TECHNICAL REPORT STANDARD TITLE PAGE

1. Report No.	2. Government Accession No.	3. Recipient's Catalog No.
FHWA/TX-88+381-2		

4. Title and Subtitle
SHEAR CAPACITY OF HIGH STRENGTH PRESTRESSED CONCRETE GIRDERS

5. Report Date
January 1988

6. Performing Organization Code

7. Author(s)
David L. Hartmann, J. E. Breen, and M. E. Kreger

8. Performing Organization Report No.
Research Report 381-2

9. Performing Organization Name and Address
Center for Transportation Research
The University of Texas at Austin
Austin, Texas 78712-1075

10. Work Unit No.

11. Contract or Grant No.
Research Study 3-5-84-381

12. Sponsoring Agency Name and Address
Texas State Department of Highways and Public Transportation; Transportation Planning Division
P. O. Box 5051
Austin, Texas 78763-5051

13. Type of Report and Period Covered
Interim

14. Sponsoring Agency Code

15. Supplementary Notes
Study conducted in cooperation with the U. S. Department of Transportation, Federal Highway Administration. Research Study Title: "Optimum Design of Bridge Girders Made Using High Strength Concretes and Deflection of Long-Span Prestressed Concrete Beams"

16. Abstract

Recent studies have shown that it is commercially feasible to produce prestressed concrete girders utilizing concrete strengths in the 12,000 psi range. However current codes and specification provisions for important structural parameters such as shear strength are largely empirical and are based on tests using concrete strengths less than 6000 psi. This program was undertaken to evaluate the adequacy of current design provisions for shear capacity when applied to high strength concrete girders.

This report summarizes the results of the shear testing of ten pretensioned girder specimens made from concretes with compressive strengths ranging from 10,800 psi to 13,160 psi. Both monolithically cast slabs of high strength concrete and compositely cast slabs of 3300 psi and 5350 psi concrete were utilized. Web reinforcement ratios varied from unreinforced webs and very lightly reinforced webs near current minimum web reinforcement ratios to very heavily reinforced webs with web reinforcement substantially above current maximum shear capacity limits. The tests indicated that the current maximum shear reinforcement limits could be substantially increased.

In addition to the laboratory tests performed, a comprehensive evaluation of shear tests in high strength concrete girders reported in American literature was carried out. All of the test results were evaluated in comparisons with the current AASHTO/ACI provision, the compression field theory recommendations of the Canadian Code, and the variable inclination truss models proposed in Study 248. All three methods gave generally conservative results for both reinforced and prestressed high strength concrete members. These design methods are acceptable for concrete strengths ranging to at least 12,000 psi. All three design procedures showed little change in conservatism as a function of concrete strengths. The tests indicated that the current maximum shear reinforcement limits could be substantially increased.

17. Key Words	18. Distribution Statement
shear capacity, prestressed concrete girders, high strength, parameters, testing, strengths, pretensioned, reinforcement	No restrictions. This document is available to the public through the National Technical Information Service, Springfield, Virginia 22161.

19. Security Classif. (of this report)	20. Security Classif. (of this page)	21. No. of Pages	22. Price
Unclassified	Unclassified	272	

Form DOT F 1700.7 (8-69)

SHEAR CAPACITY OF HIGH STRENGTH PRESTRESSED CONCRETE GIRDERS

by

David L. Hartmann
J.E. Breen
M.E. Kreger

Research Report 3-5-84-381-2

Research Project 3-5-84-381

"Optimum Design of Bridge Girders Made Using High Strength Concretes and Deflection of Long-Span Prestressed Concrete Beams"

Conducted for

Texas
State Department of Highways and Public Transportation

In Cooperation with the
U.S. Department of Transportation
Federal Highway Administration

by

CENTER FOR TRANSPORTATION RESEARCH
BUREAU OF ENGINEERING RESEARCH
THE UNIVERSITY OF TEXAS AT AUSTIN

January 1988

The contents of this report reflect the views of the authors who are responsible for the facts and accuracy of the data presented herein. The contents do not necessarily reflect the official views or policies of the Federal Highway Administration. This reports does not constitute a standard, specification, or regulation.

TABLE OF CONTENTS

LIST OF FIGURES (cont.)

LIST OF FIGURES (cont.)

LIST OF FIGURES (cont.)

LIST OF FIGURES (cont.)

LIST OF TABLES

Table Page

CHAPTER 1
INTRODUCTION

1.1 Background

Shear in high strength prestressed concrete girders combines the well studied problem of shear in prestressed concrete with the less researched behavior of high strength concrete. The use of high strength concrete, f'_c from 7000 to 13000 psi, is increasing in bridge applications as well as in buildings and other structures. Presently the normal AASHTO/ACI shear provisions are used to predict the capacity of high strength prestressed concrete.

There are several reasons why current shear provisions must be re-examined or used cautiously for high strength concrete. Current AASHTO/ACI shear equations are quite empirical. The nature of current provisions have not changed substantially since their introduction in the 1963 ACI Code. For the most part these empirical equations were derived using results from tests having concrete strengths less than 6000 psi. In many locations it is possible to mass produce concretes with useful compressive strengths of 12000 psi or more. In all the shear equations for both reinforced and prestressed concrete, concrete strength is a primary variable in capacity calculations. Extrapolating empirical equations for concretes with twice the compressive strength of those used in the original formulation is dangerous. Another consideration is that some physical properties are known to change with increasing concrete strength. The effect of changing physical properties on empirical equations is difficult to predict without test data. The shortage of test data is the third reason that caution must be exercised in the use of current AASHTO/ACI shear provisions. To date only 32 shear tests have been reported in American literature for high strength prestressed concrete. Those tests are for a relatively narrow range of concrete strengths, shear reinforcement, prestress force, and shear span to depth ratios. Additionally a number of tests have been conducted on high strength reinforced concrete beams. While not of direct use they do provide information as to whether trends exist for increasing concrete strength. The fact remains, however, that test data for shear capacity of high strength prestressed concrete is currently quite limited.

There is also some dissatisfaction with the current method of shear capacity calculations due to its complexity. Over the last ten to fifteen years a number of shear models have been proposed as replacements for the current empirical equations. The proposed methods are based on the theory of plasticity. This provides a rational basis

as opposed to the current method's empirical nature. These models and especially the truss model that may be derived from them give the designer added insight into member behavior. They also tend to be simple, direct methods of predicting capacity. These methods, however, also need checking to insure conservatism when used to predict the shear capacity of high strength concrete.

1.2 Objectives and Scope

The primary objective of this investigation was to add to the meager existing data base of shear tests in high strength prestressed concrete. Several secondary goals were set as well. The first was to find the cracking load of the prestressed members which current American practice takes as the concrete's contribution to shear. Additionally it was desired to observe behavior of beams with shear reinforcement in excess of the levels allowed by current specifications. This was to determine whether current reinforcement limits could be raised as concrete strength increases. The last major goal was to compare the results for high strength concrete shear tests reported in the literature and obtained in this investigation to several proposed shear capacity models. This was to provide a basis for judgement of the merits of different shear capacity models.

To fulfill these goals a series of ten tests were conducted on high strength prestressed girders. A variety of shear rein- forcement values were used to broaden the data base. Some specimens had extremely heavy shear reinforcement to allow observation on behavior of such members. A wide range of measurements were taken during testing to give added information. Cracking loads were noted during testing. All available test results reported in American literature as well as the results of this experimental program were compared to the predictions of a number of shear capacity models.

The work done in this study will be organized in the following way. Chapter 2 will contain a brief literature review on the information available about high strength concrete. Additional information obtained from trial batches for the current project will also be noted. Chapter 3 contains a review of the bases for a number of shear capacity models. The tests reported in the literature are also evaluated in this section. A general description of the current study test specimens, test procedures, and equipment is given in Chapter 4. Chapter 5 contains the results and an evaluation of the results for the test specimens of this project. Chapter 6 contains a summary of results and conclusions drawn from this work. Supplemental information on high strength concrete and prestressing strand development is given in Appendices A and B respectively.

CHAPTER 2
HIGH STRENGTH CONCRETE

2.1 Introduction

High strength concrete offers many advantages related to physical performance and economics. High strength concrete has, in recent years, proven itself in applications such as bridges, buildings and offshore oil structures [14,22,24,25,41]. Optimum use of high strength concrete, however, can only come with familiarity of the production requirements and physical properties.

The following chapter is not an indepth study of either production requirements or all properties determined to date for high strength concrete. It is rather intended as background information important to the more specific topic of shear in high strength prestressed concrete girders.

2.2 Production of High Strength Concrete

Successful production of high strength concrete requires extreme care in all steps of the production process. The first step is to determine the strength needed and the age at which the strength is required. The strength level indicates the general requirements for the batch. A 12000 psi mix will demand more careful selection of materials and production control than a 9000 psi mix. Strength in the trial batches must be higher than the required f'_c to guarantee a minimum number of tests below the specified strength as stated by AASHTO and ACI 318. Sufficient strength is absolutely essential, but excess strength becomes uneconomical. Knowing when the specified strength is required is as important as knowing the strength. A mix for use in a prestressed precasting yard which needs high strength at from 12-24 hours will be different than one for a building column needing full strength several months later. High strength concrete generally continues to gain substantial strength for 90 days and beyond [10]. It has become common practice to specify high strength concrete strengths at 56, 90, or even 180 days [10,22]. Again 12000 psi at 28 days would require different mix proportions than 12000 psi at 90 days. Economically it is important to know specifically what strength one needs and when one needs it at the outset of high strength concrete production.

Once the general strength goals have been determined, development of a mix to meet these goals must begin. Reference [9] is a good starting point. It gives quantitative suggestions on initial trial batches. As would be expected, high strength concrete requires

a very low water to cement ratio. Ratios as low as 0.25 are not uncommon. The production of high strength concrete requires good quality for all constituents of the mix. For more information on the individual material requirements References [9,10,11,36] all offer valuable suggestions. As suggested in Reference [9] it is best to try several different mixes in the initial trial batches.

Trial batches with the initial mix designs are critical to successful application of high strength concrete. First the trial batches indicate if sufficient strength can be obtained from the mix proportions and materials used. If not, refinements must be made to obtain greater strength. If sufficient strength has been obtained then decisions can be made as to which mix will be the most economical. Generally several trial batches are required if an optimized mix design is desired. Trial batches serve other purposes as well. They indicate if the various mix components, especially admixtures, are compatible. Also a determination can be made whether the mix is providing sufficient workability. Production of the trial batches under field conditions gives more realistic indications of actual batch performance than laboratory mixes.

Control of production techniques must be strict for success with high strength concrete [10,22]. Actual requirements are the same as normal strength concrete, but it is imperative that they be adhered to without compromise. Batching weights must match the mix design as accurately as possible. Steps need to be taken at the ready mix plant to insure proper gradation of aggregates. Even more importantly the water content of the aggregates must be closely monitored. Water content changes have the greatest effect of all variables on concrete strength [20]. Inaccurate estimation of the aggregates' water content, which affects the quantity of additional water added at batching, can result in either balling of the concrete due to lack of mixing water or too high a slump. In general if balling occurs, so much water must be added at the batch plant to break up the balls that the batch must be discarded. If the slump is too high, the water content is already too high and the mix must be rejected. Once the correct slump is obtained at the batch plant further water additions must not be allowed. The order in which materials are loaded into the truck can affect the resulting concrete. Mixing proves to be critically important as well. For satisfactory performance all the materials, especially admixtures, must be thoroughly mixed. At the jobsite the addition of water must be strictly forbidden. Any admixtures added need to be carefully measured and thoroughly mixed before casting begins. Casting high strength concrete requires proper manpower and equipment. Due to the high cement content and low water content workability time is often shortened even with the use of retarders, particularly during hot weather.

Provisions must be made to quickly cast and thoroughly consolidate the concrete upon arrival. Curing becomes more critical in high strength concrete production. Curing must begin as soon as possible to insure good quality concrete. Given the already low water content in high strength concrete, drying must be prevented to allow proper hydration. High strength concrete tends to be more susceptible to shrinkage cracking. This is especially true if silica fume is used [37]. The curing method whether ponding, spraying, covering, etc. should keep the concrete moist during its initial curing.

2.3 Current Work

2.3.1 Trial Batches. A portion of the preliminary work for this project involved doing a series of trial batches. The objective was to obtain a mix that satisfied the strength requirements for the shear specimens. The general strength goal was 12000 psi at 28 days with a 9 inch slump and using a 3/8" aggregate. Much of the work was done jointly with another project. Reference [11] contains complete coverage of these and other batches. In the following paragraphs the same batch numbering system as Reference [11] will be used. All told 22 trial batches were carried out. The last trial batch was used for the test specimens which were cast on four separate occasions. The following are some observations from these trial batches.

2.3.1.1 Air dried versus moist curing. Curing conditions were one of the variables investigated during the trial batch phase of this project. ACI 318 requires concrete to meet the specified strength after curing as per ASTM C31. The pertinent provision is Section 9.3 which states that test specimens should be removed "from the molds at the end of 20 ± 4 h and stored in a moist condition at $73.4° \pm 3°$ F. ($23° \pm 7°$ C.) until the moment of test." Moist curing is defined as immersion in saturated lime water or setting in a moist room. The Texas Department of Highways and Public Transportation commonly specifies a seven day moist cured beam break for concrete acceptance. This is not representative of actual field curing conditions. Tests were run on both beams and cylinders which were moist cured and ones which were air dry cured using a curing compound.

Table 2.1 gives moist cured strength at 28 days and air dry cured strengths at 28 days and later. Mixes 28-31 are the four shear specimen casts corresponding to Specimens 3-1 and 3-2, Specimens 3-3 and 3-4, Series 1, and Series 2. Figure 2.1 gives normalized results of the strength of air cured cylinders at various dates compared to moist cured strength at 28 days. It will be noted that most values fall within 10% of

Table 2.1 Moist and air dry cured strengths at 28 days and later

MIX	MOIST	AIR DRIED								
	28 DAY (1)	DAY	STRENGTH (2)	(2)/(1)	DAY	STRENGTH (3)	(3)/(1)	DAY	STRENGTH (4)	(4)/(1)
07	9800	28	9490	.97	56	9320	.95			
10	9870	28	10230	1.04	56	10450	1.06			
11	9480	28	9580	1.01	54	9940	1.05			
12	9410	28	8940	.95	54	9900	1.05			
13	8670	28	9100	1.05	56	10000	1.15			
14	9873	28	10310	1.04	56	11190	1.13	91	11380	1.15
15	10470	28	10990	1.05	56	11240	1.07	91	11500	1.10
16	10620	28	9920	.93						
17	8900	28	9270	1.04	56	10140	1.14	91	10820	1.22
18	10360	28	10750	1.04						
28	12420	28	12000	.97	44	13020	1.05			
29	10660	28	10750	1.01	55	10780	1.01			
30	11120	28	10860	.98						
31	13010	28	10540	.81	68	10800	.83			

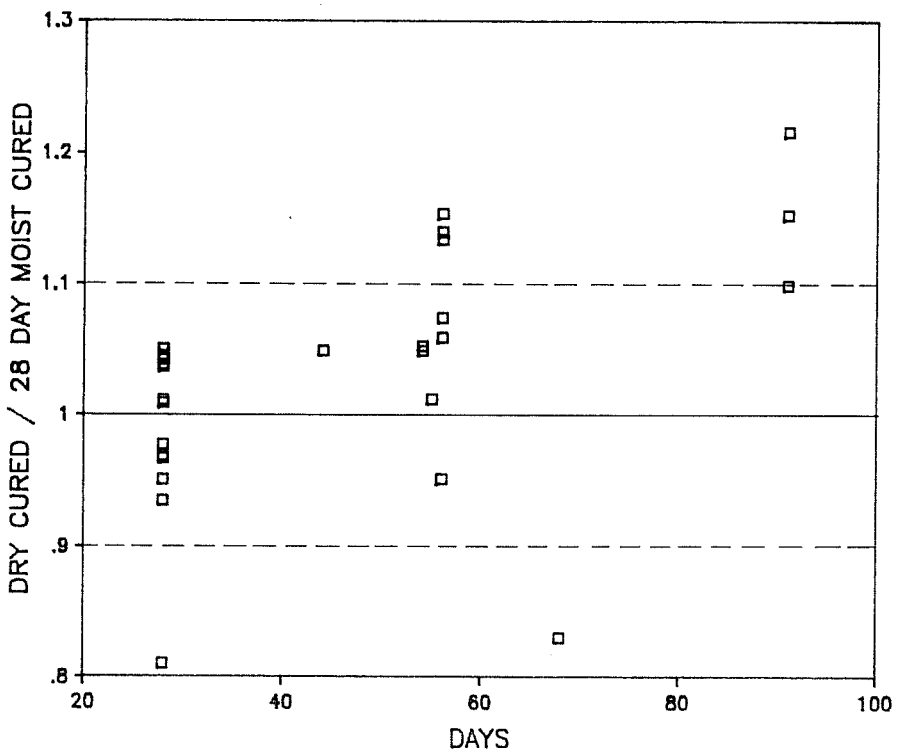

Fig. 2.1 Normalized plot of air dried cured compressive strength at 28 days and later divided by 28-day moist cured strength

unity. The higher values indicate slight conservatism while lower values are unconservative. The two very low values indicate a potential problem. The vast majority of the points shown are for concrete batches poured over the summer. The temperature range was approximately 75° to 105° F daily for the first part of the curing. Based on the maturity concept for strength development the dry cured specimens should have done quite well. From further evaluation of the data Carrasquillo noted that up to 15 days dry cured cylinders were stronger, but from 28 days until the end of testing moist cured were stronger [11]. It is reasonable to assume that the early heat helped the dry cured concrete develop strength quickly, but that desiccation prevented the concrete from curing completely. The two very low readings were for a batch cast during cold weather. Due to the cold temperature, about 35° F at cast and less than 70° F during curing, the maturity of the concrete was low. The concrete still dried so that hydration slowed. The net result is a mix in which the dry concrete was significantly lower than moist cured cylinders.

The literature has noted a significant link between curing conditions and tensile strength of high strength concrete. The tensile strength was measured using 6"x6"x20" beams cast in steel molds. The data presented herein is for moist cured cylinders at 7 days and 28 days and moist and dry cured beams at 7 days and 28 days (Table 2.2). The beam strengths are compared with the square root of the moist cured cylinders at a given date. Figures 2.2 and 2.3 show the results plotted against concrete strength at 7 and 28 days respectively. There are several trends in the data. There is quite obviously a difference between the moist cured and dry cured beams. The dry cured beams had about 60% of the strength of moist cured beams at both 7 and 28 days. There is a modest increase in the coefficient of tensile strength divided by the square root of compressive strength as the age increases. The relative increase between moist and dry cured is essentially the same. This would indicate that either tensile strength increases more with age than the square root of the compressive strength or that the tensile strength does not change as a square root function of the compressive strength.

2.3.1.2 Effect of aggregate. The coarse aggregate can have a major influence on the strength of concrete. Table 2.3 gives pertinent aggregate properties. After a number of trial batches had been conducted it was decided that the aggregate was not sufficiently strong to allow higher concrete strength. Table 2.4 contains the highest strength obtained out of each batch. It should be noted that the date of the highest strength varied due to modifications in the testing schedule that occurred as the trial batches proceeded. Figure 2.4 shows the results graphically. It will be noted that for

Table 2.2 Moist and dry cured beam strengths at 7 and 28 days

MIX	7 DAY					28 DAY				
	CYLINDERS	BEAMS				CYLINDERS	BEAMS			
	MOIST (1)	MOIST (2)	(2)/√(1)	AIR DRY (3)	(3)/√(1)	MOIST (4)	MOIST (5)	(5)/√(4)	AIR DRY (6)	(6)/√(4)
01	9200	1229	12.8			11190				
02	9170	1059	11.1			11000				
03	8730	1094	11.7			9920				
04	9730	1029	10.4			11060				
05	9150	974	10.2			10440				
06	8930	1098	11.6			10850				
07	8470	952	10.3	531	5.8	9800	1092	11.0	688	6.9
08A	9360	1212	12.5			10610				
08B	9420	1233	12.7			10630				
09	9210	1135	11.8			10140				
10	8770	1271	13.6	720	7.7	9870	1323	13.3	783	7.9
11	7730	1100	12.5	710	8.1	9480	1260	12.9	770	7.9
12	7310	1160	13.6	700	8.2	9410	1430	14.7	750	7.7
13	7660	1020	11.7	580	6.6	8670	1300	14.0	680	7.3
14	9710	1140	11.6	550	5.6	9870	1390	14.0	730	7.3
15	10040	1320	13.2	810	8.1	10470	1430	14.0	920	9.0
16	8640	1010	10.9	570	6.1	10615	1300	12.6	800	7.8
17	7950	930	10.4			9570	1083	11.1		
18	9210	870	9.1			11030	1190	11.3		
19	9200	1270	13.2			10930	1280	12.2		
20	9810	1200	12.1			11620	1590	14.8		
		AVERAGE	11.8		7.0		AVERAGE	13.3		7.9
		ST. DEV.	1.2		1.0		ST. DEV.	1.4		.7

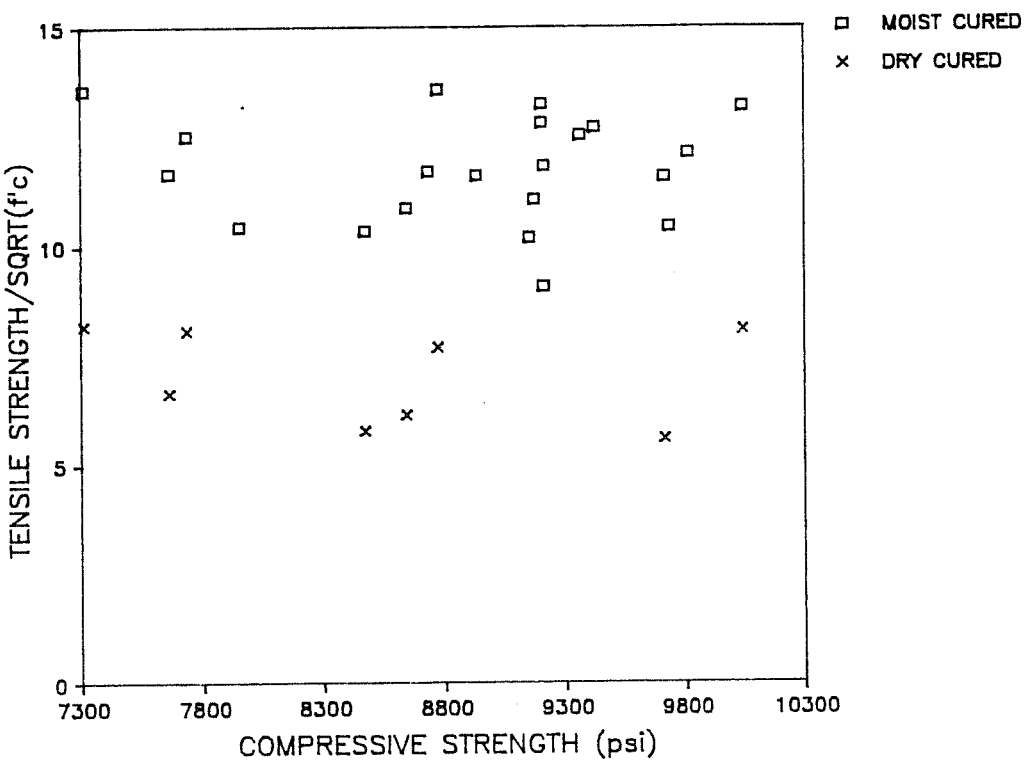

Fig. 2.2 Tensile strength versus square root of moist cured compressive strength at 7 days

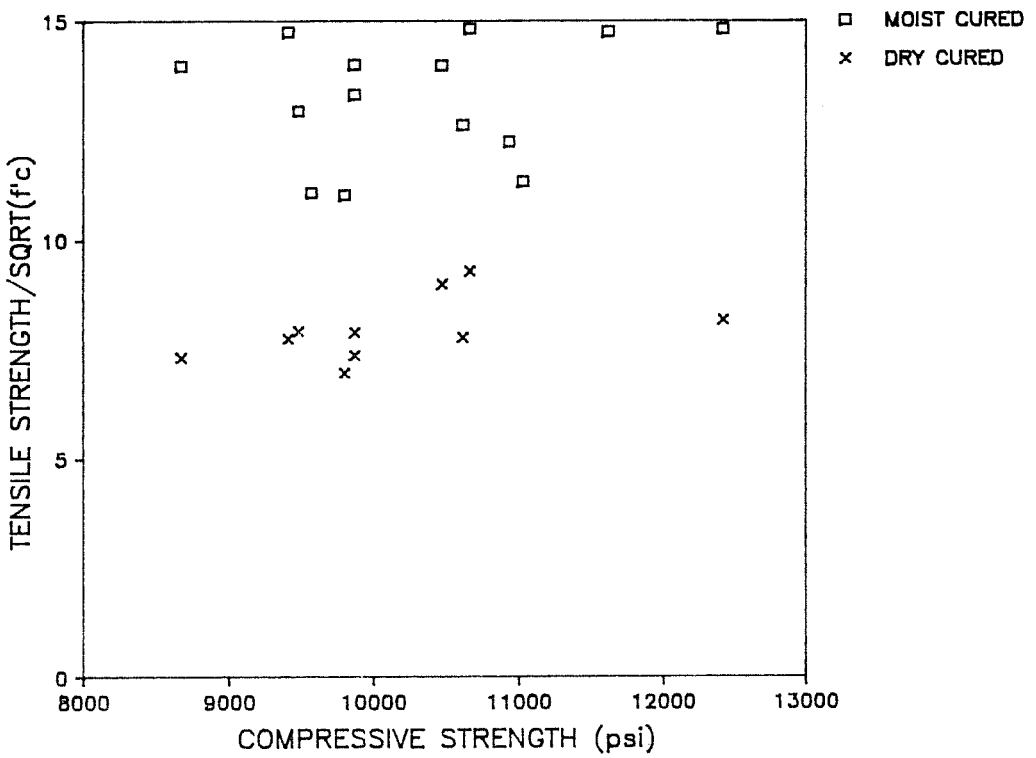

Fig. 2.3 Tensile strength versus square root of moist cured compressive strength at 28 days

Table 2.3 Properties of coarse aggregates used in high strength concrete mixes.

COARSE AGGREGATE DESIGNATION	COARSE AGGREGATE PROPERTIES
AGGREGATE A	Crushed limestone ASTM C33 No. 8, 3/8-in. to #8 BSG_{ssd} = 2.53 DRUW = 94 pcf AC_{ssd} = 3.0%
AGGREGATE B	Crushed limestone ASTM C33 No. 8, 3/8-in. to #8 BSG_{ssd} = 2.43 DRUW = 91 pcf AC_{ssd} = 4.5%
AGGREGATE C	Crushed limestone ASTM C33 No. 57, 1-in. to #4 BSG_{ssd} = 2.79 DRUW = 99 pcf AC_{ssd} = 0.5%
AGGREGATE D	Crushed limestone ASTM C33 No. 8, 3/8-in. to #8 BSG_{ssd} = 2.79 DRUW = 100 pcf AC_{ssd} = 0.5%

Table 2.4 Maximum compressive strength for each mix

BATCH	COARSE AGGREGATE	AGE (DAYS)	COMPRESSIVE STRENGTH (psi)
01	A	56	11790
02	A	56	12140
03	A	56	10410
04	A	56	11830
05	A	56	11280
06	A	56	11650
07	A	56	10210
08A	A	56	11260
08B	A	56	11360
09	A	56	10870
10	A	91	11550
11	A	91	11650
12	A	91	10980
13	A	91	11650
14	A	91	12930
15	A	91	12560
16	A	92	12330
17	B	92	10750
18	B	92	11480
19	A	90	12440
20	C	90	14310
21	D	96	16110

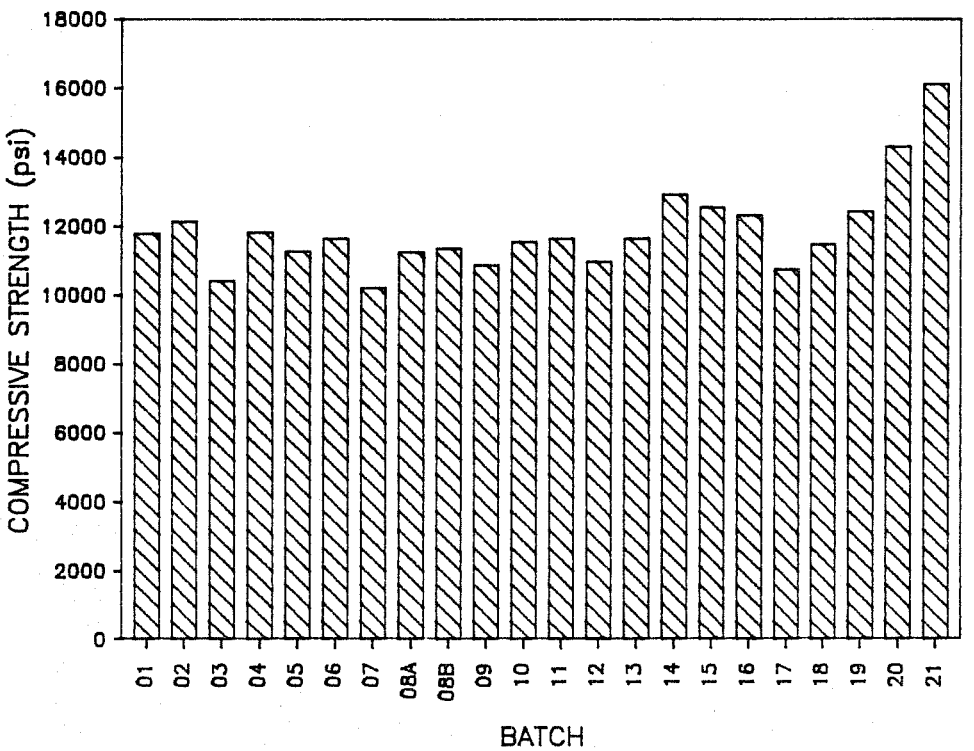

Fig. 2.4 Maximum compressive strength for each batch

batchs 01 through 19, using Aggregates A and B, maximum strength was between 10000 psi and 13000 psi with the majority below 12000 psi. The breaks were going through the aggregate without bond failure. Several batches were conducted with a stronger limestone. The 1" maximum size, Aggregate C, used in trial batch 20 gave a high strength of 14300 psi. The 3/8" maximum size, Aggregate D, used in trial batch 21 gave strengths up to 16110 psi. The coarse aggregate appears to have limited concrete strength in batches 01-19. This provides further evidence that the coarse aggregate has a major effect on the strength of high strength concrete.

2.3.2 Problems with use. For all of high strength concrete's advantages there are certain problems which should be considered. Batching concrete with a very low water to cementitious materials ratio, about 0.25, is delicate. Good knowledge of the aggregates' water content is essential. If too little water is added during batching the concrete will form balls and not mix properly. Generally if this occurs so much water must be added to break up the balls that the resulting batch is unacceptable. If too much water is added initially the slump will be out of the acceptance range and the batch must be discarded. Once a good mix has been obtained several casting difficulties can occur. The mixes can become quite stiff in only a short time, especially in hot weather. Redosing with superplasticizer is an option, but speed in casting is better policy. Crusting between lifts is possible in hot, dry weather; therefore, compaction must penetrate the previous lift. Finishing holds even greater trouble. Workability in the forms is short lived and the rocky nature of the mix makes finishing more difficult. Curing must be done very well or problems can occur. In the laboratory plastic shrinkage cracks occurred in several instances while the formwork was still on. Thin sections are especially vulnerable to this. In other cases surface cracking was visible within a few minutes of final screeding. Curing must be quick and thorough. Successful use of high strength concrete requires care in batching, casting, and curing.

2.4 Properties of High Strength Concrete

2.4.1 General. The physical properties of high strength concrete tend to be somewhat different than for normal strength concrete. Only those properties pertinent to shear in prestressed concrete will be discussed herein. References [10,13,35] all have additional information. The most important property is the higher compressive strength. High strength is actually a fairly loose term implying greater strength than is generally used at a certain location. Usually this means strengths in excess of 6000 psi. While

strength is the most obvious and easily measured property, other properties do have a major effect on structural performance.

2.4.2 Stress-strain behavior. The stress-strain behavior in uniaxial compression changes some as concrete strength increases. Figure 2.5 shows the general trend. The slope of the stress-strain curve is steeper and more linear up to about 80% of ultimate capacity [35]. The strain at maximum stress is somewhat higher than for normal strength concrete [12]. The descending branch of high strength concrete is steeper. It is stated that the descending branch becomes almost a vertical line [43]. Special methods must be employed to obtain the descending branch. The ultimate strain at failure is lower than for normal strength concrete.

2.4.3 Modulus of elasticity. The steeper stress-strain curve for high strength concrete means the modulus of elasticity is higher. The increase in modulus of elasticity does not, however, in general match the value predicted by $E_c = 33(w_c)^{1.5}\sqrt{f'_c}$ (psi). This equation tends to overestimate the actual modulus. Other equations for the modulus of elasticity have been proposed with

$$E_c = (40000\sqrt{f'_c} + 1.0 \times 10^6)(w_c/145)^{1.5}$$

(psi) by Carrasquillo et al. being widely accepted (Fig. 2.6) [12]. The modulus is greatly influenced by the coarse aggregate [19].

2.4.4 Tensile strength. The tensile strength of concrete is typically measured either by a modulus of rupture test or splitting tensile test. The values of tensile strength are highly dependent upon drying as found by this project and in the literature. Moist cured beams show substantially higher strengths than predicted by the current AASHTO Specification. Dry cured, however, only show a small difference. Proposals have been made for increased predictions of tensile strength. More recently however the feeling has been to use more traditional and conservative values predicted by current equations [12,35].

2.4.5 Miscellaneous. Several other properties have minor influences on shear in high strength concrete. Total shrinkage at later ages is said to be about the same as for normal strength concrete. High strength concrete does, however, see more of its total shrinkage at early ages than does normal strength concrete. Unit creep tends to be much lower in high strength concrete. Given the fact that it is stressed higher, total creep stays about the same. This indicates that total prestressed losses should be of

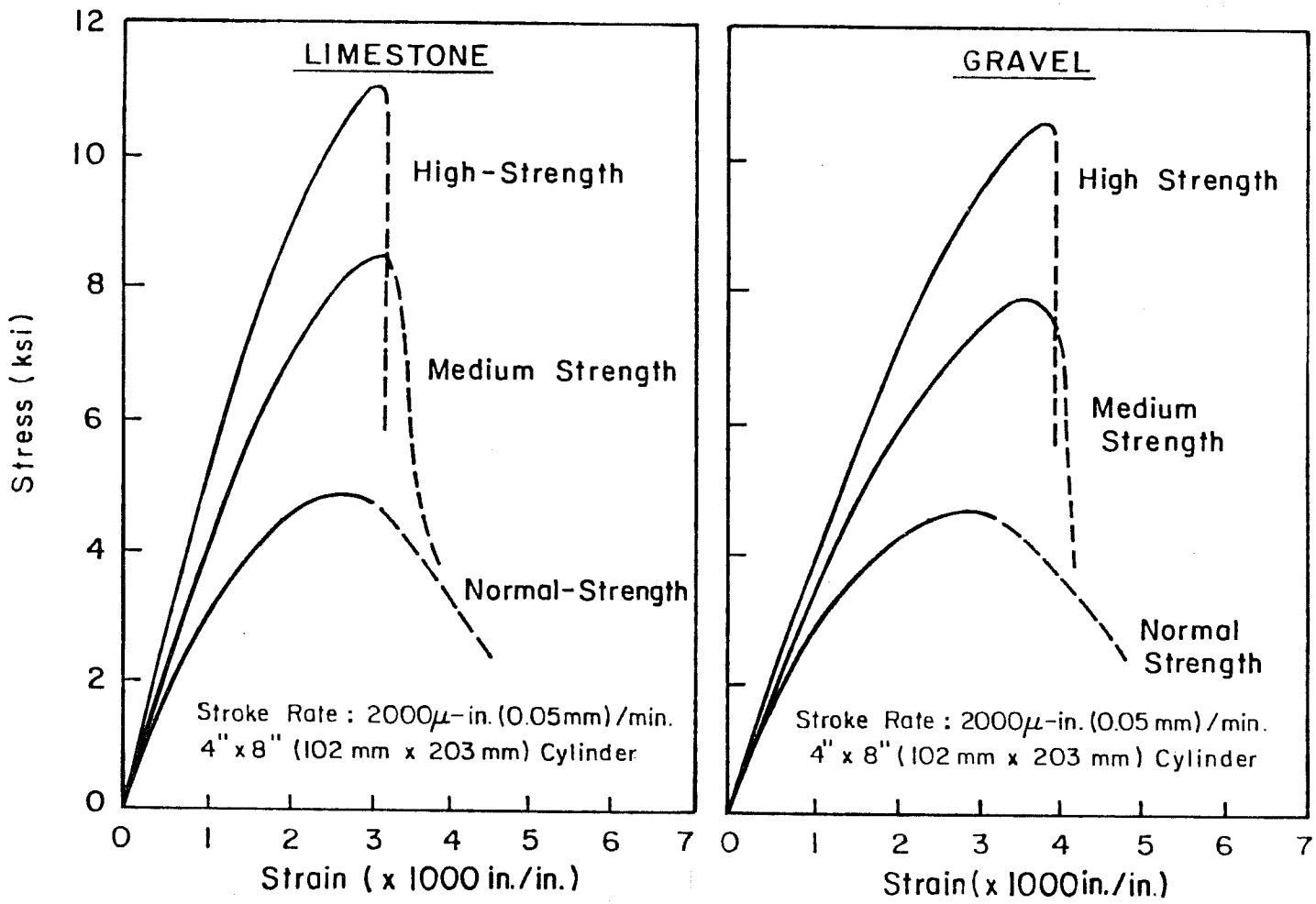

Fig. 2.5 Stress-strain curves for normal, medium and high strength concrete [12]

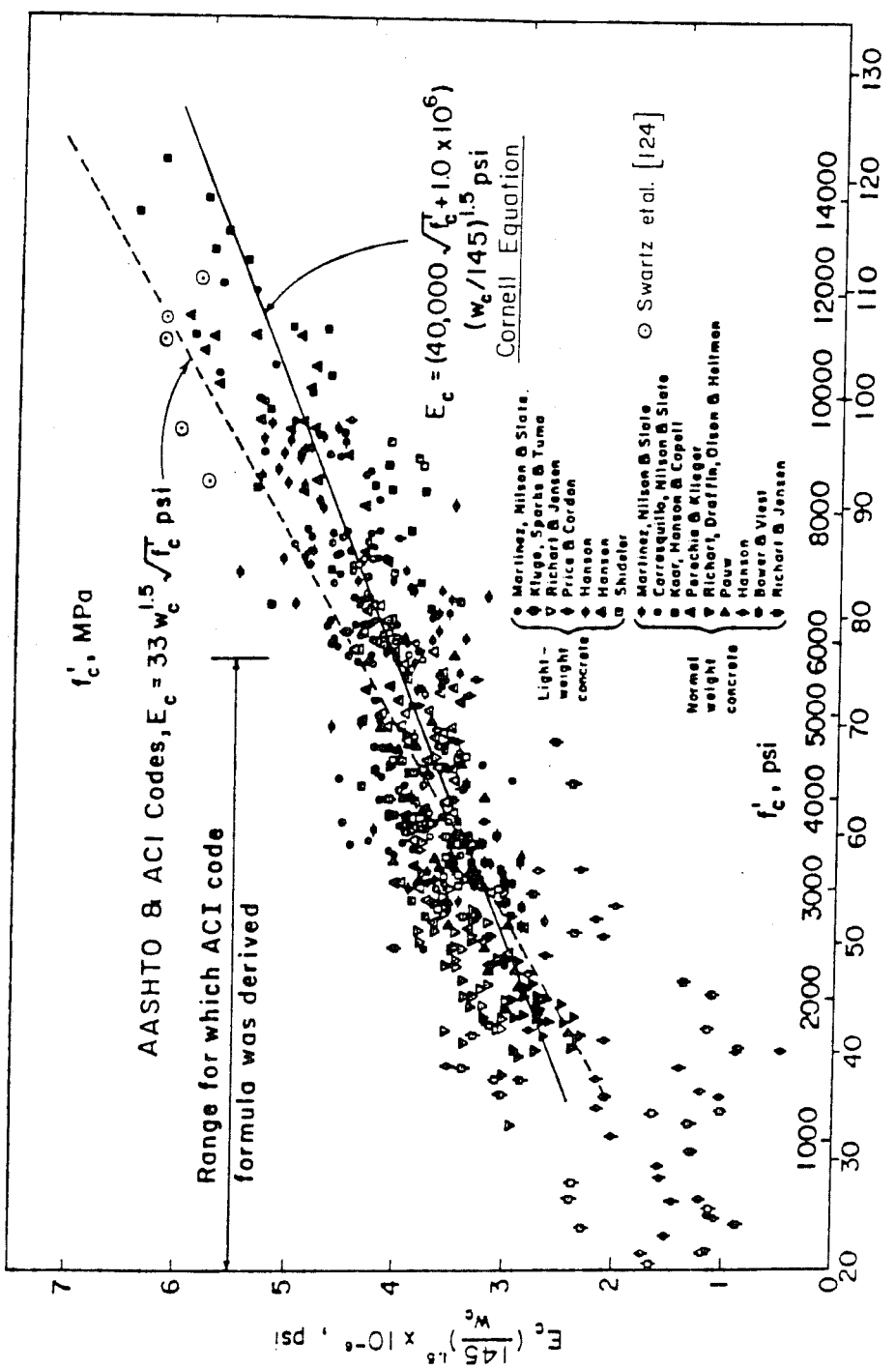

Fig. 2.6 Modulus of elasticity versus compressive strength [29]

CHAPTER 3
SHEAR CAPACITY MODELS

3.1 Introduction

Shear is one of the primary modes of failure in structural concrete. For over 30 years shear has been extensively researched and discussed [7,8]. A number of empirical and conceptual models have been presented over the course of time. Given all of this effort, however, a completely satisfactory solution has not been attained.

A number of currently popular shear capacity models will be discussed herein. The models range from highly empirical to highly theoretical. The assumptions of each model will be discussed and some comments will be made on their rationality and ease of use. The three most popular models will be compared with the test results available for shear in high strength concrete.

3.2 AASHTO and ACI (Current)

Current AASHTO and ACI shear provisions are highly empirical. The major provisions of the two are identical [2,5]. A full history of the development of each can be found in Reference [40]. For the present purpose only the bases of current provisions are discussed.

The general basis of the Code provisions, Code referring to both ACI and AASHTO in this discussion, is summarized in

$$V_u \leq \phi(V_c + V_s) \tag{3.1}$$

where

V_u = factored shear force at a section

V_c = nominal shear strength provided by concrete

V_s = nominal shear strength provided by shear reinforcement

ϕ = strength reduction factor equal to 0.85 for shear

This explicitly states that total shear resistance is the sum of a concrete contribution and a steel contribution.

The steel contribution to shear is based on a 45° truss model. The original formulation came from W. Ritter in 1899 and was extended by E. Morsch. An assumption was made that the crack angle was 45°. From equilibrium, and rearranging terms the familiar equation for the steel contribution is

$$V_s = \frac{A_v f_y d}{d} \tag{3.2}$$

where

A_v = area of shear reinforcement within a distance s

f_y = specified yield strength of shear reinforcement

d = distance from extreme compression fiber to centroid of longitudinal reinforcement

s = spacing of shear reinforcement in direction parallel to longitudinal reinforcement

The basic philosophy for the current design procedure is that

> "shear reinforcement restrains growth of inclined cracking, providing increased ductility, and a warning in situations in which the sudden formation of inclined cracking in an unreinforced web may lead directly to distress [8]."

ACI-ASCE Committee 426 goes on to state:

> "In addition to any shear carried by the stirrup itself, when an inclined crack crosses shear reinforcement, the steel may contribute significantly to the capacity of the member by increasing or maintaining the shear transferred by interface shear transfer, dowel action, and arch action."[8]

The underlying conceptual truss model has thus been pushed to the background. The shear reinforcement is seen to a significant degree as a means of maintaining the concrete contribution at ultimate.

While there is an underlying physical model for the steel contribution, the concrete contribution consists of empirical equations which try to include the most important parameters affecting behavior. The V_c term as used in the Code is an attempt

to account for the four major shear transfer mechanisms [8]. The four mechanisms are shear transfer by concrete shear stress, interface shear transfer, dowel shear, and arch action. Each of these four mechanisms can have a varying influence under different circumstances. The practicality of the situation is that the V_c terms were derived to correlate sufficiently well with the test results available. A major assumption is that the shear taken by the concrete at cracking can be carried at ultimate in a reinforced beam and that this shear supplements the shear contribution of the truss model as reflected in the V_s term [7].

For reinforced concrete there are two equations for V_c, under normal loading conditions. One equation is

$$V_c = (1.9\sqrt{f_c'} + 2500\,\rho_w[V_u d/M_u])b_w d \leq 3.5\sqrt{f_c'}b_w d \tag{3.3}$$

where

$\sqrt{f_c'}$ = square root of specified compressive strength of concrete

$\rho_w = A_s/b_w d$

A_s = area of longitudinal reinforcement

V_u = factored shear load at a section

M_u = factored moment at section

b_w = web width

d = distance from extreme compression fiber to centroid of longitudinal tension reinforcement

The origin of this equation dates back to the early 1960's and ACI-ASCE Committee 326. This equation tried to realistically indicate the influence of three primary variables: the ratio of longitudinal reinforcement ρ_w, the quantity M/Vd, and the concrete strength f_c' which represented the concrete quality. From the starting point of

$$f_{t(max} = f_t/2 + [(f_t/2)^2 + v^2]^{0.5} \tag{3.4}$$

and

$$v = v/bd \tag{3.5}$$

where

V = total shear

v = shear stress

f_t = tensile strength of concrete,

the equations were manipulated into two dimensionless parameters. The available test data was then plotted in terms of these two parameters (Fig. 3.1). A bilinear curve was chosen to represent the data. The lower portion of the curve was chosen to be almost a lower bound since failures in this range were observed to have little reserve strength after diagonal cracking. The upper limit on the curve was chosen more as an average value since these specimens demonstrated substantial reserve strength. The tests from which this equation was derived were all reported by January 1, 1960. Thus this equation was derived by curve fitting the available data using what was considered the three most important parameters.

The second equation for shear in reinforced concrete is

$$V_c = 2\sqrt{f'_c} b_w d \tag{3.6}$$

This equation was first used in the 1963 Building Code. The equation gave a simple, reasonably conservative estimate to the tests used to obtain Equation (3.3). The only advantage to Equation (3.6) is its extreme simplicity. The current equations for the concrete contribution in reinforced concrete stem from empirical curve fitting done in the early 1960's.

Three separate equations are given for the concrete contribution in prestressed members. The first equation is

$$2\sqrt{f'_c} b_w d \leq V_c(0.6\sqrt{f'_c} + 700[V_u d/M_u]) b_w d \leq 5\sqrt{f'_c} b_w d \tag{3.7}$$

Several additional limitations include $V_u d/M_u \leq 1.0$ and the value given must be less than that given for web shear cracking inside the development length. This equation was added in the 1971 ACI Code as a simplified method of computing V_c compared to the more detailed equations [4]. Figure 3.2 shows the data used to obtain this equation. It should be noted that the nondimensional parameters used for the derivation are the

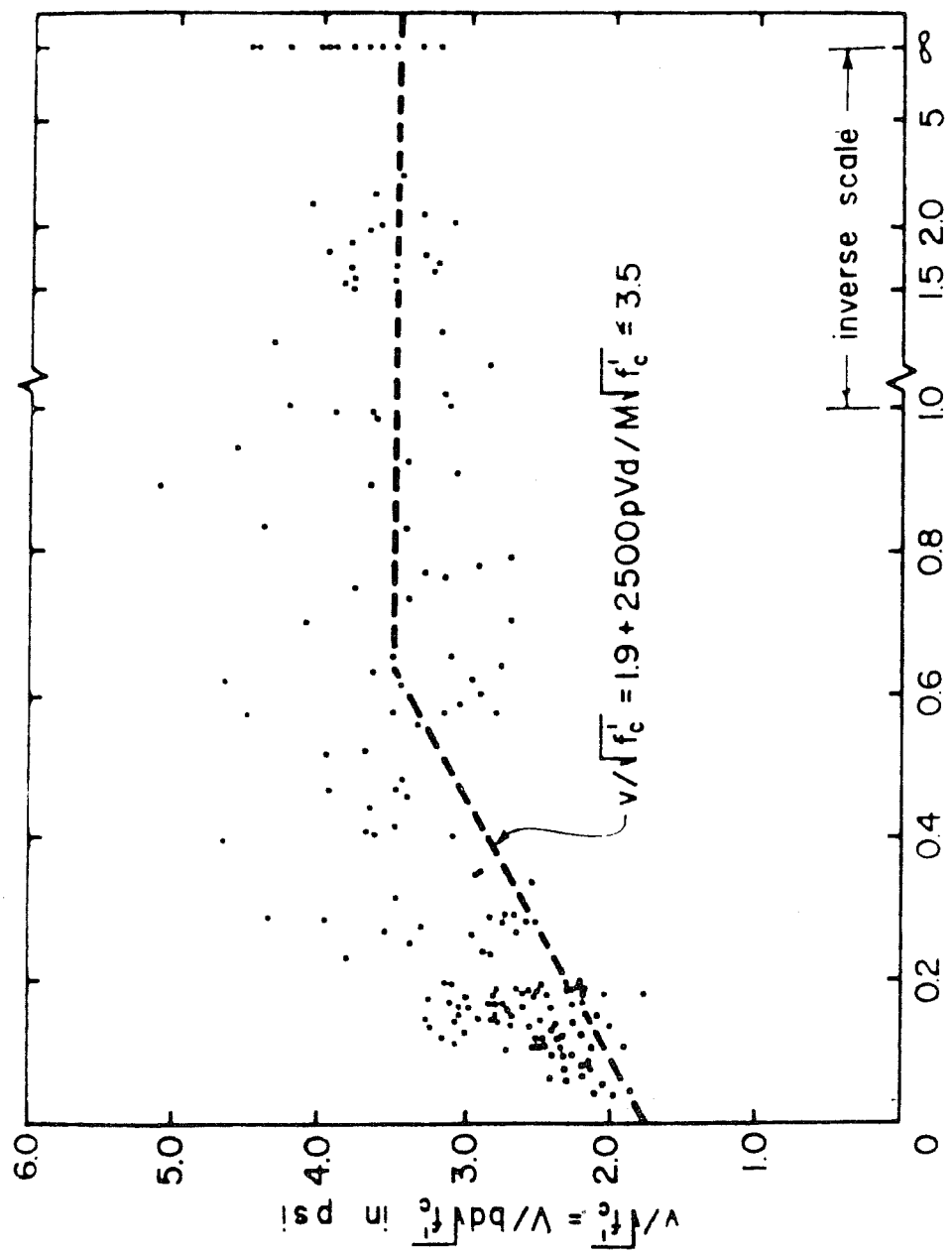

Fig. 3.1 Data points used in derivation of Eq. (3.3) [Ref.6].

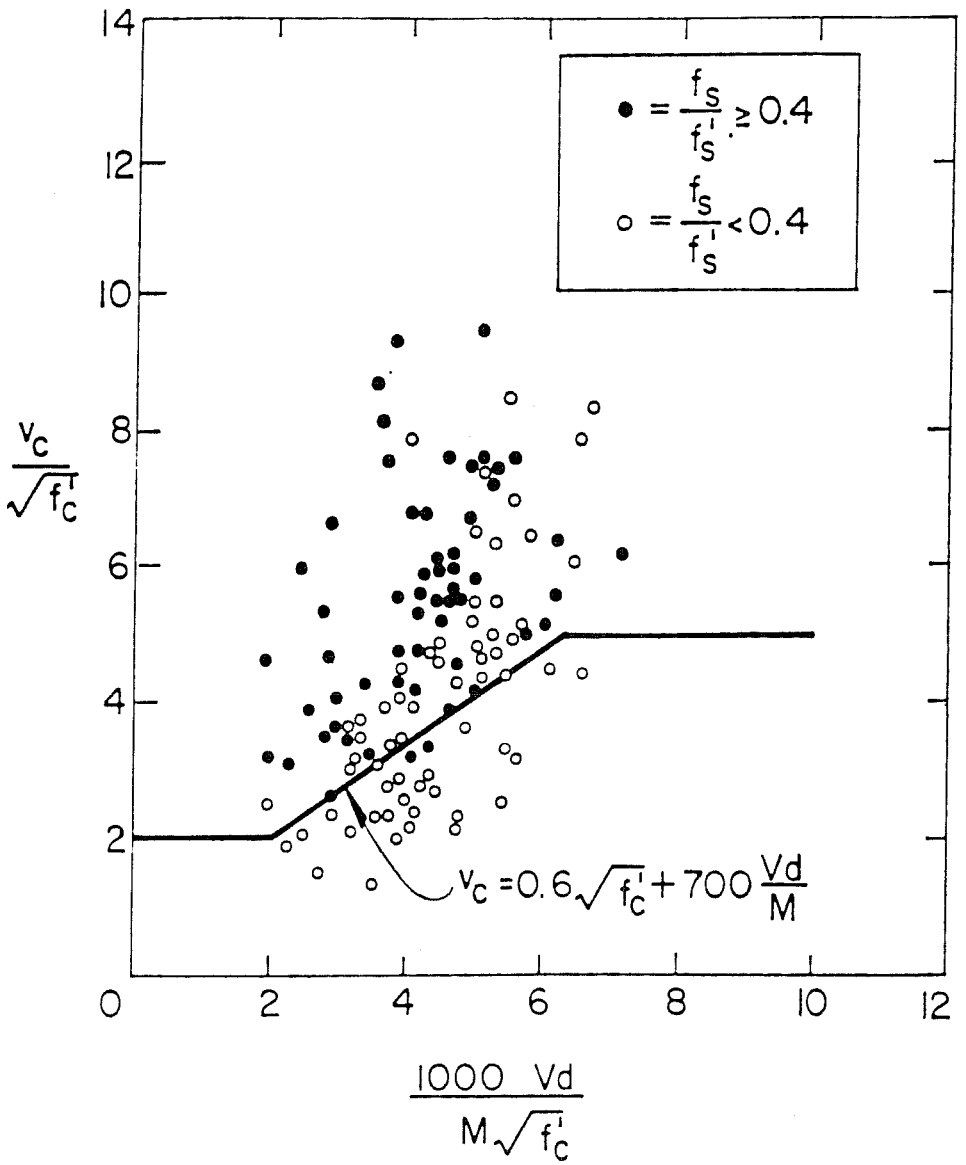

Fig. 3.2 Data points used to formulate Eq. (3.7) [Ref. 27].

same as for Equation (3.3). Furthermore there is no term in the equation related to the prestress force. The equation restriction that the effective prestress force be greater than 40% of the tensile strength of the flexural reinforcement was required to maintain conservatism. The $V_c \leq 5\sqrt{f'_c} b_w d$ was an attempt to prevent web shear cracking.

A more detailed calculation is given for inclined cracking in prestressed concrete.

$$1.7\sqrt{f'_c} \leq V_{ci} = 0.6\sqrt{f'_c} b_w d V_d + (V_i M_{cr}/M_{max} \tag{3.8}$$

where

$$M_{cr} = (I/y_t)(6\sqrt{f'_c} + f_{pe} - f_d)13.10 \tag{3.9}$$

I = moment of inertia of the section resisting externally applied factored loads

y_t = distance from centroidal axis of gross section, neglecting reinforcement, to extreme fiber in tension

V_d = shear force at section due to unfactored dead load

V_i = factored shear force at section due to externally applied loads occurring simultaneously with M_{max}

M_{max} = maximum factored moment at section due to externally applied loads

M_{cr} = moment causing cracking at section due to externally applied loads

f_{pe} = compressive stress in concrete due to effective prestress force only (after allowance for all prestress losses) at extreme fiber of section where tensile stress is caused by externally applied loads

f_d = stress due to unfactored dead load at extreme fiber of section where tensile stress is caused by externally applied loads

This equation has been essentially the same since the 1963 ACI Code. The major term of this equation is $V_i M_{cr}/M_{max}$. In the original formulation by Sozen and Hawkins [43] and later used by ACI 318-63 [3] the term was $M_{cr}/(M/V) - (d/2)]$. This can be derived with reference to Figure 3.3. Section B-B represents the section to be considered and has a shear and moment of V and M. The shear crack is assumed to have a horizontal projection equal to d. The occurrence of a flexure crack at d/2 towards the support from

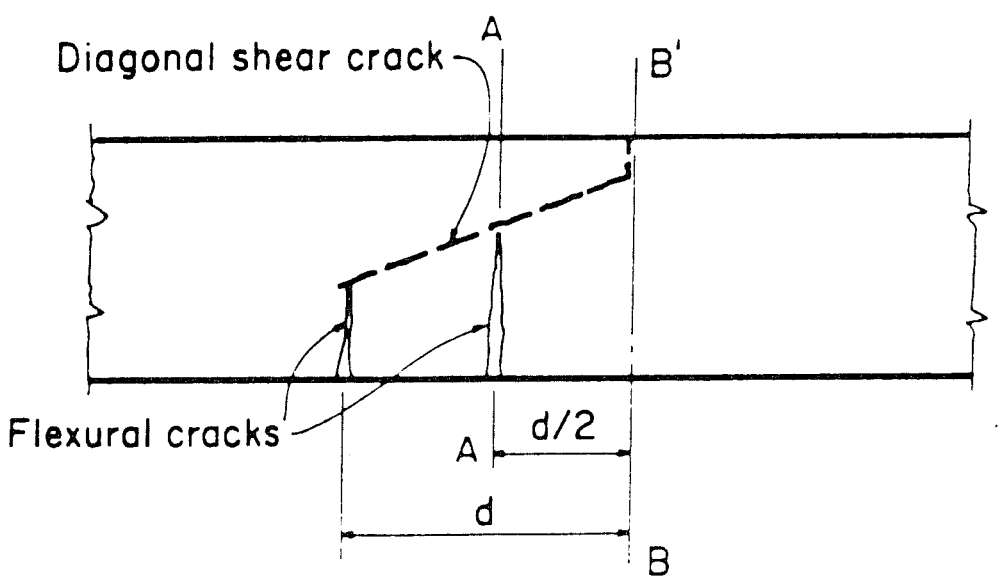

Fig. 3.3 Model used in derivation of Eq. (3.8) [Ref. 6].

B-B was taken as a sign of impending inclined cracking. Assuming that the moment at A-A is M_{cr} and the difference in shear at A-A and B-B is small one gets M-M_{cr}=Vd/2 which can be rearranged to the form used. This was changed in the 1971 ACI Code by the removal of the d/2 term. This effectively causes one to compute the flexural cracking load at the point of interest rather than d/2 back towards the support. The dead load shear, V_d was considered separately for two reasons [6]:

1. Dead load is usually uniformly distributed, whereas live load can have any distribution.
2. The dead load effect is always computed for the prestressed section alone. The live load effect is computed for the composite section in composite construction.

The $0.6\sqrt{f'_c}b_w d$ term was added to account for the added shear needed to cause the inclined crack. Figure 3.4 shows the data originally used to derive this equation. The lower limit of $1.7\sqrt{f'_c}b_w d$ was added since the only points falling below this had extremely low prestress forces.

The final equation for V_c estimates the web shear cracking, V_{cw},

$$V_{cw} = (3.5\sqrt{f'_c} + 0.3f_{pc})b_w d + V_p \tag{3.10}$$

where

f_{pc} = compressive stress in concrete (after allowance for all prestress losses) at centroid of cross- section resisting externally applied loads or at junction of web and flange when the centroid lies within the flange. (In a composite member, f_{pc} is resultant compressive stress at centroid of composite section, or web and flange when the centroid lies within the flange, due to both prestress and moments resisted by precast member acting alone.

V_p = vertical component of effective prestress force at section

The equation was first used in the 1963 ACI Code. It can be derived based on the assumption that web shear equals the tensile strength of the concrete. The maximum principal tensile stress generally occurs near the centroid of the cross-section. The capacity is

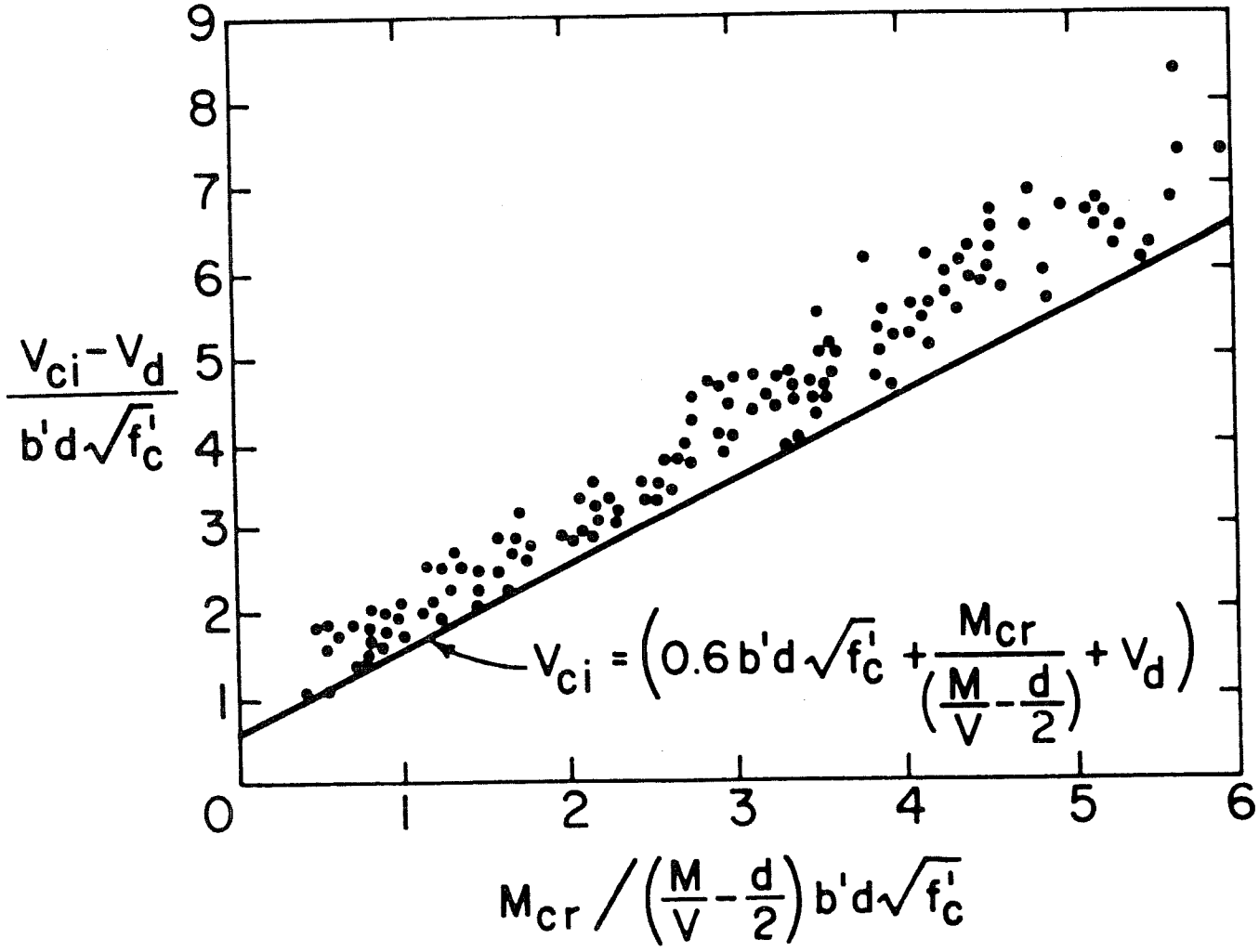

Fig. 3.4 Data points used in calibration of Eq. (3.8) [Ref. 6].

$$f_t = [v_{cw}^2 + (f_{pc}/2)^2]^{0.5} - f_{pc}/2 \tag{3.11}$$

where

f_t = tensile strength of concrete

v_{cw} = shear stress

By rearrangement this becomes

$$v_c = f_t[1 + (f_{pc}/f_t)]^{0.5} \tag{3.12}$$

The tensile stress was set so $f_t = 3.5\sqrt{f_c'}$ which yields

$$V_{cw} = 3.5\sqrt{f_c'}[1 + (f_{pc}/(3.5\sqrt{f_c'}))]^{0.5} b_w d \tag{3.13}$$

This equation was simplified to the Code equation (Fig 3.5). The V_p term was added to account for shear balanced by the prestress force.

3.3 Plasticity Theories

3.3.1 Introduction. The theory of plasticity provides a mathematical basis for collapse load calculations. While the mathematical proofs are beyond the scope of this work and indeed would prove to be of little help, several basic concepts provide background for the work done using the theory of plasticity [28,33,48]. The yield condition for a material is a central concept. It is a mathematical description of which stresses are allowable. Given a set of generalized stresses, Q_1, Q_2, ... Q_n the yield condition is defined as $f(Q_1, Q_2 \ldots Q_n) = 0$. The yield condition can be visualized as a surface in n-dimensional space. If f¡0, the point determined by the generalized stresses lies within the surface and does not give yielding. If f=0, the point lies on the yield surface and hence yielding occurs. The condition f>0 implies a point outside the yield surface which corresponds to stresses that cannot occur. The flow law is a second major concept in plasticity. The flow law is defined as

$$Q_1 = f/\lambda Q_1 \qquad (i = 1,2,...n) \tag{3.14}$$

where

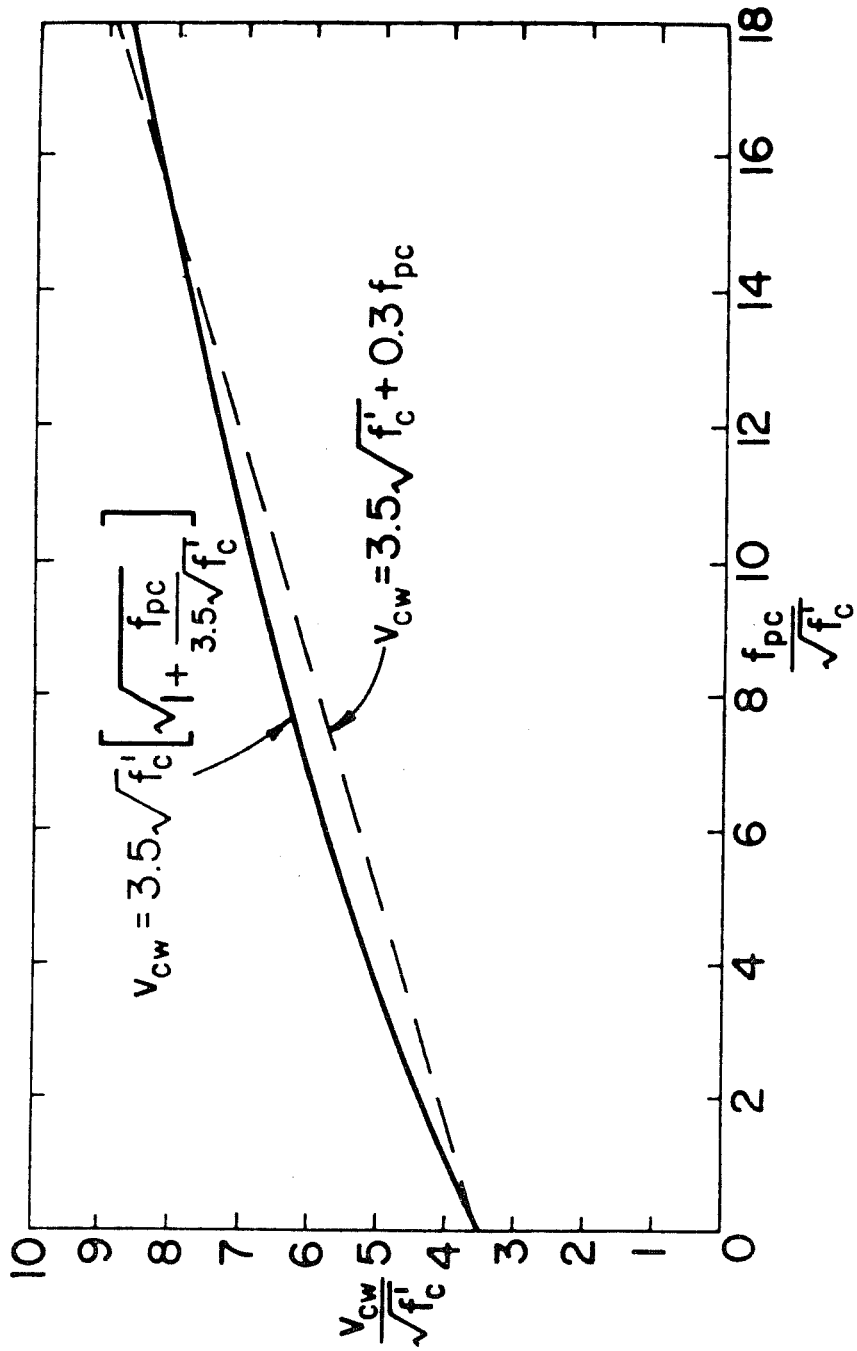

Fig. 3.5 Comparison of derived and approximate formulas for Eq. (3.10) [Ref. 6].

q_i = the generalized strain corresponding to Q_i

λ = a nonnegative number

The flow law governs the plastic strain changes at constant stress.

Starting from the yield condition and flow rules it is possible to derive the theorems of limit analysis. The lower bound theorem states: "A load system based on a statically admissible stress field which does not violate the yield condition is a lower bound on the ultimate load [48]." "A statically admissible stress distribution is a distribution which satisfies the equilibrium equations and the statistical boundary conditions [33]." This essentially says that any assumed internal distribution of stresses which does not exceed yield at any point gives a load carrying capacity less than or equal to the actual capacity. Use of the lower bound theorem will in all cases be conservative. The upper bound theorem states: "A load system which is in equilibrium with a kinematically admissible velocity field (i.e. a mechanism) is an upper bound of the ultimate load [48]." A kinematically admissible velocity field is a displacement field compatible with the geometrical boundary conditions. A mechanism satisfying the upper bound theorem gives a load equal to or greater than the actual capacity and is therefore unconservative. The theory of plasticity also states that there is a unique and exact solution such that both the upper and lower bound theorems are satisfied.

The solution procedures are different for the two limit theorems. Solution for a lower bound is accomplished by use of the equations of equilibrium. Upper bound solutions are derived by equating the external work done to the internal dissipation for the assumed mechanism.

While the framework for plastic analysis is in place, the quality of the results is extremely dependent upon the quality of the constitutive equations. The constitutive model defines the yield condition which determines failure of the plastic model. In Figure 3.6 it can be seen that steel can be reasonably well modelled as either elastic-plastic or rigid-plastic. Concrete on the other hand does not show plastic tendencies (Fig. 3.7). The way constitutive equations are handled by the various plastic models will be discussed for each model.

3.3.2 Danish model. Nielsen and his co-workers at the Technical University of Denmark have been among the leaders in applying the theory of plasticity to shear problems [32,33,34]. A number of assumptions were made in the derivation of the plastic models. Most important are the ones dealing with the constitutive models for concrete

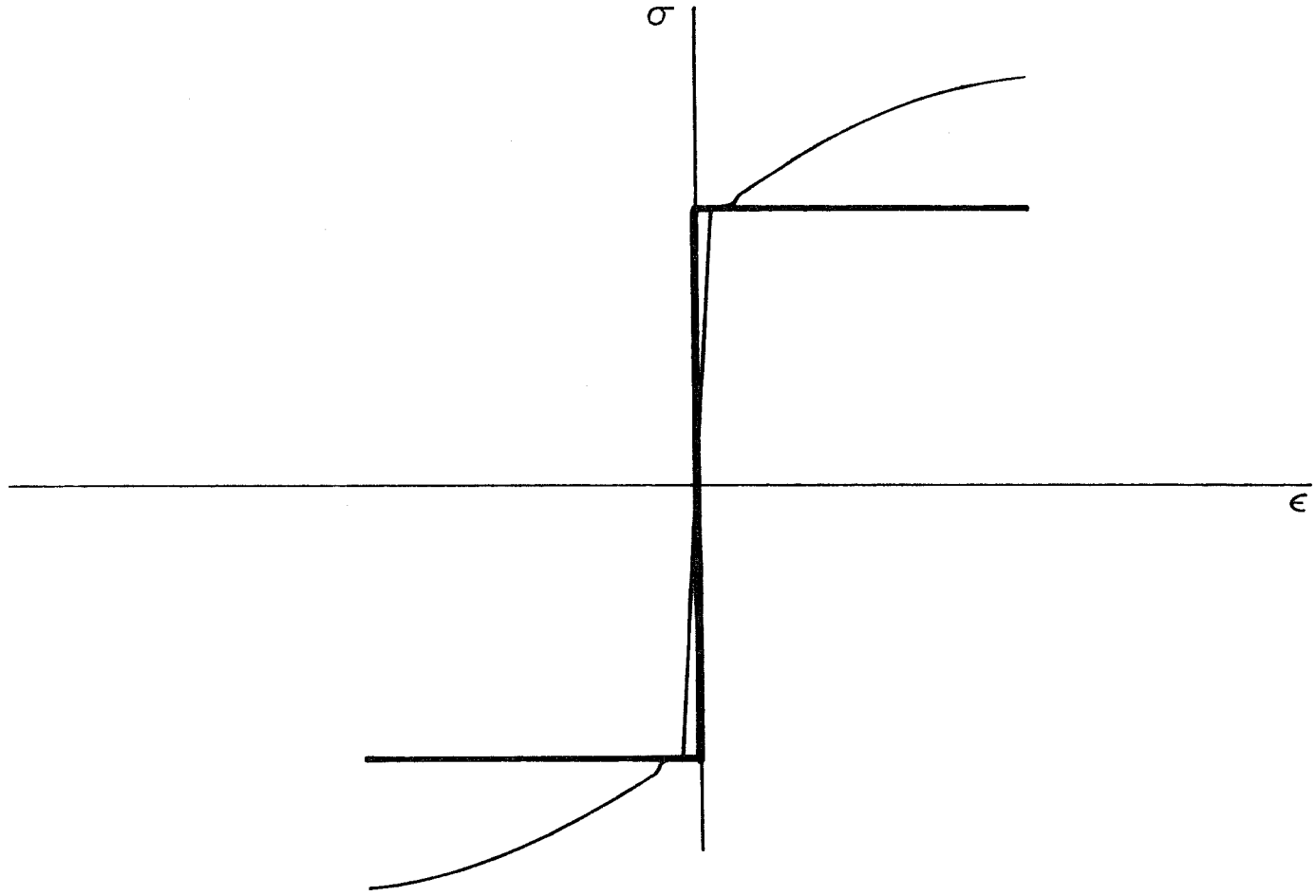

Fig. 3.6 Comparison of rigid-plastic model to steel stress-strain curve.

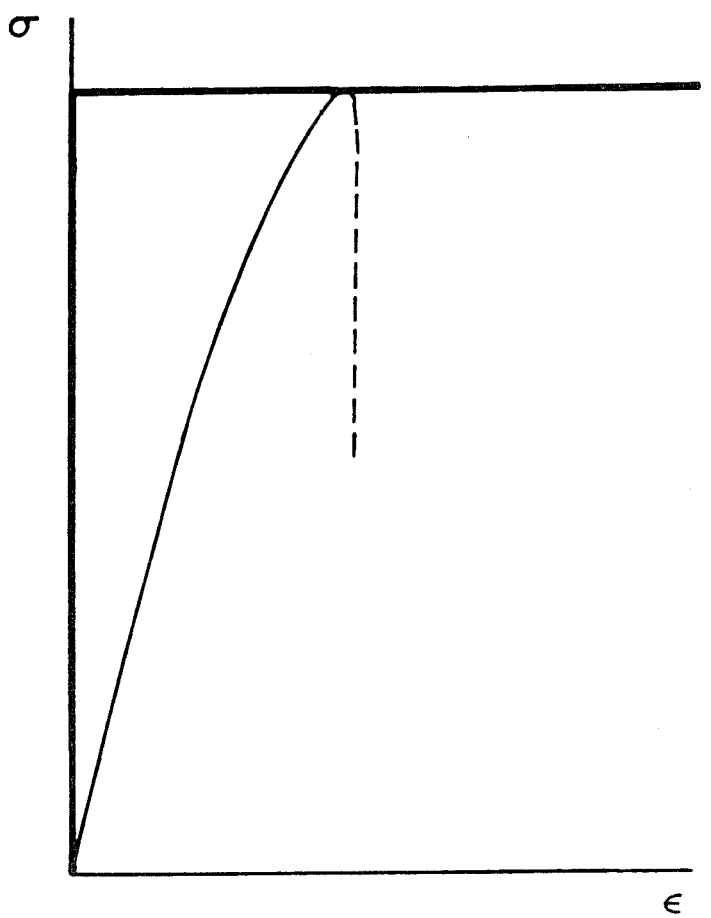

Fig. 3.7 Comparison of rigid-plastic model to high strength concrete stress-strain curve.

and steel. Nielsen chose to use a rigid-plastic model for the concrete based on the modified Coulomb failure criteria. Since the beam is assumed to be in plane stress the model gives a square yield locus with a compressive yield stress of f_c and zero tensile capacity (Fig. 3.8). A value for compressive yield less than uniaxial compressive strength must be used to obtain good results. The reinforcement is also assumed to be rigid-plastic and capable only of axial tension or compression (Fig. 3.9). Beyond material assumptions several modelling constraints are applied. The members considered are horizontal and of constant depth and have a web of constant thickness. The compression zone is idealized as a stringer carrying compressive force C and the tensile zone is modelled as a stringer carrying tensile force F. Both stringers are considered rigid-plastic and are assumed not to yield. Finally stirrups are to be spaced close enough to allow use of an equivalent stirrup stress.

The solution process involves both the upper and lower bound theorems. The cases treated to date include simply supported beams with vertical and/or inclined shear reinforcement for concentrated and distributed loads as well as beams without shear reinforcement subject to concentrated and distributed loads. Based on the assumptions above, especially that the stringers are not yielding, the best estimate for capacity comes from assuming both the web concrete and shear reinforcement to be at yield. With this it is straightforward to solve the equilibrium equations for a lower bound solution. The assumed failure mechanism for the upper bound solution is one of displacement rather than rotation. The case of a beam with shear reinforcement and two concentrated loads illustrates the mechanism (Fig. 3.10). Inclined cracks are assumed at an angle θ. Region I is assumed to displace vertically with respect to regions II. Equating the internal and external work gives the upper bound solution.

Based on their work with plasticity Nielsen et al. proposed the following design rules based on the lower bound theorem. The first step is to divide the beam into design zones. Each design zone is κh long where $\kappa = cot\theta$. A constant shear value, τ', is determined for each design zone (Fig. 3.11). The transverse reinforcement is determined by

$$A_v = \frac{V_d s}{f_y h \kappa} \tag{3.15}$$

where

$V_d =$ design shear

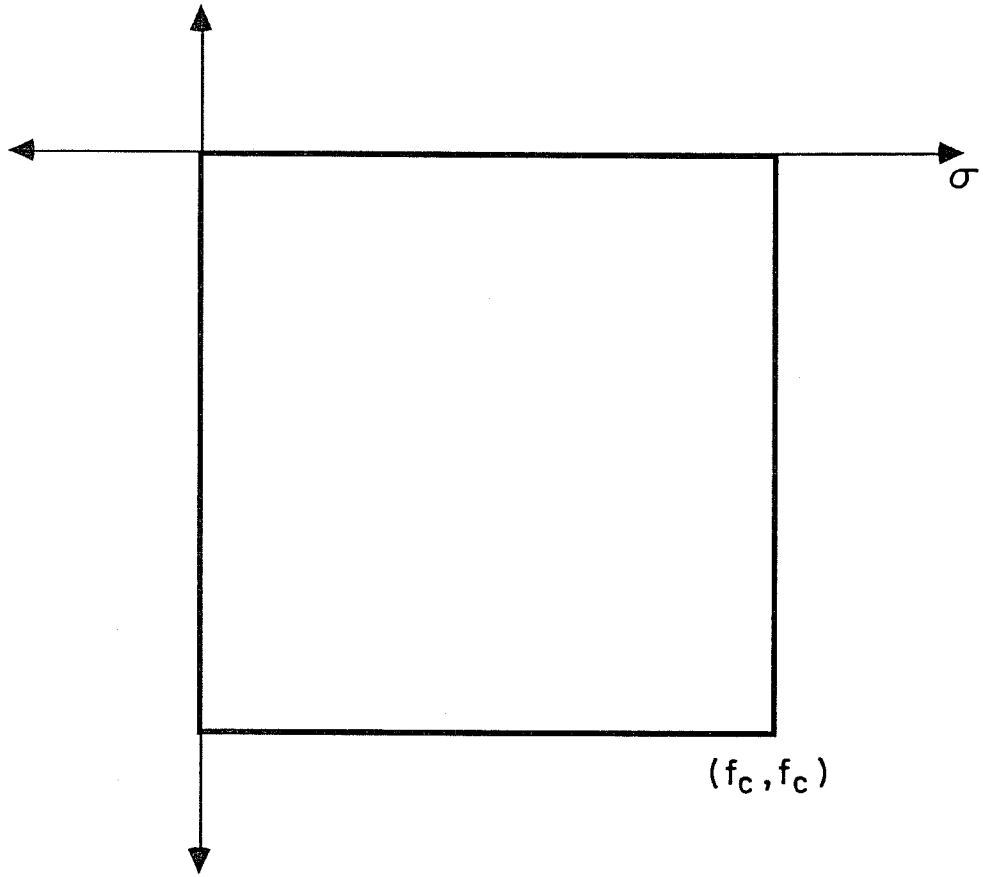

Fig. 3.8 Concrete yield locus.

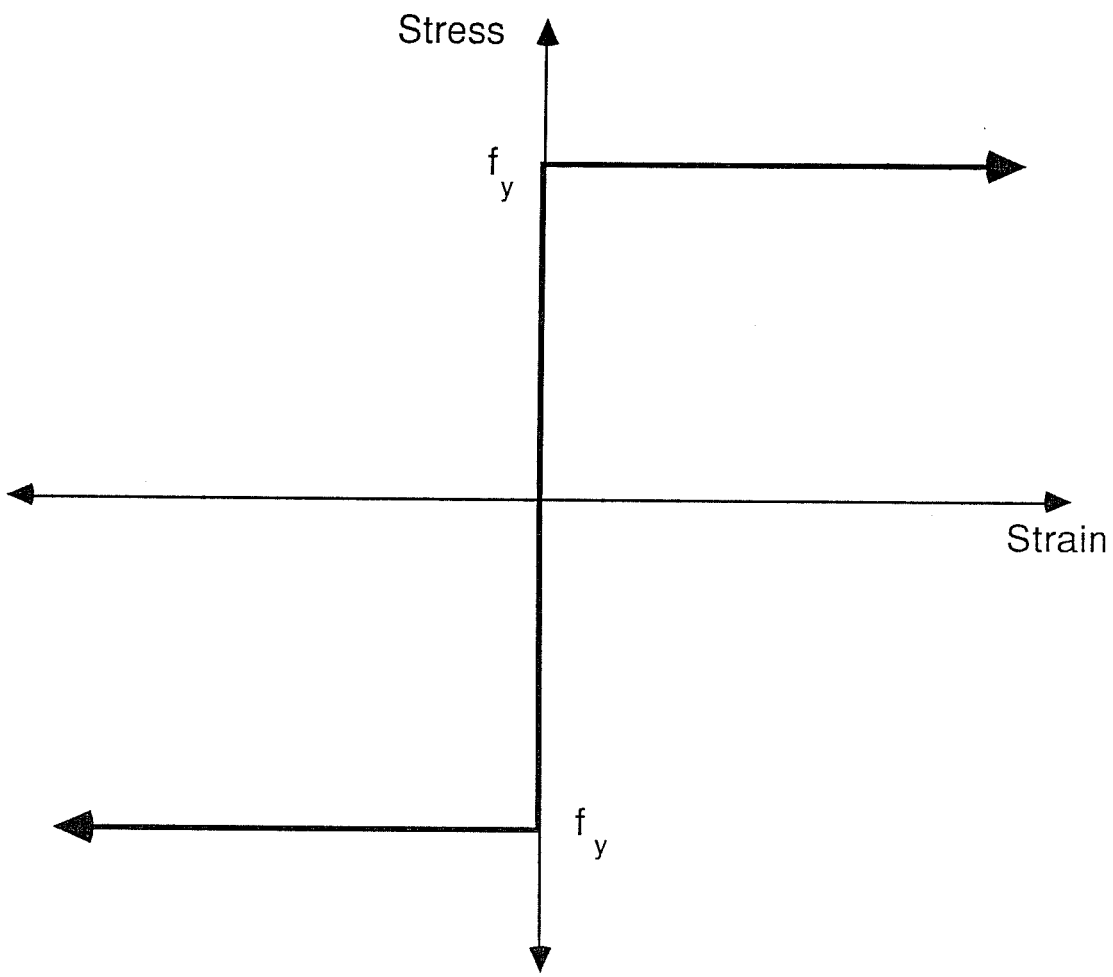

Fig. 3.9 Rigid-plastic model for steel.

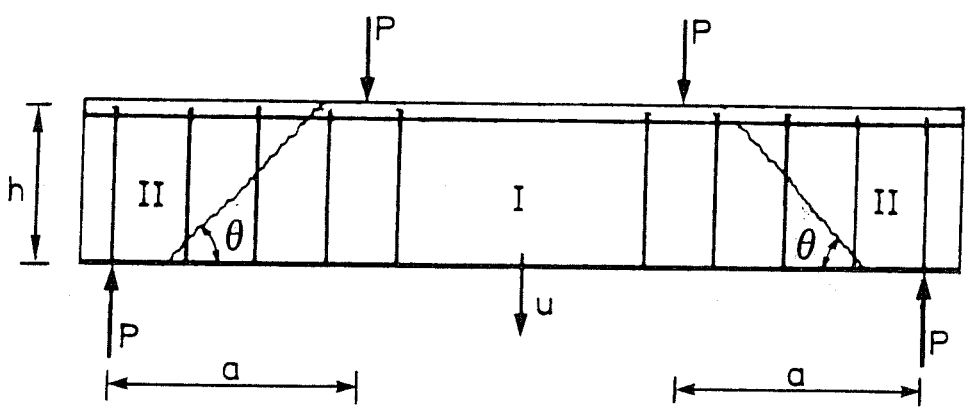

Fig. 3.10 Assumed failure mechanism for Danish model [Ref. 32].

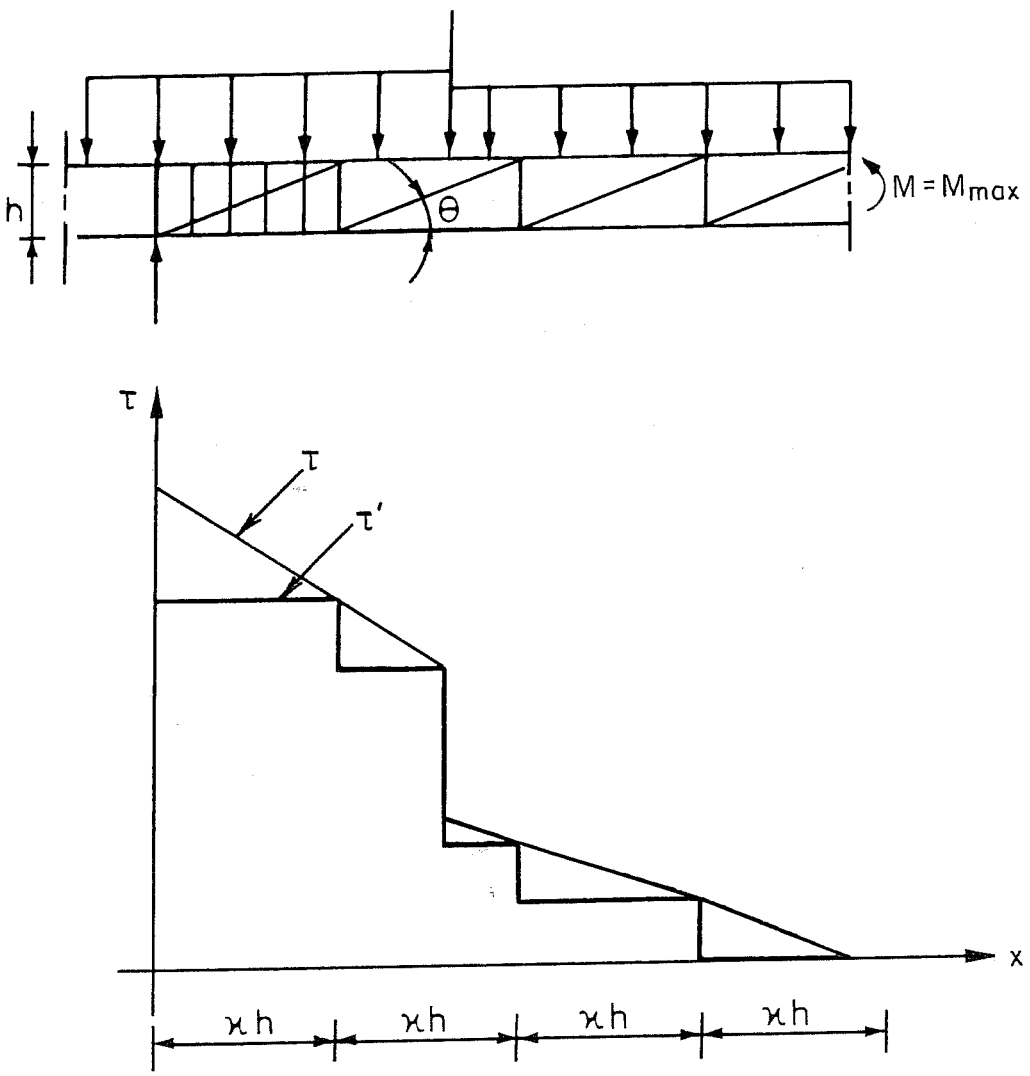

Fig. 3.11 Shear design zones using the Danish model [Ref. 32].

h = distance between stringers

s = stirrup spacing

f_y = shear reinforcement yield stress

A check on concrete stress is also required

$$f_d = (V/bh)(\kappa + 1/\kappa) \leq \nu f'_c \tag{3.16}$$

where f_d is the concrete stress in the diagonal compression field. The longitudinal reinforcement must meet two conditions. The tension chord must carry at least

$$A_s f_y = M/h + V\kappa/2 \tag{3.17}$$

at every section and at the support

$$T_o = \kappa R/2 \tag{3.18}$$

where

R = reaction

T_o = tension chord requirement.

Limits are placed on the value of κ to prevent too large a deviation from elastic behavior. For beams with constant longitudinal reinforcement: $1 \leq \kappa \leq 2.5$ or $21.8° \leq \theta \leq 45°$. For beams with curtailed reinforcement: $1 \leq \kappa \leq 2.0$ giving $26.5° \leq \theta \leq 45°$. The tighter limit for beams with curtailed reinforcement is an attempt to prevent stirrups from yielding at service load.

The recommended concrete effectiveness factor is

$$\nu = 0.7 - (f'_c/29000) \qquad (f'_c \textit{ in psi}) \tag{3.19}$$

The equation was limited to concrete strengths less than 8700 psi.

3.3.3 Swiss Model. Thurlimann and his co-workers at the Swiss Federal Institute of Technology have also been leaders in the work with plasticity based models [26,46,47,48]. Thurlimann used a somewhat different set of assumptions than Nielsen. The

predominant difference is that Thurlimann assumed both the web and the longitudinal reinforcement yields. This allows formation of a mechanism without having the concrete reach yield. Rigid-plastic material behavior is assumed as well as only axial resistance from reinforcement. For the concrete a square yield criterion with no tensile strength is assumed. Additionally an upper limit is set on the concrete to prevent a premature failure. Also a limit is placed on the inclination of the concrete compression field, α, and thereby on the amount of redistribution of internal forces. The flow rule or failure mechanism is uniaxial yielding of the reinforcement opening up the final cracks perpendicular to the crack direction. Finally the reinforcement is assumed to be properly detailed so that no local failures are possible.

Thurlimann and his co-workers solved both the upper and lower bound solutions for a beam subjected to shear based on the above assumptions. The lower bound solution can be obtained given the shear web element of Figure 3.12. The diagonal force D:

$$D = V/sin\alpha \tag{3.20}$$

The concrete compressive stress f_d:

$$f_d = D/(bh\ cos\alpha) = V/(b\ h\ sin\alpha\ cos\alpha) \tag{3.21}$$

The stringer forces:

$$upper\ stringer\ =\ -M/h + (V/2)cot\alpha \tag{3.22}$$

$$lower\ stringer\ =\ M/h + (V/2)cot\alpha \tag{3.23}$$

The stirrup forces are:

$$s = V(b/h)tan\alpha \tag{3.24}$$

The assumed failure comes from yielding of the stirrups and the lower stringer. Setting the applied shear and moment equal to their ultimate values, V_p and M_p, the following relationships can be derived.

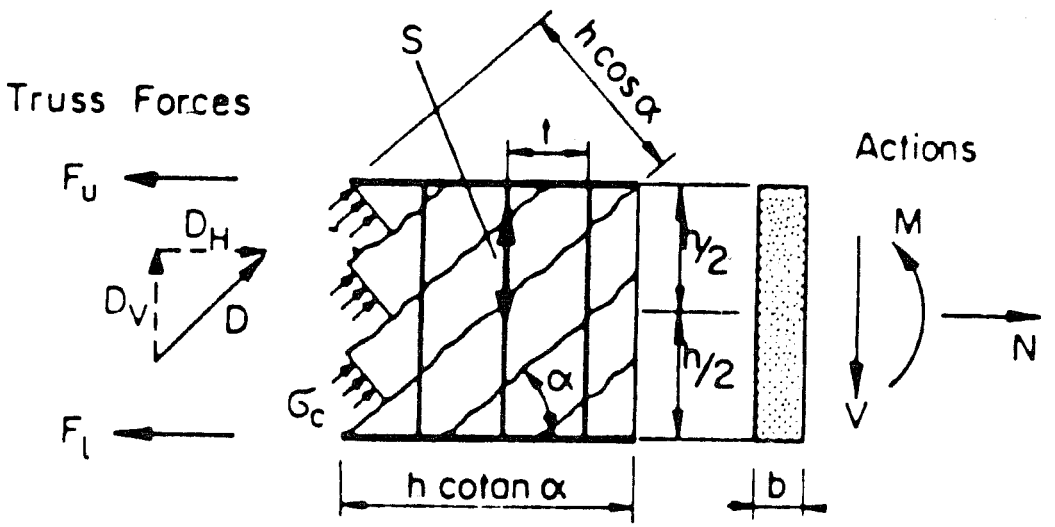

Fig. 3.12 Shear web element [Ref. 47].

$$F_{y1} = M_p/h + (1/2)V_p^2 t/s_y h \tag{3.25}$$

$$M_{po} = f_{y1} h \quad for\ V_p = 0 \tag{3.26}$$

$$V_{po} = 2F_{y1} s_y (h/t) \quad for\ M_p = 0 \tag{3.27}$$

This gives the interaction formula

$$\frac{M_p}{M_{po}} + \frac{V_p^2}{V_{po}^2} = 1 \tag{3.28}$$

The kinematic or upper bound solution is based on Figure 3.13. The solution of the work equations gives the same results as the lower bound solution. Thus the results are unique. Several additional considerations arise from the upper bound solution. The mean crack strain ϵ_R is defined in Figure 3.14. It is related to the reinforcement strains as follows:

yielding of longitudinal reinforcement $\epsilon_1 = \epsilon_y$

$$\epsilon_R = \epsilon_y (1 + cot^2 \alpha) \tag{3.29}$$

yielding of web reinforcement $\epsilon_s = \epsilon_y$

$$\epsilon_R = \epsilon_y (1 + tan^2 \alpha) \tag{3.30}$$

Figure 3.15 shows the ratio of ϵ_R/ϵ_y for the web and longitudinal reinforcement as α changes. It can be noted that as α moves away from 45° one of the strains increases very rapidly. A large increase in ϵ_R indicates that the cracks are opening very wide. If cracks open too wide, aggregate interlock deteriorates destroying the members redistribution capabilities.

Several practical limitations become obvious from the moment-shear interaction equation and the crack width versus yield strain diagram. Thurlimann noted that at ϵ_R/ϵ_y values of about 5 the failure mechanisms begin to change. Either shear or flexural failures become possible without both of the reinforcements yielding. To get failures consistent with those assumed, limits were placed on the range of α:

$$0.5 \leq tan\alpha \leq 2.0 \tag{3.31}$$

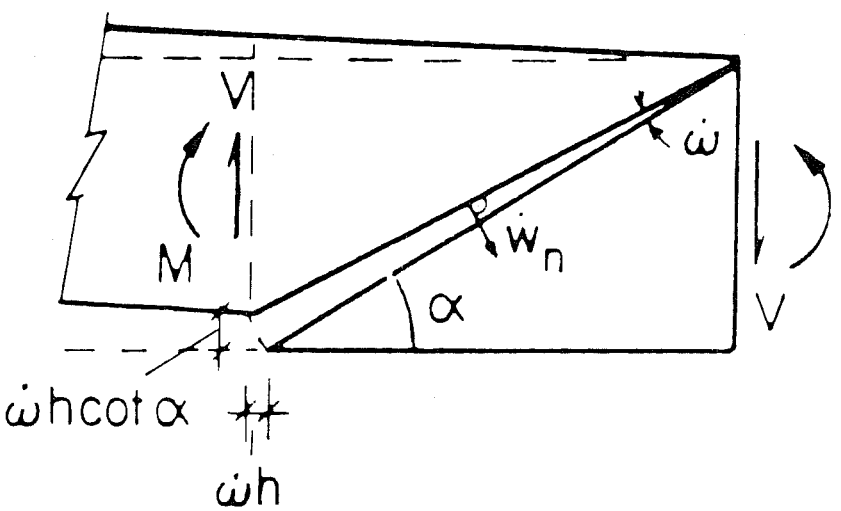

Fig. 3.13 Assumed failure mechanism for the Swiss model [Ref. 46].

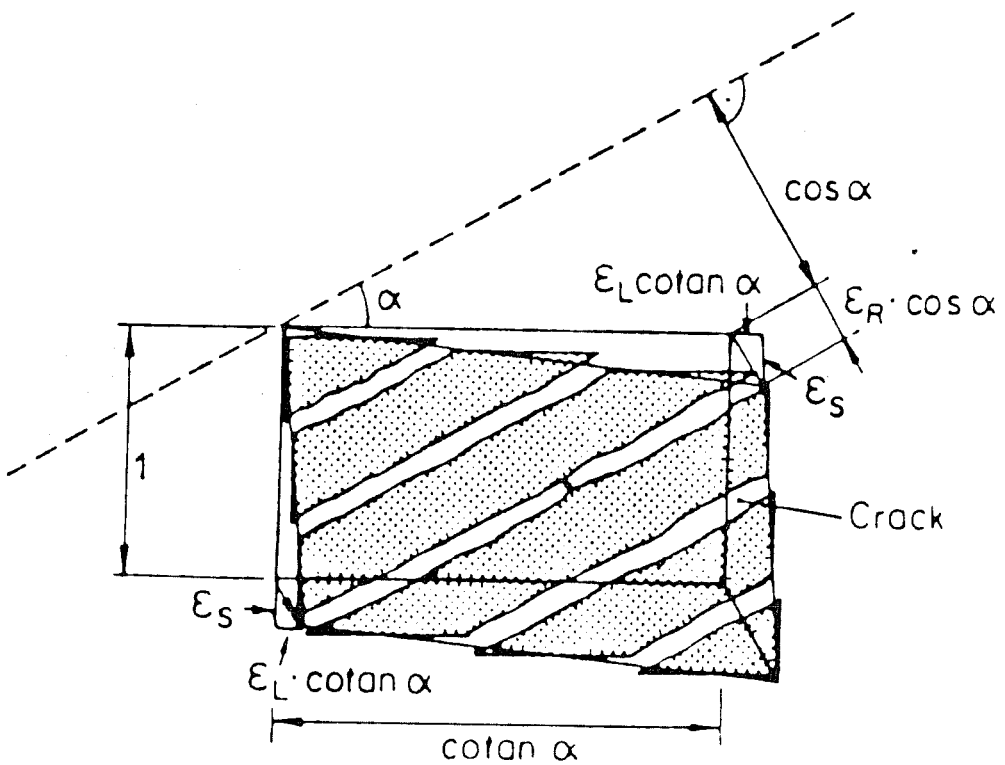

Fig. 3.14 Mean crack strain ϵ_R [Ref. 47].

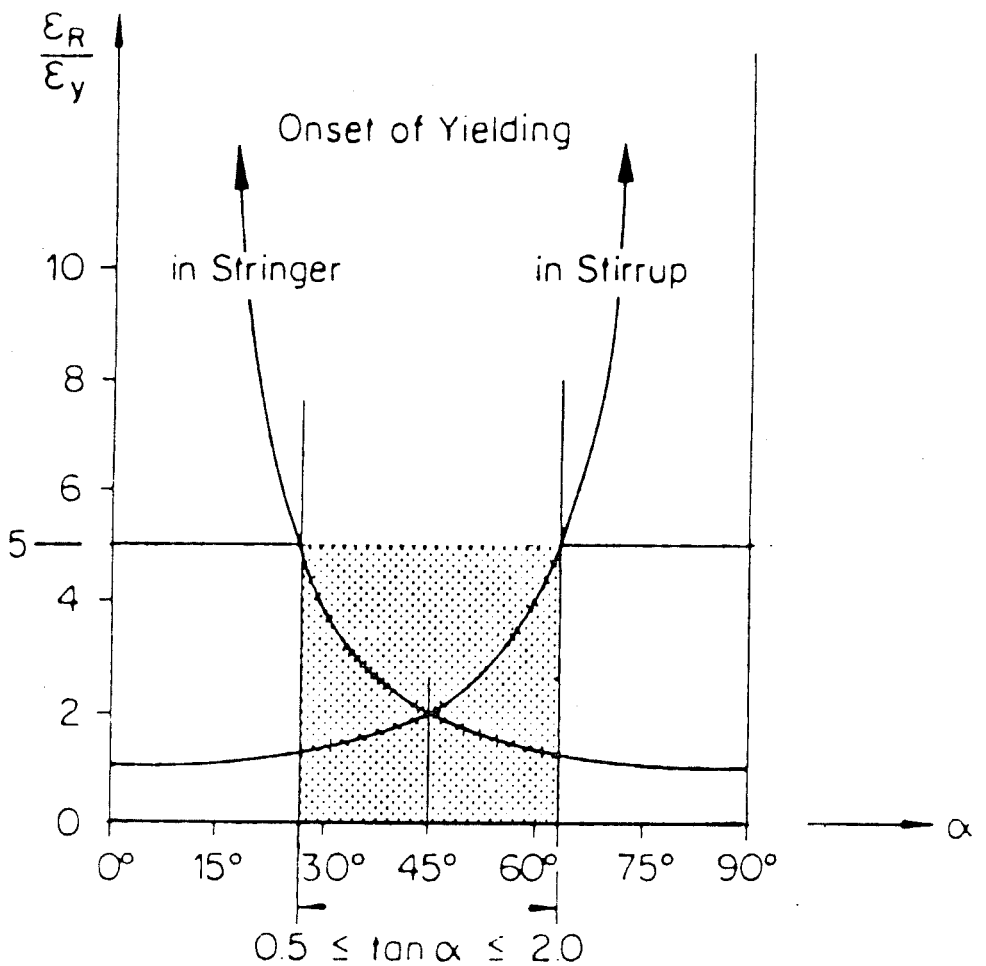

Fig. 3.15 Change in mean crack strain with change in α [Ref. 47].

$$26.5° \leq \alpha \leq 63.5° \tag{3.32}$$

The values are not exact limits but give a general range for transitions of failure mechanisms. Within this range a combined mechanism of both reinforcements yielding occurs. Outside this range either shear or flexure controls.

In addition to the limit placed on the angle α there is a material limit as well. The limit is based on crushing of the concrete. The relationship is:

$$(V_{pc}/V_{po}) = (V_{fc}h/M_{po}) * [1 - (P_{sc}/f_{cd}] \tag{3.33}$$

where

$$\mathrm{V}_{fc} = (/1/2)f_c dh \tag{3.34}$$

P_{sc} = shear flow producing failure

$$= \tau d = f_{cd}(P_y/f_{cd}) * 1 - [(P_y/f_{cd})] \tag{3.35}$$

The crushing of the concrete represents a different failure mechanism not requiring the longitudinal reinforcement to yield. The limits on α are to insure that a combined mechanism of failure will occur.

The 1978 CEB Model Code included this model as the Refined Method [18]. The major change from the model mentioned is that α has the following limits

$$3/5 \leq tan\alpha \leq 5/3 \tag{3.36}$$

$$31° \leq \alpha \leq 59° \tag{3.37}$$

A check on web crushing is required

$$V_u \leq 0.30 f_{cd} b_w d sin2\alpha \tag{3.38}$$

where

b_w = web width

d = effective depth

f_{cd} = design concrete stress = f'_c/ϕ

The general design is controlled by

$$V_u \leq V_r = V_{tr} + V_c \tag{3.39}$$

where

V_u = design load

V_r = factored resistance

V_{tr} = truss contribution

V_c = concrete contribution

The truss contribution is given by

$$V_{tr} = (A_{sw}/s) \bullet 0.9 d f_{ywd} (cot\alpha + cot\theta) sin\alpha \tag{3.40}$$

where

A_{sw} = web reinforcement

f_{ywd} = yield stress of web reinforcement divided by a safety factor

d = effective depth of beam

s = stirrup spacing

α = angle of compression diagonals

θ = angle of stirrups to the horizontal

There are three ranges for the concrete contribution. The first region is called uncracked

$$V_u \leq 2.5 \tau_{RD} b_w d \qquad V_c = 2.5 \tau_{RD} b_w d \tag{3.41}$$

where

$$\tau_{RD} = .24 f_{ctd} \tag{3.42}$$

f_{ctd} = design concrete tensile strength

= tensile strength divided by resistance safety factor

The next region is the transition zone

$$2.5\tau_{RD} b_w d < V_u < 7.5\tau_{RD} b_w d \qquad V_c = (1/2)(7.5\tau_{RD} b_w d - V_u) \tag{3.43}$$

The last region is the full truss zone:

$$V_u \geq 7.5\tau_{RD} b_w d \qquad V_c = 0 \tag{3.44}$$

Finally there is a provision to increase the longitudinal reinforcement over the value required for flexure by the amount

$$\Delta F_{t1} = \frac{V_{sd}^2 S}{2\ A_{sw}\ f_{ywd}\ d\ sin\alpha} - V_{sd} cot\alpha \tag{3.45}$$

where

V_{sd} = design shear force

ΔF_{t1} = design stress of longitudinal reinforcement

3.3.4 Diagonal compression field theory. Diagonal compression field theory has its origin in plasticity models such as that of Thurlimann [15,16,17]. Collins and his co-workers, however, diverged from strict application of the theory of plasticity. The major assumption is that concrete can carry no tension and that the shear will be carried by a diagonal compression field. At this level all three plasticity models are the same. Rather than formally following the limit analysis theorems of plasticity, Collins et al. chose to develop a procedure where equilibrium and compatibility are satisfied at all load stages rather than just at ultimate. The procedure is analogous to a moment-curvature analysis for flexure.

Diagonal compression field theory requires that appropriate relations for stresses, strains, and constitutive equations be determined. For this work the stresses are assumed to act over an effective area defined by $b_w jd$ where b_w is web width and jd is the effective depth for shear. The model requires the presence of stirrups. From

equilibrium considerations three generalized stresses are derived σ_t, average transverse compressive stress, σ_t average longitudinal compressive stress, and f_d average principle compressive stress. Each of these average stresses can be written in terms of an average shear stress, v, and the angle of inclination of f_d to the horizontal, α where

$$v = V/(b_w jd) \tag{3.46}$$

and V = total applied shear

The average strains are considered in a similar manner. The compatibility condition can be stated as

$$tan^2\alpha = \frac{\epsilon_d + \epsilon_1}{\epsilon_d + \epsilon_t} \tag{3.47}$$

where

ϵ_l = average value of longitudinal tensile strain

ϵ_t = average value of transverse tensile strain

ϵ_d = average value of principal compressive strain

For the diagonal compression field to work, the average stress must be tied to the average strain through constitutive equations. For steel the average stress-average strain relationships can be pictured as elastic-plastic. The use of elastic-plastic relationships are required if compatibility is considered since rigid-plastic materials only deform at yield. The concrete constitutive equations are, as always, more subject to uncertainty. Several suggestions have been made as to the proper model for this use. Reference [17] had two relationships given for an average concrete modulus. The recommended one was simply a straight line function whose value was the crushing strength of concrete divided by the strain at peak stress. In the same paper the limit on concrete stress was determined as a function of the diameter of the Mohr's circles for stress and strain at ultimate. It was felt that size of the stress circle that causes failure is related to the size of the coexisting strain circle. Reference [16] carried the upper limit out to the following simple expression

$$f_{du} = \frac{5.5f'_c}{4 + \lambda_m/\epsilon_d} \tag{3.48}$$

where

$$\lambda_m = 2\epsilon_d + \epsilon_l + \epsilon_r \tag{3.49}$$

f_{du} = limiting concrete stress

ϵ_d = 0.002 assumed

More recently the following constitutive equations were proposed [49].

$$f_{c2} = f_{c2max}[2(\epsilon_2/\epsilon_o - \epsilon_2/\epsilon_o)^2] \tag{3.50}$$

where

$$\frac{f_{c2max}}{f'_c} = \frac{1}{0.8 - 0.34(\epsilon_1/\epsilon_o)} \leq 1.0 \tag{3.51}$$

f_{c2} = principle compressive stress in concrete

ϵ_2 = principle compressive strain in concrete

ϵ_1 = principle tensile strain in concrete

ϵ_o = strain at peak concrete stress

That equation also had provisions for considering tensile strength of concrete. The accuracy of the concrete constitutive model effects the capabilities of diagonal compression field theory.

Given the preceding relationships it is possible to determine full behavior of members subject to shear. Collins considered three phases of behavior. The first is prior to steel yielding. Compression field theory can predict the angle of the initial cracks. The next stage of behavior had the transverse steel yielding. This is followed by a change in α up to the ultimate load. Compression field theory allows failure to be caused by either yielding of the longitudinal reinforcement or by crushing of the web. It is possible to track through beam behavior from zero load to ultimate and to determine the failure mechanism all using compression field theory.

Compression field theory formed the basis of the General Method in the 1984 Canadian Code [21]. That Code is set up so that a design is acceptable if it satisfies a series of Code provisions. The angle of the diagonal compression strut, θ, can be chosen as any value between 15° and 75°. To prevent premature diagonal crushing

$$f_2 < f_{2max} \tag{3.52}$$

where

$$\mathrm{f_2} = tan\theta + (1/tan\theta)](V_f/b_v d_v) \tag{3.53}$$

$$\mathrm{f_{2max}} = \lambda\phi_c f'_c/(0.8 + 170\epsilon_1) \leq \lambda\phi_v f'_c \tag{3.54}$$

unless concrete is triaxially confined

$$\epsilon_1 = \epsilon_x + 0.002)/tan^2\theta \tag{3.55}$$

$\mathrm{V_f}$ = factored shear force at section

$\mathrm{b_v}$ = minimum effective web width within depth $\mathrm{d_v}$

$\mathrm{d_v}$ = effective shear depth, which can be taken as the distance, measured perpendicular to the neutral axis, between the resultants of the tensile and compressive forces due to flexure but need not be taken less than 0.9 d.

λ = factor to account for low density concrete

ϕ_c = resistance factor for concrete

In Equation (3.55) ϵ_x may be taken as 0.002 or calculated from a plane section analysis under factored loads. If

$$V_f \leq 12.04\ \lambda\phi_c\ \sqrt{f'_c} b_w d \tag{3.56}$$

$\mathrm{b_w}$ may be used for $\mathrm{b_v}$.

To insure yielding of the transverse reinforcement

$$\epsilon_t > f_y/E_s \tag{3.57}$$

where $\epsilon_t = \epsilon_1 - \epsilon_x - 0.002$ (3.58)

The transverse reinforcement is designed so that

$$V_R \geq V_f \tag{3.59}$$

where

$$\mathrm{V}_r = (\phi_s A_v f_y/s)(d_v/tan\theta) = \phi_p V_p \tag{3.60}$$

A_v = area of shear reinforcement perpendicular to the axis of a member within a distance, s

f_y = specified yield stress of nonprestressed reinforcement

s = spacing of shear reinforcement measured parallel to the longitudinal axis of the member

ϕ_s = resistance factor for reinforcement

ϕ_p = resistance factor for prestressing tendons

V_p = component in the direction of the applied shear of the effective prestressing force.

An additional amount of longitudinal reinforcement over that needed for flexure alone is required at a section. The added tensile load, N_v, is

$$N_v = V_f/tan\theta \tag{3.61}$$

The Canadian Code has two added sections in the General Method. The first is for handling problems near geometric discontinuities or concentrated loads. The procedure calls for the use of concrete struts and tension ties joined at nodal regions. Provisions are given for allowable stresses. This type of model will be discussed further in Section 3.4.2 The second added provision is one on serviceability. This is included to ensure reasonably small crack widths at service loads.

3.4 Truss Models

3.4.1 Ramirez. In recent work done at the University of Texas Ramirez and Breen proposed a design procedure based on the truss model. The work was based on the plasticity models previously discussed but principally on the work of Thurlimann. In Ramirez's work the emphasis was shifted from the plasticity based proofs to the conceptual use of a truss model to show the flow of forces. The detailed work was

reported in References [38,39,40] and only a brief summary of the conceptual basis and design procedures will be given herein.

The basic assumptions for the truss model are the same as used by Thurlimann. Yielding of both the longitudinal and transverse reinforcement is required. This requires an upper limit on the diagonal concrete stresses to prevent crushing. The reinforcement can only resist axial loads. The reinforcement is properly detailed so that local crushing and bond failures are prevented.

The truss model can be used in a six step design procedure. The first step is to pick an appropriate truss system for the loading and support conditions under consideration. This basically entails dividing the beam into convenient design segments. The second step requires assuming an angle for the compression diagonal inclination, α. Acceptable values are $25° \leq \alpha \leq 65°$ and a value which fits the truss system should be chosen. The lower α values require less shear reinforcement. The next step is to check the concrete stress in the compression diagonals. This is to insure that web crushing does not occur. The web reinforcement can then be calculated. Consideration needs to be given to spacing limits and to make certain minimum reinforcement values are met. The area of longitudinal reinforcement must be calculated for the combined actions of flexure and shear. Finally, all reinforcement must be properly detailed. Since the model relies on both web and longitudinal reinforcement reaching yield, poor details resulting in premature failure would be extremely serious.

Numerical guidelines were added to the conceptual framework given above. The member's shear resistance comes from three components, the concrete contribution V_c, the truss contribution V_{tr}, and the component in the direction of applied shear of the effective prestress force V_p. The model is equally applicable to reinforced and prestressed concrete. The angle of inclination for the compression diagonals is

$$25° \leq \alpha \leq 65° \tag{3.62}$$

The compressive stress in the compression diagonals, f_d shall be less than $30\sqrt{f'_c}$ where:

$$f_d = V/(b_w z \cos\alpha \sin\alpha) \tag{3.63}$$

z = distance between stringers

The concrete contribution can be calculated as

a) reinforced concrete members

$$V_c = (1/2)[6\sqrt{f_c'} - v_u]b_w z \tag{3.64}$$

$$but \quad 0 \leq V_c \leq 2\sqrt{f_c'}b_w z$$

b) prestressed concrete members

$$V_c = (K/2)[(4+2K)\sqrt{f_c'} - v_u]b_w z \tag{3.65}$$

$$but \quad 0 \leq V_c \leq 2K\sqrt{f_c'}b_w z$$

where

$$K = [1 + (f_{ps}/2\sqrt{f_c'}^2]^{0.5} \tag{3.66}$$

but $1.0 \leq K \leq 2.0$ and K=1.0 if stress at extreme tension fiber at the section exceeds $6\sqrt{f_c'}$ due to the computed ultimate load and the applied effective prestress force.

If V_u exceeds $1\sqrt{f_c'}b_w z$ then minimum web reinforcement equal to

$$A_v = 1.0\sqrt{f_c'}[b_w s/f_y] \tag{3.67}$$

must be added. The truss contribution is given by

$$V_{tr} = [S_y z]/[tan\alpha \bullet s] \tag{3.68}$$

where

S_y = total stirrup force over spacing s

The bottom reinforcement is calculated by

$$F_{y1} = M_u/z + (V_u/2)cot\alpha \tag{3.69}$$

Additional detailing requirements as well as provisions for torsion can be found in Reference [39].

3.4.2 Strut and tie model. Schlaich et al. at the Institut fur Massivbau at Stuttgart have a more refined truss model called the strut and tie model [42]. The strut and tie model condenses all stresses into compression and tension members and joins them by nodes. The model is based on the lower bound theory of plasticity. The authors themselves describe the method as one of sufficient, not perfect, accuracy. The real aim of the strut and tie method is to determine the flow of forces in a member. Given this flow of forces, struts and ties can be sized to cover the required forces. In this way the entire structure can be designed for a consistent level of safety.

The strut and tie model defines two types of regions in a structure. The B-regions are areas where the internal state of stress can easily be derived from sectional forces such as moments, shears, and axial forces. In these regions stresses can be calculated based on section properties up to cracking. In the cracked state a normal truss model gives the desired results. The second type is the D- region. The D-regions include all areas where the strain distribution is significantly nonlinear such as at concentrated loads, corners, openings, etc. In the uncracked state such regions can be designed based on linear elastic stress analysis. In the cracked state typical current design is based on "experience" or "standard practice." The strut and tie model allows a reasonable design of such regions since the compression and tensile forces are followed throughout the region. From this it can be seen that the strut and tie model is an extension of the truss model.

The strut and tie model allows for a consistent design of the entire structure. A first step is to perform a sufficiently accurate structural analysis. Schliach et al. had several suggestions for appropriate types of analysis. The structure should also be broken up into B and D-regions. In general, D-regions extend a distance approximately equal to the effective depth of the member on either side of the discontinuity. The B-regions may be dimensioned using the results from the structural analysis and the truss model. The D- regions are where the true advantages of the strut and tie model become apparent. Using the sectional forces that occur at the edge of the D-region and any externally applied forces a flow path needs to be developed. The recommendation is to adapt "the struts and ties of the model to the direction and size of the internal forces as they would appear from the theory of elasticity." This provides for adequate serviceability as well as a conservative estimation of ultimate capacity. The loadpaths should begin and end

at the center of gravity of corresponding stress diagrams. They should take the shortest smooth route in between and have the appropriate direction at D-region boundaries. The best load path model is one which minimizes the strain energy of the steel ties.

For design use stress limits must be imposed on the concrete struts and nodal regions. The 1984 Canadian Code has some guidelines on allowable stresses in the nodes. The recommendations of Schlaich et al. will, however, be included here. The model allows for concrete struts and steel and concrete tension ties. The struts and ties are joined at nodes. It is stated

> "that a whole D-region is safe, if the pressure under the most heavily loaded bearing plate or anchor plate is less than 0.6 f_{cd} (or exceptionally 0.4 f_{cd}) and if all significant tensile forces are covered by reinforcement and further if sufficient development lengths are provided for reinforcement [42]."

The following recommendations were given for strut stresses. For current purposes f_{cd} is defined as

$$f_{cd} = .85 f'_c / \lambda_c \tag{3.70}$$

where

$\lambda_c =$ a partial safety factor

$f^*_{cd} = 1.0 f_{cd}$ for undisturbed uniaxial state of compressive stress

$0.8 f_{cd}$ if tensile strains in the cross direction or transverse tensile reinforcement may cause cracking parallel to the strut with normal crack width; this also applies to node regions where tension bars are anchored or cross

$0.6 f_{cd}$ as above for skew cracking or skew reinforcement

$0.4 f_{cd}$ for skew cracks of extraordinary crack width. This occurs if modelling deviates substantially from the theory of elasticity's flow of force.

Through necessity, concrete tensile ties are allowed. The following guidelines are given for their use. A limit is placed on their use to cases where they are used for equilibrium and where progressive collapse is not expected. This can be assumed

satisfied if in any area of the stress field a cracked failure zone can occur without the increased tensile stresses in the remaining section exceeding the tensile strength f_{ct}. The cracked failure zone A_c shall be taken as

$$A_c \geq 4d_g^2 \text{ and } \geq A_{ct}/10 \tag{3.71}$$

where

d_g = diameter of the largest aggregate

A_{ct} = area of the tensile zone

It is stated that the most important thing is to determine where tensile forces are required and to place reinforcement there if possible.

3.5 Rationality and Ease of Use

Rationality and ease of use are important factors in evaluating the qualities of different models. While these issues are somewhat subjective, certain topics deserve consideration. A rational model has a firm physical basis. The model should give a clear indication of the mechanisms and paths used to transfer loads to the supports. It should also be consistent in its treatment of internal mechanisms. For ease of use the model must give the designer clear understanding of what is required. In addition, the parameters used should be simple and easily defined physical properties.

The models discussed have various levels of rationality. The AASHTO/ACI equations are more empirical relationships than rational models. The steel contribution does have a solid physical basis, but the current design philosophy hides even that. The concrete contributions are empirical relationships containing various numbers of pertinent parameters. Together they provide a reasonably accurate, and conservative model, but they do not indicate member behavior or how forces are transferred to supports. The method does not treat internal mechanisms consistently. The current method is not very rational. The two strict plasticity models provide a rational picture of member behavior. Both the Danish and the Swiss models use the limit theorems to obtain exact solutions for the original assumptions made. The Danish model with its assumption of concrete crushing is, however, quite restricted in application. Only a few exact solutions have been obtained. The design procedure basically uses the conservative lower bound theorem. The Swiss Model with its assumption of longitudinal and transverse reinforcement yielding is more general. The model can consistently handle a wide range

of problems. The models also give a clear picture of the mechanisms at work. Both models are consistent, rational methods although certain practical limitations must be added to insure compliance with the original assumptions. Compression field theory in its pure form is a rational method. It uses equilibrium and compatibility tied together by generalized constitutive equations. The model can give a good picture of member behavior throughout the full range of behavior. Load paths and shear transfer mechanisms are subordinate to the mathematical treatment but still provide insight into member behavior. In its Code format, however, compression field theory has been reduced to a series of fairly complicated equations. Their basis is still rational, but the basis and any physical insight gained from that has been covered over. The truss model provides a design procedure that uses the physical basis of the Swiss plasticity and still emphasizes the picture of structural behavior. The method is consistent and gives a designer a good understanding of the mechanisms used to carry the load. The truss model provides a rational method of design. The strut and tie model provides the designer with a clear, consistent method for designing the entire structure. Some parts of the model are not mathematically pure, but the advantages from following the load paths far outweigh any disadvantages. The model gives an excellent picture of the mechanisms and paths used to transfer loads to the supports.

The ease of use varies between the models discussed. The AASHTO/ACI method is not particularly easy to use. The equations for the concrete contribution are in many cases long and confusing. Compression field theory is also not easy to use. The model was condensed down to a series of complex equations to check various parameters. The Danish, Swiss, and truss models are all similar from the design standpoint. The checks and design procedures are easy to use. They also give a good picture of behavior helping the designer in complex situations. The Danish model has the advantage of not requiring a concrete contribution. All three methods are straightforward to use. The strut and tie model is somewhat more difficult to use than the plasticity and truss models. It does, however, provide results for situations where the other models do not work very well. The added difficulty is just a slight inconvenience given the much better picture of structural behavior obtained.

3.6 Comparison with Test Results

3.6.1 Introduction. Comparison to test results provides a basis for judgement on the safety and accuracy of a shear capacity model. For a model to be of

value other than just as a conceptual aid, it must be able to reasonably predict actual capacities. For present purposes three currently popular models will be compared to the available test results for shear in high strength concrete [1,23,30]. The results will be compared to current AASHTO/ACI provisions, the 1984 Canadian Code General Method,and the truss model. Both reinforced and prestressed concrete tests will be used since the plasticity based models do not distinguish between the two cases at ultimate.

3.6.2 Current AASHTO and ACI Provisions.

3.6.2.1 Reinforced, without stirrups. Presently there are 53 shear tests reported on reinforced high strength concrete beams without shear reinforcement in American literature. Table 3.1 gives some of the specimen properties, the test results, and the values predicted by the Code. Equation (3.3) is the more general formula including concrete strength, M/Vd, and the percentage of longitudinal reinforcement. A comparison with test results shows moderate conservatism with an average test/predicted value of 1.27. There is a fair, but expected amount of scatter in the data. Figure 3.16 shows the results plotted against concrete compressive strength. Figure 3.17 shows the test data plotted in terms of the nondimensional parameters used in the original formulation. It will be noted that the tests all have low $1000\rho(Vd/M\sqrt{f'_c})$ values. More importantly all the unconservative values are for values of $1000\rho(Vd/M\sqrt{f'_c})$ in the range of 0.15 and lower. The results are not substantially different than the original data points used for the range tested to date. From Figure 3.18 it can be seen that Equation (3.3) becomes unconservative as the a/d ratio increases. While the trend is general, the Cornell tests show the greatest sensitivity to the a/d ratio. Figure 3.19 shows the relationship between the percentage of longitudinal reinforcement and Equation (3.3) accuracy. The data from Cornell is the only group that shows a strong trend with a change in ρ. From this data Equation (3.3) becomes unconservative as ρ decreases. Equation (3.6) is the simplified formula and only includes the concrete strength. This formula is more conservative with and average test/predicted ratio of 1.41. Since only one major variable was considered, greater variability would be expected. This proves to be the case in the tests reported. The comparison with Equation (3.6) can be seen in Figure 3.20. There are about the same number of unconservative results using either Equation (3.3) or (3.6).

The AASHTO/ACI equations are reasonably conservative. The a/d ratio and percentage of reinforcement seem to be the more critical issue than concrete strength in the present equations.

Table 3.1 AASHTO/ACI prediction for reinforced beams without stirrups

SPECIMEN	SOURCE (REF.)	f'c (psi)	a/d	pv	TEST (K) (1)	ACI EQ. (3.6) (K) (2)	(1)/(2)	ACI EQ. (3.3) (K) (3)	(1)/(3)
A1	1	8820	4	.0393	13	7.51	1.73	8.12	1.60
A2	1	8820	3	.0393	14	7.51	1.86	8.45	1.66
A3	1	8820	2.7	.0393	14	7.51	1.86	8.59	1.63
A4	1	8820	2.3	.0393	14.3	7.51	1.90	8.85	1.62
A5	1	8820	2	.0393	17	7.51	2.26	9.1	1.87
A7	1	8820	4	.0177	8.5	7.69	1.11	7.76	1.10
A8	1	8820	3	.0177	9.5	7.69	1.24	7.91	1.20
A9	1	8820	2.7	.0177	11	7.69	1.43	7.98	1.38
A10	1	8820	2.3	.0177	11	7.69	1.43	8.1	1.36
A11	1	8820	2	.0177	12	7.69	1.56	8.21	1.46
B1	1	9720	4	.0504	11.5	7.83	1.47	8.68	1.32
B2	1	9720	3	.0504	12.75	7.83	1.63	9.1	1.40
B3	1	9720	2.7	.0504	14	7.83	1.79	9.29	1.51
B4	1	9720	2.3	.0504	14	7.83	1.79	9.61	1.46
B5	1	9720	2	.0504	17.5	7.83	2.23	9.94	1.76
B7	1	9720	4	.0225	10	8.07	1.24	8.24	1.21
B8	1	9720	3	.0225	10.5	8.07	1.30	8.44	1.24
B9	1	9720	2.7	.0225	10.5	8.07	1.30	8.52	1.23
B10	1	9720	2.3	.0225	12.5	8.07	1.55	8.67	1.44
B11	1	9720	2	.0225	14	8.07	1.73	8.82	1.59
C1	1	9330	4	.0664	12	7	1.71	8.16	1.47
C2	1	9330	3	.0664	11	7	1.57	8.66	1.27
C3	1	9330	2.7	.0664	9	7	1.29	8.88	1.01
C4	1	9330	2.3	.0664	12.5	7	1.79	9.27	1.35
C5	1	9330	2	.0664	15	7	2.14	9.66	1.55
C7	1	9330	4	.0326	8	7.85	1.02	8.29	.97
C8	1	9330	3	.0326	10	7.85	1.27	8.56	1.17
C9	1	9330	2.7	.0326	10	7.85	1.27	8.69	1.15
C10	1	9330	2.3	.0326	9.25	7.85	1.18	8.9	1.04
C11	1	9330	2	.0326	14.5	7.85	1.85	9.12	1.59

Table 3.1 (continued)

SPECIMEN	SOURCE (REF.)	f'c (psi)	a/d	pv	TEST (K) (1)	ACI EQ. (3.6) (K) (2)	(1)/(2)	ACI EQ. (3.3) (K) (3)	(1)/(3)
A0-7-3a	03	5460	3.6	.0336	15	10.42	1.44	11.54	1.30
A0-7-3b	03	6040	3.6	.0336	14	10.96	1.28	12.06	1.16
A0-11-3a	03	10870	3.6	.0336	15	14.7	1.02	15.61	.96
A0-11-3b	03	10820	3.6	.0336	15	14.67	1.02	15.58	.96
A0-15-3a	03	11800	3.6	.0336	19	15.32	1.24	16.2	1.17
A0-15-3b	03	13590	3.6	.0336	22.5	16.44	1.37	17.26	1.30
A0-15-3c	03	13320	3.6	.0336	21.5	16.27	1.32	17.1	1.26
A0-7-2	03	6550	2.5	.0336	18	11.41	1.58	13.21	1.36
A0-11-2	03	11500	2.5	.0336	20	15.12	1.32	16.73	1.20
A0-15-2a	03	12150	2.5	.0336	24	15.54	1.54	17.13	1.40
A0-15-2b	03	10060	2.5	.0336	18	14.14	1.27	15.8	1.14
F1	32	9500	4	.012	12.9	14.33	.90	14.16	.91
F2	32	9500	4	.025	14.75	14.31	1.03	14.74	1.00
F3	32	10000	2	.012	17.85	14.7	1.21	15.07	1.18
F4	32	10000	2	.025	25.5	14.66	1.74	16.22	1.57
F5	32	9200	6	.012	9.65	14.1	.68	13.76	.70
F6	32	9200	6	.025	13.5	14.09	.96	14.15	.95
F8	32	5800	4	.01	10.05	11.2	.90	11.1	.91
F9	32	11600	4	.016	14	15.84	.88	15.79	.89
F10	32	9500	4	.033	16.83	13.96	1.21	14.74	1.14
F13	32	5800	4	.012	10.7	11.2	.96	11.19	.96
F14	32	5800	4	.025	14.25	11.17	1.28	11.76	1.21
F15	32	11300	4	.025	14.9	15.6	.96	15.97	.93
						AVE	1.41	AVE	1.27
						STD DEV	.36	STD DEV	.25

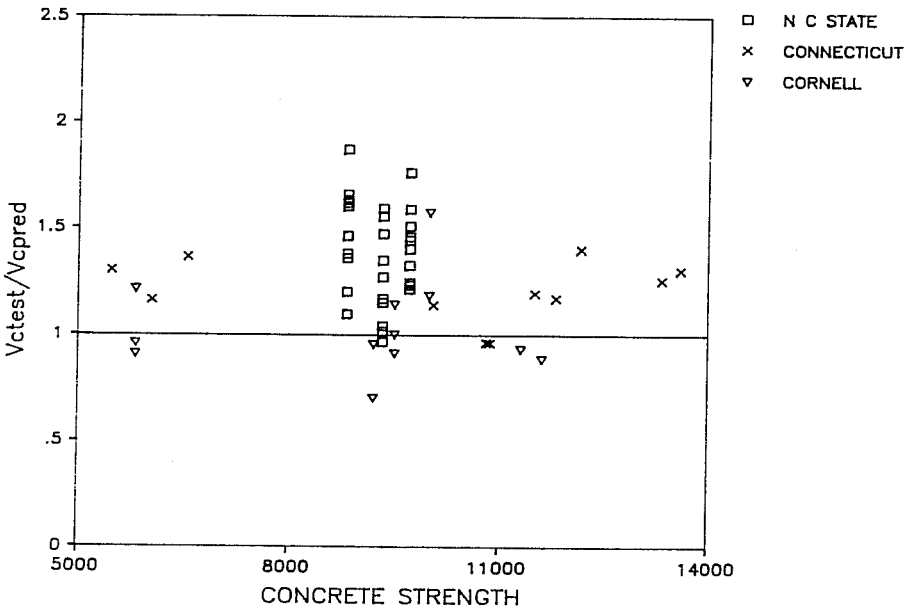

Fig. 3.16 Test/predicted values versus concrete strength for reinforced beams without stirrups using AASHTO/ACI.

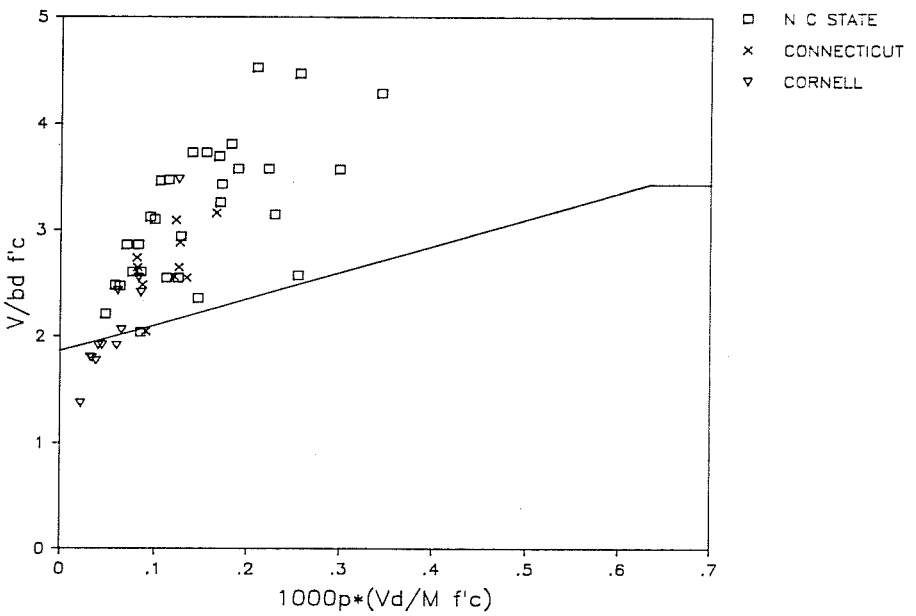

Fig. 3.17 High strength test results plotted in form used to derive Eq. (3.3).

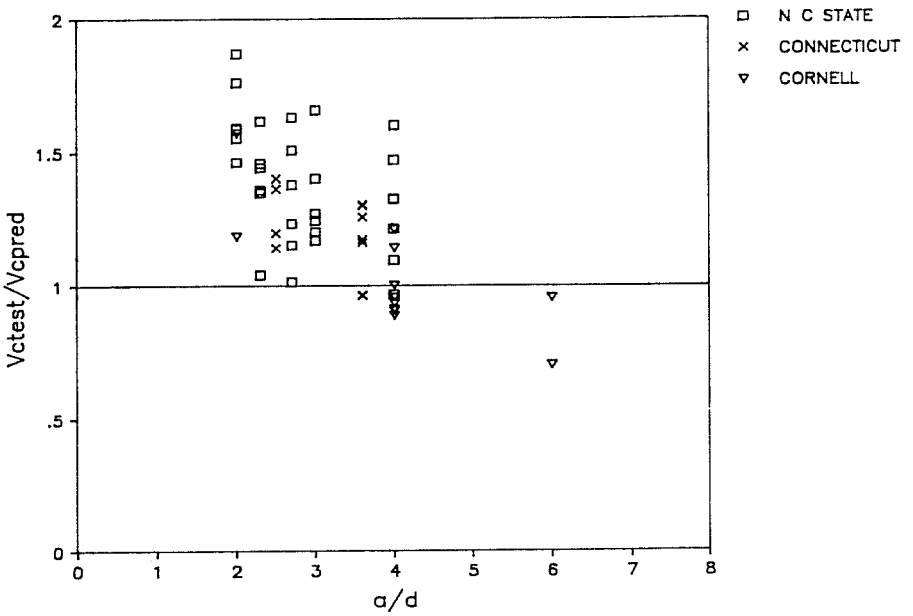

Fig. 3.18 Test results/predicted values versus a/d ratio for reinforced beams without stirrups using AASHTO/ACI.

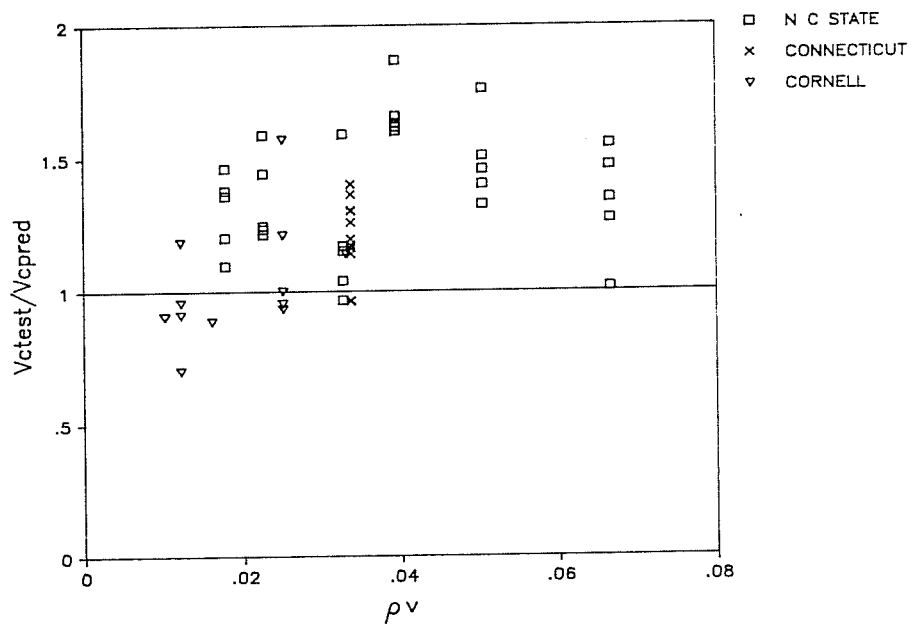

Fig. 3.19 Test results/predicted values versus ρ for reinforced beams without stirrups using AASHTO/ACI.

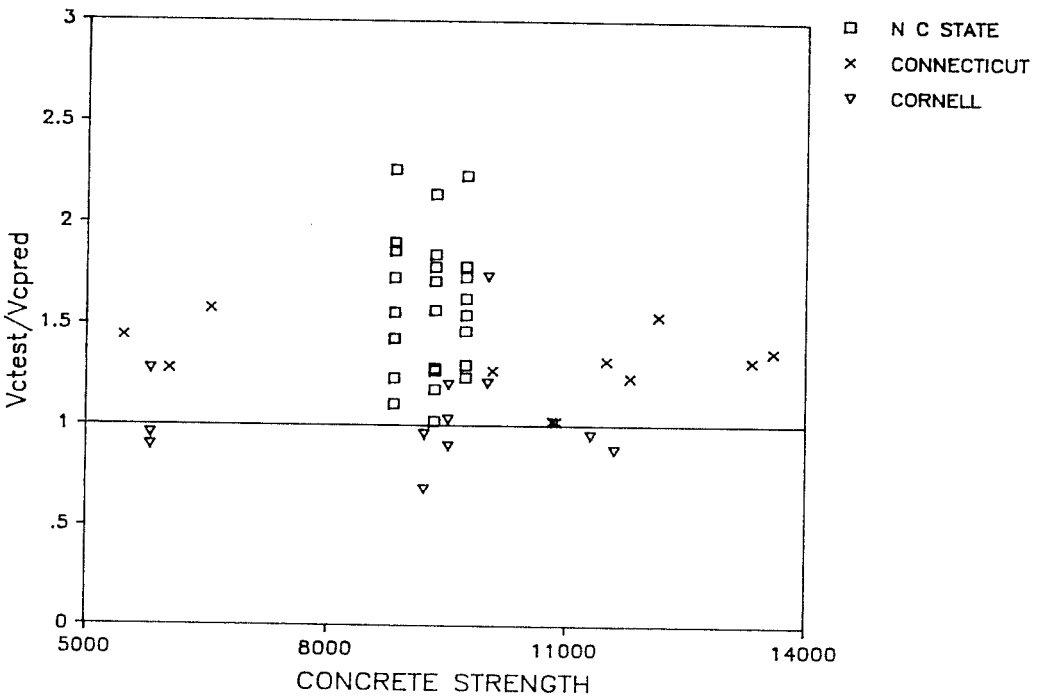

Fig. 3.20 Test results/Eq. (3.6) versus concrete strength for reinforced beams without stirrups.

3.6.2.2 Reinforced, with stirrups. American literature only contains 11 shear tests on high strength reinforced concrete beams with stirrups. Table (3.2) contains the test results and Code predictions. From Figures 3.21 and 3.22 it can be seen that both equations for the concrete contribution plus the steel contribution give conservative results.

The Cornell report stated that the Code equations become more conservative as concrete strength increases. The Connecticut report stated that for low values of shear reinforcement the equations become less conservative as concrete strength increases. From Figures 3.23, 3.24, and 3.25, which show results for various values of shear reinforcement, there does not appear to be a consistent trend in the data.

For the range of tests run to date the AASHTO/ACI provisions for reinforced concrete beams with shear reinforcement provide a conservative estimate of shear capacity.

3.6.2.3 Prestressed, without stirrups. AASHTO and ACI have three equations for the concrete contribution in prestressed concrete. The Cornell report stated that the cracking load for prestressed members with and without stirrups is the same. Based on this, the cracking load for members with stirrups will also be considered in this evaluation (Table 3.3).

Equation (3.7) is a general equation for both inclined and web shear cracking. It does not have a term considering the prestress force. Some of the specimens are very close to or just under the limit that prestress force should be greater than or equal to 40% of the tensile capacity. Since all were within several percent of 40%, all specimens were included. The equation is extremely conservative. The average value of test results divided by predicted results was 3.38. There was significant scatter but all values were well over 2.0 (Fig. 3.26). Given the basis, the limitations, and the extreme conservatism of the equation; its value is very limited.

Equation (3.10) is for web shear cracking. The equation was in all cases conservative with an average comparison value of 1.16. There was very small scatter in the data. There are no dramatic trends in the data for increasing concrete strength (Fig. 3.27). The tests with different a/d ratios suggest that there may be a trend towards decreasing conservatism with increasing a/d. There is not at present enough data to confirm this trend.

Table 3.2 AASHTO/ACI predictions for reinforced beams with stirrups

SPECIMEN	SOURCE (REF.)	f'c	a/d	pvfy (psi)	TEST (K) (1)	V tot EQ. (3.6) (K) (2)	(1)/(2)	V tot EQ. (3.3) (K) (3)	(1)/(3)
B50-7-3	03	5780	3.6	50	21.1	14.24	1.48	15.35	1.37
B50-11-3	03	8660	3.6	50	22	16.65	1.32	17.64	1.25
B50-15-3	03	12030	3.6	50	25	18.99	1.32	19.86	1.26
B100-7-3	03	6830	3.6	100	27.1	18.7	1.45	19.76	1.37
B100-11-3	03	9950	3.6	100	34.1	21.11	1.62	22.06	1.55
B100-15-3	03	11880	3.6	100	26	22.42	1.16	23.29	1.12
B150-7-3	03	6750	3.6	150	30	22.16	1.35	23.22	1.29
B150-11-3	03	10080	3.6	150	36.3	24.73	1.47	25.67	1.41
B150-15-3	03	12000	3.6	150	33.7	26.02	1.30	26.89	1.25
G3	32	9100	4	140	26.4	24.14	1.09	24.95	1.06
G4	32	9100	4	94	33.1	20.65	1.60	21.45	1.54
G5	32	5800	4	94	25.45	18.35	1.39	18.95	1.34
						AVE	1.38	AVE	1.32
						STD DEV	.15	STD DEV	.14

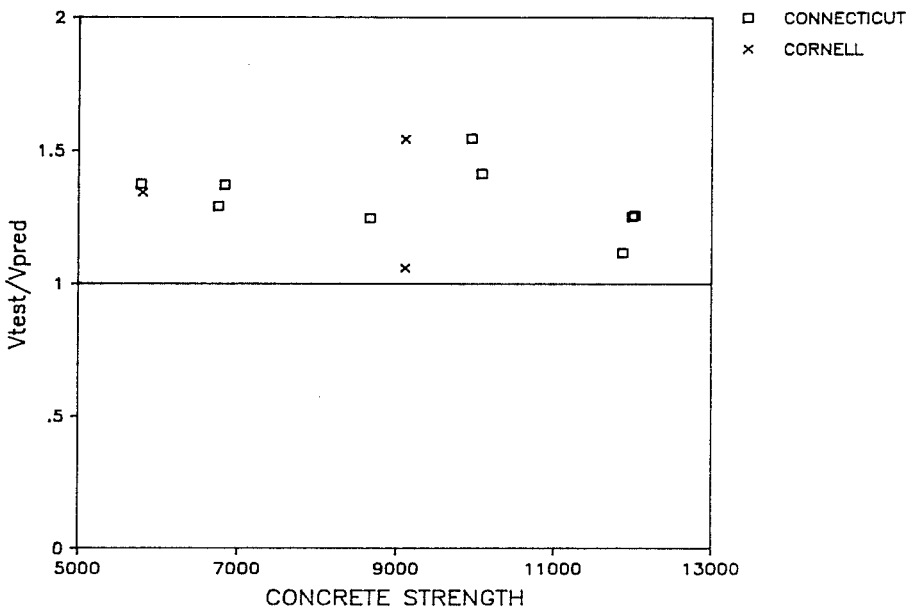

Fig. 3.21 Test results for reinforced beams with stirrups/ (AASHTO/ACI) using Eq. (3.3) versus concrete strength.

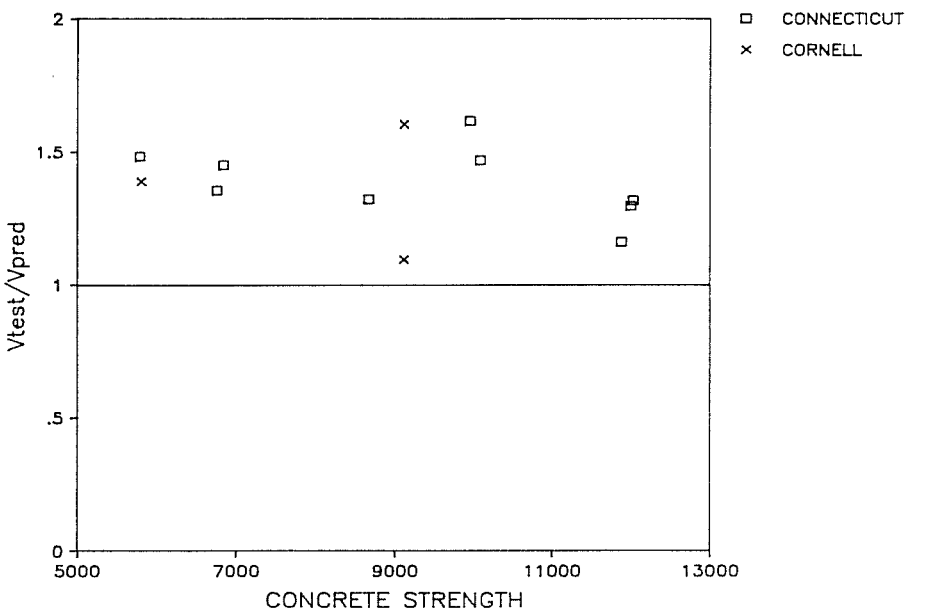

Fig. 3.22 Test results/ predicted values versus concrete strength for reinforced beams with stirrups using AASHTO/ACI method and Eq. (3.6).

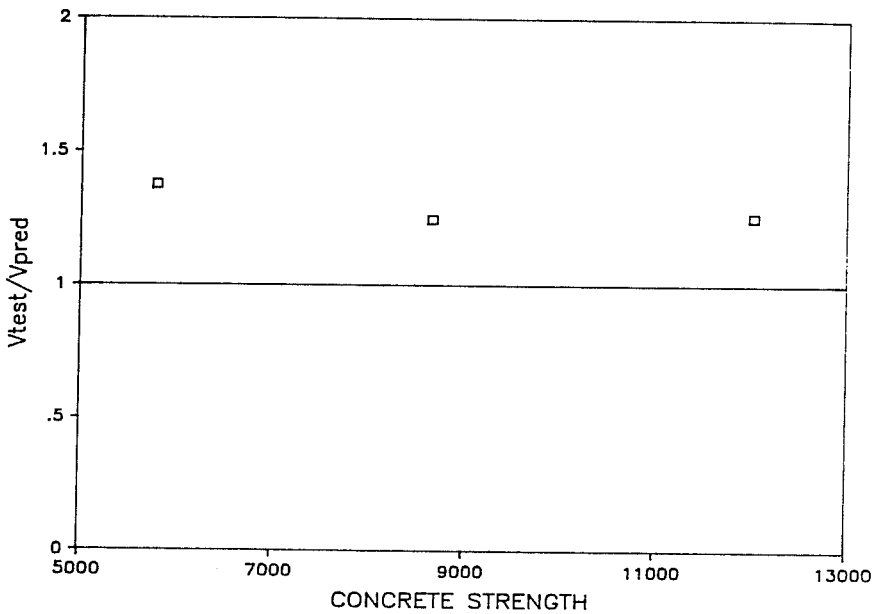

Fig. 3.23 Test results/predicted values versus concrete strength for reinforced beams with stirrups ($\rho_v f_y \leq 50$ psi).

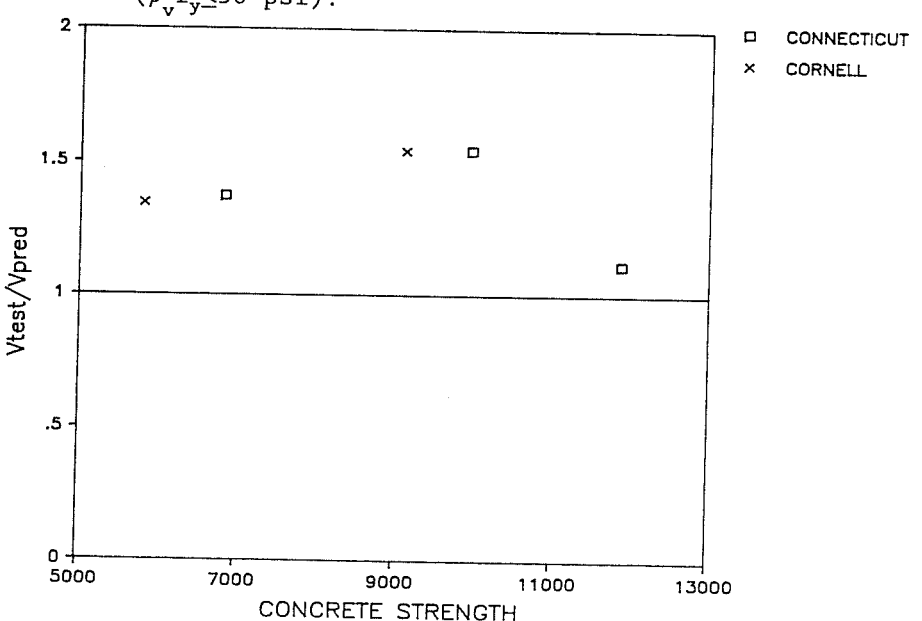

Fig. 3.24 Test results/predicted values versus concrete strength for reinforced beams with stirrups ($50 < \rho_v f_y \leq 100$ psi).

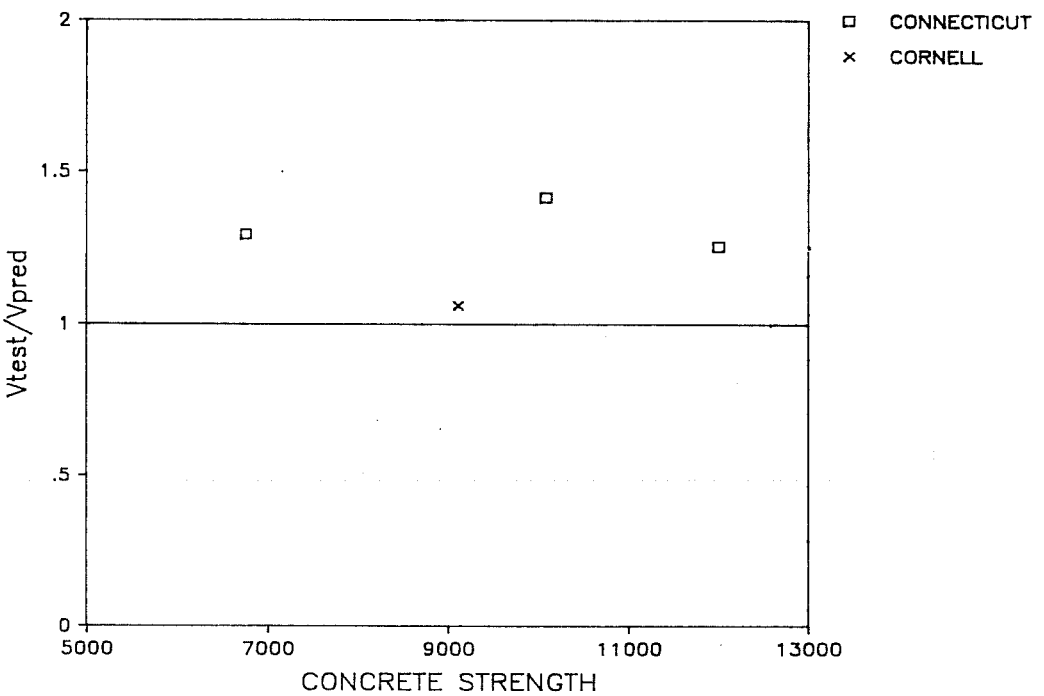

Fig. 3.25 Tests results/predicted values versus concrete strength for reinforced beams with stirrups ($100 < \rho_v f_y \leq 150$ psi).

Table 3.3 AASHTO/ACI predictions for prestressed beams without stirrups

SPECIMEN	SOURCE (REF.)	f'c	a/d	TEST (K) (1)	GENERAL (K) (2)	(1)/(2)	Vci (K) (3)	(1)/(3)	Vcw (K) (4)	(1)/(4)
CW1	32	11100	2.9	31.1	8.8	3.53			24.32	1.28
CW2	32	11100	3.75	28	7.2	3.89			24.27	1.15
CW3	32	11100	5	26.4	6.1	4.33			24.12	1.09
CW4	32	11400	3.75	28.6	7.3	3.92			24.65	1.16
CW5	32	11300	3.75	27.9	7.2	3.88			24.42	1.14
CW6	32	11300	3.75	25.2	7.2	3.50			21	1.20
CW7	32	11250	3.75	23.8	7.2	3.31			20.7	1.15
CW8	32	6000	3.75	20.2	6.7	3.01			18.05	1.12
CW9	32	8850	3.75	22.7	7	3.24			19.55	1.16
CW10	32	10600	3.75	24.4	7.2	3.39			20.3	1.20
CW11	32	8100	3.75	21.5	6.9	3.12			18.8	1.14
CW12	32	5800	3.75	19.2	6.7	2.87			17.4	1.10
CW13	32	10500	3.75	27.6	7.2	3.83			24	1.15
CW14	32	10700	3.75	27.8	7.2	3.86			24.2	1.15
CW15	32	10200	3.75	22.6	7.1	3.18			19.9	1.14
CW16	32	10600	3.75	27.5	7.2	3.82			24.1	1.14
CW17	32	10100	3.75	27.7	7.1	3.90			23.9	1.16
CI1	32	11100	7.8	17.5	7.1	2.46	15.91	1.10		
CI2	32	11100	5.8	26	7.1	3.66	20.79	1.25		
CI3	32	11100	4	27.2	7.1	3.83			23.32	1.17
CI4	32	11400	5.8	24.4	7.2	3.39	21.07	1.16		
CI5	32	11300	5.8	26.9	7.1	3.79	20.89	1.29		
CI6	32	11300	5.8	20	7.1	2.82	16.82	1.19		
CI7	32	11250	5.8	18.3	7.1	2.58	16.49	1.11		
CI8	32	6000	5.8	19.2	5.6	3.43	15.5	1.24		
CI9	32	8850	5.8	19.6	6.3	3.11	16.06	1.22		
CI10	32	10600	5.8	18.8	6.9	2.72	16.3	1.15		
CI11	32	8100	5.8	18	6	3.00	15.5	1.16		
CI12	32	5800	5.8	18.6	5.6	3.32	14.9	1.25		
CI13	32	10500	5.8	18	6.9	2.61	20.7	.87		
CI14	32	10700	5.8	24.2	7	3.46	21	1.15		
CI15	32	10200	5.8	17.6	6.8	2.59	16	1.10		
CI16	32	10600	5.8	26.3	6.9	3.81	20.9	1.26		
CI17	32	10100	5.8	25.5	6.8	3.75	20.7	1.23		
					AVE	3.38	AVE	1.17	AVE	1.16
					STD DEV	.47	STD DEV	.10	STD DEV	.04

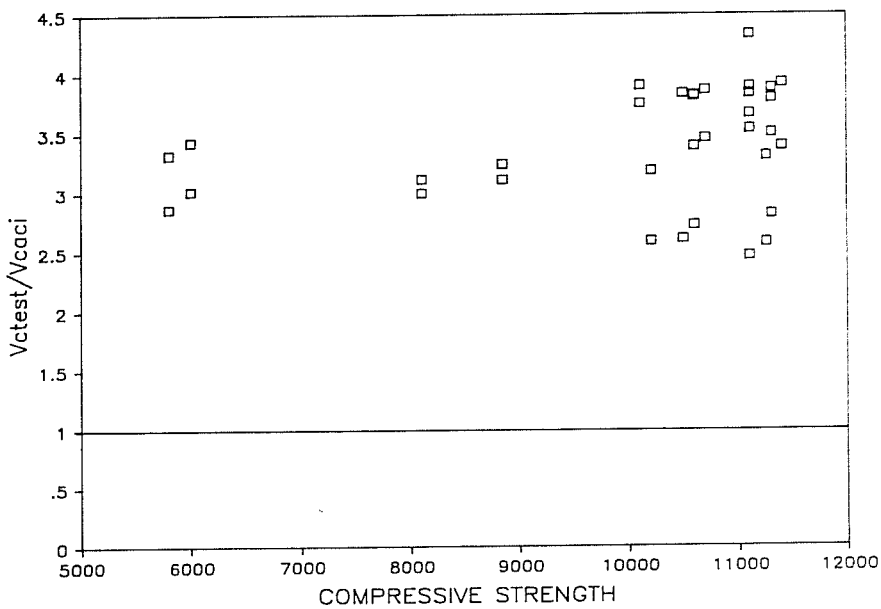

Fig. 3.26 Prestressed cracking load/ Eq. (3.7) versus concrete strength.

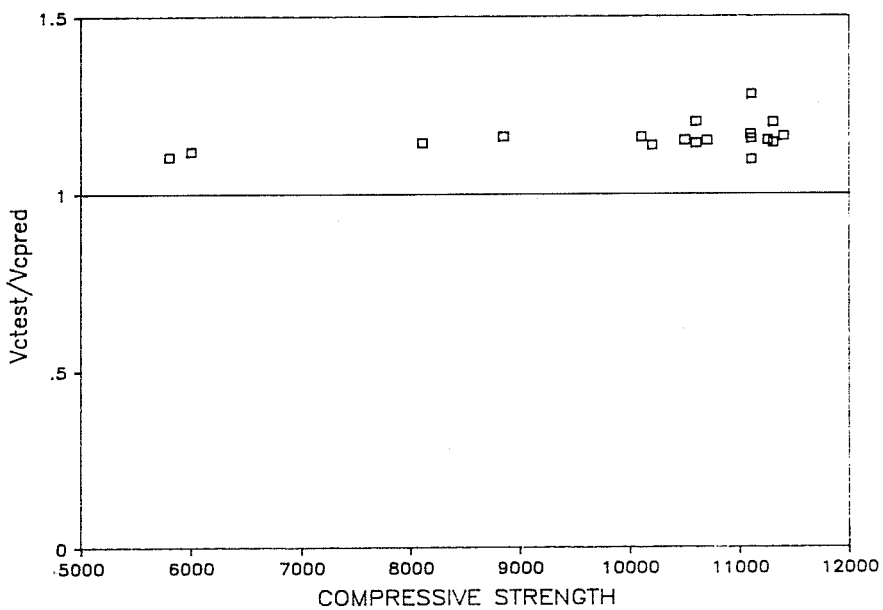

Fig. 3.27 Prestressed web shear cracking / Eq. (3.10) versus concrete strength for AASHTO/ACI.

Equation (3.8) is used to predict flexure shear cracking. The equation was conservative in all but one case which the authors said had some experimental deficiency. There appears to be no major trend for increasing concrete strength (Fig. 3.28).

The Code provisions for prestressed members give conservative predictions for the cracking load.

3.6.2.4 Prestressed, with stirrups. There are 16 tests on high strength prestressed beams with shear reinforcement reported in American literature. The test results are compared to the Code predicted value of $V_c + V_s$, (Table 3.4). For V_c both the general expression and the appropriate specific expressions are used.

Use of the general expression results in extremely conservative predictions with an average test/predicted ratio of 2.11.

Use of the specific equations gives more accurate, conservative results. The test/predicted ratio was on average 1.16 with low scatter. The Code predictions are in all cases conservative (Fig. 3.29). There do not appear to be consistent trends in the data for changing concrete strength, amount of web reinforcement, or prestress force.

3.6.3 1984 Canadian Code

3.6.3.1 No stirrups. The 1984 Canadian Code General Method is based on compression field theory. The General Method does not have a concrete contribution term as such. It does set a limit on the amount of shear that can be taken without stirrups. The following equation is used to predict the cracking load for reinforced and prestressed members in crack width calculations.

$$V_{cr} = \{2.4\lambda\sqrt{f'_c}[1 + f_{pc}(4.8\lambda\sqrt{f'_c})]^{0.5}\}b_w d \quad (in\ psi) \tag{3.72}$$

This equation will be used for an evaluation of shear tests without reinforcement.

Table (3.5) contains the results of the reinforced concrete tests. The prestress term in Equation (3.72) is 1.0 for reinforced concrete. The Canadian Code limit for d_v = .9d was used throughout. The Code prediction is generally conservative in its prediction of shear capacity. The average value of 1.29 is slightly lower than the similar AASHTO/ACI equation. The standard deviation is nearly as good as the long AASHTO/ACI equation, (3.3). There are no distinct trends in the data for changing concrete strength (Fig. 3.30).

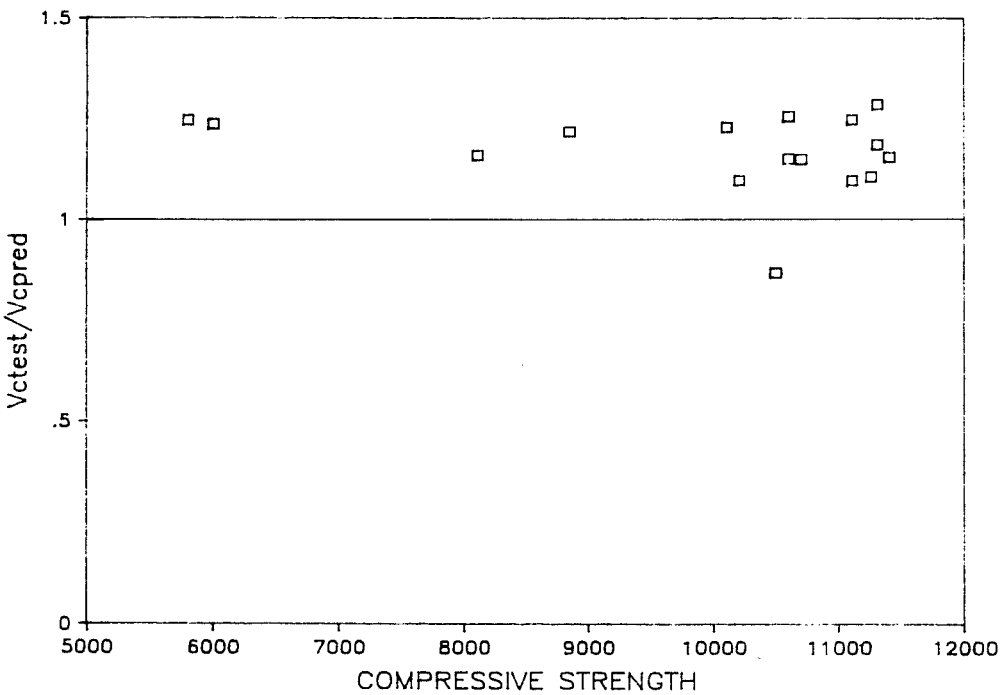

Fig. 3.28 Prestressed inclined cracking/Eq. (3.8) versus concrete strength for AASHTO/ACI.

Table 3.4 AASHTO/ACI predictions for prestressed beams with stirrups

SPECIMEN	SOURCE (REF.)	f'c	a/d	d (in)	pvfy (psi)	TEST (K) (1)	Vcg+Vs (K) (2)	(1)/(2)	Vc+Vs (K) (3)	(1)/(3)
CW10	32	10600	3.75	14.4	346	39.00	17.16	2.27	29.7	1.31
CW11	32	8100	3.75	14.4	346	35.20	16.86	2.09	28.2	1.25
CW12	32	5800	3.75	14.45	346	31.60	16.70	1.89	26.8	1.18
CW13	32	10500	3.75	14.47	346	41.00	17.21	2.38	33.4	1.23
CW14	32	10700	3.75	14.46	495	42.20	21.52	1.96	37.7	1.12
CW15	32	10200	3.75	14.4	346	33.80	17.06	1.98	29.3	1.15
CW16	32	10600	3.75	14.47	346	42.00	17.21	2.44	33.5	1.25
CW17	32	10100	3.75	14.47	135	32.00	11.01	2.91	28.2	1.13
CI10	32	10600	5.8	11.2	289	31.80	16.61	1.91	24.2	1.31
CI11	32	8100	5.8	11.2	289	28.60	15.71	1.82	23.4	1.22
CI12	32	5800	5.8	11.2	289	27.50	15.31	1.80	22.8	1.21
CI13	32	10500	5.8	11.2	289	34.80	16.61	2.10	28.6	1.22
CI14	32	10700	5.8	11.2	462	37.00	22.52	1.64	33.7	1.10
CI15	32	10200	5.8	11.2	289	27.20	16.51	1.65	23.9	1.14
CI16	32	10600	5.8	11.2	289	36.70	16.61	2.21	28.8	1.27
CI17	32	10100	5.8	11.2	112	29.10	10.56	2.75	24.3	1.20
							AVE	2.11	AVE	1.16
							STD DEV	.35	STD DEV	.06

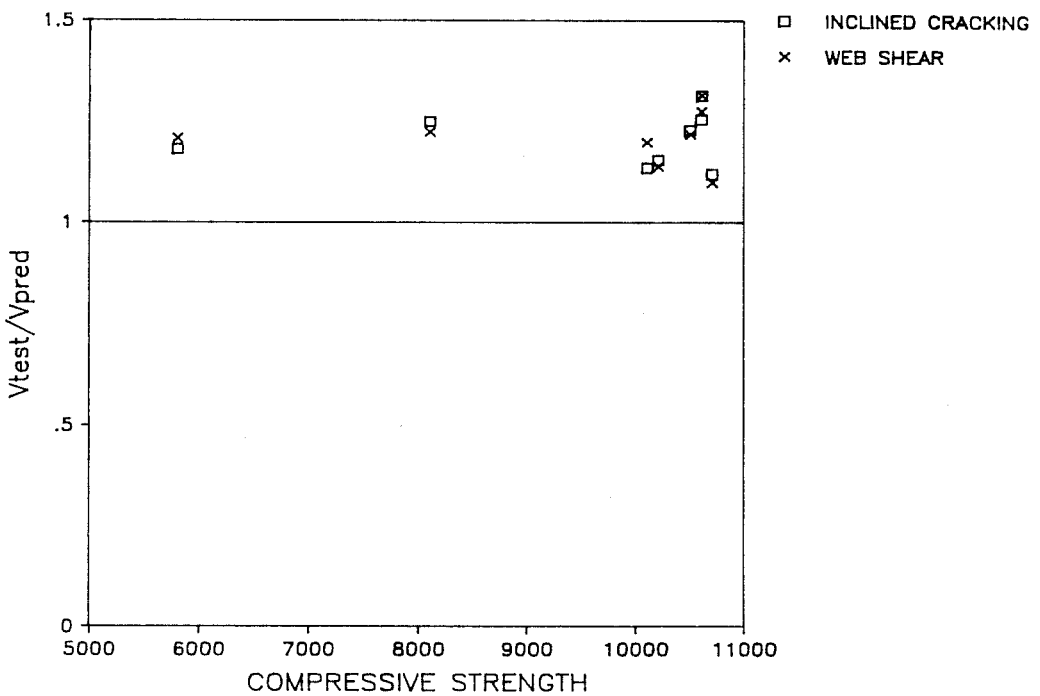

Fig. 3.29 Test results/predicted values versus concrete strength for prestressed beams with stirrups using AASHTO/ACI.

Table 3.5 Canadian code predictions for reinforced beams with stirrups

SPECIMEN	SOURCE (REF.)	f'c (psi)	a/d	d (in)	TEST (K) (1)	CANADIAN	(1)/(2)
A1	1	8820	4	8.00	13	9.05	1.44
A2	1	8820	3	8.00	14	9.05	1.55
A3	1	8820	2.7	8.00	14	9.05	1.55
A4	1	8820	2.3	8.00	14.3	9.05	1.58
A5	1	8820	2	8.00	17	9.05	1.88
A7	1	8820	4	8.19	8.5	9.26	.92
A8	1	8820	3	8.19	9.5	9.26	1.03
A9	1	8820	2.7	8.19	11	9.26	1.19
A10	1	8820	2.3	8.19	11	9.26	1.19
A11	1	8820	2	8.19	12	9.26	1.30
B1	1	9720	4	7.94	11.5	9.43	1.22
B2	1	9720	3	7.94	12.75	9.43	1.35
B3	1	9720	2.7	7.94	14	9.43	1.49
B4	1	9720	2.3	7.94	14	9.43	1.49
B5	1	9720	2	7.94	17.5	9.43	1.86
B7	1	9720	4	8.19	10	9.72	1.03
B8	1	9720	3	8.19	10.5	9.72	1.08
B9	1	9720	2.7	8.19	10.5	9.72	1.08
B10	1	9720	2.3	8.19	12.5	9.72	1.29
B11	1	9720	2	8.19	14	9.72	1.44
C1	1	9330	4	7.25	12	8.43	1.42
C2	1	9330	3	7.25	11	8.43	1.30
C3	1	9330	2.7	7.25	9	8.43	1.07
C4	1	9330	2.3	7.25	12.5	8.43	1.48
C5	1	9330	2	7.25	15	8.43	1.78
C7	1	9330	4	8.13	8	9.46	.85
C8	1	9330	3	8.13	10	9.46	1.06
C9	1	9330	2.7	8.13	10	9.46	1.06
C10	1	9330	2.3	8.13	9.25	9.46	.98
C11	1	9330	2	8.13	14.5	9.46	1.53

74

Table 3.5 (continued)

SPECIMEN	SOURCE (REF.)	f'c (psi)	a/d	d (in)	TEST (K) (1)	CANADIAN	(1)/(2)
A0-7-3a	03	5460	3.6	11.75	15	10.46	1.43
A0-7-3b	03	6040	3.6	11.75	14	11.00	1.27
A0-11-3a	03	10870	3.6	11.75	15	14.75	1.02
A0-11-3b	03	10820	3.6	11.75	15	14.72	1.02
A0-15-3a	03	11800	3.6	11.75	19	15.37	1.24
A0-15-3b	03	13590	3.6	11.75	22.5	16.50	1.36
A0-15-3c	03	13320	3.6	11.75	21.5	16.33	1.32
A0-7-2	03	6550	2.5	11.75	18	11.45	1.57
A0-11-2	03	11500	2.5	11.75	20	15.17	1.32
A0-15-2a	03	12150	2.5	11.75	24	15.60	1.54
A0-15-2b	03	10060	2.5	11.75	18	14.19	1.27
F1	32	9500	4	10.625	12.9	12.47	1.03
F2	32	9500	4	10.5625	14.75	12.40	1.19
F3	32	10000	2	10.625	17.85	12.80	1.40
F4	32	10000	2	10.5625	25.5	12.72	2.00
F5	32	9200	6	10.625	9.65	12.27	.79
F6	32	9200	6	10.5625	13.5	12.20	1.11
F8	32	5800	4	10.723	10.05	9.83	1.02
F9	32	11600	4	10.5625	14	13.70	1.02
F10	32	9500	4	10.5	16.83	12.32	1.37
F13	32	5800	4	10.625	10.7	9.74	1.10
F14	32	5800	4	10.5625	14.25	9.69	1.47
F15	32	11300	4	10.5625	14.9	13.52	1.10
						AVE	1.29
						STD DEV	.26

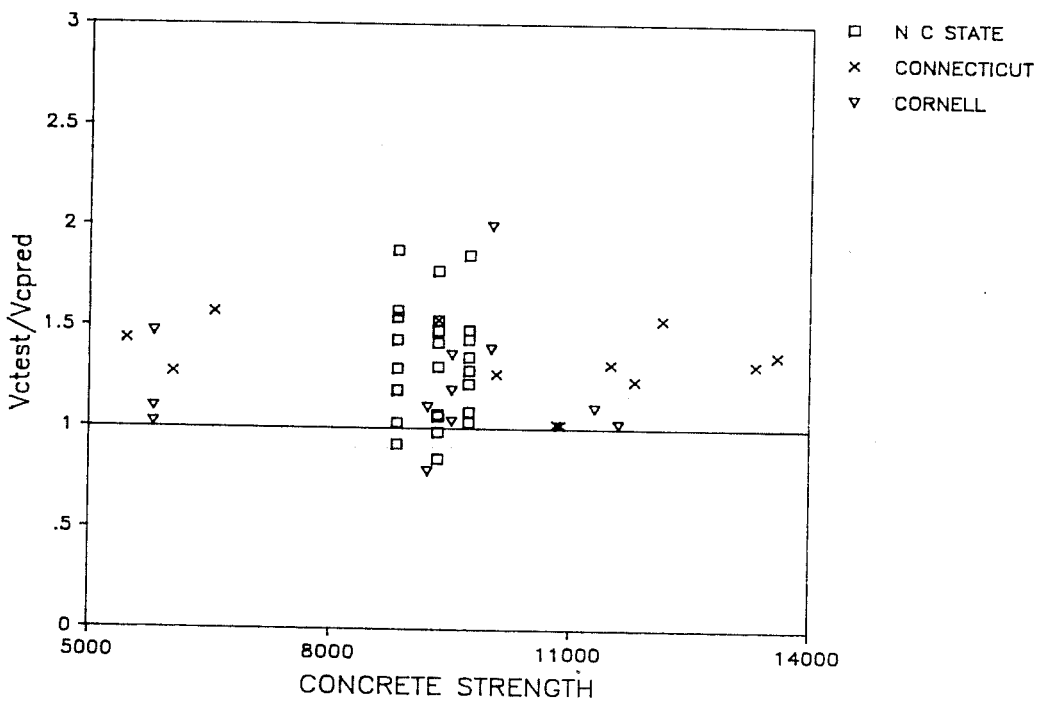

Fig. 3.30 Concrete contribution in reinforced beams/ Eq. (3.72) from Canadian Code versus concrete strength.

The prestressed beam tests are given in Table (3.6). For prestressed members the prestress term increases the predicted cracking load. The prediction is quite conservative with the average ratio of test/predicted being 1.70. Figure 3.31 shows that there is a distinct difference in behavior between web shear and inclined cracking loads. The web shear loads are predicted much more conservatively, with an average value of 1.85. Inclined shear cracking has an average ratio of 1.39. There appears to be a slight tendency towards decreasing conservatism for increasing concrete strength for inclined cracking.

Figure 3.32 shows all the specimens without shear rein- forcement on one plot. It shows that the equation does give reasonably consistent, conservative results for both reinforced and prestressed beams.

3.6.3.2 Reinforced, with stirrups. Table (3.7) has the results predicted by the Canadian Code General Method for reinforced beams with stirrups. A value of 0.002 was used throughout for ϵ_x as allowed by the Code. The angle θ was chosen so that $f_2=f_{2max}$ with ϕ factors equal to 1.0. The values of V_f in the equation for f_2 were chosen so that $V_f = \rho_v f_y / tan\theta$. This allowed a closed form solution given $\rho_v f_y$ and f'_c. The results gave V_r predicted equal to V_f assumed. Anchorage was assumed to be acceptable since a development overhang was provided. Figure 3.33 shows the results versus concrete strength. The General Method is conservative in all but one case and no trends are apparent. An average test/predicted value of 1.67 was obtained. Plotting test/predicted versus $\rho_v f_y$ leads to sharply decreasing conservatism (Fig. 3.34). The tests reported to date are for a small range of $\rho_v f_y$ values. Currently $\rho_v f_y$ could be as high as 800 psi for 10000 psi concrete. Data is needed for high $\rho_v f_y$ values to determine whether the trend continues or if high conservatism at low $\rho_v f_y$ values comes from a contribution by the concrete.

3.6.3.3 Prestressed, with stirrups. The solution method used for prestressed beams is identical to that for reinforced concrete beams. The results of the calculations are shown in Table 3.8. The results plotted against concrete are shown in Figure 3.35. The average test/predicted value is 1.90. With the exception of two specimens with light shear reinforcement there seems to be a tendency towards decreasing conservatism. Figure 3.36 shows the results plotted against $\rho_v f_y$. The data shows a sharp decrease in conservatism with increasing $\rho_v f_y$. The results do seem to be somewhat asymptotical to unity. This indicates that the high conservatism for low $\rho_v f_y$ may be due to a concrete contribution.

Table 3.6 Canadian code prediction for cracking load in prestressed beams

SPECIMEN	SOURCE (Ref.)	f'c	a/d	d (in)	PRESTRESS FORCE (K)	fpc (ksi)	TEST (K) (1)	Vcr (K) (2)	(1)/(2)
CW1	32	11100	2.9	14.4	136.4	1.62	31.10	14.98	2.08
CW2	32	11100	3.75	14.4	135.6	1.61	28.00	14.94	1.87
CW3	32	11100	5	14.4	134.1	1.60	26.40	14.88	1.77
CW4	32	11400	3.75	14.2	138	1.64	28.60	14.96	1.91
CW5	32	11300	3.75	14.9	136.2	1.62	27.90	15.57	1.79
CW6	32	11300	3.75	14.4	102.3	1.22	25.20	13.55	1.86
CW7	32	11250	3.75	14.5	99.8	1.19	23.80	13.51	1.76
CW8	32	6000	3.75	14.4	101.5	1.21	20.20	11.06	1.83
CW9	32	8850	3.75	14.4	100.5	1.20	22.70	12.45	1.82
CW10	32	10600	3.75	14.4	98.8	1.18	24.40	13.11	1.86
CW11	32	8100	3.75	14.4	96.4	1.15	21.50	11.92	1.80
CW12	32	5800	3.75	14.4	96.8	1.15	19.20	10.75	1.79
CW13	32	10500	3.75	14.4	135.8	1.62	27.60	14.70	1.88
CW14	32	10700	3.75	14.4	137.2	1.63	27.80	14.84	1.87
CW15	32	10200	3.75	14.5	97.3	1.16	22.60	12.97	1.74
CW16	32	10600	3.75	14.9	136.4	1.62	27.50	15.28	1.80
CW17	32	10100	3.75	14.4	136.7	1.63	27.70	14.56	1.90
CI1	32	11100	7.8	9.9	136	1.49	17.50	14.97	1.17
CI2	32	11100	5.8	9.9	135.4	1.49	26.00	14.94	1.74
CI3	32	11100	4	9.9	134.3	1.48	27.20	14.90	1.83
CI4	32	11400	5.8	9.6	137.2	1.51	24.40	14.69	1.66
CI5	32	11300	5.8	10.5	135.9	1.49	26.90	15.96	1.69
CI6	32	11300	5.8	9.9	102.3	1.12	20.00	13.59	1.47
CI7	32	11250	5.8	9.9	99.6	1.09	18.30	13.45	1.36
CI8	32	6000	5.8	9.9	101.6	1.12	19.20	11.07	1.73
CI9	32	8850	5.8	9.9	100.4	1.10	19.60	12.47	1.57
CI10	32	10600	5.8	9.9	98.9	1.09	18.80	13.16	1.43
CI11	32	8100	5.8	9.9	96.8	1.06	18.00	11.96	1.50
CI12	32	5800	5.8	9.9	97.2	1.07	18.60	10.77	1.73
CI13	32	10500	5.8	9.9	135.4	1.49	18.00	14.69	1.23
CI14	32	10700	5.8	9.9	137.8	1.51	24.20	14.87	1.63
CI15	32	10200	5.8	9.9	97.4	1.07	17.60	12.92	1.36
CI16	32	10600	5.8	10.5	136.8	1.50	26.30	15.68	1.68
CI17	32	10100	5.8	9.9	136.5	1.50	25.50	14.55	1.75
								AVE	1.70
								STD DEV	.20

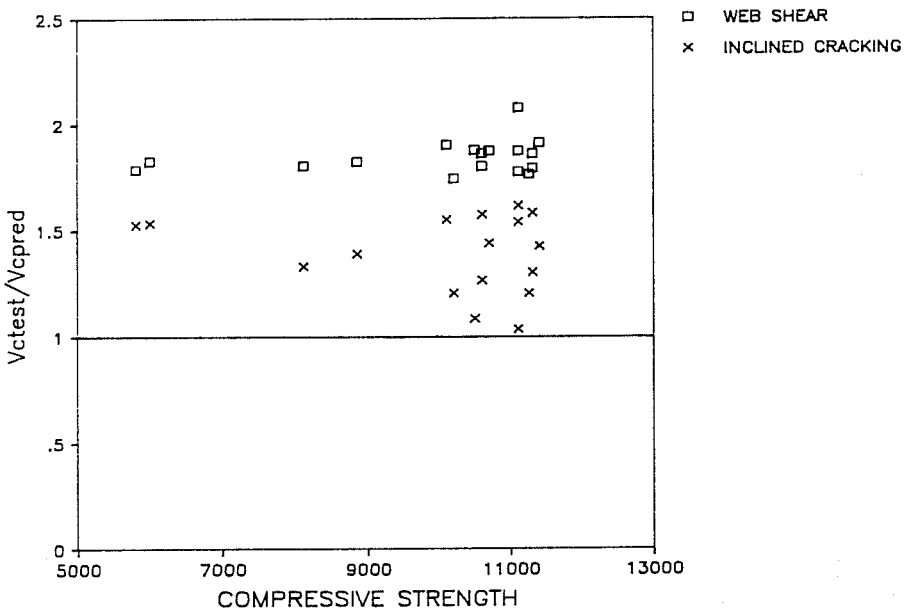

Fig. 3.31 Concrete contribution in prestressed beams/Eq. (3.72) from Canadian Code versus concrete strength.

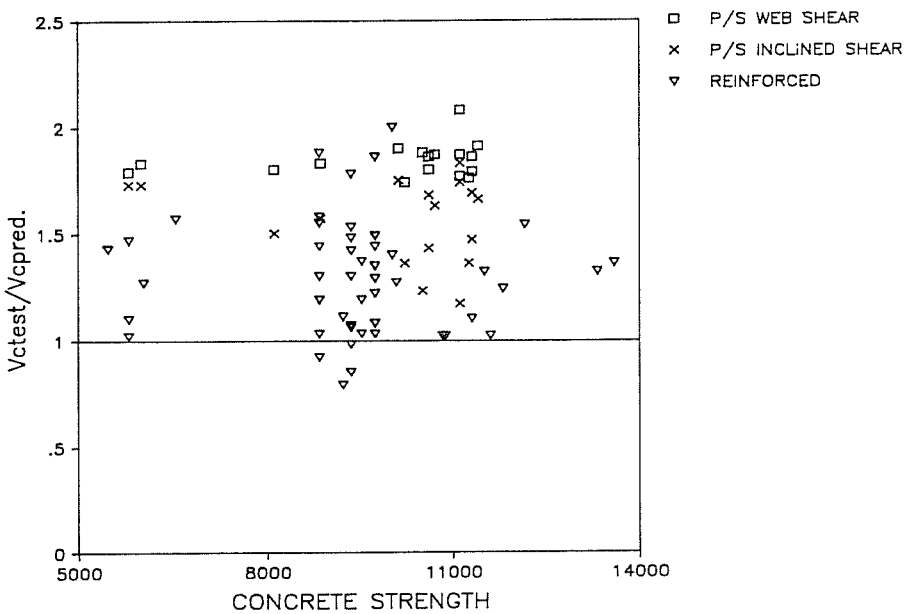

Fig. 3.32 Cracking loads for reinforced and prestressed beams/Canadian Code prediction, Eq. (3.72), versus concrete strength.

Table 3.7 Canadian code predictions for reinforced beams with stirrups

SPECIMEN	SOURCE (REF.)	f'c	a/d	pvfy (psi)	dv (in)	TEST (K) (1)	θ (°)	Vr (K) (2)	(1)/(2)
B50-7-3	03	5780	3.6	50	10.58	21.1	16.3	10.8	1.95
B50-11-3	03	8660	3.6	50	10.58	22.0	15.0	11.8	1.86
B50-15-3	03	12030	3.6	50	10.58	25.0	15.0	11.8	2.12
B100-7-3	03	6830	3.6	100	10.58	27.1	18.7	18.7	1.45
B100-11-3	03	9950	3.6	100	10.58	34.1	17.0	20.8	1.64
B100-15-3	03	11880	3.6	100	10.58	26.0	16.2	21.9	1.19
B150-7-3	03	6750	3.6	150	10.58	30.0	21.0	24.8	1.21
B150-11-3	03	10080	3.6	150	10.58	36.3	18.8	27.9	1.30
B150-15-3	03	12000	3.6	150	10.58	33.7	18.0	29.4	1.15
G3	32	9100	4	140	9.38	26.4	19.0	26.7	.99
G4	32	9100	4	94	9.32	33.1	17.1	20.0	1.66
G5	32	5800	4	94	9.58	25.5	19.2	18.0	1.41
								AVE	1.49
								STD DEV	.34

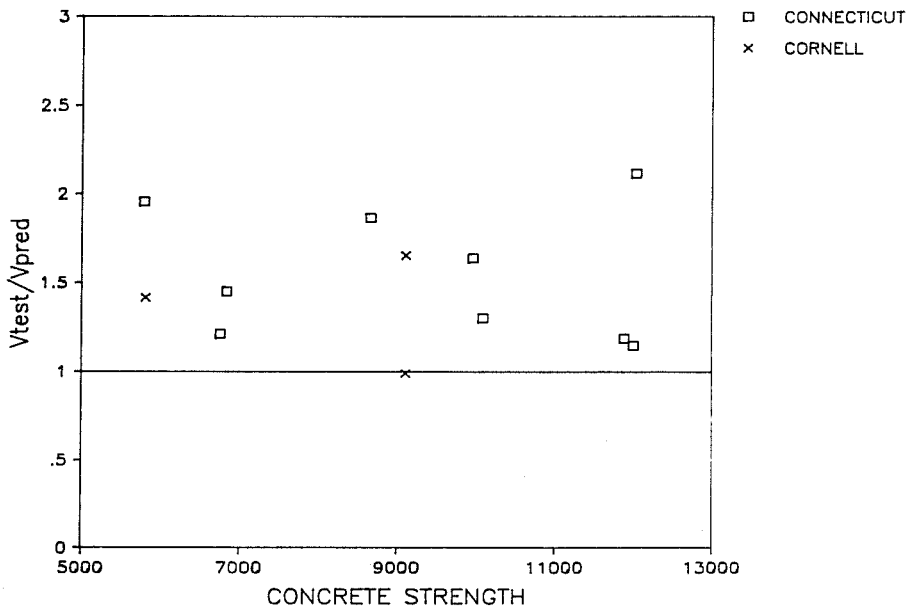

Fig. 3.33 Reinforced beams with stirrups / Canadian Code versus concrete strength.

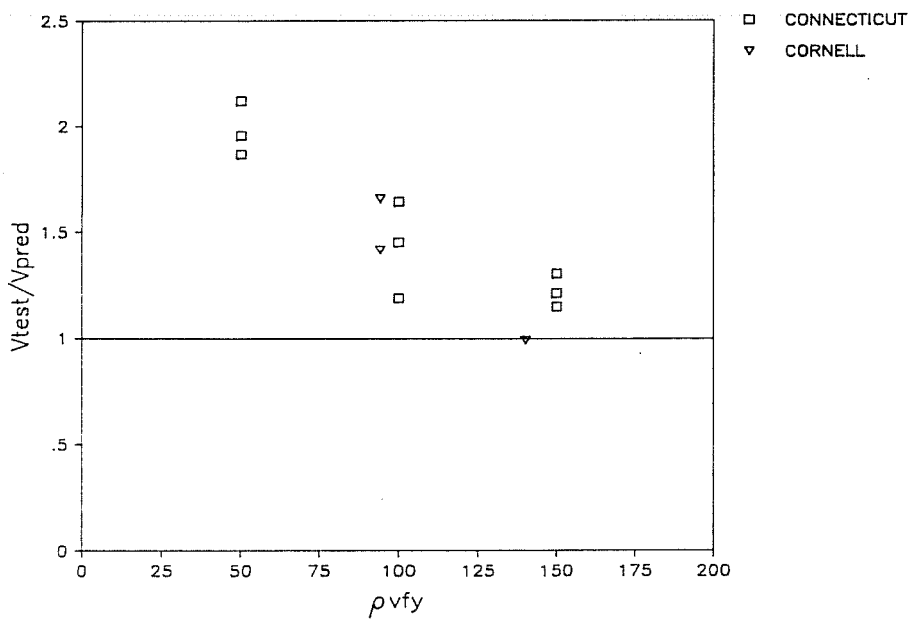

Fig. 3.34 Reinforced beams with stirrups/ Canadian Code versus $\rho_v f_y$.

Table 3.8 Canadian code prediction for prestressed beams with stirrups

SPECIMEN	SOURCE (REF.)	f'c	a/d	dv (in)	pvfy (psi)	TEST (K) (1)	θ (°)	Vr (K) (2)	(1)/(2)
CW10	32	10600	3.75	13.0	346	39.0	23.3	20.9	1.87
CW11	32	8100	3.75	13.0	346	35.2	25.1	19.2	1.83
CW12	32	5800	3.75	13.0	346	31.6	27.7	17.1	1.84
CW13	32	10500	3.75	13.0	346	41.0	23.4	20.8	1.97
CW14	32	10700	3.75	13.0	495	42.2	25.7	26.7	1.58
CW15	32	10200	3.75	13.0	346	33.8	23.6	20.6	1.64
CW16	32	10600	3.75	13.4	346	42.0	23.3	21.5	1.95
CW17	32	10100	3.75	13.0	135	32.0	18.3	10.6	3.02
CI10	32	10600	5.8	8.9	289	31.8	22.2	18.9	1.68
CI11	32	8100	5.8	8.9	289	28.6	23.8	17.5	1.63
CI12	32	5800	5.8	8.9	289	27.5	26.3	15.6	1.76
CI13	32	10500	5.8	8.9	289	34.8	22.2	18.9	1.84
CI14	32	10700	5.8	8.9	462	37.0	25.2	26.2	1.41
CI15	32	10200	5.8	8.9	289	27.2	22.4	18.7	1.45
CI16	32	10600	5.8	9.4	289	36.7	22.2	20.0	1.84
CI17	32	10100	5.8	8.9	112	29.1	17.4	9.5	3.05
								AVE	1.90
								STD DEV	.46

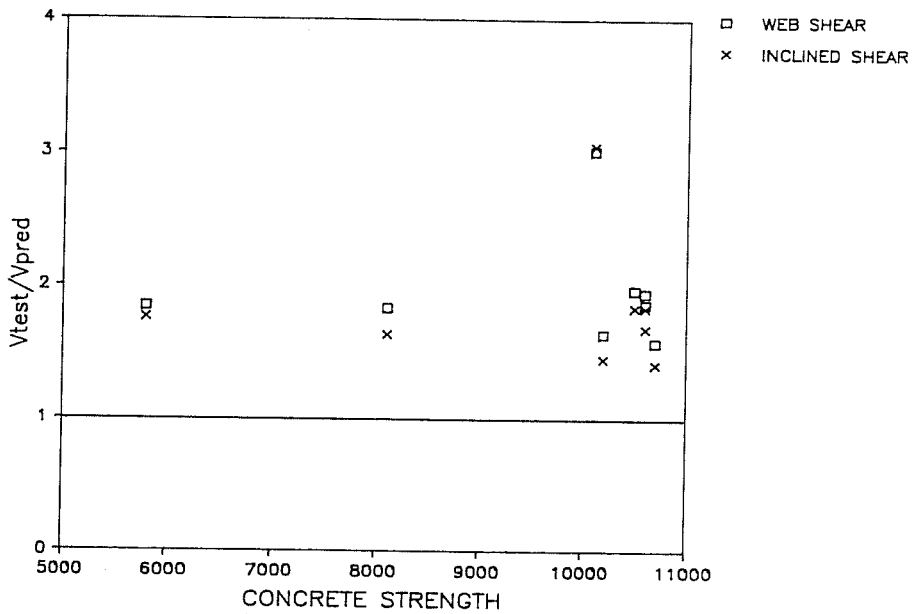

Fig. 3.35 Prestressed beams with stirrups / Canadian Code versus concrete strength.

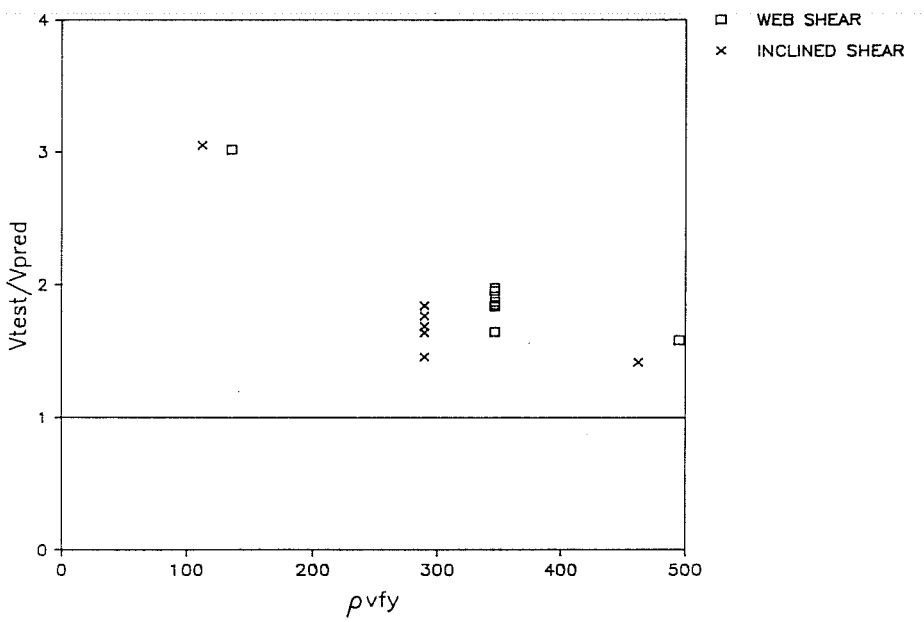

Fig. 3.36 Prestressed beams with stirrups / Canadian Code versus $\rho_v f_y$.

Figure 3.37 shows all the specimens with shear reinforcement plotted against concrete strength. The figure indicates that the Canadian Code General Method is consistent in its prediction of both reinforced and prestressed members. Figure 3.38 shows all the tests plotted versus $\rho_v f_y$. Plotted in this fashion there appears to be a distinction in performance not accounted for by the method. Reinforced and prestressed members show similar behavior for increasing $\rho_v f_y$. A strong possibility for the origin of this change in agreement as previously mentioned is that the method does not consider a concrete contribution. This would also explain why the prestressed specimens were so conservative. Prestress increases the amount of shear resisted by the concrete increasing the conservatism of the results.

3.6.4 Truss Model

3.6.4.1 Reinforced, no stirrups. Table 3.9 gives the predicted values for the concrete contribution for the truss model proposed by Ramirez. For specimens with low shear reinforcement values the truss contribution to V_u is considered to be supplemented by a concrete contribution. In beams with no reinforcement, a case that is strictly not allowed in the truss model, the concrete must carry both compression and tension associated with the shear. The current purpose is to determine if the maximum allowable concrete contribution is conservative for high strength concrete. Since most of the beams were not close to yielding of the longitudinal rein- forcement at the shear failure loads, assumptions were made for z values. A common assumption is that z=7/8 d. For current purposes the smaller of 7/8 d or z at flexural ultimate was used as z. The average test/predicted value was 1.67 with a substantial amount of scatter (Fig. 3.39). The limiting value of concrete contribution to shear is generally conservative.

3.6.4.2 Prestressed, no stirrups. Table 3.10 contains the truss model predictions for prestressed girders with no shear reinforcement. Again the lower estimate of z at ultimate or 7/8 d was used for z. The z at ultimate was based on Code calculations for moment capacity. The d used was a best estimate considering both prestressed and non-prestressed reinforcement. This was necessary since the report did not explicitly state the d for the specimens. A zero value was assumed for v_u in the calculations. All calculated K values were greater than the limit value of 2.0. Ramirez further limited K to 1.0 at sections where the extreme tension fiber stress exceeded $6\sqrt{f'_c}$. As a practical matter K=2.0 was chosen and V_c calculated. This value was used to back calculate a moment and stresses to check the limit on K.

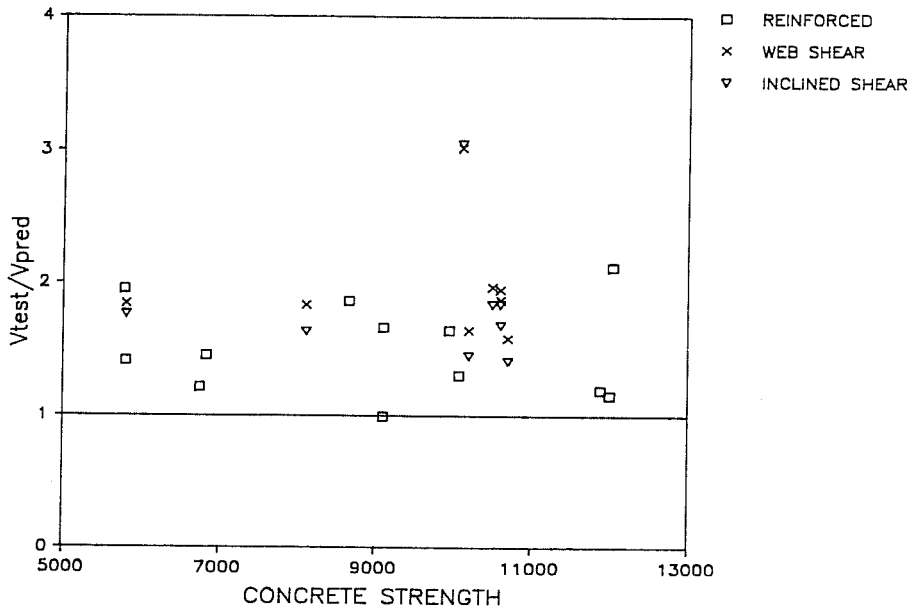

Fig. 3.37 All specimens with stirrups / Canadian Code versus concrete strength.

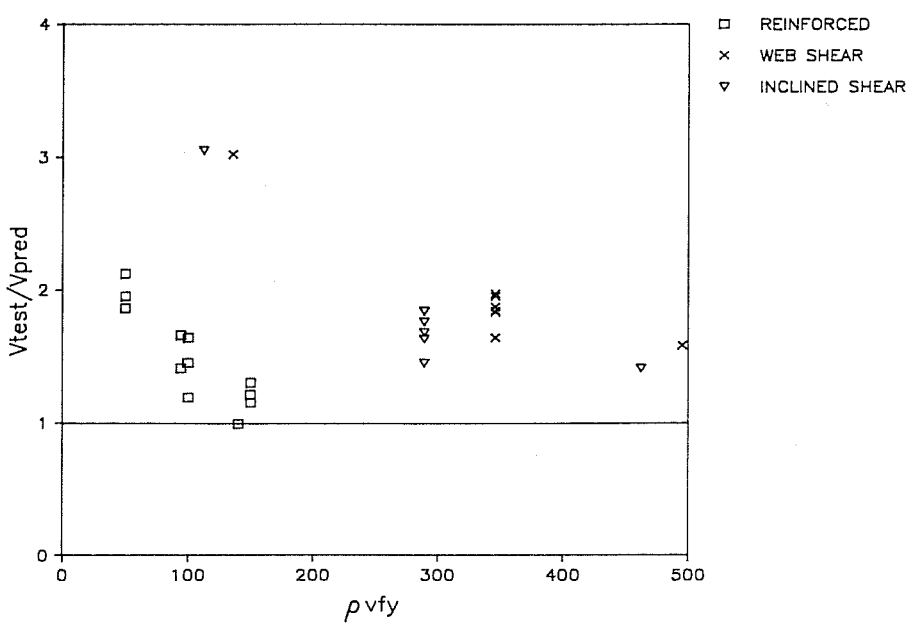

Fig. 3.38 All specimens with stirrups / Canadian Code versus $\rho_v f_y$.

Table 3.9 Truss model predictions for reinforced beams without stirrups

SPECIMEN	SOURCE (REF.)	f'c (psi)	a/d	z (in)	TEST (K) (1)	TRUSS (K) (2)	(1)/(2)
A1	1	8820	4	6.74	13	6.33	2.05
A2	1	8820	3	6.74	14	6.33	2.21
A3	1	8820	2.7	6.74	14	6.33	2.21
A4	1	8820	2.3	6.74	14.3	6.33	2.26
A5	1	8820	2	6.74	17	6.33	2.69
A7	1	8820	4	7.17	8.5	6.73	1.26
A8	1	8820	3	7.17	9.5	6.73	1.41
A9	1	8820	2.7	7.17	11	6.73	1.63
A10	1	8820	2.3	7.17	11	6.73	1.63
A11	1	8820	2	7.17	12	6.73	1.78
B1	1	9720	4	6.49	11.5	6.40	1.80
B2	1	9720	3	6.49	12.75	6.40	1.99
B3	1	9720	2.7	6.49	14	6.40	2.19
B4	1	9720	2.3	6.49	14	6.40	2.19
B5	1	9720	2	6.49	17.5	6.40	2.74
B7	1	9720	4	7.17	10	7.07	1.41
B8	1	9720	3	7.17	10.5	7.07	1.49
B9	1	9720	2.7	7.17	10.5	7.07	1.49
B10	1	9720	2.3	7.17	12.5	7.07	1.77
B11	1	9720	2	7.17	14	7.07	1.98
C1	1	9330	4	5.75	12	5.55	2.16
C2	1	9330	3	5.75	11	5.55	1.98
C3	1	9330	2.7	5.75	9	5.55	1.62
C4	1	9330	2.3	5.75	12.5	5.55	2.25
C5	1	9330	2	5.75	15	5.55	2.70
C7	1	9330	4	7.11	8	6.87	1.16
C8	1	9330	3	7.11	10	6.87	1.46
C9	1	9330	2.7	7.11	10	6.87	1.46
C10	1	9330	2.3	7.11	9.25	6.87	1.35
C11	1	9330	2	7.11	14.5	6.87	2.11

Table 3.9 (continued)

SPECIMEN	SOURCE (REF.)	f'c (psi)	a/d	z (in)	TEST (K) (1)	TRUSS (K) (2)	(1)/(2)
A0-7-3a	03	5460	3.6	8.98	15	7.96	1.88
A0-7-3b	03	6040	3.6	9.25	14	8.63	1.62
A0-11-3a	03	10870	3.6	9.84	15	12.31	1.22
A0-11-3b	03	10820	3.6	9.84	15	12.28	1.22
A0-15-3a	03	11800	3.6	9.84	19	12.83	1.48
A0-15-3b	03	13590	3.6	9.84	22.5	13.77	1.63
A0-15-3c	03	13320	3.6	9.84	21.5	13.63	1.58
A0-7-2	03	6550	2.5	9.44	18	9.17	1.96
A0-11-2	03	11500	2.5	9.84	20	12.66	1.58
A0-15-2a	03	12150	2.5	9.84	24	13.02	1.84
A0-15-2b	03	10060	2.5	9.84	18	11.84	1.52
F1	32	9500	4	9.3	12.9	12.69	1.02
F2	32	9500	4	9.24	14.75	12.61	1.17
F3	32	10000	2	9.3	17.85	13.02	1.37
F4	32	10000	2	9.24	25.5	12.94	1.97
F5	32	9200	6	9.3	9.65	12.49	.77
F6	32	9200	6	9.24	13.5	12.41	1.09
F8	32	5800	4	9.38	10.05	10.00	1.00
F9	32	11600	4	9.24	14	13.93	1.00
F10	32	9500	4	9.18	16.83	12.53	1.34
F13	32	5800	4	8.96	10.7	9.55	1.12
F14	32	5800	4	8.92	14.25	9.51	1.50
F15	32	11300	4	9.24	14.9	13.75	1.08
						AVE	1.67
						STD DEV	.46

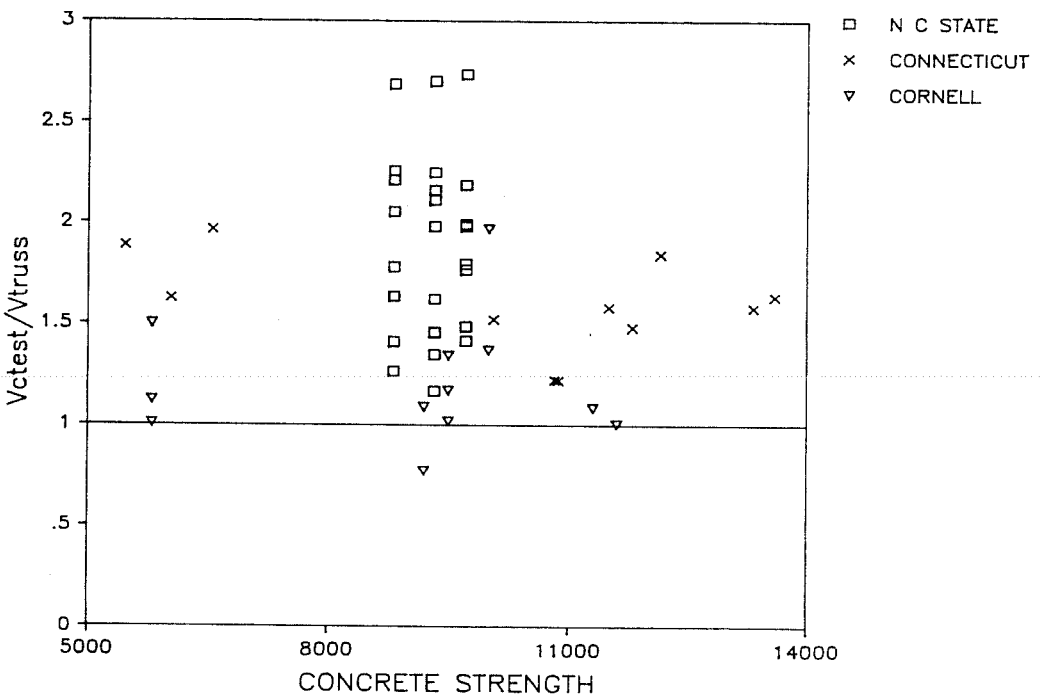

Fig. 3.39 Reinforced beams without stirrups / Eq. (3.64) of truss model versus concrete strength.

Table 3.10 Truss model predictions for prestressed beams without stirrups

SPECIMEN	SOURCE (REF.)	f'c	a/d	z (in)	K act	K all	TEST (K) (1)	Vc (K) (2)	(1)/(2)
CW1	32	11100	2.9	12.4	2.95	2.00	31.1	10.5	2.98
CW2	32	11100	3.75	12.4	2.93	2.00	28.0	10.5	2.68
CW3	32	11100	5	12.4	2.94	2.00	26.4	10.5	2.53
CW4	32	11400	3.75	12.4	2.95	2.00	28.6	10.6	2.70
CW5	32	11300	3.75	11.9	2.94	2.00	27.9	10.1	2.76
CW6	32	11300	3.75	12.4	2.57	2.00	25.2	10.5	2.39
CW7	32	11250	3.75	12.7	2.60	2.00	23.8	10.8	2.21
CW8	32	6000	3.75	9.7	2.95	2.00	20.2	6.0	3.36
CW9	32	8850	3.75	11.8	2.72	2.00	22.7	8.9	2.56
CW10	32	10600	3.75	12.6	2.59	2.00	24.4	10.4	2.35
CW11	32	8100	3.75	12.6	2.72	2.00	21.5	9.1	2.37
CW12	32	5800	3.75	9.4	2.93	2.00	19.2	5.7	3.35
CW13	32	10500	3.75	12.3	2.98	2.00	27.6	10.1	2.74
CW14	32	10700	3.75	12.3	2.98	2.00	27.8	10.2	2.73
CW15	32	10200	3.75	11.3	2.60	2.00	22.6	9.1	2.48
CW16	32	10600	3.75	11.6	2.98	2.00	27.5	9.6	2.88
CW17	32	10100	3.75	12.6	3.02	2.00	27.7	10.1	2.73
CI1	32	11100	7.8	8.7	2.84	2.00	17.5	11.0	1.59
CI2	32	11100	5.8	8.7	2.83	2.00	26.0	11.0	2.36
CI3	32	11100	4	8.7	2.84	2.00	27.2	11.0	2.47
CI4	32	11400	5.8	8.4	2.84	2.00	24.4	10.8	2.27
CI5	32	11300	5.8	9.2	2.83	2.00	26.9	11.7	2.29
CI6	32	11300	5.8	8.7	2.48	2.00	20.0	11.1	1.80
CI7	32	11250	5.8	8.7	2.51	2.00	18.3	11.1	1.65
CI8	32	6000	5.8	8.6	2.85	2.00	19.2	8.0	2.40
CI9	32	8850	5.8	8.7	2.63	2.00	19.6	9.8	2.00
CI10	32	10600	5.8	8.7	2.51	2.00	18.8	10.7	1.75
CI11	32	8100	5.8	8.7	2.63	2.00	18.0	9.4	1.92
CI12	32	5800	5.8	8.6	2.83	2.00	18.6	7.9	2.37
CI13	32	10500	5.8	8.7	2.87	2.00	18.0	10.7	1.68
CI14	32	10700	5.8	8.7	2.88	2.00	24.2	10.8	2.24
CI15	32	10200	5.8	8.7	2.51	2.00	17.6	10.5	1.67
CI16	32	10600	5.8	9.2	2.88	2.00	26.3	11.4	2.31
CI17	32	10100	5.8	8.7	2.91	2.00	25.5	10.5	2.43
								AVE	2.38
								STD DEV	.44

The actual/predicted value was 2.38 with moderate scatter. Little can be said about the model other than it is quite conservative. Figure 3.40 shows the results graphically.

3.6.4.3 Reinforced, with stirrups. The results of reinforced beams with shear reinforcement are given in Table 3.11. The same assumptions for z were used as above. In these specimens a v_u value consistent with the final predicted V_u was desired for computing V_c. Since the specimens were in the transition zone, V_c changed as the truss contribution changed. Figure 3.41 shows the relative contribution of V_c and V_{tr} for various V_u values. For computation purposes

$$V_u = 2\sqrt{f_c'} b_w z + (2/3) * V_{tr} \tag{3.73}$$

The truss contribution can be calculated given section properties, shear reinforcement, and an assumption for α. After V_u is obtained, V_c can be calculated and a check made that $V_c + V_{tr} + V_u$. Also, a check must be made that $V_c > 0$. Finally, the diagonal compression strut stresses must be checked to insure that an appropriate value of α was originally chosen.

The test/predicted value was 1.42 with only moderate scatter. The data shows a tendency towards decreasing conservatism as concrete strength increases (Fig. 3.42). The data is more sensitive to changes in $\rho_v f_y$ (Fig. 3.43). There is a general decrease in conservatism as $\rho_v f_y$ increases. This may in part be due to underestimating the concrete contribution at low $\rho_v f_y$ values. Figure 3.44 shows the diagonal compressive strut stress/allowable stress versus $\rho_v f_y$. The percentage increases steadily with increasing $\rho_v f_y$.

3.6.4.4 Prestressed, with stirrups. Truss model predictions for the prestressed beams with stirrups are given in Table 3.12. The same z values were used as in Section 3.6.4.2. Approximately half the shear span had an extreme tension fiber stress greater than $6\sqrt{f_c'}$ so K=1.0 was used throughout.

A value of $\alpha = 25°$ was assumed for each specimen. The procedure outlined in Section 3.6.4.3 was used again. It should be noted that if K=2.0 the concrete contribution decreases more rapidly giving $V_u = V_c + 1/2V_{tr}$. It was found that for all but 2 specimens the concrete contribution was zero. Those two specimens had light shear reinforcement. The average test/predicted value was 2.11 with substantial scatter. The

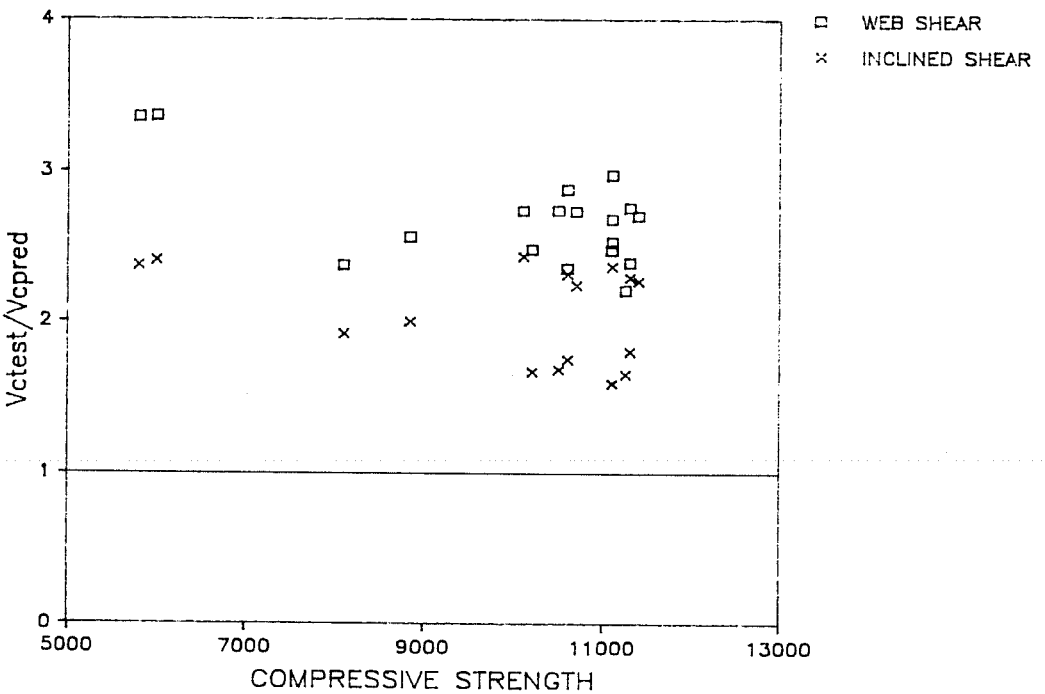

Fig. 3.40 Prestressed beams without stirrups / truss model predictions versus concrete strength.

Table 3.11 Truss model predictions for reinforced beams with stirrups

SPECIMEN	SOURCE (REF.)	f'c	a/d	pvfy (psi)	z (in)	TEST (K) (1)	Vc EQ (3.) (K) (2)	ø (°)	Vtr EQ (3.) (K) (3)	Vtot (2)+(3) (K) (4)	(1)/(4)
B50-7-3	03	5780	3.6	50	9.14	21.1	6.4	25.0	5.9	12.3	1.72
B50-11-3	03	8660	3.6	50	10.01	22.0	9.0	25.0	6.4	15.5	1.42
B50-15-3	03	12030	3.6	50	10.28	25.0	11.3	25.0	6.6	17.9	1.39
B100-7-3	03	6830	3.6	100	9.54	27.1	5.4	25.0	12.3	17.6	1.54
B100-11-3	03	9950	3.6	100	10.23	34.1	7.9	25.0	13.2	21.0	1.62
B100-15-3	03	11880	3.6	100	10.28	26.0	9.0	25.0	13.2	22.3	1.17
B150-7-3	03	6750	3.6	150	9.51	30.0	3.3	25.0	18.4	21.6	1.39
B150-11-3	03	10080	3.6	150	10.25	36.3	5.8	25.0	19.8	25.5	1.42
B150-15-3	03	12000	3.6	150	10.49	33.7	7.0	25.0	20.2	27.3	1.24
G3	32	9100	4	140	9.12	26.4	5.8	25.0	19.2	25.0	1.06
G4	32	9100	4	94	9.12	33.1	7.9	25.0	12.9	20.8	1.59
G5	32	5800	4	94	8.76	25.5	5.2	25.0	12.4	17.6	1.45
										AVE	1.42
										STD DEV	.18

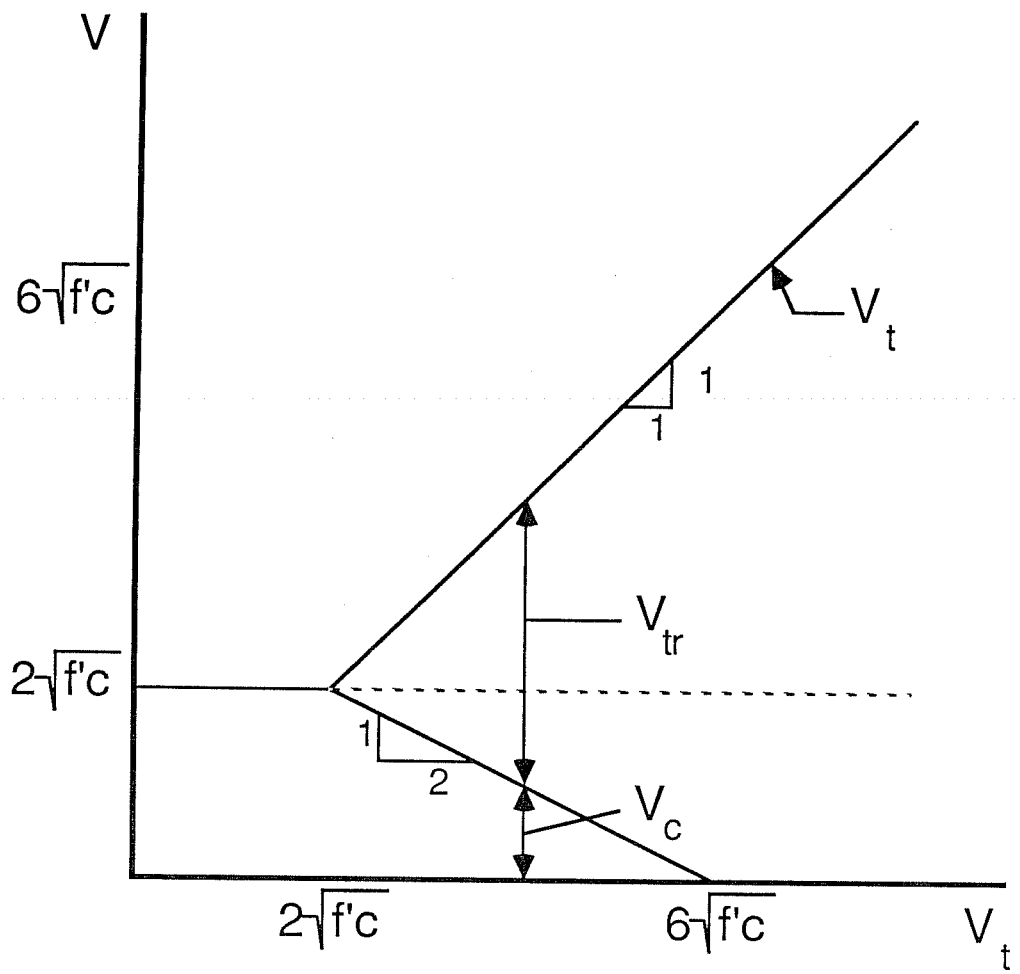

Fig. 3.41 Truss contribution in the transition zone.

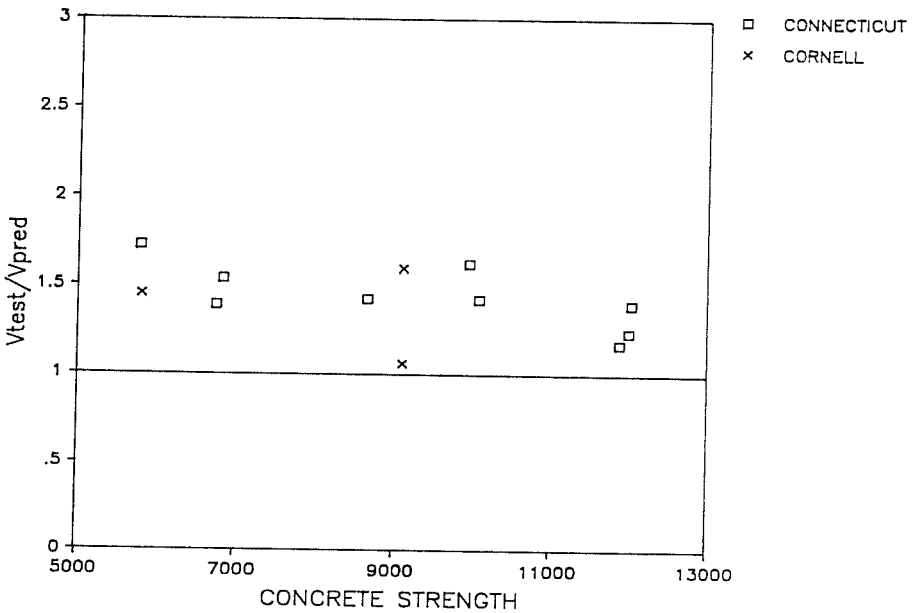

Fig. 3.42 Reinforced beams with stirrups / truss model versus concrete strength.

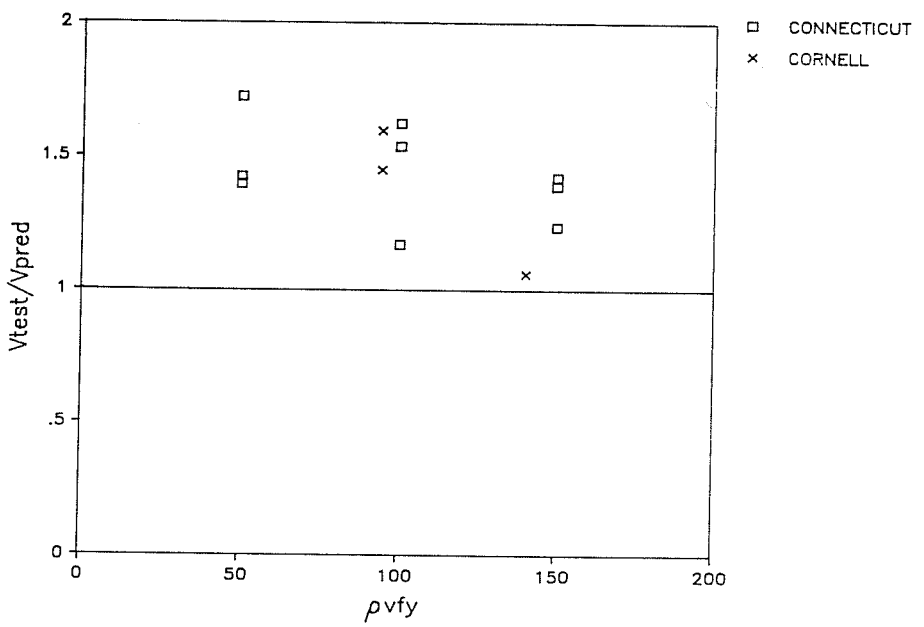

Fig. 3.43 Reinforced beams with stirrups / truss model versus $\rho_v f_y$.

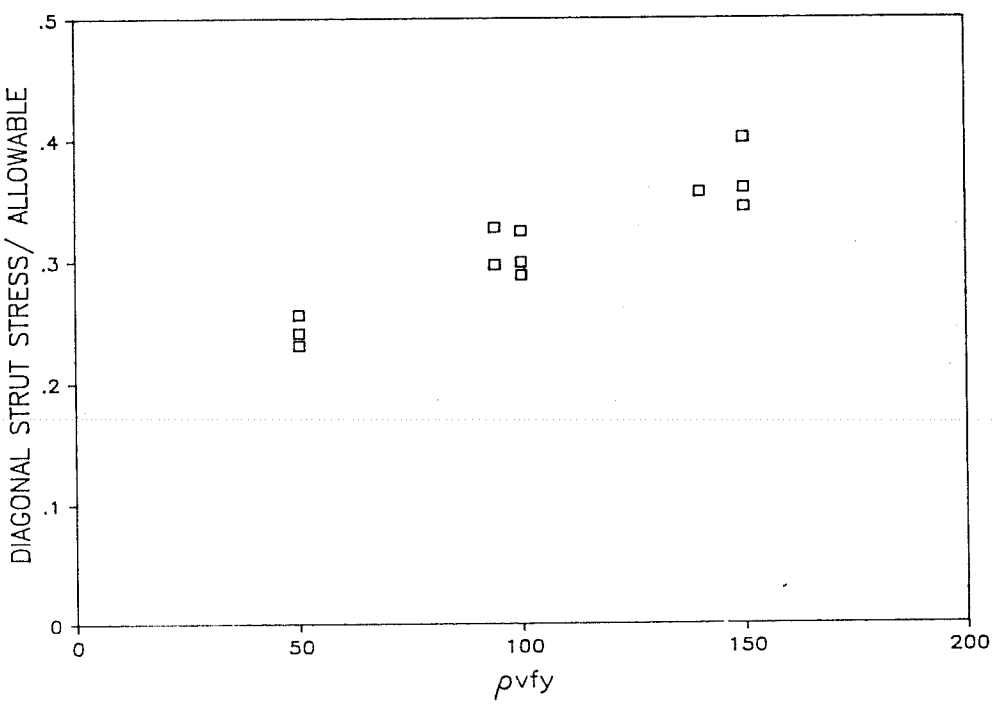

Fig. 3.44 Inclined compression diagonal stress at failure/ allowable versus $\rho_v f_y$.

Table 3.12 Truss model predictions for prestressed beams with stirrups

SPECIMEN	SOURCE (REF.)	f'c	z (in)	pvfy (psi)	K all	α (°)	TEST (K) (1)	Vc (K) (2)	Vtr (K) (3)	Vc+Vtr (K) (4)	(1)/(4)
CW10	32	10600	12.6	346	1.0	25.0	39.0	.0	18.7	18.7	2.09
CW11	32	8100	12.6	346	1.0	25.0	35.2	.0	18.7	18.7	1.88
CW12	32	5800	9.4	346	1.0	25.0	31.6	.0	13.9	13.9	2.27
CW13	32	10500	12.3	346	1.0	25.0	41.0	.0	18.3	18.3	2.25
CW14	32	10700	12.3	495	1.0	25.0	42.2	.0	26.1	26.1	1.62
CW15	32	10200	11.3	346	1.0	25.0	33.8	.0	16.8	16.8	2.02
CW16	32	10600	11.6	346	1.0	25.0	42.0	.0	17.2	17.2	2.44
CW17	32	10100	12.6	135	1.0	25.0	32.0	2.6	7.3	9.9	3.22
CI10	32	10600	8.7	289	1.0	25.0	31.8	.0	16.2	16.2	1.97
CI11	32	8100	8.7	289	1.0	25.0	28.6	.0	16.2	16.2	1.77
CI12	32	5800	8.6	289	1.0	25.0	27.5	.0	16.0	16.0	1.72
CI13	32	10500	8.7	289	1.0	25.0	34.8	.0	16.2	16.2	2.15
CI14	32	10700	8.7	462	1.0	25.0	37.0	.0	25.9	25.9	1.43
CI15	32	10200	8.7	289	1.0	25.0	27.2	.0	16.2	16.2	1.68
CI16	32	10600	9.2	289	1.0	25.0	36.7	.0	17.1	17.1	2.15
CI17	32	10100	8.7	112	1.0	25.0	29.1	3.2	6.3	9.4	3.09
										AVE	2.11
										STD DEV	.47

results are plotted against concrete strength in Figure 3.45. The results were also plotted against $\rho_v f_y$ (Fig. 3.46). The trend of decreasing conservatism as $\rho_v f_y$ increases is again apparent. Shear failures originating from inclined cracking are somewhat less conservatively predicted than those originating from web shear cracking. The extreme conservatism at low $\rho_v f_y$ values would indicate that the method substantially underestimates the concrete's contribution. Figure 3.47 shows the concrete compression strut stress/allowable versus $\rho_v f_y$.

3.6.5 Summary. The numerical predictions for each of the three models have been compared to the available test results. On average all models were conservative for all cases. There were, however, a number of tests that were unconservative. The amount of scatter in the data as indicated by the standard deviation varied considerably between models and between types of beams.

The different methods will be evaluated statistically as a means of comparing relative accuracies. For present purposes values at which there is 95% confidence that 90% of the values are above and that 90% of the values are below will be computed. This particular choice of confidence level and limits is somewhat arbitrary, but will serve current purposes. The values computed give an indication on how closely the model predicts behavior. Line 1 of Figure 3.48 shows data that is very tightly bunched about the mean. This indicates a model that is highly accurate. Line 2 on the other hand would represent a model with considerable scatter in its predictions.

Table 3.13 contains the results of the statistical evaluation. Upper and lower confidence limits were computed by:

$$X = x \pm K\mu$$

where K is a factor dependent on the confidence level, percent of members above or below, and the number of test points [31]. Values of K not explicitly given were obtained through interpolation. The results given for reinforced beams are based on Equation 3.3. The results for prestressed beams are based on using the appropriate values of V_{ci} or V_{cw}. The comparison will only be conducted for members with shear reinforcement at ultimate since both Canadian and truss methods are not meant for unreinforced members.

The results are shown graphically in Figure 3.49. It is quite obvious that the AASHTO/ACI equations give accurate results and that they give the smallest scatter.

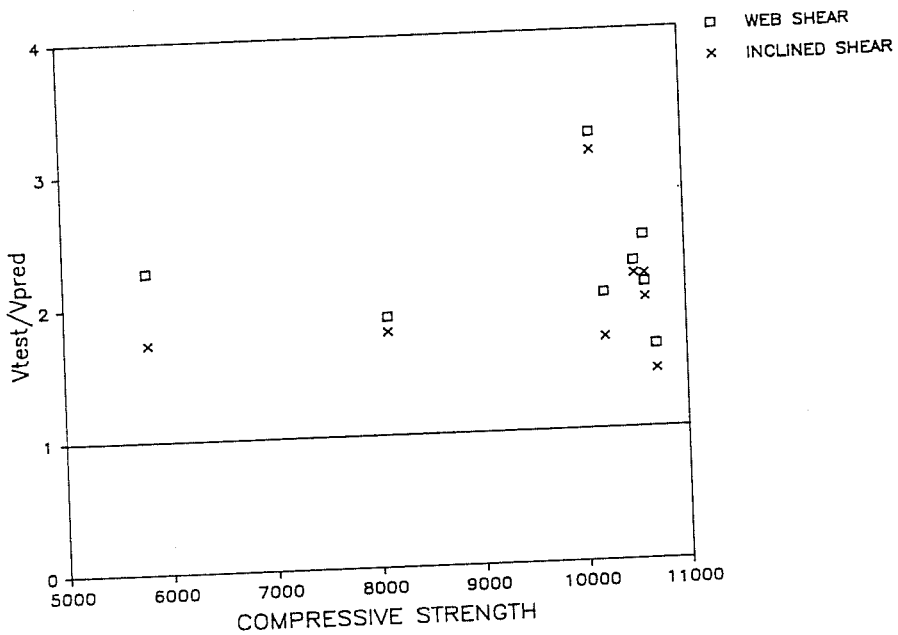

Fig. 3.45 Prestressed beams with stirrups / truss model versus concrete strength.

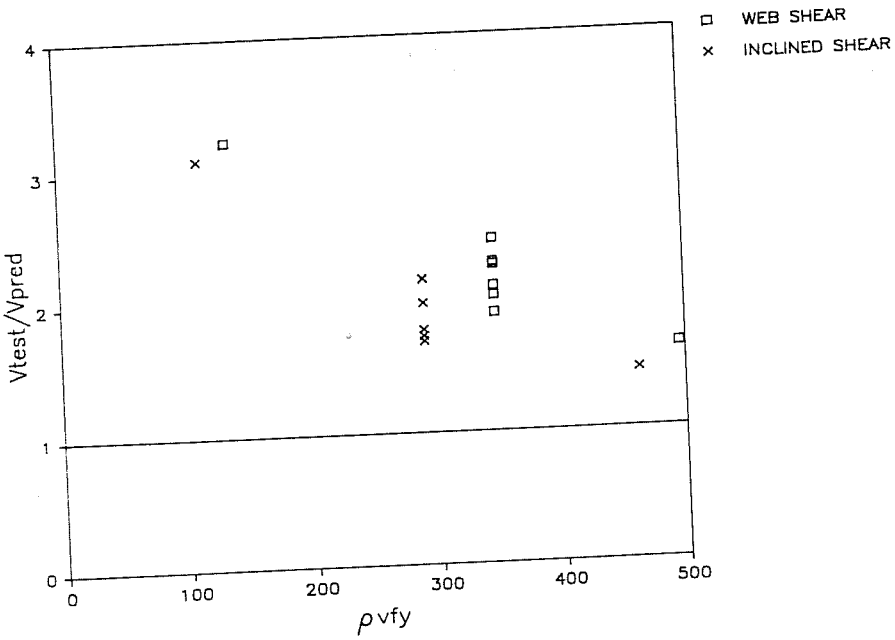

Fig. 3.46 Prestressed beams with stirrups / truss model versus $\rho_v f_y$.

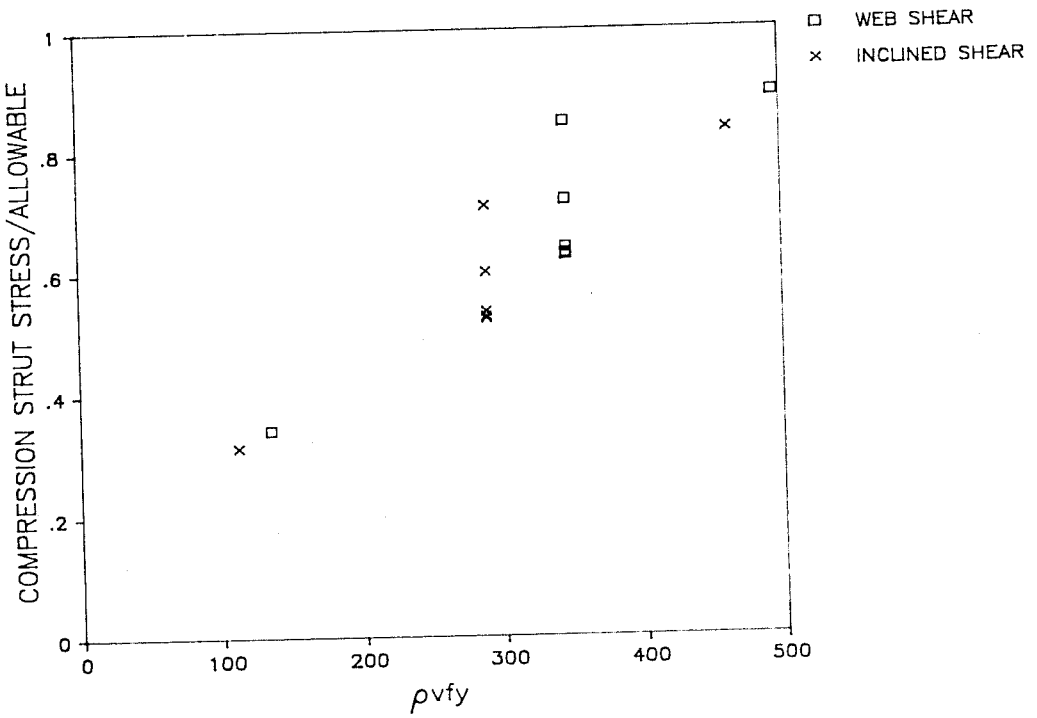

Fig. 3.47 Inclined compression diagonal stress at failure/ allowable versus $\rho_v f_y$.

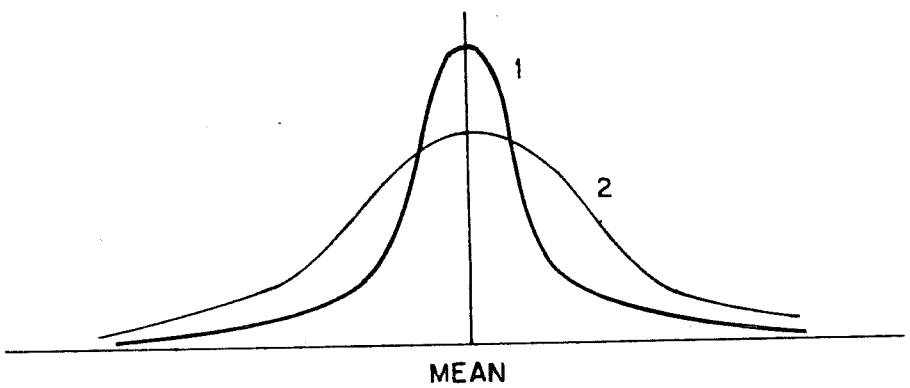

Fig. 3.48 Relative scatter for well bunched and widely scattered data.

Table 3.13 Statistical comparison of model predictions

METHOD		REIN. CRACKING (N=53)	REIN. ULTIMATE (N=12)	PRES. CRACKING (N=34)	PRES. ULTIMATE (N=16)
ACI	MEAN	1.27	1.32	1.16	1.16
	STD DEV	.25	.14	.07	.06
	UP. LIMIT	1.68	1.62	1.28	1.28
	LOW LIMIT	.86	1.02	1.04	1.04
CANADIAN	MEAN	---	1.49	---	1.9
	STD DEV	---	.34	---	.46
	UP. LIMIT	---	2.23	---	2.82
	LOW LIMIT	---	.75	---	.98
TRUSS	MEAN	1.67	1.42	2.38	2.11
	STD DEV	.46	.18	.44	.47
	UP. LIMIT	2.42	1.81	3.14	3.05
	LOW LIMIT	.92	1.03	1.62	1.17

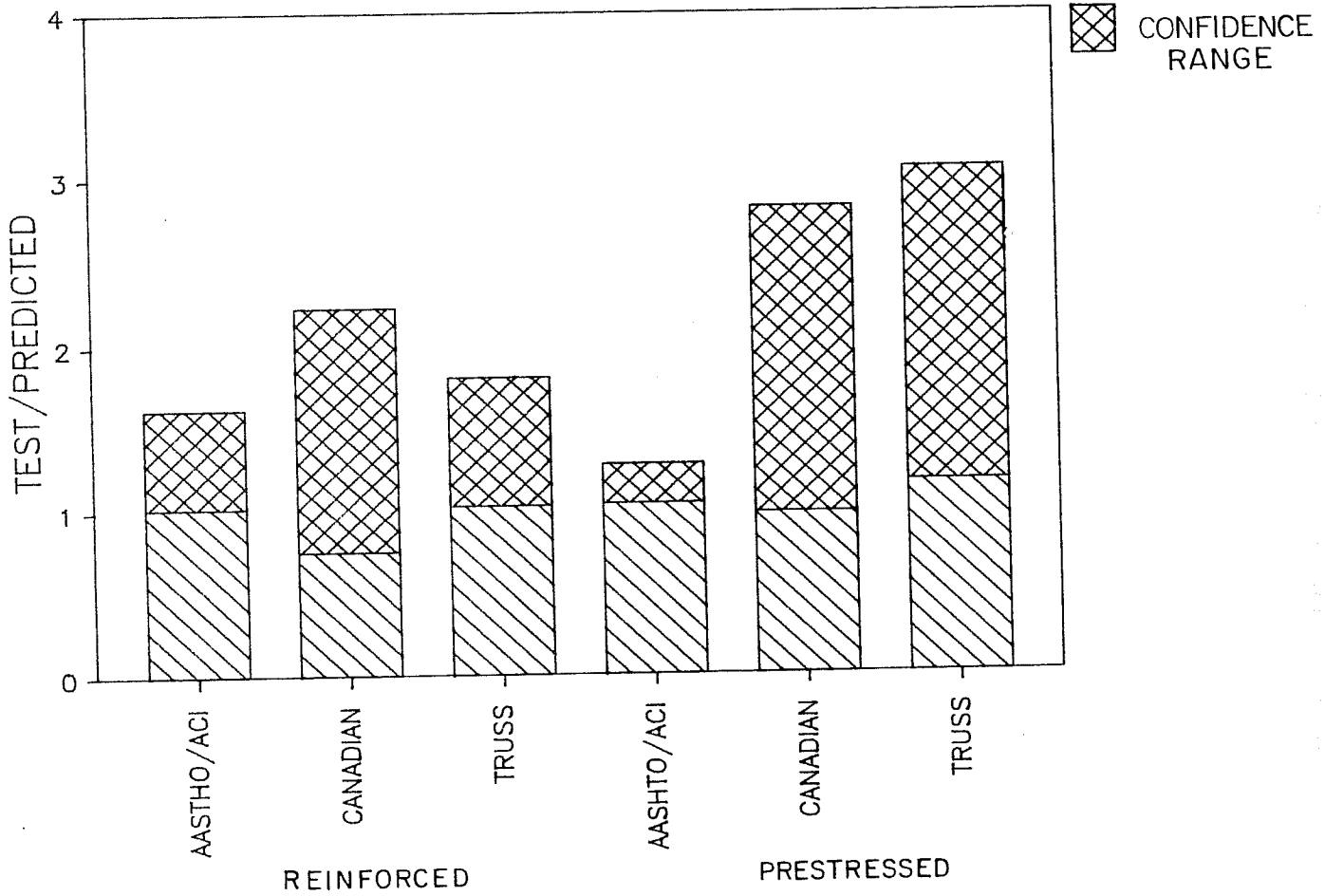

Fig. 3.49 Statistical comparison of the methods for reinforced and prestressed concrete at ultimate.

The Canadian Code General Method gives substantial scatter. Furthermore the limit values for both reinforced and prestressed beams are below one. The truss model gives substantial scatter. The truss model does, however, give limit values greater than one. So far as accuracy goes AASHTO/ACI does the best job for high strength members reported failing in shear.

One important question at the outset of this investigation was what trends would form in the data as concrete strength increases. While a few isolated tests conducted holding all but the concrete strength constant may show some trend, the data base taken as a body shows little change in conservatism with changing concrete strength. Factors such as a/d ratio, percentage of longitudinal reinforcement, and level of shear reinforcement all showed much greater influences than concrete strength. For the available test results, increasing concrete strength has not made the current methods evaluated unconservative.

CHAPTER 4
EXPERIMENTAL PROGRAM

4.1 Introduction

The goal of the experimental portion of this program was to determine the failure loads and behavior in shear of prestressed girders made of high strength concrete. The specimens were designed to examine a wide range of shear reinforcement values. The reinforcement values were chosen to fill gaps in the meager existing data base for shear tests of high strength prestressed concrete beams.

Ten shear tests were performed in this project. Six girders were cast specifically as shear specimens. The other four shear tests were conducted on end sections of the flexural specimens tested by Castrodale [13]. Further information on the flexural tests of these specimens are contained in the companion report 381-3. The six shear specimens were a modified version of the flexural specimens. The six shear specimens had a shear span to depth ratio, a/d, of 3.0 while the end sections of the flexural specimens had an a/d ratio of 3.2.

The amount of shear reinforcement was the primary variable in this investigation. Shear reinforcement values, V_s, ranged from zero to $15\sqrt{f'_c}b_w d$. The quantity of shear reinforcement had a direct effect on the size and spacing of the web reinforcement.

Several minor variables were considered as well. The location of supports proved critical to behavior. Several stirrup details were evaluated. The effects of concrete strength and prestress force on shear cracking were also studied.

4.2 Description and Design of Test Specimens

4.2.1 Series 1. Series 1 consisted of three girders. Figure 4.1 shows the cross-section dimensions and properties of the section used in Series 1 and 2. All girders were 16 ft long. The shear and flexural reinforcement used in Series 1 is shown in Figure 4.2. Throughout the project the prestressing strands were placed in a grid pattern 1 1/4" on center. Load points and support locations are illustrated in Figure 4.3. All three girders of this series were cast at one time using a long line prestressing bed. This assured identical concrete and prestress force in all three girders.

The primary variable was the amount of shear reinforcement. Specimen 1-1 had no shear reinforcement excluding end detail steel which extended from the end of the girder to 7.5 inches into the shear span past the support centerline (Fig. 4.4).

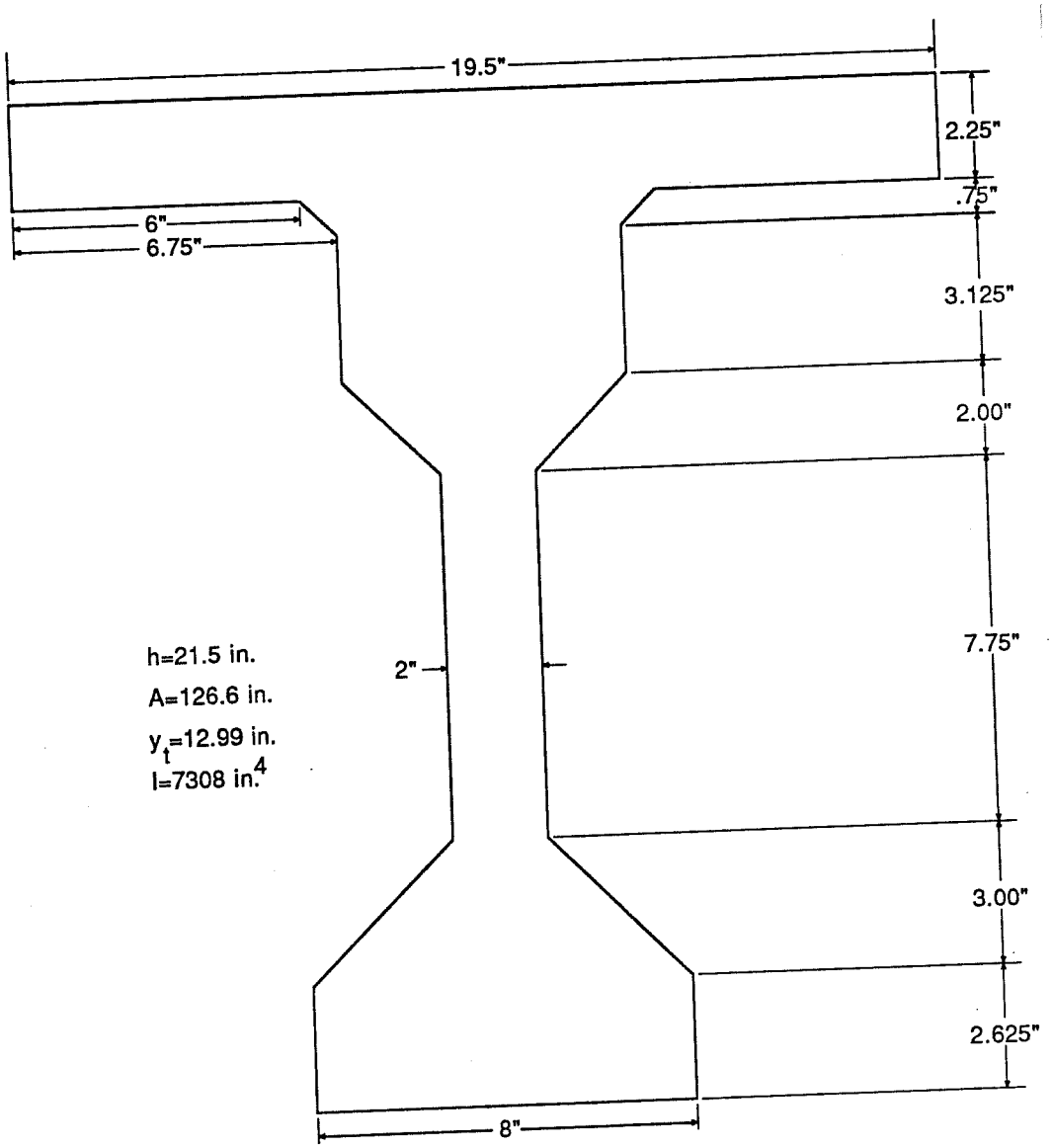

Fig. 4.1 Series 1 and 2 cross-section.

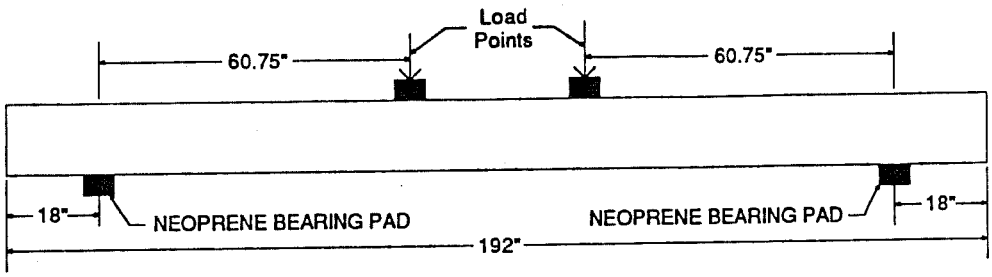

Fig. 4.3 Load and support locations for Series 1

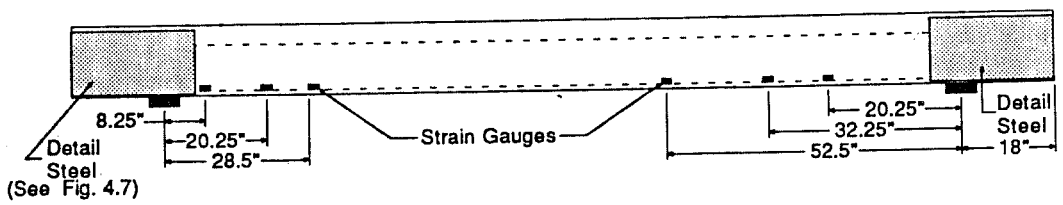

Fig. 4.4 Specimen 1-1 strain gauge locations V_s=0.

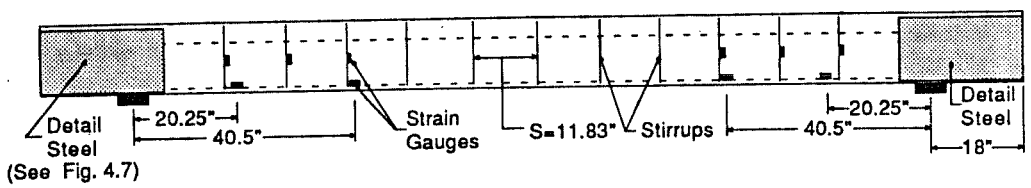

Fig. 4.5 Specimen 1-2 stirrup and stain gauge locations V_s= 50 b_wd.

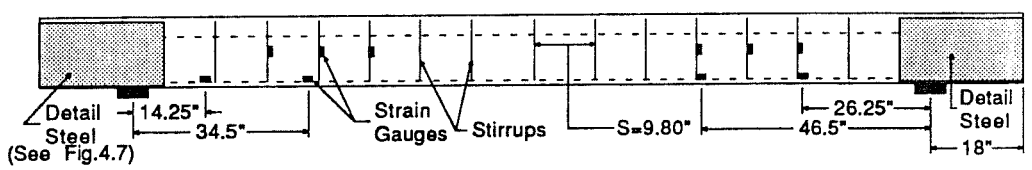

Fig. 4.6 Specimen 1-3 stirrup and strain gauge locations $V_s = 1\sqrt{f'_c}b_w d = 109 b_w d$.

Specimen 1-2 had the Code minimum $V_s=50b_wd$ of shear reinforcement. To maintain spacing limits, special #1.5 Mexican deformed reinforcing bars were used for the shear reinforcement. The location of the normal stirrups in the shear span as well as the location of internal strain gauges is shown in Figure 4.5. In all girders a pair of stirrups were used at each stirrup location. Specimen 1-3 had a $V_s = 1\sqrt{f'_c}b_w d$ equivalent web reinforcement quantity using a nominal concrete strength of 12000 psi. The $1\sqrt{f'_c}$ was 109 psi. In this specimen #2 Mexican deformed reinforcement was used due to spacing considerations. The stirrup spacing and strain gauge locations for Specimen 1-3 are shown in Figure 4.6.

Each specimen was designed so that the flexural capacity would be moderately, about 1.33 times, higher than the expected shear capacity as estimated using ACI/AASHTO Code provisions [2,5]. For design purposes a nominal concrete strength of 12000 psi was used. V_{cw} and V_{ci} were calculated using an estimate for the prestress force. Web shear cracking, V_{cw}, controlled for all specimens of this project. The estimate of the total shear force, V_n, was $V_n = V_{cw} + V_s$. Since all three girders were cast long line, the prestress force had to be the same for all. Specimen 1-3 controlled the design. Adjustments in the design were made until the reinforcement provided the behavior desired.

The prestressed reinforcement was designed to satisfy both release stress limits and ultimate strength requirements. AASHTO requirements for tendon stresses and concrete release stresses were met. Prestress loss calculations were also performed to estimate prestress force at the time of test. This prestress force was used to estimate the concrete contribution. The ultimate flexural capacity was determined using a slightly modified version of program MOMCURV developed by Castrodale [13]. The modification consisted of using a triangular stress block for the entire compression zone including the deck.

In addition to the main longitudinal and web reinforcement, the girders had some auxiliary reinforcement. The most important was the end detail steel. The detail steel, shown in Figure 4.7, was used in all girders of Series 1 and 2 including Specimen 1-1 which had no other shear reinforcement. End detail steel stirrups were the same size as the stirrups used as the main shear reinforcement. No. 1.5 stirrups were used for Specimens 1-1 and 1-2 while #2 stirrups were used for Specimen 1-3. Design of this detail steel was based on the Texas SDHPT Standard Detail, (Fig. 4.8) and AASHTO

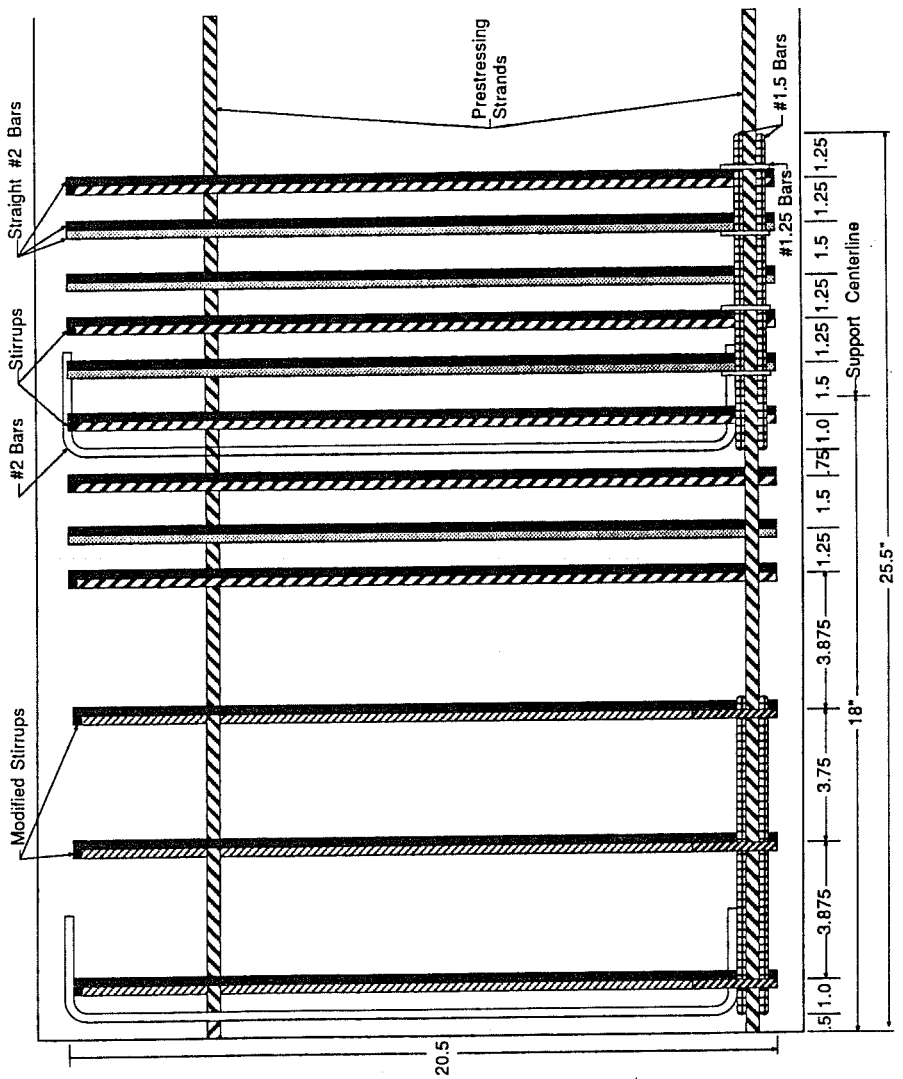

Fig. 4.7 End detail steel (all units in inches).

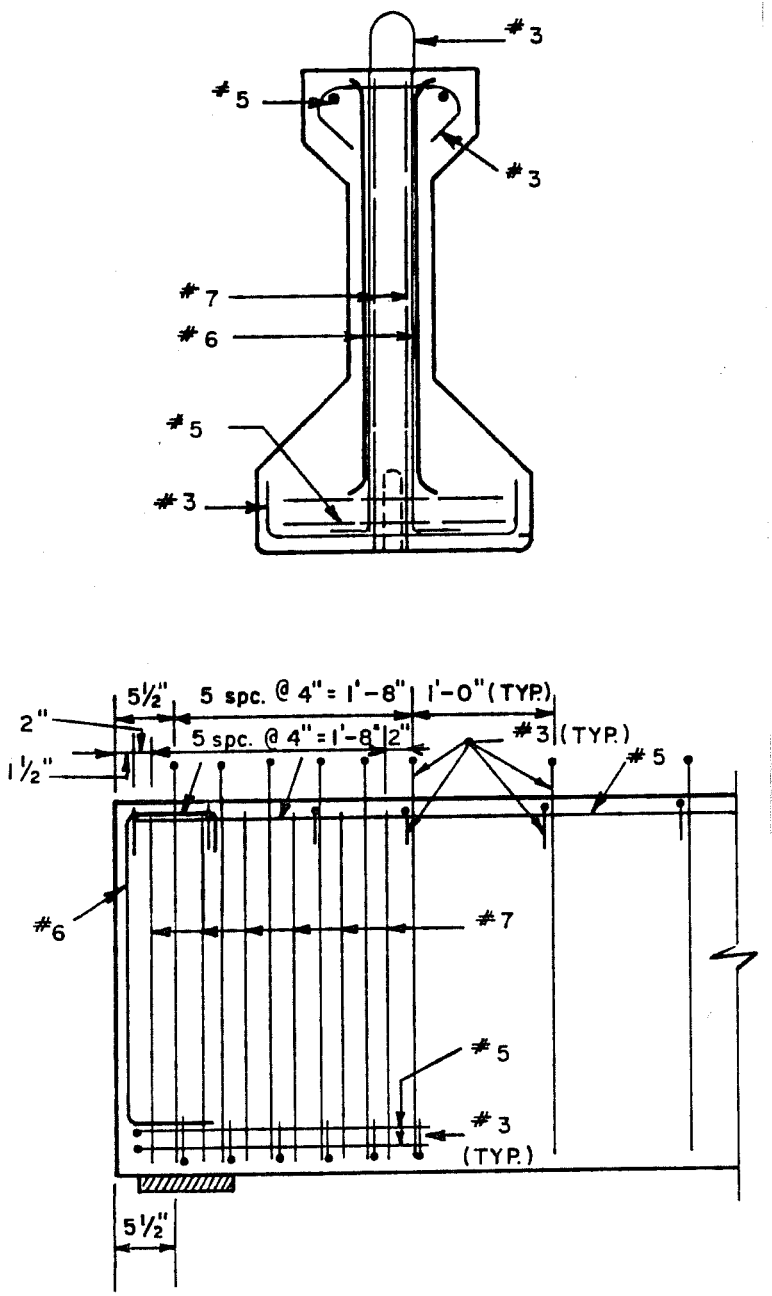

Fig. 4.8 Texas SDH&PT standard end details.

requirements. All girders also had a minimum amount of steel in the deck. The steel was proportioned to satisfy temperature and shrinkage requirements from the ACI.

The cross-section chosen and the support overhang used were governed by considerations of Series 2 and will be discussed therein.

4.2.2 Series 2. Series 2 consisted of three girders. Figure 4.9 shows the location of supports and load points. The cross section and reinforcement are shown in Figure 4.10. The girders were again cast and stressed simultaneously using the long line pretensioning method.

The primary variable in Series 2 was the amount of shear reinforcement. Specimen 2-1 had $V_s = 12\sqrt{f'_c}b_w d$ equivalent shear reinforcement. Specimens 2-2 and 2-3 each had $V_s = 15\sqrt{f'_c}b_w d$ equivalent shear reinforcement. A nominal value of 12000 psi was again used for f'_c. Specimen 2-2 and Specimen 2-3 had different stirrup details as can be seen by comparing the stirrups in Figures 4.10 and 4.11. To maintain a reasonable stirrup spacing #3 bars were used in all beams of Series 2. Figures 4.12 and 4.13 show the stirrup layout and strain gauge locations for Specimen 2-1 and Specimens 2-2 and 2-3 respectively.

The design procedure was essentially the same as described for Series 1. It was desired to keep the same cross-section for both Series 1 and 2. Since Series 2 had the higher shear reinforcement, it was the critical design case. The section chosen was deemed the best of a number of trial sections. The layout of prestressing strands and use of nonprestressed reinforcement was governed by both strength requirements and prestressing bed constraints.

The same end detail reinforcement and deck steel were used as in Series 1 except that the stirrups shown in Figure 4.7 were changed to #3 bars for Series 2.

The decision to use a support overhang came from the desire to prevent an anchorage failure from causing a general shear failure. Based on a comparison of tension chord requirements versus strand development and laboratory constraints, a value of 18 in. from the centerline of the support to the end of the girder was chosen. This overhang was kept constant throughout Series 1 and 2.

4.2.3 Series 3. Series 3 consisted of shear tests performed on the lightly damaged ends of the flexural specimens previously tested by Castrodale. For full details on flexural design of these specimens see Reference [13]. Specimens 3-1 and 3-2 came from opposite ends of the same flexural specimen while Specimens 3-3 and 3-4 did likewise.

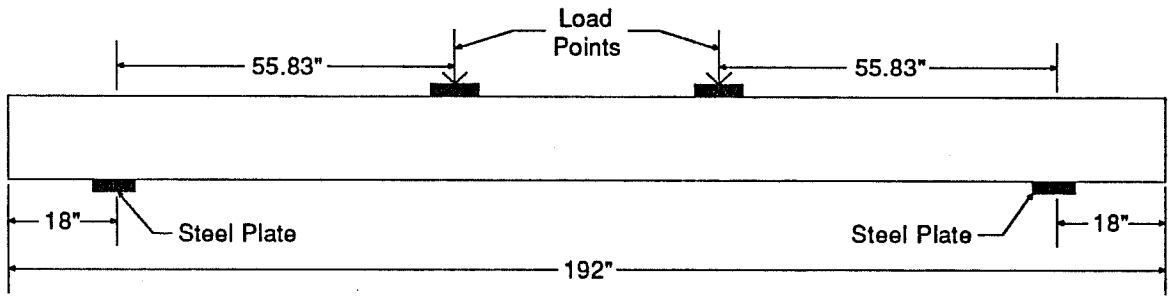

Fig. 4.9 Load and support locations for Series 2

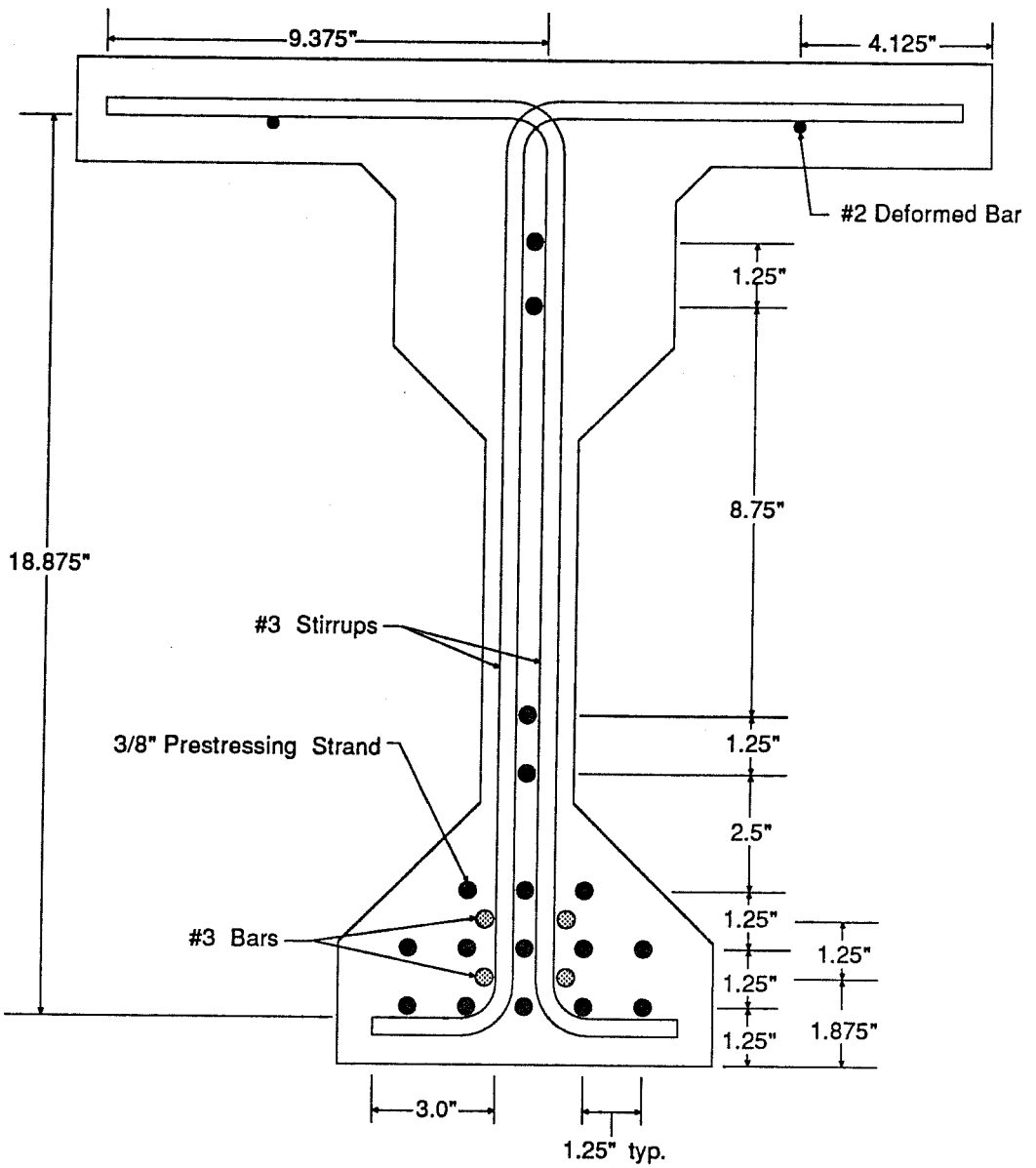

Fig. 4.10 Series 2 reinforcement.

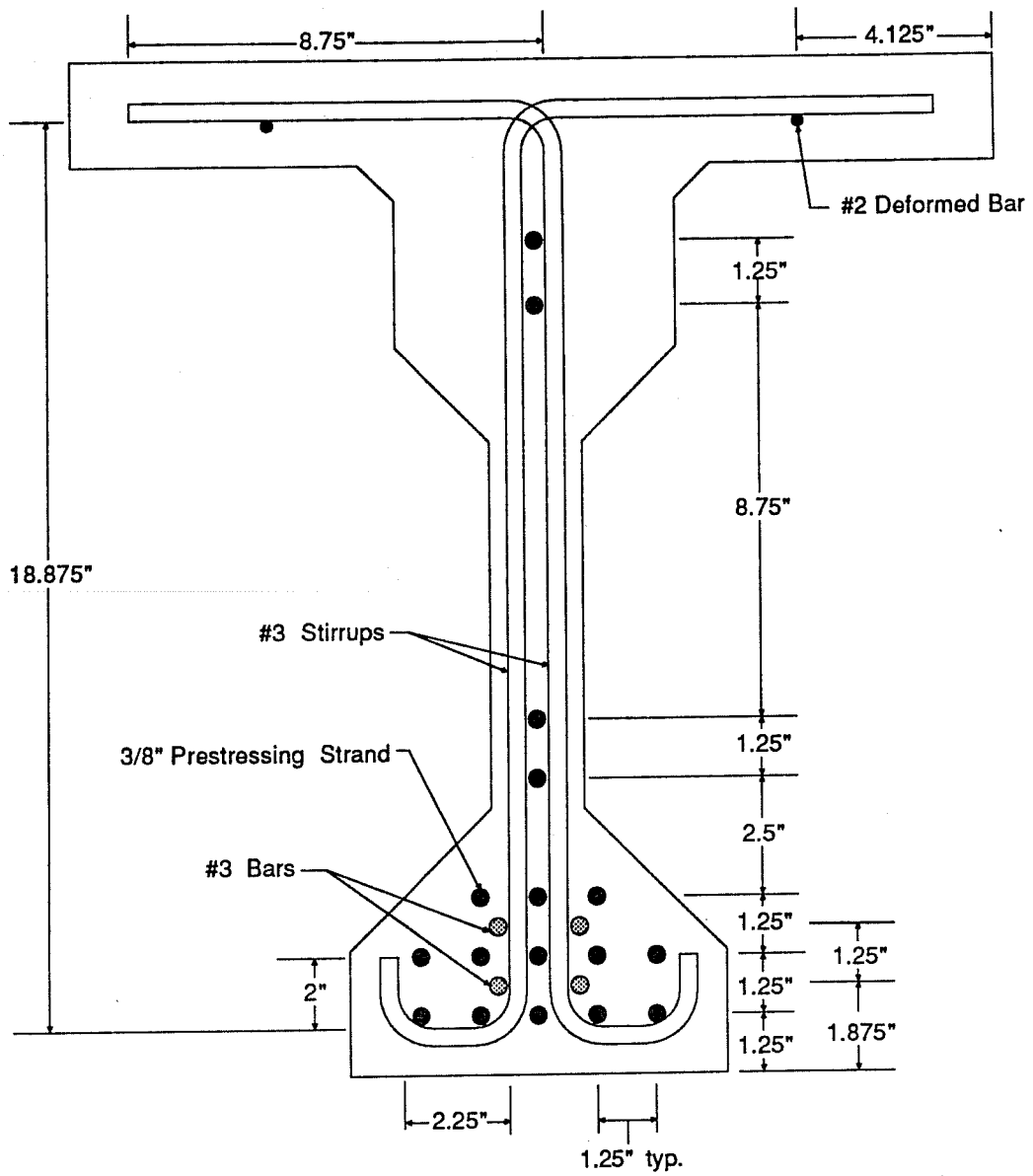

Fig. 4.11 Modified stirrup detail, Specimen 2-3.

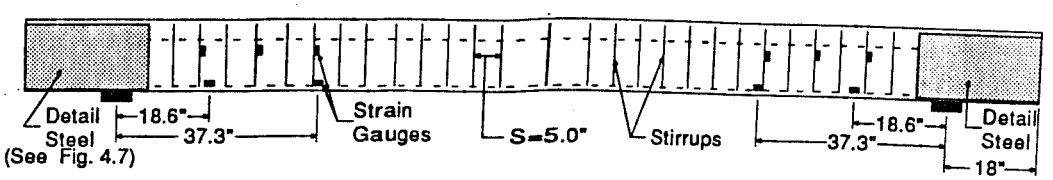

Fig. 4.12 Specimen 2-1 stirrup and strain gauge locations $V_s = 12\sqrt{f'_c}b_w d$.

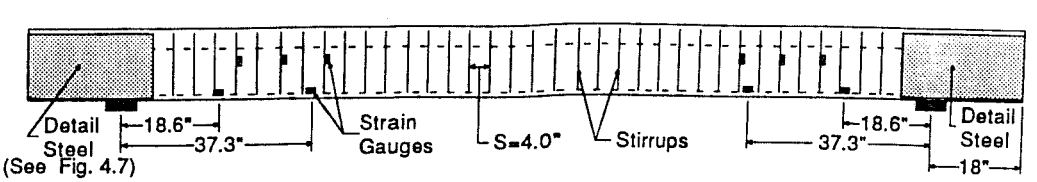

Fig. 4.13 Specimen 2-2 and 2-3 stirrup and strain gauge locations $V_s = 15\sqrt{f'_c}b_w d$.

Since the specimens were principally designed for flexural tests, there were several major differences between the specimens of Series 3 and of Series 1 and 2. The most important was that the Series 3 specimens had the girders and decks cast compositely. The high strength girders were cast and then much lower strength decks were added later. The decks had different widths than the noncomposite Series 1 and 2 specimens. The girders of Series 3 also had inclined prestressing tendons.

Because the specimens were first tested in flexure they had sustained some damage. The original girders were 49 feet long. The concrete at the location of flexural failure basically exploded leaving the prestressing strands exposed. Any remaining concrete was removed and the strands were cut separating the two ends. A total span of 17 ft 4 in. was used during the shear tests with one test having an additional 6" for development (Fig. 4.14). The ends used as shear specimens were approximately half the original 49 feet in length. The additional length was not used in the test and it extended unsupported as an overhang. The observable damage consisted principally of transverse cracks through the deck, some of which went into the girder. The cracks formed during the flexural failure and are likely due both to the dynamics of the failure and the shedding of the dead load blocks used during the flexural strength test. Other damage was suspected, but unobservable since the prestressing closed many of the cracks.

Specimens 3-1 and 3-2 had shear reinforcement of $V_s = 8\sqrt{f'_c}b_w d$ which is the maximum allowed by AASHTO. The cross-section and prestressing strands are shown in Figure 4.15. The major difference between these two specimens was the stirrup details as can be seen by comparing Figures 4.16 and 4.17. The stirrups were all #2 Mexican deformed bar. The stirrup layout and strain gauge locations are shown in Figure 4.18. In both tests actual support locations were modelled. For these specimens slightly different end details were used as illustrated in Figure 4.19a.

Specimens 3-3 and 3-4 had $V_s = 4\sqrt{f'_c}b_w d$. The strand locations and stirrup detail are shown in Figure 4.20. The stirrups were #2 Mexican deformed bar. Specimen 3-3, like Specimens 3-1 and 3-2, had the support location and detail steel modelling that of actual field conditions (Fig. 4.19a). Specimen 3-4 was provided with a 6 inch overhang. The stirrup layout and strain gauge locations are illustrated in Figure 4.21. A special end detail was provided for Specimen 3-4 and it is illustrated in Figure 4.19b.

4.3. Materials

4.3.1 Concrete. The concrete mix was designed to give a 28 day strength of 12000 psi. All batches of concrete were obtained from a local ready mix plant. The

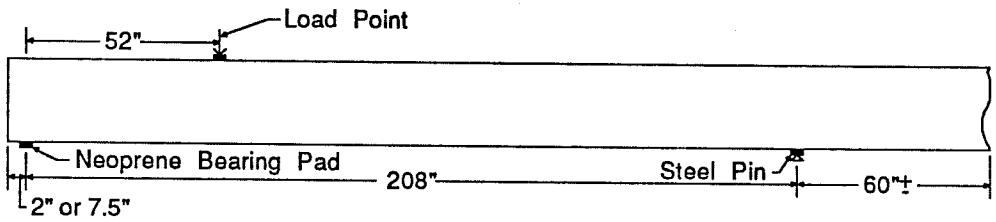

Fig. 4.14 Load and support locations for Series 3.

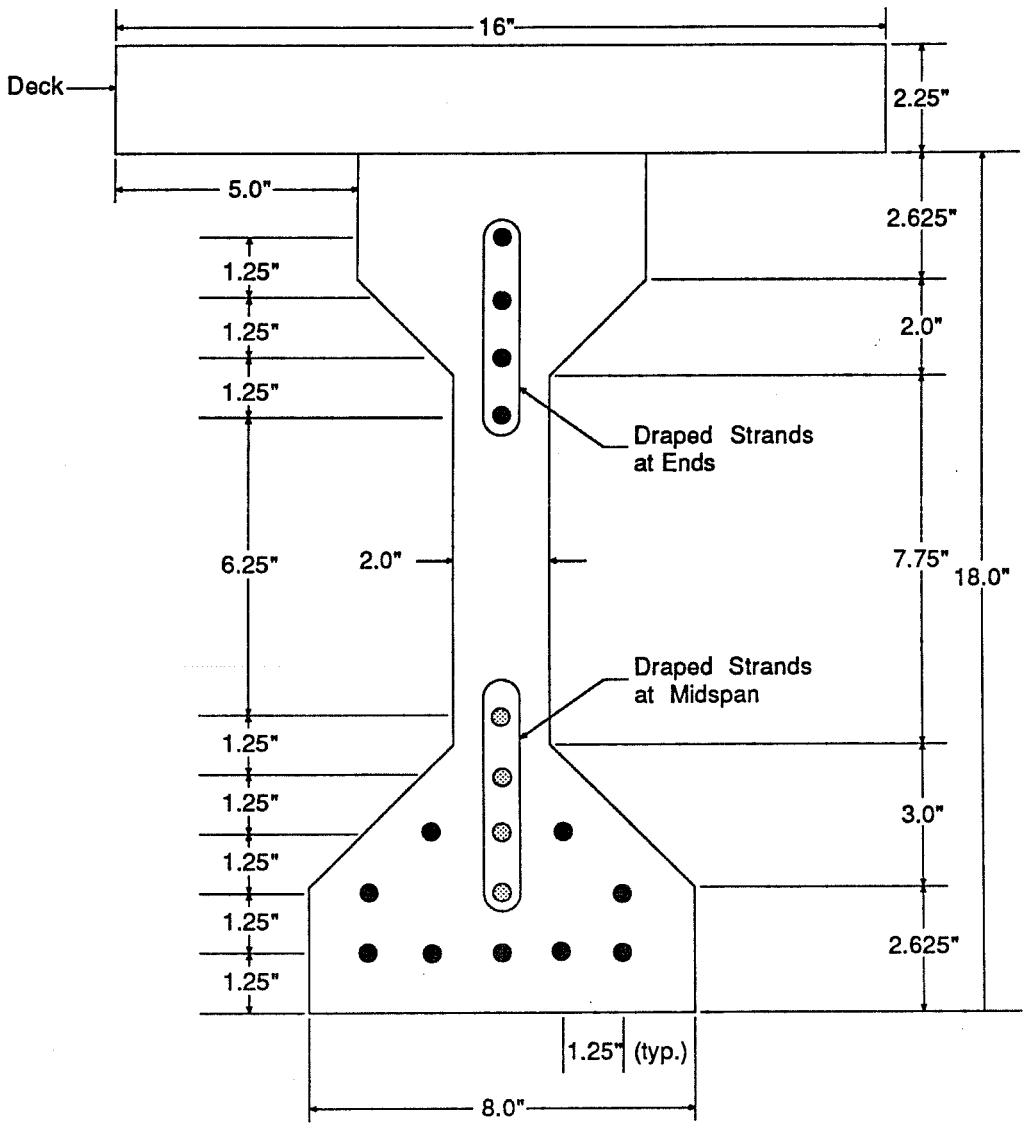

Fig. 4.15 Cross-section and strand locations for Specimens 3-1 and 3-2.

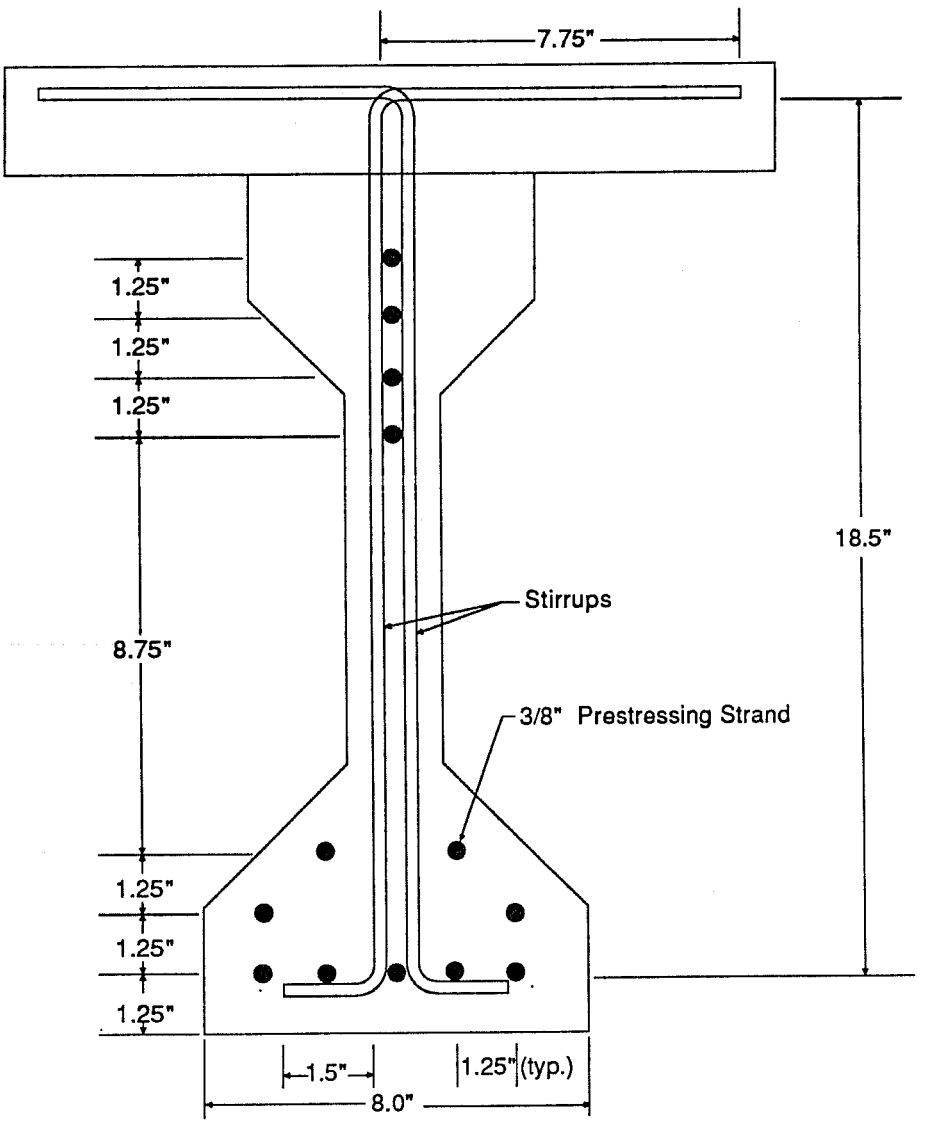

Fig. 4.16 Standard stirrup, Specimen 3-1.

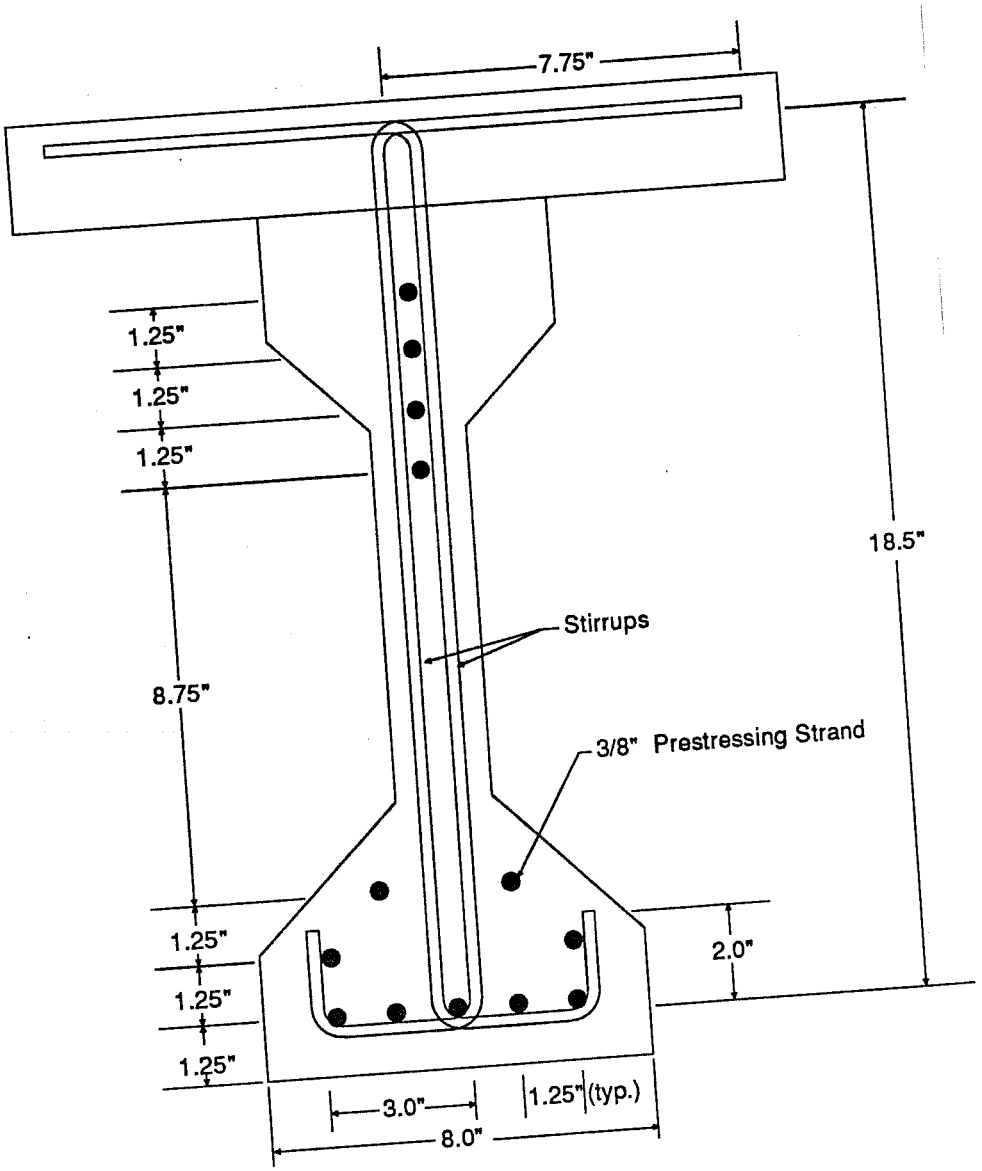

Fig. 4.17 Modified stirrup, Specimen 3-2.

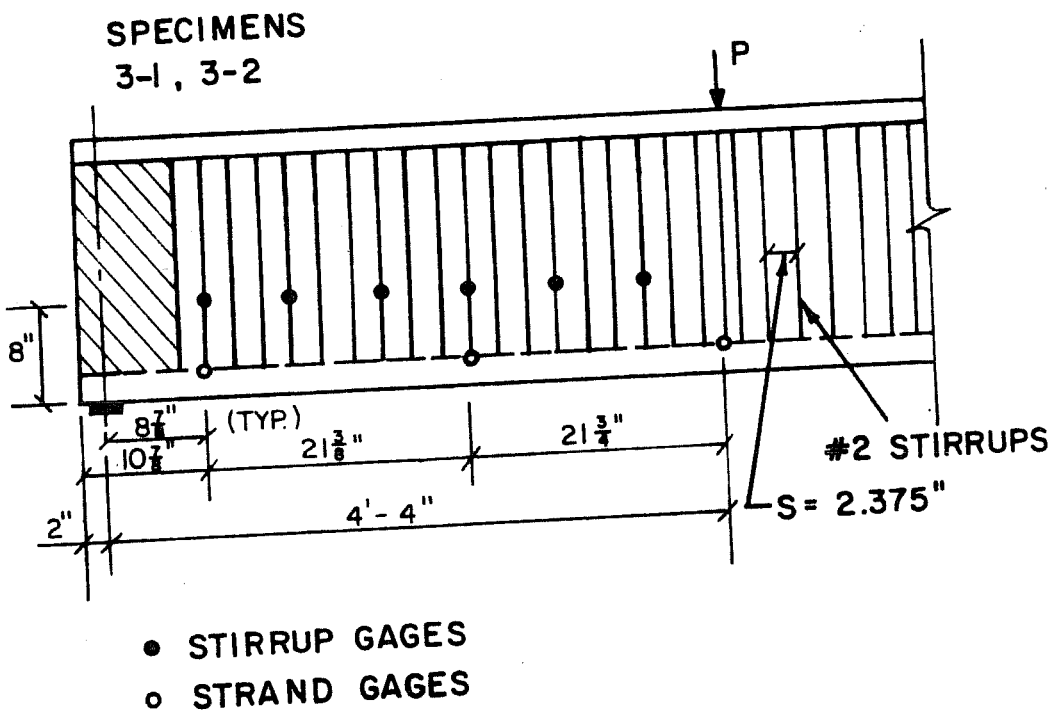

Fig. 4.18 Specimen 3-1 and 3-2 stirrup and strain gauge locations $V_s = 8\sqrt{f'_c}\,b_w d$.

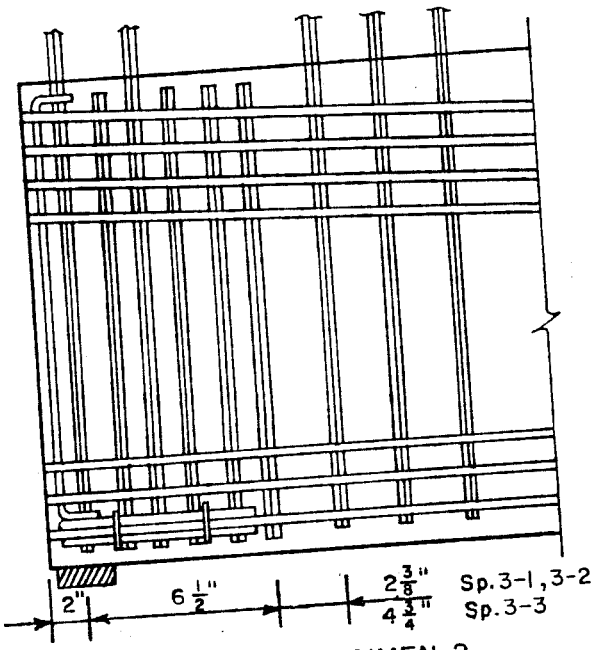

SOUTH END- SPECIMEN 2
(a)

All Reinforcing Bars are No.2 Prestressing Strands are 3/8" dia.

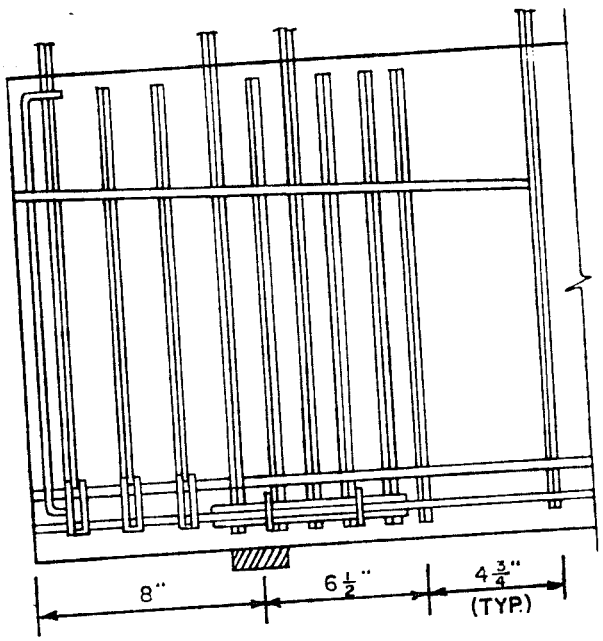

NORTH END-SPECIMEN 2
(b)

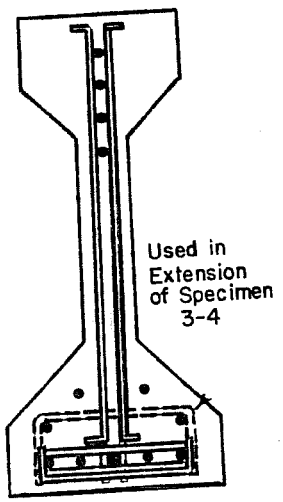

END VIEW

Fig. 4.19 End detail steel for Series 3.

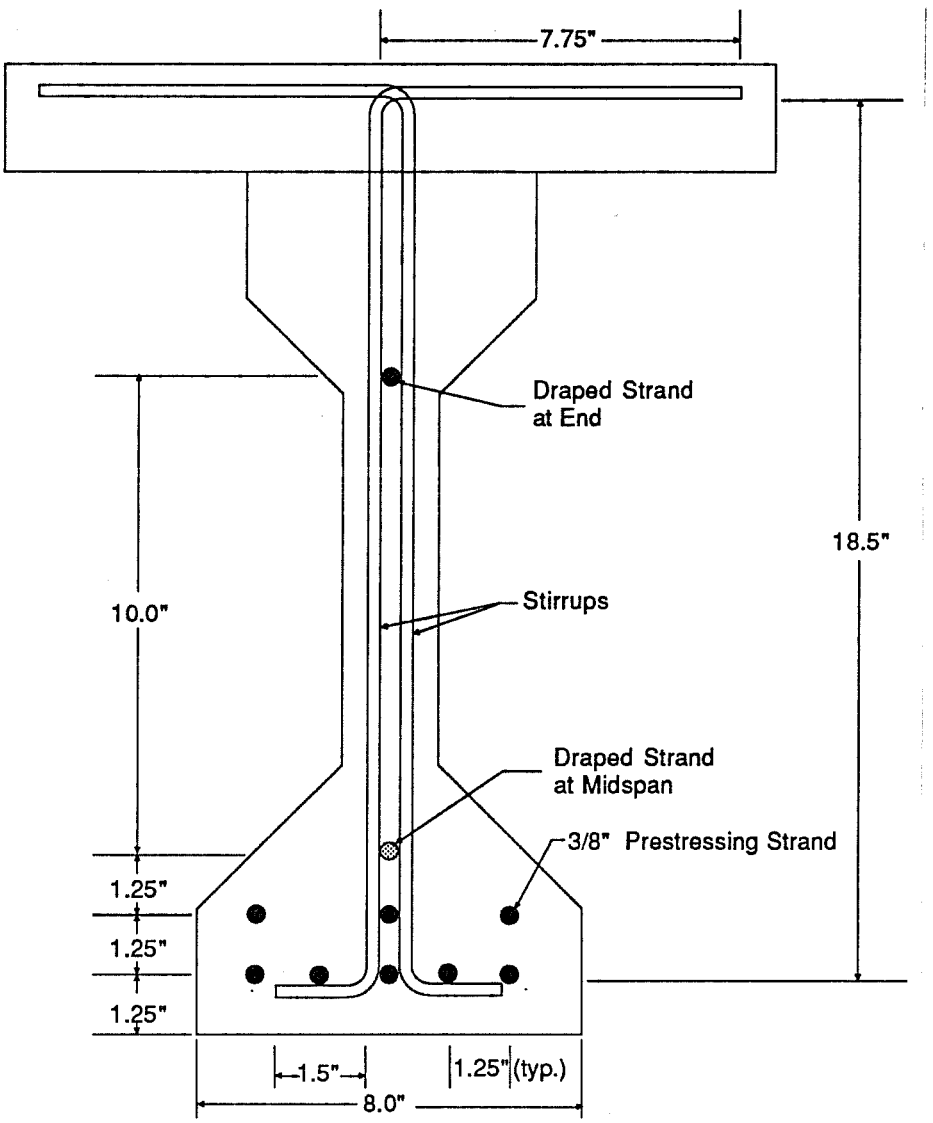

Fig. 4.20 Strand locations and stirrup details for Specimens 3-3 and 3-4.

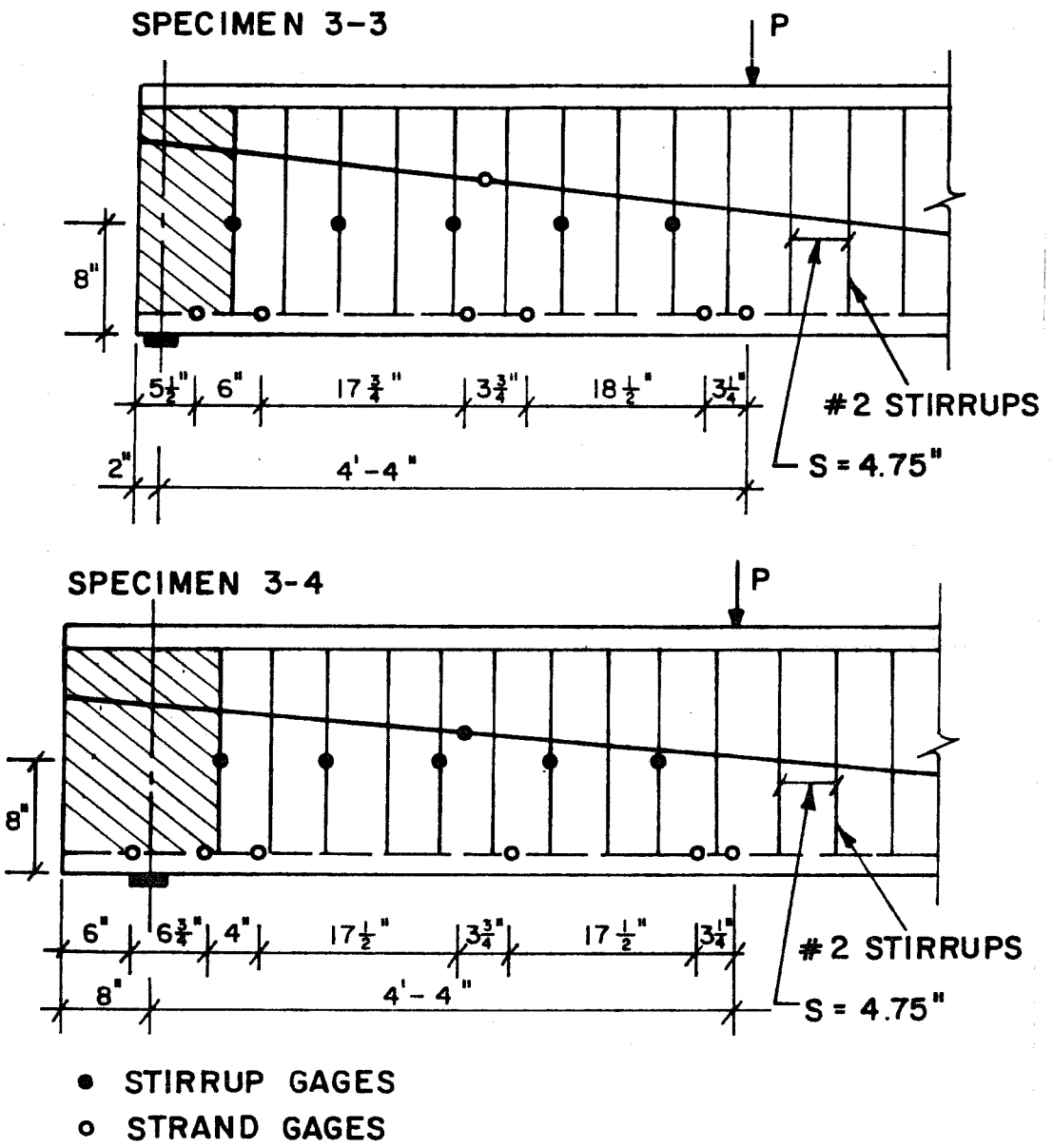

Fig. 4.21 Specimens 3-3 and 3-4 stirrup and strain gauge locations $V_s = 4\sqrt{f'_c}b_w d$.

mix used was developed through a series of trial batches reported in Chapter 2 and Reference [11]. The mix proportions and other pertinent data on the actual batches used are given in Appendix A. A very hard 3/8" crushed limestone was used to prevent aggregate failures from limiting concrete strength. Fly ash was used to replace 30% of the cement by weight.

The specimens of Series 3 had a composite low strength deck. The deck strength was approximately 4000 psi at 28 days. The properties and mix proportions of this concrete can be found in Reference [13].

A total of 14 6"x12" plastic mold cylinders, 19 6"x12" steel mold cylinders, and 10 6"x6"x20" steel mold beams were cast for each of Series 1 and 2. The beams and steel mold cylinders were tested at 7 days, 28 days, at release, and on each test day. Plastic mold cylinders were used to check strength gain. The 7 day beam specimens and 28 day cylinders were moist cured in a saturated lime bath. All other cylinders and beams were stored in the laboratory with the shear specimens. The shear specimens as well as cylinders were dry cured. They were, however, covered with a curing compound.

Tests were run with a mechanical compressometer on the release day and a couple of days after the last shear test to determine the modulus of elasticity of the concrete.

Similar steps were taken with Series 3 specimens. Full details can be found in Reference [13]. Strengths at test days, however, are included in Chapter 5.

4.3.2 Prestressing steel. A 3/8" diameter Grade 270 ksi seven wire low relaxation prestressing strand was used for all shear specimens. The strand was donated by Florida Wire and Cable Company. The load-strain behavior as given by the mill report is shown in Figure 4.22. The modulus of elasticity given by the mill report is 28,400,000 psi. Additional tests were run in the laboratory using strain gauges attached to one of the seven wires. The apparent modulus using this method is 30,500,000 psi. From this an appropriate conversion between strain gauge readings and actual strain could be determined.

The strand had been stored in the lab for approximately a year. Over this time it had become lightly rusted.

4.3.3 Nonprestressed reinforcement. Nonprestressed reinforcement was used both as shear reinforcement and longitudinal reinforcement. Because of the small specimen size and in some cases very light shear reinforcement, very small bars were

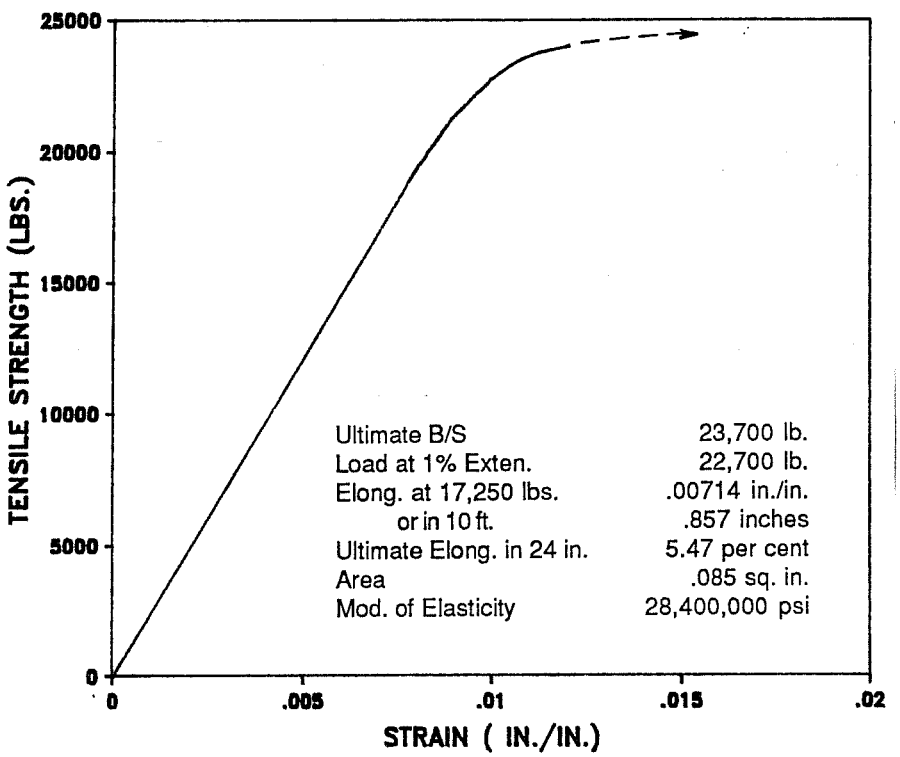

Fig. 4.22 Load-strain curve and data for prestressing strand.

required. Deformed bars of the sizes #1.25, #1.5, and #2 were obtained from a mill in Mexico [13].

Upon arrival the bars had a high yield stress but low ductility. To correct this they were sent to a local heat treatment plant. Figure 4.23 shows a typical stress-strain diagram before and after heat treatment for a #2 bar. After heat treatment the yield stress was 44 ksi with a net area of 0.0488 in.^{2}. Figure 4.24 shows the #1.5 bar properties. The final yield stress was 53800 psi with a net area of 0.0269 in.^{2}. Because only a small number of #1.5 bars were required, a portion of each bar used for a stirrup was tested to failure. The #2 bars were also used in their untreated state as temperature and shrinkage steel.

For the more heavily reinforced specimens #3 bars were used for stirrups. No. 3 bars were also used as added longitudinal reinforcement in Series 2. The yield stress was 73 ksi. Figure 4.25 shows the stress-strain behavior for the #3 bars.

4.4 Fabrication

4.4.1 Introduction. The shear tests performed are the continuation of a larger project. The fabrication of the shear specimens was essentially the same as described by Castrodale [13]. Series 3 is in fact the specimens described therein. For the sake of brevity only a brief summary and important differences will be given.

4.4.2 Formwork. The formwork used was made out of plywood. The forms were stripped and relaquered after every cast. For Series 1 and 2 it was desired to use the same girder cross-section as for Series 3 which was cast first chronologically. It was also desired to cast the deck out of high strength concrete at the same time as the girder. To facilitate this the forms were modified. A layer of porous foam rubber was placed at the top of the girder forms. This foam rubber was covered with duct tape to seal out the concrete. The deck forms were then nailed on top of this. The deck forms were covered with clear contact paper rather than being lacquered. The forms were lightly oiled before assembly. After casting the deck forms had to be removed first and then the girder forms could be removed.

4.4.3 Pretensioning procedure. All the shear specimens of this project were cast in the prestressing bed at Ferguson Laboratory. The pretensioning was done in two steps. In the first step the strands were tensioned individually to ensure uniform stressing. Each strand was tensioned to 50 ksi using a monostrand ram. The stressing operation was monitored by elongations, strain gauges, and a pressure gauge. Chucks

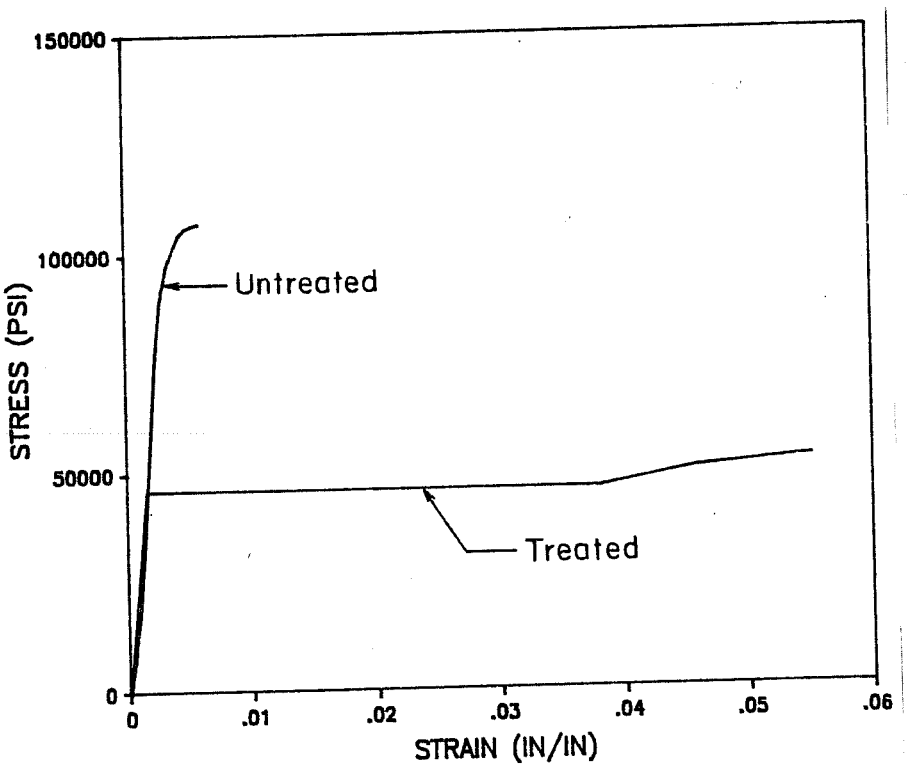

Fig. 4.23 Typical stress-strain curves for #2 deformed bars.

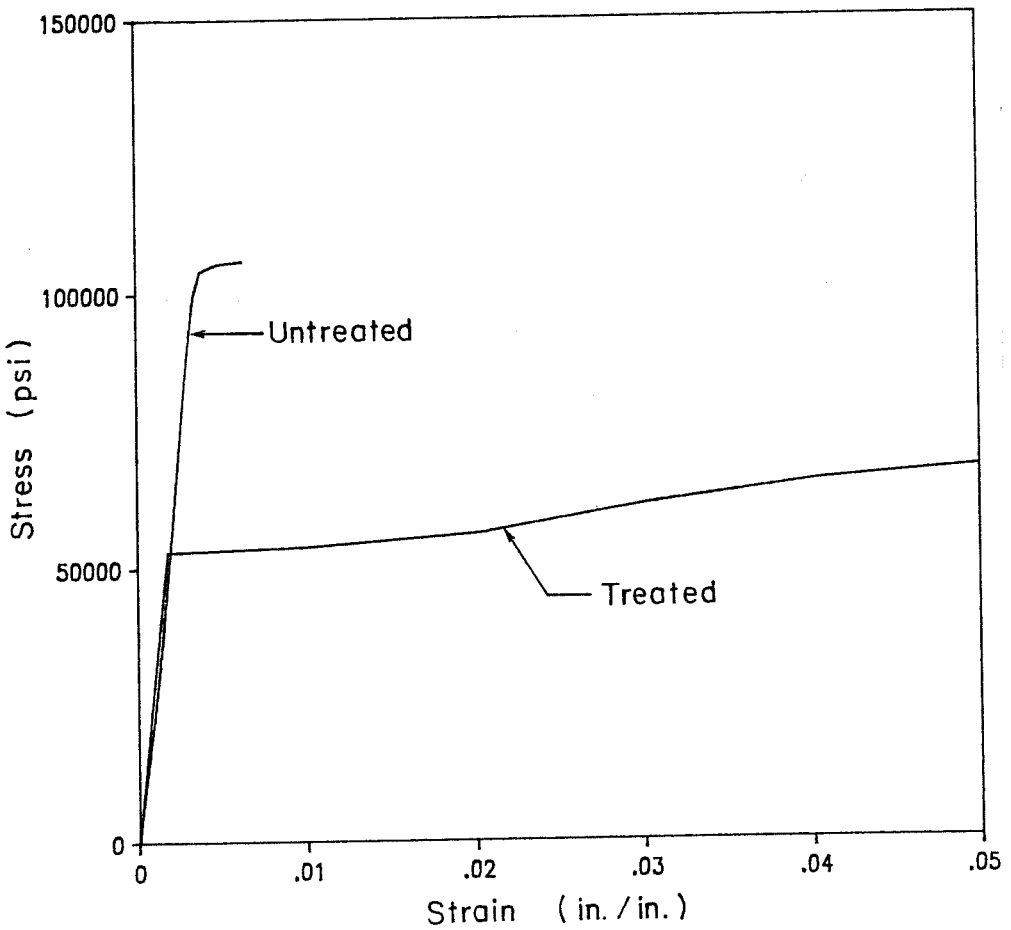

Fig. 4.24 Typical stress-strain curves for #1.5 deformed bars.

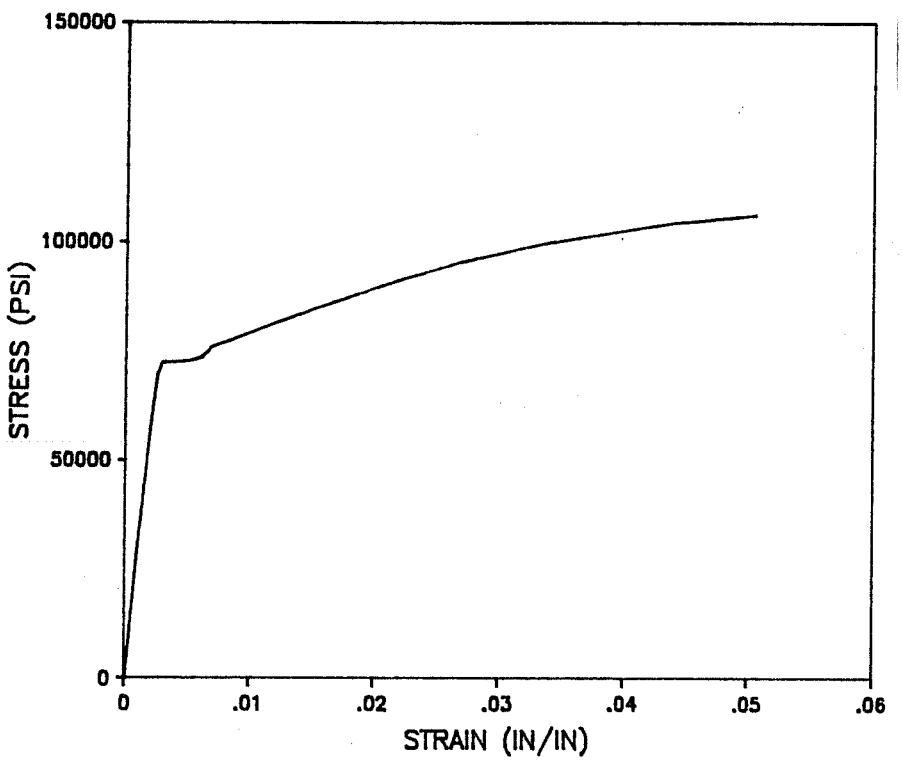

Fig. 4.25 Typical stress-strain curves for #3 deformed bars.

and wedges donated by Great Southwest Marketing Company were used throughout the project. Due to the size of the chuck and the small strand spacing a two tiered anchorage system was required. Chairs were fabricated at the laboratory to facilitate this.

The second pretensioning operation used the large hydraulic ram in the prestressing bed. The ram pulled all the strands at once. Tensioning was controlled by elongations and strain readings. Friction in the bed prevented accurate readings using a pressure gauge. The strands were tensioned to approximately 216 ksi (0.8 f_{pu}), then the bed was locked off and the ram unloaded.

At final release after the concrete girders achieved their specified strength the ram was again loaded until the nuts used to lock off the bed loosened. The nuts were backed off and the load was then gradually transferred to the specimens.

4.4.4 Girder Fabrication. All stirrups and end detail steel were prepared in the laboratory. Prestressing strands were cut, strain gauges placed, and then the strands were first tensioned. After this the stirrups and end detail steel were installed. Final tensioning was then done, and the forms were oiled and assembled. The girders were cast either one or two days after final tensioning.

4.4.5 Casting procedures. Project personnel inspected the ready mix batching to supervise the mix design and add the retarder and superplasticizer. An additional dose of superplasticizer was added to the truck at the laboratory to obtain a slump of about 9 in. The girders were cast in two lifts. The concrete was consolidated using small internal vibrators. Compaction was good even with the small clearances and large amounts of steel.

All three girders of a series were cast simultaneously. Plywood blockouts were used to separate the girders. Upon completion of the casting the concrete was screeded off. Smooth finishing was difficult due to the rocky nature of the mix. The concrete was then covered with wet burlap and plastic.

One to two days later, depending on strength gain, the forms were stripped and the specimens covered with a curing compound. Cylinders and beams were also stripped and coated on the same day.

When the specimens had gained sufficient strength, about one week later, the prestress was released and the strands between the girders were cut.

4.5. Instrumentation

4.5.1 Internal strain gauges. Internal strain gauges were mounted on both the shear and longitudinal reinforcement. Figures 4.4, 4.5, 4.6, 4.12, and 4.13 give the locations in the beams. The stirrup strain gauges were located near midheight of the specimens as illustrated in Figure 4.26. The gauges were applied and waterproofed using standard laboratory methods.

Some of the gauges of each series were continuously connected to strain indicator boxes from initial tensioning until testing. Readings were taken periodically to monitor behavior.

Strand gauges were attached to one of the seven wires. The wire gauges gave an apparent modulus of elasticity of 30.5×10^6 psi although the correct strand modulus was 28.4×10^6 psi. These values were used to adjust strain readings to indicate strand stress.

In Series 1 and 2 a Hewlett-Packard data acquisition system was used to obtain and record the strain readings. For Series 3 both internal and surface strain gauges were read manually using a switch and balance box and a strain indicator box.

4.5.2 Surface gauges. Concrete strains were measured with surface strain gauges. As a check on the prestress force, surface gauges were placed at five locations at the centerline of one girder of each series (Fig. 4.27). These gauges were monitored continuously from release through the test. The girder so instrumented was the last girder of each series tested.

For the girders of Series 1 and 2 strain rosette gauges were also used. In most cases the rosettes were placed 10 in. up from the bottom of the girder and 1 d and 2 d away from the support (Fig. 4.28). The one exception to this was Specimen 2-3 which had gauges 1.5 d and 2 d from the support.

4.5.3 Beam deflections. For the specimens of Series 1 and 2 linear potentiometers were used to measure deflections. The Riehle test machine had a potentiometer that measured head displacements. Readings were also taken to measure midspan girder displacement and pad compression in the tests which used neoprene bearing pads. The potentiometers were hooked up to the data acquisition system.

In Series 3 the readings were taken using dial gauges. The machine head displacement was recorded manually.

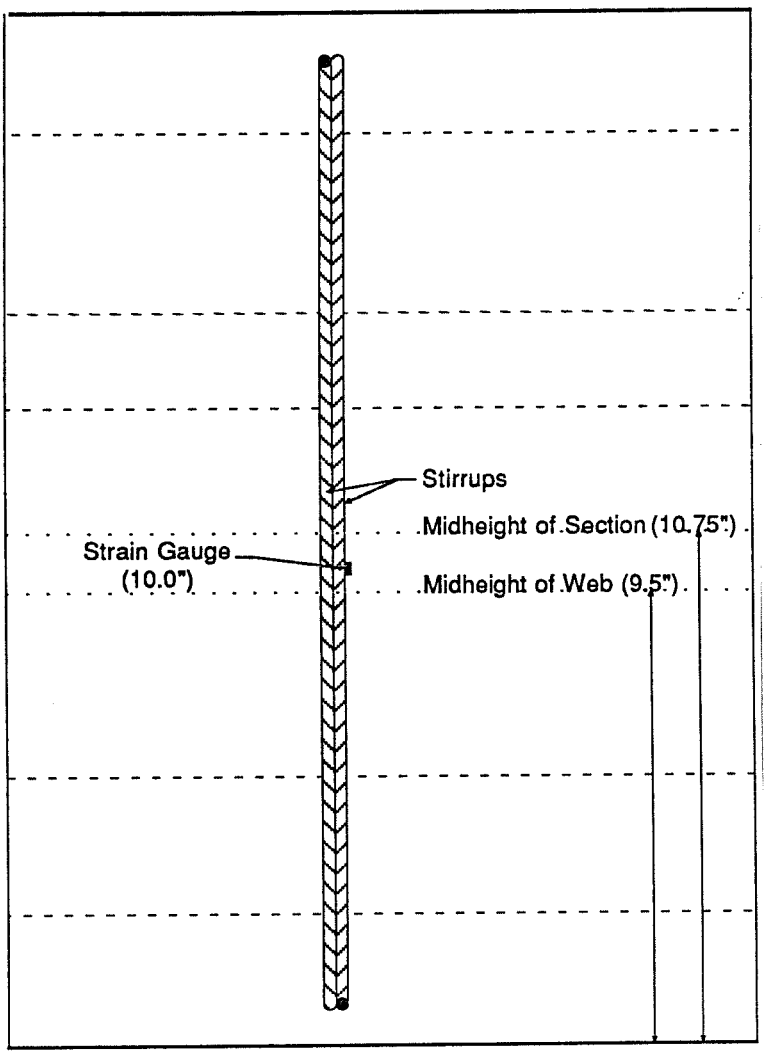

Fig. 4.26 Strain gauge location.

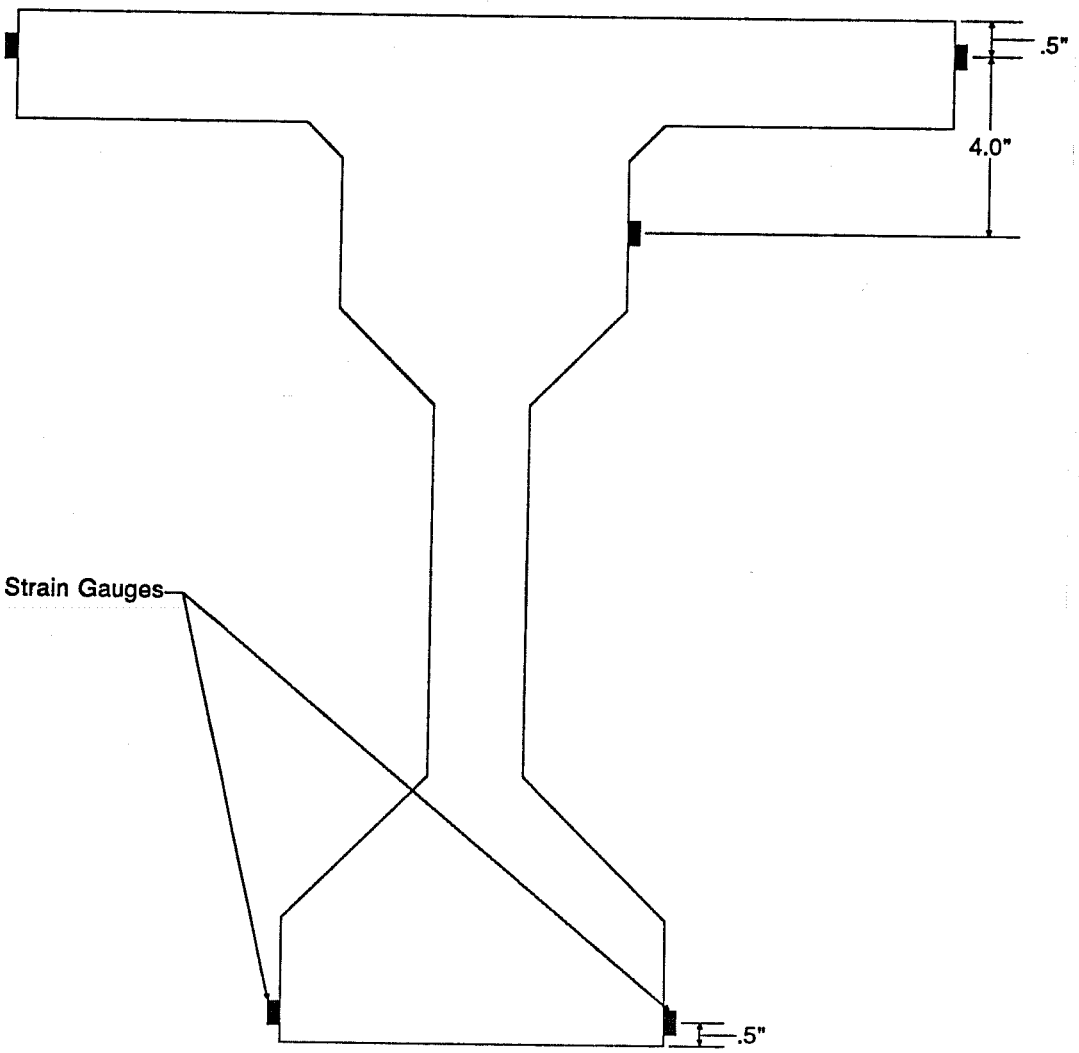

Fig. 4.27 Surface gauge locations.

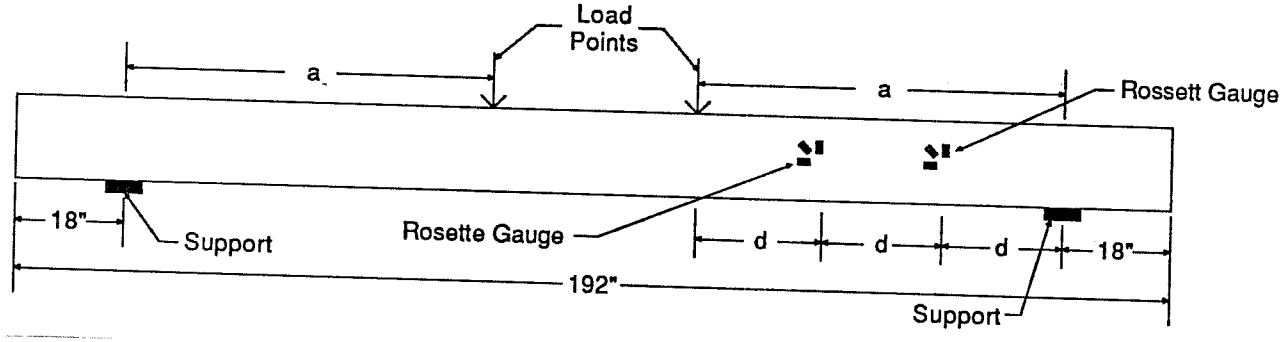

Fig. 4.28 Rosette strain gauge locations for Series 1 and 2.

4.5.4 Strand movement detection. Measurements were taken to determine the existence and amount of strand end slip. A frame was epoxied to each specimen as shown in Figure 4.29. Again either linear potentiometers or dial gauges were used to monitor slip.

4.6 Test Frame and Loading System

4.6.1 Test machine. For the majority of these shear tests, the large 600 kip Riehle test machine at Ferguson Laboratory was utilized. The test machine is of the screw type. The load and head displacement could be read on a digital display. Figure 4.30 shows the general layout of the test machine and loading system. Due to the location of the supports, a system had to be devised to span the trench that surrounds the Riehle test machine. Four W sections were paired and then bolted to the base of the test machine. The support pedestals then rested on the top of these spanning beams.

4.6.2 Loading system. Several different loading systems were needed because of the different loading requirements for Series 1 and 2 and for Series 3.

4.6.2.1 Two point loading. For the tests of Series 1 and 2 a two point loading system was used. A large spreader beam was attached to the test machine. The load points were set at the appropriate locations for the two series (Fig. 4.3 and 4.9).

Neoprene bearing pads were used for all of the tests of Series 1 and Specimen 2-1. The pads were used both under the load points and under each support. The pads were 2"x3"x7" and had nine 14 ga. steel shims in them. The pads gave little resistance to longitudinal beam displacement relative to the test machine. In several cases a small keeper was used to resist longitudinal movement. The pad use was eventually discontinued after a pad failure occurred.

After the neoprene pads proved to be ineffective for the high loads of Series 2, steel rollers were used. A pin support was placed under one end and 1 3/4" diameter steel rollers were used under the other support and both loads points (Fig. 4.31). Steel bearing plates 1"x4"x10" were used with the rollers. A layer of Hydrastone was placed between the specimen and the plates to insure even bearing.

4.6.2.2 Fixed head. For Specimen 3-3 and 3-4 a single unsymmetrical load point was used (See Fig. 4.14). The shear load was only critical in one shear span because the other shear span had only one third of the load. For these tests a fixed loading head was inserted into the test machine. The load was then applied through a

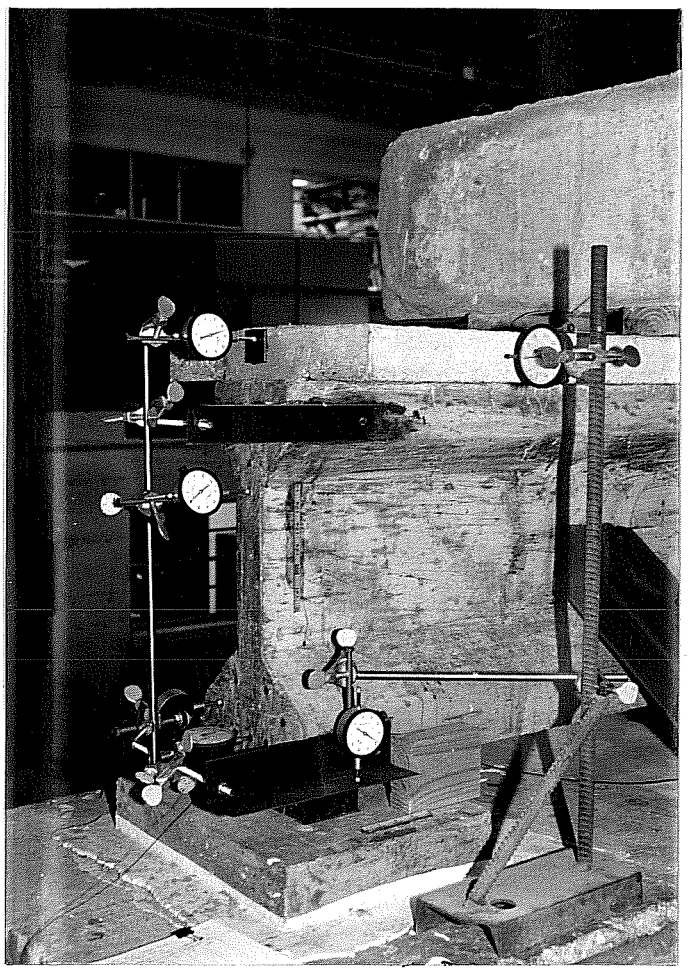

Fig. 4.29 Instrumentation frame.

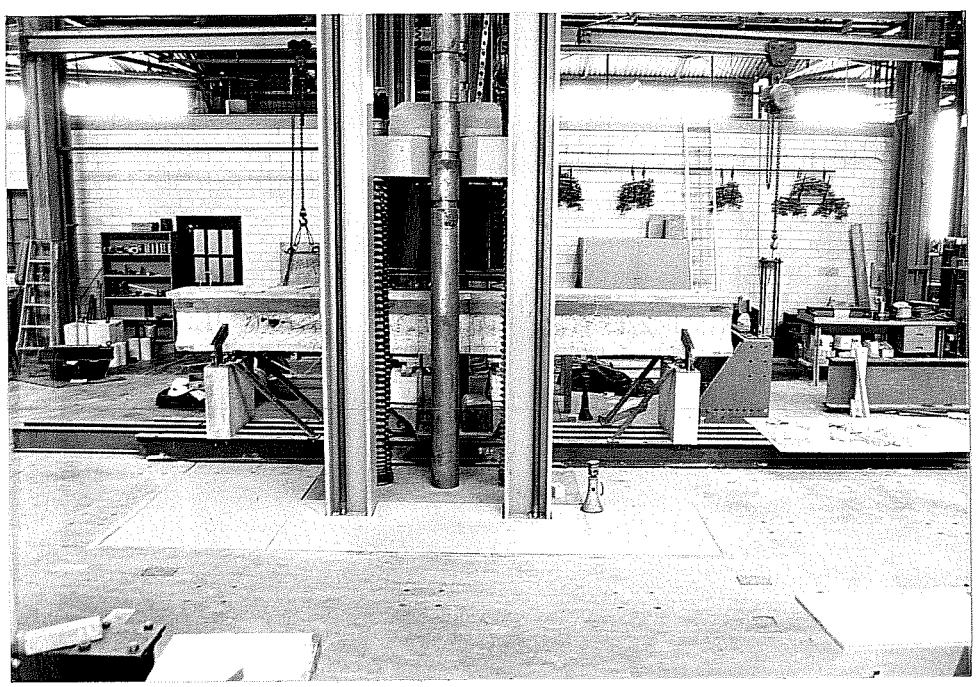

Fig. 4.30 General test setup

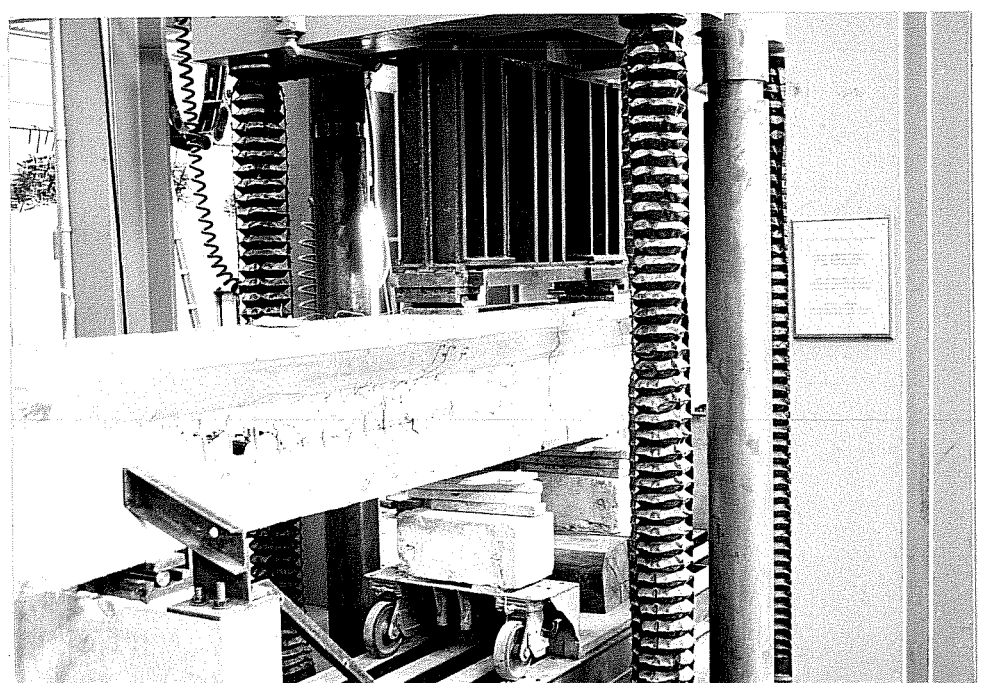

Fig. 4.31 Use of steel rollers.

neoprene bearing pad. Another neoprene pad was used as a support under the critical shear span. A steel pin connection was used at the other support.

4.6.2.3 Test frame. For Specimens 3-1 and 3-2 a completely independent load system was used (Fig. 4.32). The system consisted of Dywidag bars and a braced load head. The Dywidag bars were tied to the loading floor. A ram and load cell were suspended from the load head. Load was applied through a spherical head. The general load and support locations were the same as shown in Figure 4.14.

4.7 Test procedure

A general loading plan was determined prior to the beginning of each test. This generally involved steps of moderate fractions of the predicted cracking load. Near the predicted cracking load, single kip shear increments were used until cracking was noted. The load increments were then increased according to the predicted ultimate load. For Specimens 3-1 and 3-2, after the cracking load was reached the specimens were unloaded and then reloaded to failure. In several other tests loading had to be suspended, unloaded, and reloaded due to problems with the loading system such as excessive bearing pad displacements.

At each load stage a series of specimen strain and displacement readings were taken. The readings were either taken manually or by the data acquisition system depending on which system was in use for a given test.

Test set up checks were also made at the various load stages. These checks involved monitoring pedestal movements, beam roll, and beam displacement relative to the test machine. These readings gave an indication of test system stability and in several cases indicated the existence of problems.

At first cracking and then at regular intervals crack growth was marked. This allowed observance of crack pattern changes with load. In addition the angle the crack made to the horizontal was measured and crack width readings were taken on a number of cracks.

Pictures were taken of the beam at the same interval as cracks were marked. This allowed a permanent record to be kept of beam behavior.

Fig. 4.32 Test setup for Specimens 3-1 and 3-2.

4.8 Data Reduction

The data from Series 1 and 2 tests were stored directly onto disk by the data acquisition system. Data were converted to a form usable on the laboratory's microcomputers. The data from the tensioning operations as well as losses over time were taken manually. Data from Series #3 was all taken manually and then input into a computer.

The majority of the data reduction was done using the laboratory's computers. The calculation of effective prestress was done manually.

CHAPTER 5
TEST RESULTS

5.1 Introduction

This chapter contains the results and observations from the ten shear tests conducted in this project. All ten specimens were pretensioned high strength concrete girders. Six specimens had high strength monolithically cast decks while the other four had low strength composite decks. The principal goal of this program was to obtain data on the shear capacity of high strength prestressed concrete girders.

The primary variable was the quantity of shear reinforcement provided. Series 1 was designed with very light shear reinforcement. These tests were intended to check behavior of girders with no or very light shear reinforcement. These specimens were selected to be at the lower limits of AASHTO/ACI and are quite typical of shear reinforcement used in full scale long span structures. Series 2 was designed for extremely heavy shear reinforcement. The heavy reinforcement was intended to determine if maximum shear reinforcement levels can be raised for use with high strength concrete. Series 3 was designed to check intermediate behavior. Two specimens had the current AASHTO/ACI maximum reinforcement of $V_s = 8\sqrt{f'_c}b_w d$. The other two specimens had an intermediate level of shear reinforcement.

In the following section the individual tests will be discussed. Specimen performance will be described including cracking loads and load deflection behavior. Information from internal strain gauges and crack measurements will also be included.

The third section of this chapter will cover the tests as a group. General behavior of high strength prestressed concrete girders will be noted. The general behavior will then be compared to the assumptions of the shear capacity models of Chapter 3. Finally, the test data will be compared with the numerical predictions of the shear capacity models.

5.2 Test Behavior

5.2.1 Specimen 1-1. Specimen 1-1 was a prestressed girder with no shear reinforcement. The principle goal was to evaluate the cracking load of this type member. The load was applied in two kip shear increments to 10.0 kips and in one kip shear increments to 21.0 kips. After this the load was increased by 0.5 kip shear increments until each end cracked. First inclined cracking occurred in the web at a shear of 26.0

kips. The load dropped substantially, but returned to the cracking load. Load was then increased until the second end cracked at 27.0 kips. On each end the first cracks extended from the bottom flange all the way up to the top flange. Several cracks formed on each end (Fig. 5.1 (a)). After each end cracked the beam was unloaded.

The beam was reloaded to the previous cracking load of 27 kips. Some extension of the cracks was noted during the reloading. The beam was then loaded in 0.5 kip shear increments until failure. Relatively few additional cracks were noted. The existing cracks did, however, open extremely wide as the load increased. Crack widths were on the order of 1/4 in. at failure. Flexure cracks were noted at a shear of 32.0 kips. Flexure-like cracks formed in the shear span at a shear of 29.0 kips (Fig. 5.1 (b)). At this stage, however, there were no cracks in the constant moment region. As the load increased the shear cracks propagated into the bottom flange. Shortly prior to failure they had progressed nearly through the bottom flange.

There were no flexure-shear cracks. The ultimate shear capacity was 34.5 kips (Fig. 5.2). At failure the crack went completely through the bottom flange just outside the detail steel. The web exploded with the concrete struts basically intact. There was no debonding or slip of the prestressing strands prior to failure.

The load-deflection behavior of Speciment 1-1 is shown in Figure 5.3. The displacements were determined based on the measured head displacement of the test machine corrected by an estimate of the compression of the neoprene pads used. This was required due to difficulties with linear potentiomenters. It can be noted that there were substantial drops in load after each end cracked. Upon reloading the beam was not as stiff. This was due to the presence of shear cracking since the beam had not cracked flexurally. The load-deflection curve did flatten appreciably before shear failure occurred.

Measurements were taken on strand strain during the test. Figure 5.4 shows the strand strain given by gauge 5 through the two load cycles. On the second cycle the strains were higher for a given load. As the flexure-like cracks formed in the shear span the strand strains began to increase more rapidly as the load increased. Figure 5.5 shows the strain in all the strand gauges for the second cycle. The estimated pretension strain was $6000\mu\epsilon$. Assuming yield to be at 1% strain the strands in Specimen 1-1 did not yield prior to failure.

Measurements of the angle of inclination were taken for some of the cracks that formed. The cracks closest to the support and load point ranged from about 35°

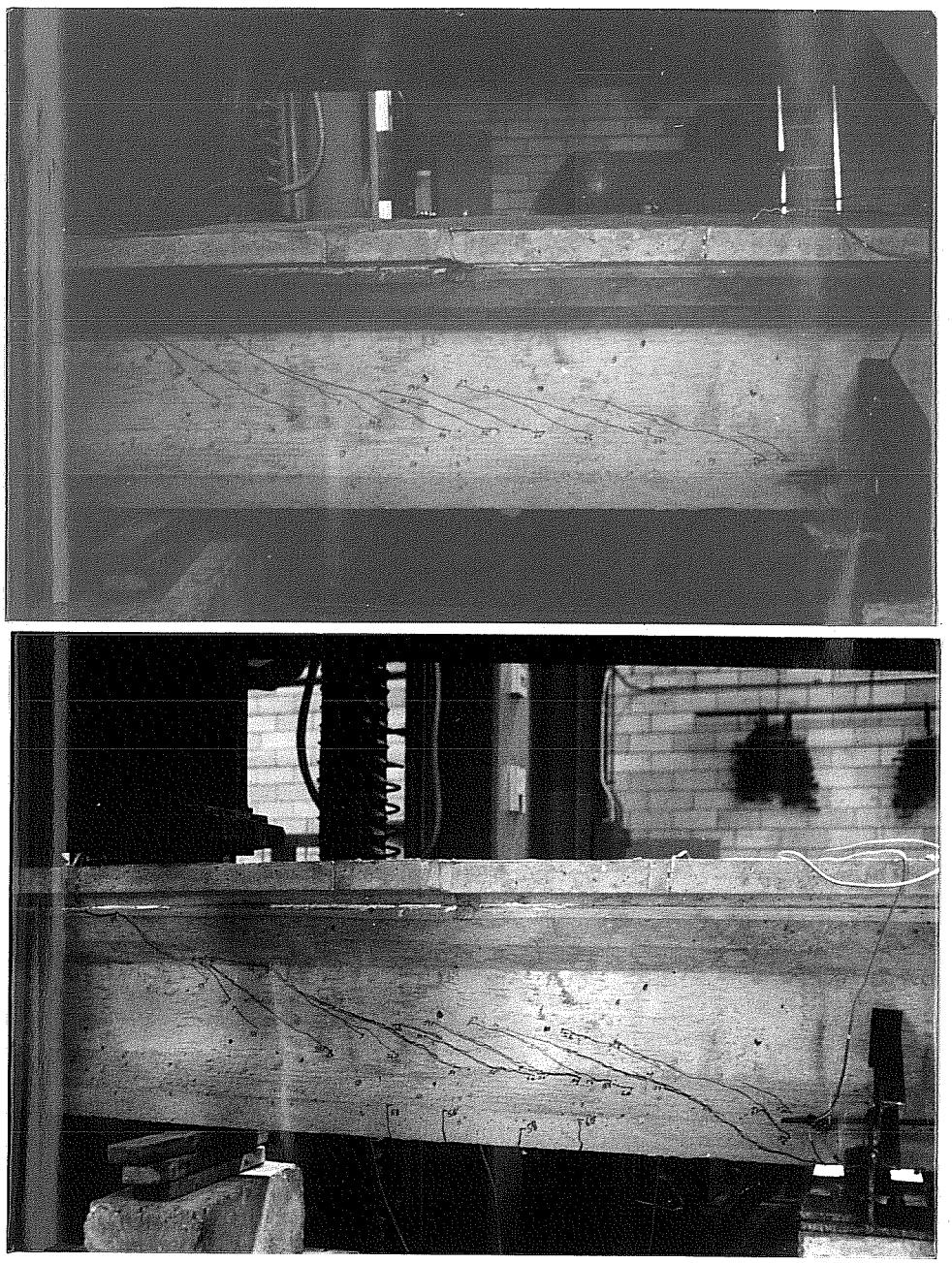

Fig. 5.1 Specimen 1-1 during testing.

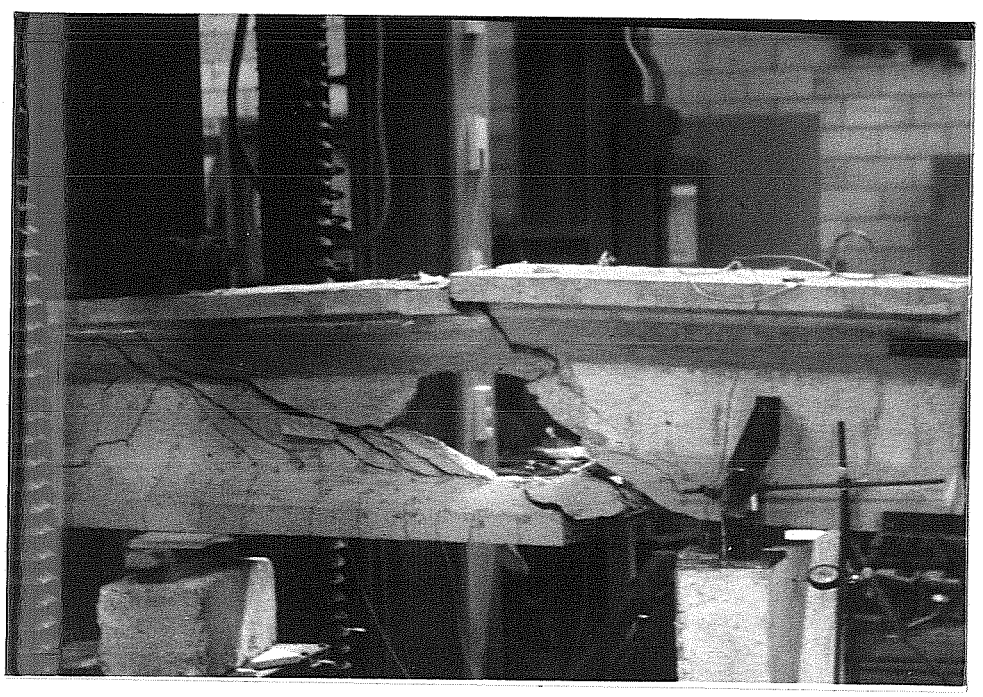

Fig. 5.2 Specimen 1-1 at failure.

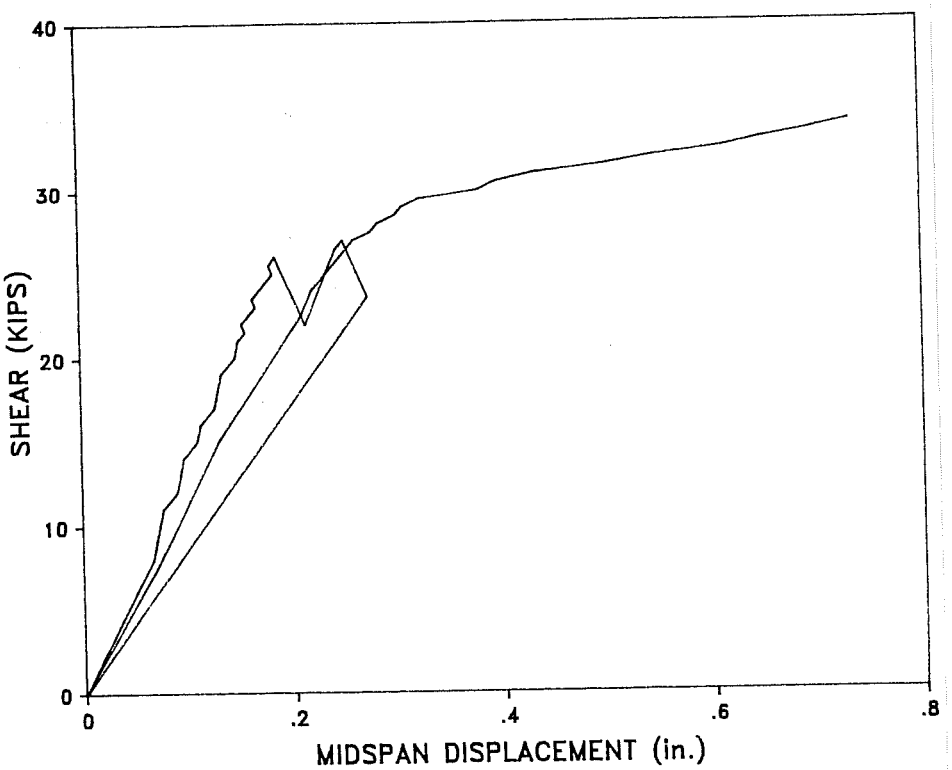

Fig. 5.3 Load-deflection behavior for Specimen 1-1.

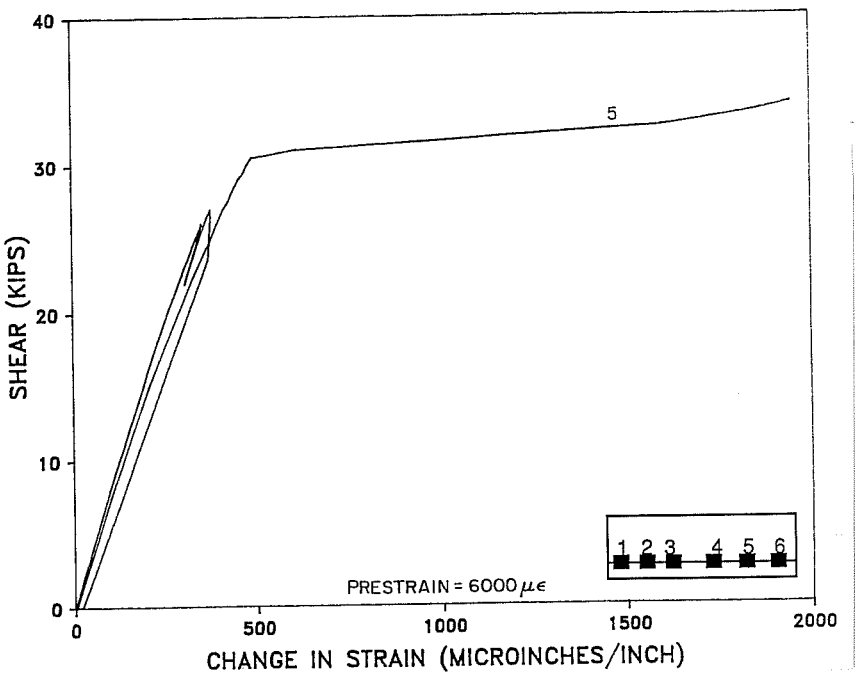

Fig. 5.4 Strains measured by strand gauges through complete loading sequence for Specimen 1-1.

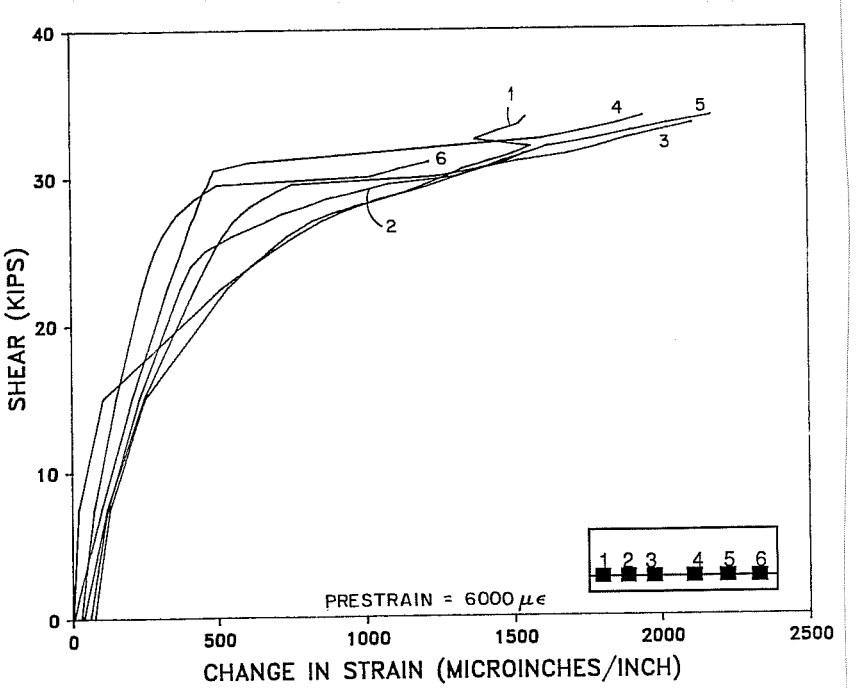

Fig. 5.5 Strand strain gauge readings for final load cycle of Specimen 1-1.

to 50°. The intermediate cracks ranged from 16° to 30°. As previously mentioned the crack widths became extremely wide as the load increased.

5.2.2 Specimen 1-2. Specimen 1-2 was designed for the AASHTO/ACI minimum of 50 psi of shear reinforcement. The shear reinforcement consisted of #1.5 deformed bars. The specimen was loaded at 2.5 kip shear increments up to 20.0 kips. It was then loaded at one kip increments until first cracking at 22.0 kips. The other shear span cracked at 24.0 kips. The cracks extended from the bottom flange all the way to the top flange. Figure 5.6 (a) shows the crack patterns at first cracking. The load was increased to 26.0 kips, but the test had to be suspended due to excessive shear in the neoprene bearing pads.

Specimen 1-2 was reloaded after the pads had been reset. The load was returned to its previous value and increased by one kip shear increments to failure. A small keeper was used to reduce pad shear. The cracks extended somewhat during reloading. The cracks grew very wide as the load increased (Fig. 5.6 (b)). Few additional cracks formed after first cracking. Flexure-like cracks formed at about the same time in the shear span and the constant moment region. As the load neared failure the shear cracks extended deep into the bottom flange. Failure load was 33.5 kips. Failure occurred due to fracture of all the stirrups which crossed the failure plane. The stirrup closest to the support fractured across one crack while the rest of the stirrups failed across an adjacent crack. The failure crack went through the end of the detail steel. No flexure-shear cracks were noted. Figure 5.7 shows the specimen after failure. There was no slip of the strands during loading.

The load-displacement behavior of Specimen 1-2 is shown in Figure 5.8. The displacement was determined from readings taken at midspan by a linear potentiometer corrected for the pad compression readings given by other potentiometers. The plot again shows considerable flattening prior to shear failure.

The prestressing stands saw only limited strain during the test. Figure 5.9 shows one of the gauges through both load cycles. Figure 5.10 shows all four gauges on the second load cycle. The strand strains were increasing more rapidly with load as failure approached. The pretension strain was again $6000\mu\epsilon$. The added strain of approximately $1500\mu\epsilon$ was not enough to begin yielding of the prestressing strands.

The stirrup strain measurements do not generally provide a good indication of behavior for Specimen 1-2. Figure 5.11 shows some interesting stirrup behavior. It will be noted that on the first cycle the stirrup sees very little strain until cracking. In the

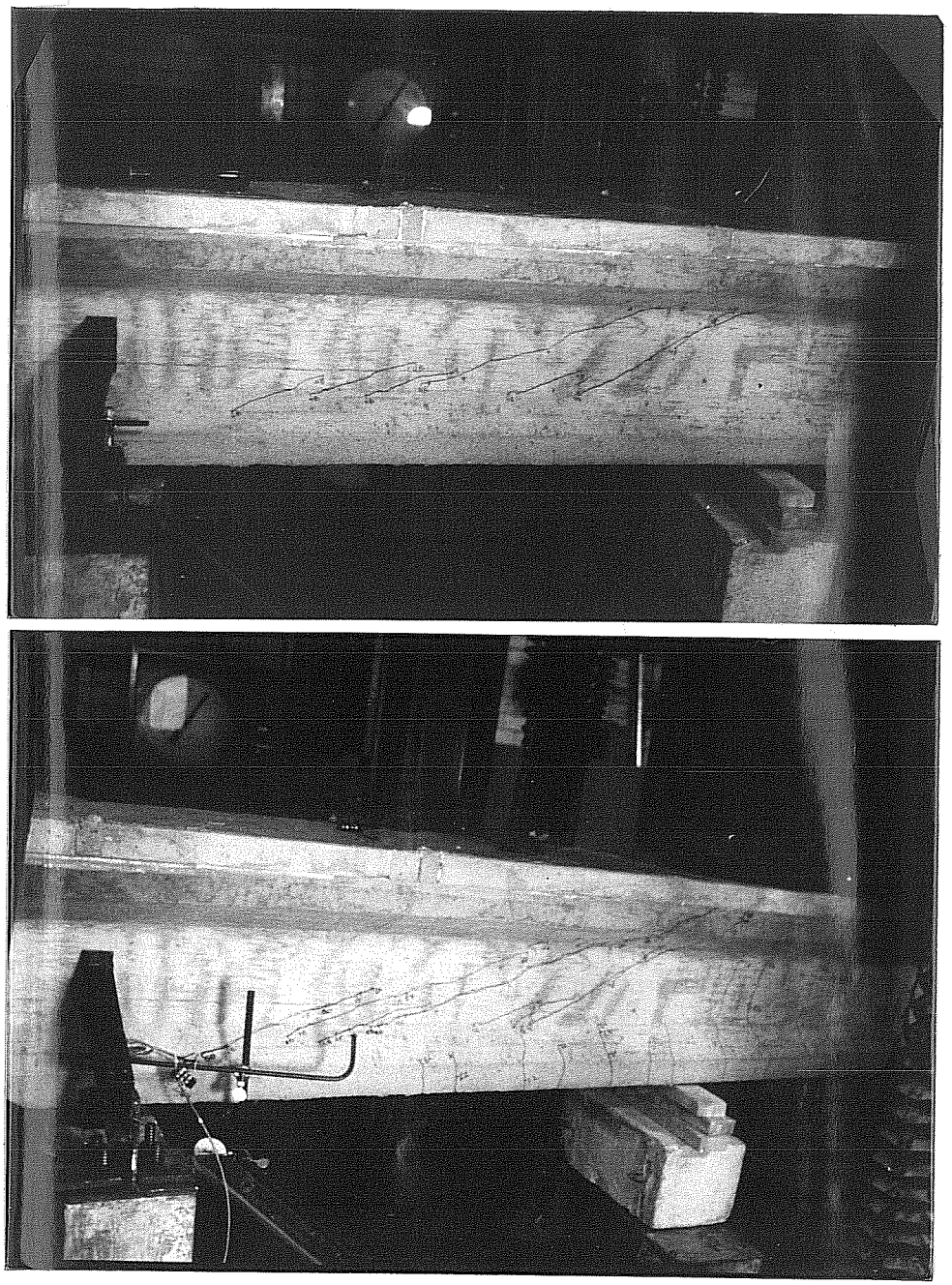

Fig. 5.6 Specimen 1-2 during loading.

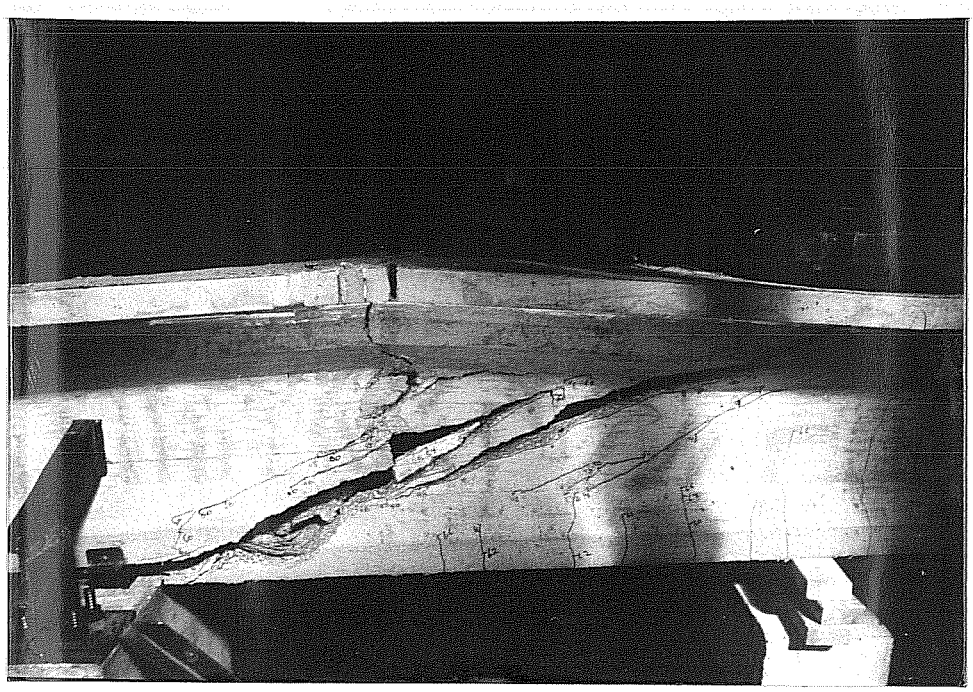

Fig. 5.7 Specimen 1-2 at failure.

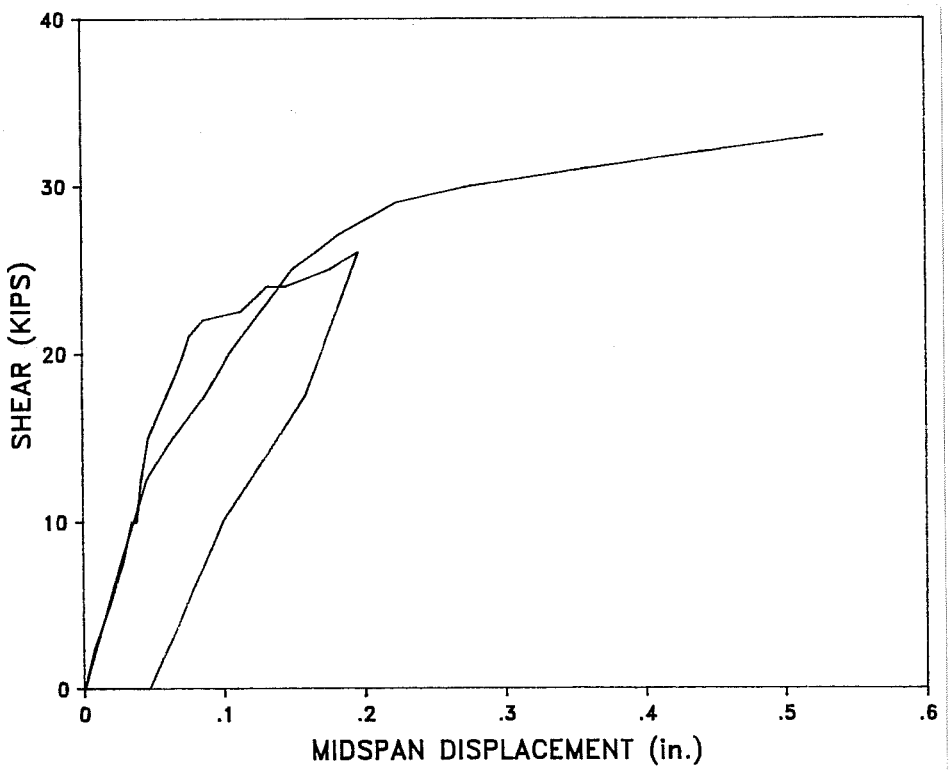

Fig. 5.8 Load-deflection curve for Specimen 1-2.

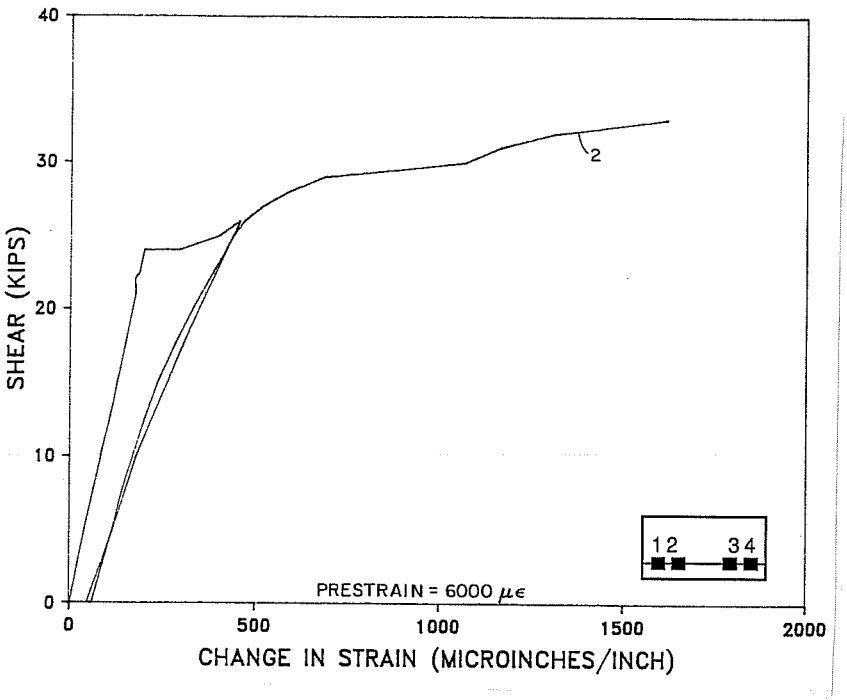

Fig. 5.9 Strand strain readings for Gauge 2 through complete loading cycle for Specimen 1-2.

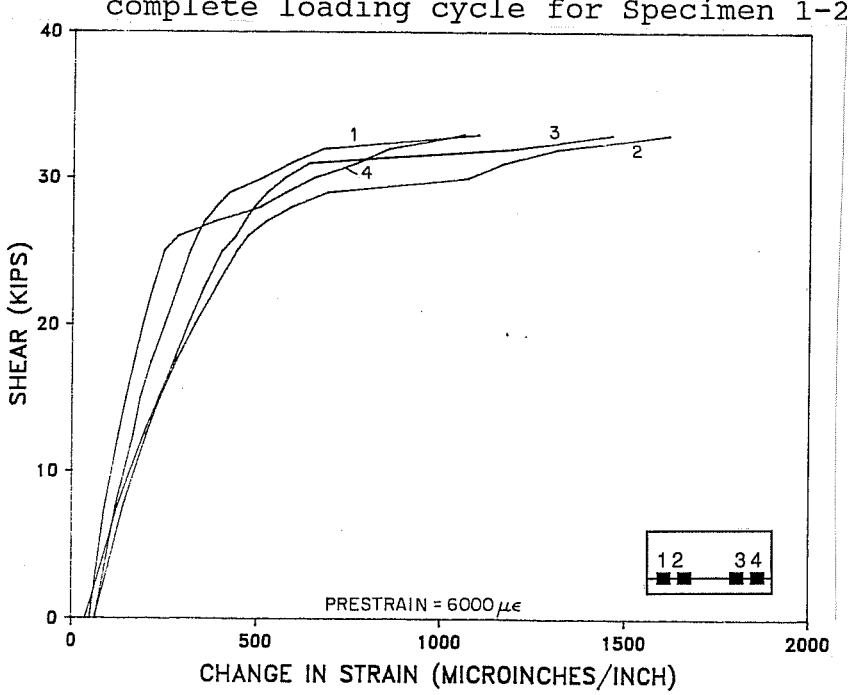

Fig. 5.10 Strand strain readings for all gauges for last load cycle of Specimen 1-2.

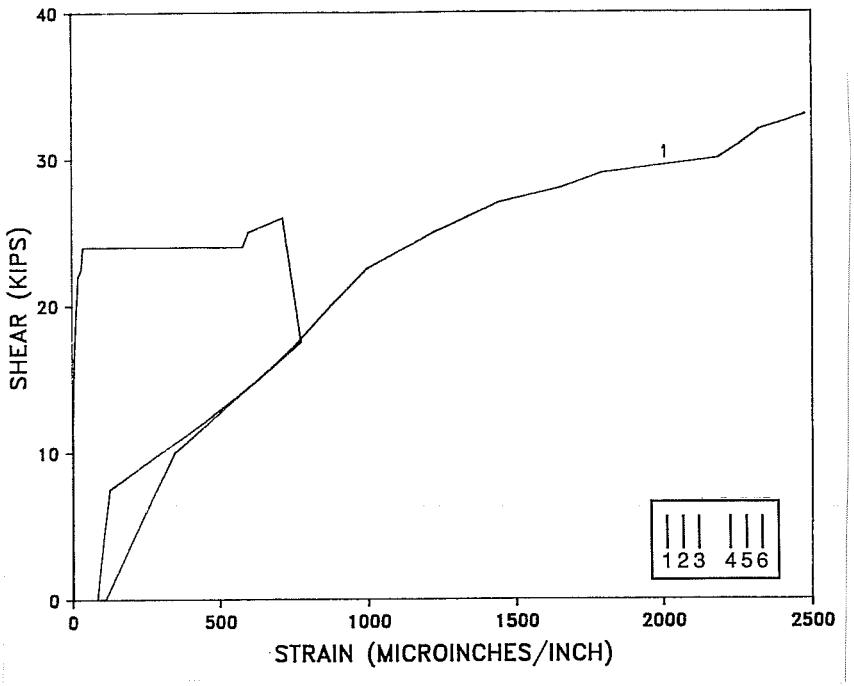

Fig. 5.11 Stirrup strain for gauge 1 through complete loading of Specimen 1-2.

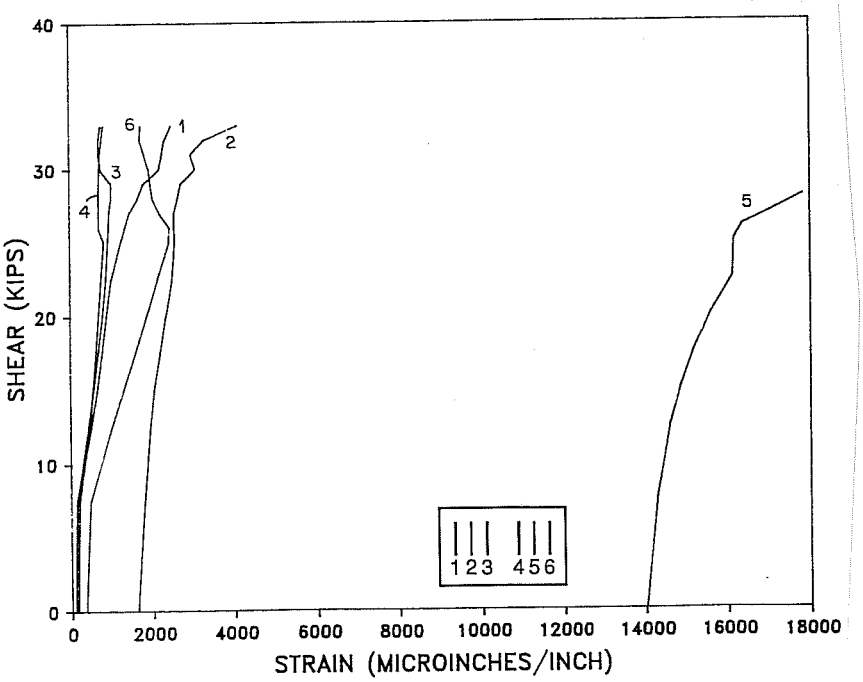

Fig. 5.12 Strirrup strains for last loading of Specimen 1-2.

second cycle the stirrup strains for any applied load. Only one gauge gives an indication of strain seen by the stirrups during the second loading (Fig. 5.12). The other gauges were away from the cracks.

Crack angles and widths were measured during the test. The crack angles varied from 20° to 35°. Cracks that formed either close to the support or close to the load point had steeper angles than cracks forming in the middle of the shear span. Crack widths were read using a plastic card with comparison marks of varying widths. The initial cracks were approximately 0.010 in. wide. At a shear of 32.0 kips some crack widths had grown in excess of 1/16 in wide.

5.2.3 Specimen 1-3. Specimen 1-3 was designed for $V_s = 1\sqrt{f'_c}b_w d$ for f'_c=12000 psi. Specimen 1-3 was loaded in 2.5 kip shear increments up to 20.0 kips. It was loaded in one kip increments thereafter to failure. First cracking occurred at 25.85 kips of shear. The other shear span cracked at a shear of 27.0 kips. The cracks ran from the bottom flange to the top flange. The crack widths increased greatly as the load was increased. The first flexure cracks formed in the constant moment region at a shear of 31.0 kips. Cracking patterns were similar to that of Specimen 1-2. At a load of 33.0 kips flexure-shear cracks were observed. The ultimate load was 35.85 kips. Final failure occurred when all the stirrups crossing the failure plane fractured. The failure crack went through the bottom of the specimen at the end of the detail steel. The deck on the failure end delaminated at the load point. No strand slip occurred during testing. Figure 5.13 shows the failed specimen.

The load-displacement behavior of Specimen 1-3 is shown in Figure 5.14. The curve shows significant flattening before failure occurs.

The prestressing strand strains are shown in Figure 5.15. The strands behaved very linearly up to shear cracking. After shear cracking the strains increased more rapidly, but it was not until flexural cracking that the strands saw subtantial strain. With a prestrain of 6000$\mu\epsilon$ the gauges do not indicate yield of the strand.

The stirrup gauges show interesting behavior (Fig. 5.16). In each span the stirrups showed very little strain up to cracking. Then one stirrup showed very large strains and another quit, likely due to high strains. The stirrups obviously did see very large strains since each one that crossed the failure crack fractured.

Crack angles and widths were again measured. Most cracks were inclined from 25° to 35°. Initial crack widths were about 0.005 in. The cracks measured grew much

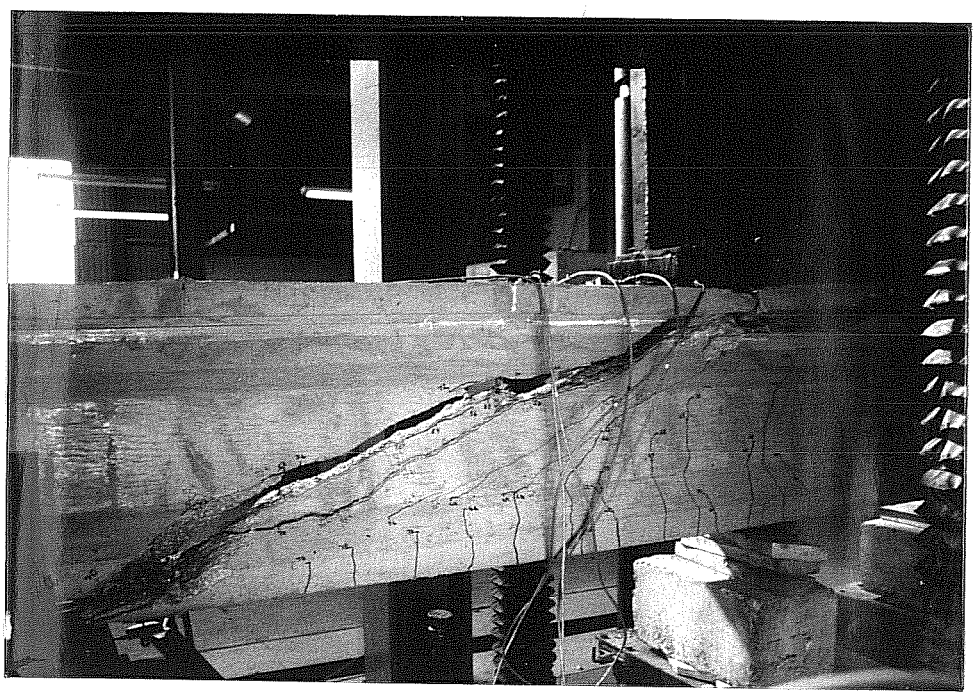

Fig. 5.13 Specimen 1-3 at failure.

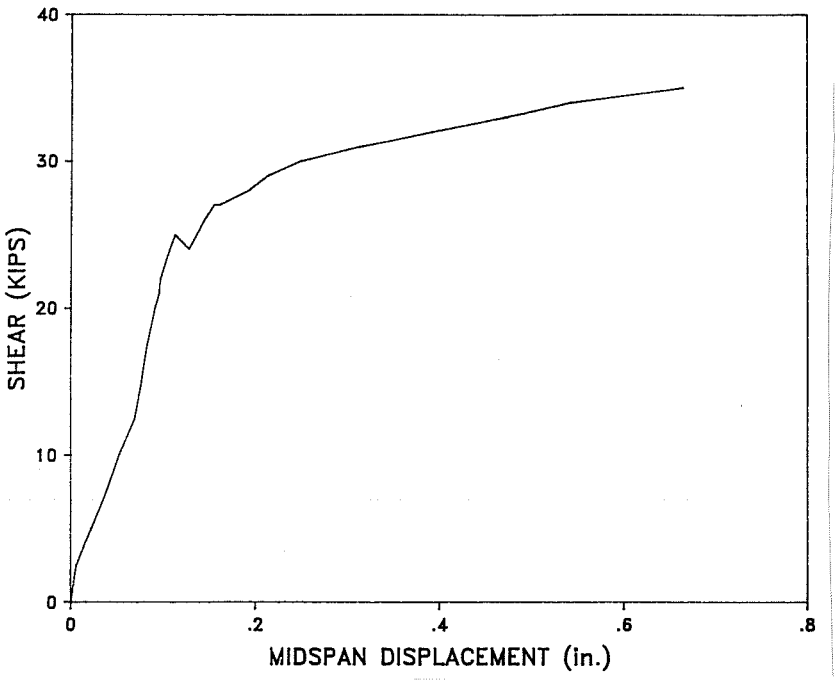

Fig. 5.14 Load-deflection curve for Specimen 1-3.

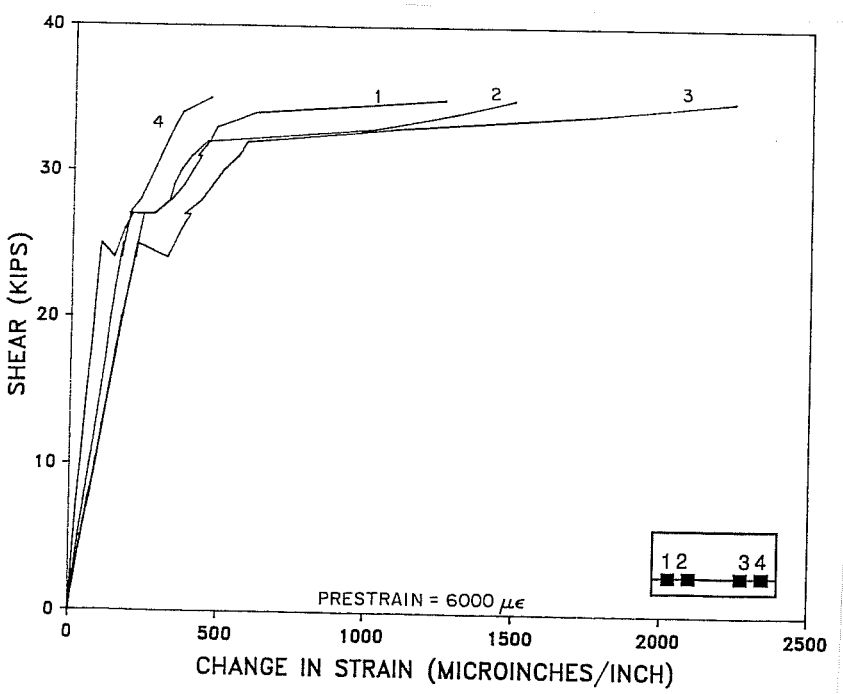

Fig. 5.15 Strand strains for Specimen 1-3.

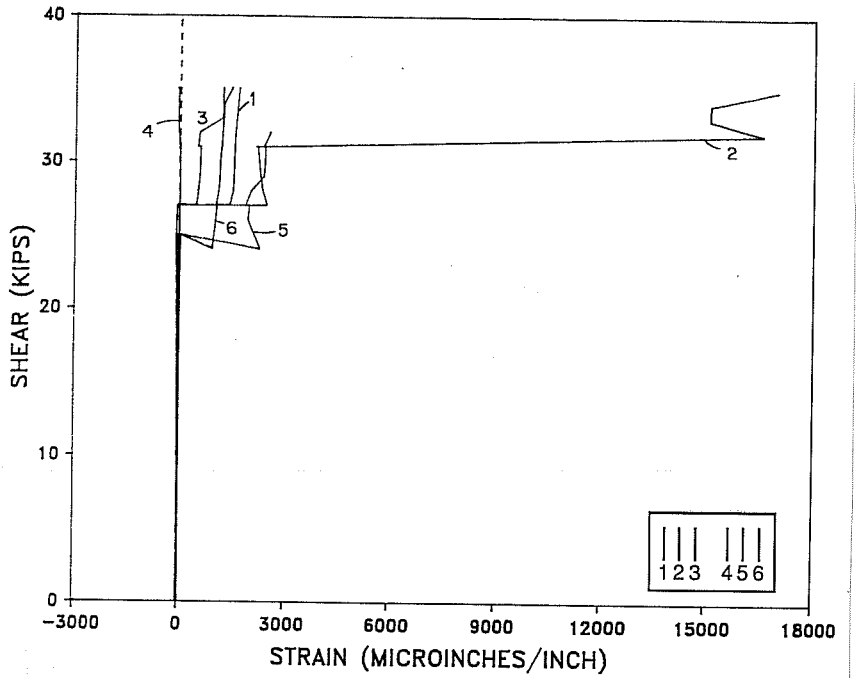

Fig. 5.16 Stirrup strains for Specimen 1-3.

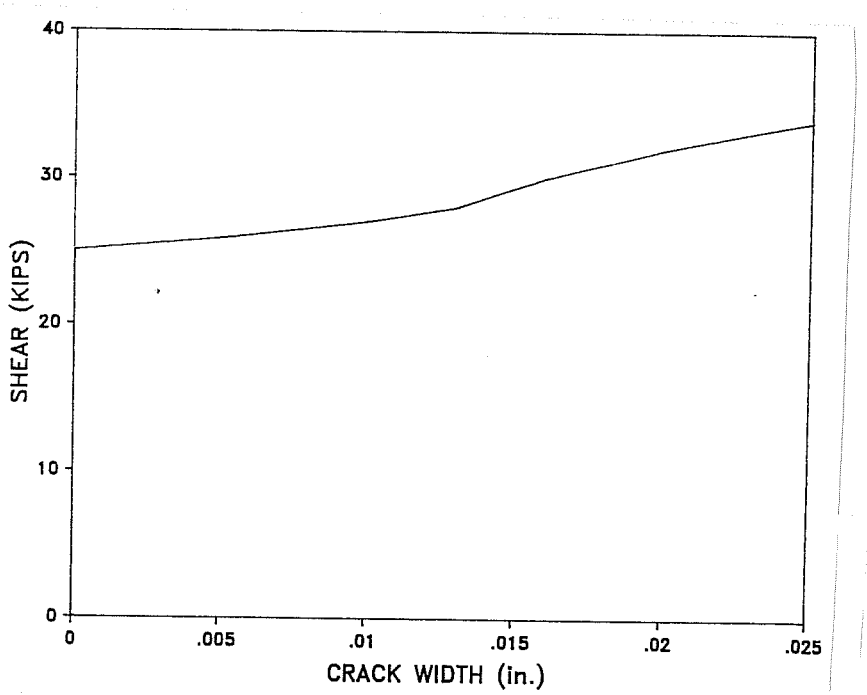

Fig. 5.17 Typical crack width versus load for Specimen 1-3.

wider as load increased. At a shear of 34.0 kips most cracks measured were 0.25 in. or more in width. Figure 5.17 shows the change in width for a typical crack.

5.2.4 Specimen 2-1. Specimen 2-1 was designed for a $V_s = 12\sqrt{f'_c}b_w d$ with f'_c=12000 psi. Specimen 2-1 was loaded in 2.5 kip increments up to a shear load of 30.0 kips. At a shear value of 32.0 kips shear cracks were noted. The specimen had suffered from shrinkage cracking before to formwork removal. All shrinkage cracks were closed at the time of the shear cracking. The second shear span cracked at 34.0 kips. Figure 5.18 (a) shows the initial cracking. The cracks were short and very fine with widths about 0.002 in. The load was increased in two kip increments to 80 kips and then by one kip until failure. The number of cracks increased greatly as the load increased (Fig. 5.18 (b)). The crack widths stayed very small. The first flexural cracks became apparent at 60.0 kips. The flexural cracks that opened formed at the existing shrinkage cracks. The cracks rapidly increased in height. Flexure- shear cracking was observed at 70 kips. Failure came from web crushing at 97 kips. Much of the web was blown off explosively at failure. Concrete spalled off over a region about 50 inches long (Fig. 5.19). The shear span was just under 56 inches long. Most of the concrete that blew off came from close to the bottom flange. In one location there was a hole completely through the web. After failure a large crack was observed just behind the support in the overhang. Prior to failure no slip was noted in the strands. After failure a number of strands pulled in. This was due to loss of bond because the strands were exposed in some areas. The bottom layer of steel did not slip to any significant degree.

Figure 5.20 shows the load-deflection curve for Specimen 2-1. The displacements are corrected for pad compression. The curve indicates a loss of stiffness for increasing load. It does not, however, show really pronounced flattening near failure.

The strand behavior is shown in Figure 5.21. The two gauges shown are for similar locations in the beam. The initial pretension strain was 5300$\mu\epsilon$. With an added strain of only approximately 1000$\mu\epsilon$ the strands were not near yield in the shear span.

One of the nonprestressed reinforcing bars was also gauged (Fig. 5.22). The bar underwent 2890 microstrains during testing. Yield strain was 2520$\mu\epsilon$. The bar was precompressed by 1900$\mu\epsilon$ due to prestressing. The bar did not yield.

Stirrup performance is indicated in Figure 5.23. Very small strains occurred up to cracking. After cracking the stirrup strains increased steadily with load. The figure shows that some but not all of the instrumented stirrups yielded. The outer stirrup on each end gave readings below yield.

Fig. 5.18 Specimen 2-1 during testing.

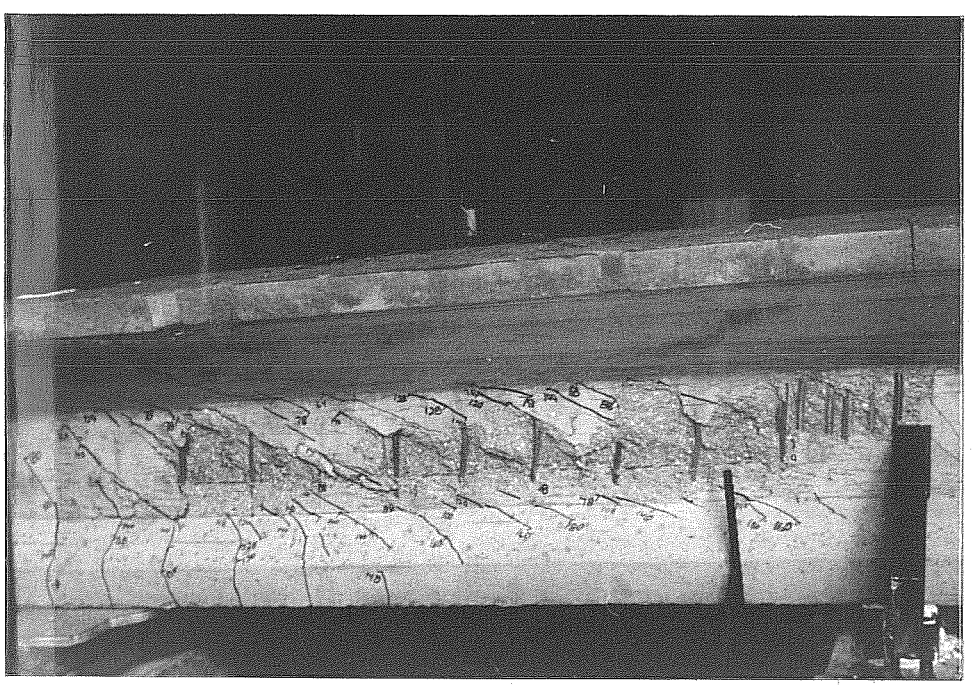

Fig. 5.19 Specimen 2-1 at failure.

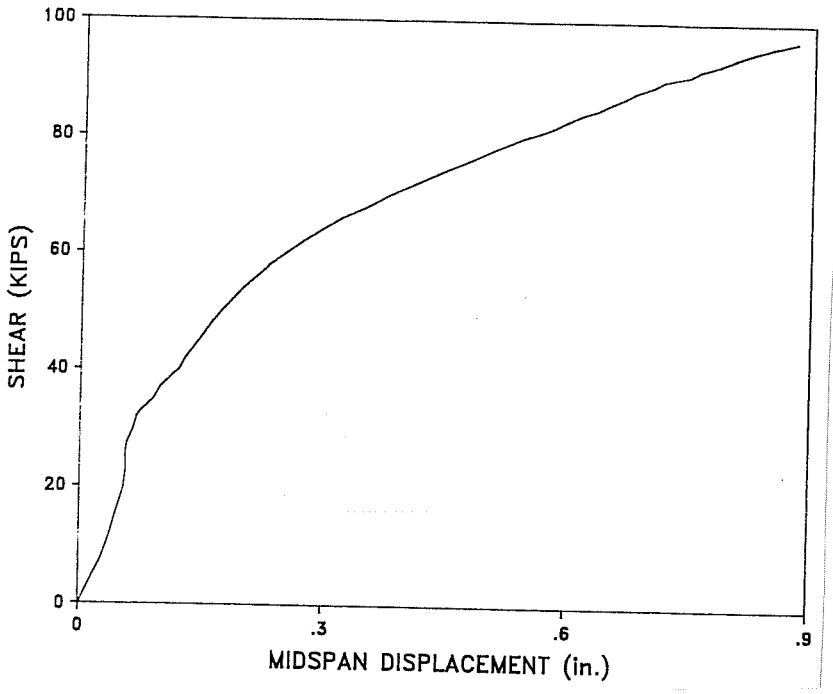

Fig. 5.20 Load-deflection curve for Specimen 2-1.

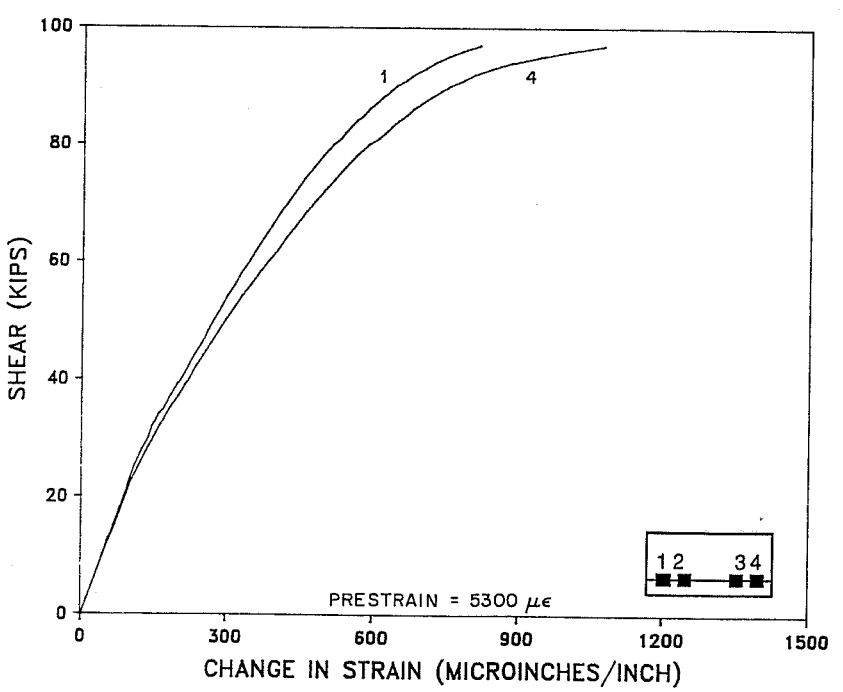

Fig. 5.21 Strand strains for Specimen 2-1.

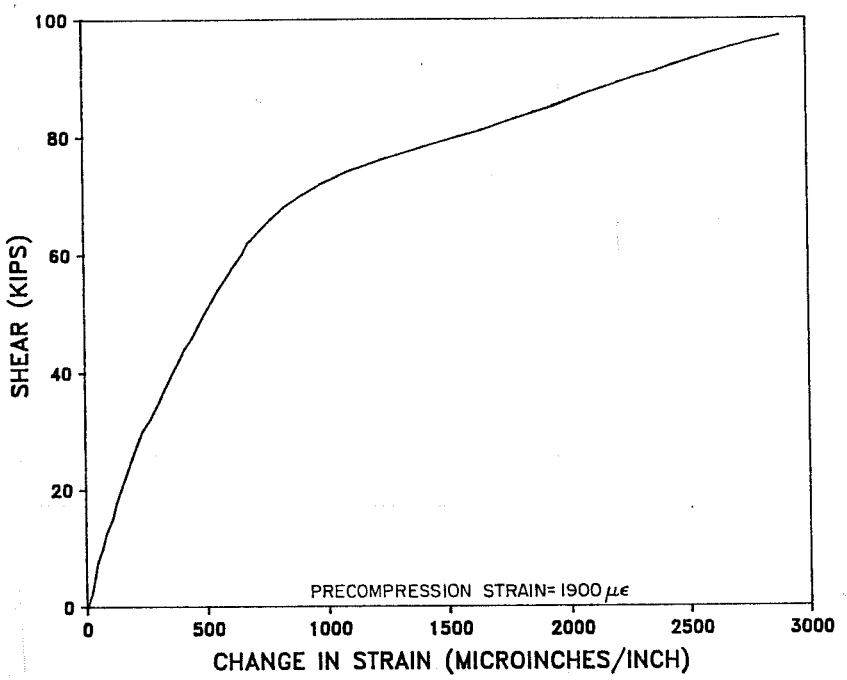

Fig. 5.22 Nonprestressed reinforcement strains for Specimen 2-1.

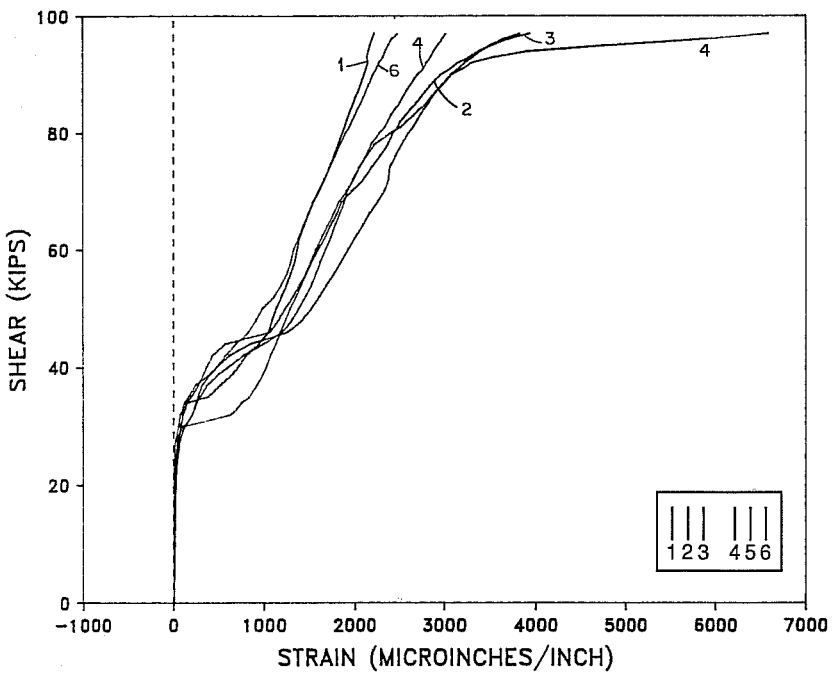

Fig. 5.23 Stirrup strains for Specimen 2-1.

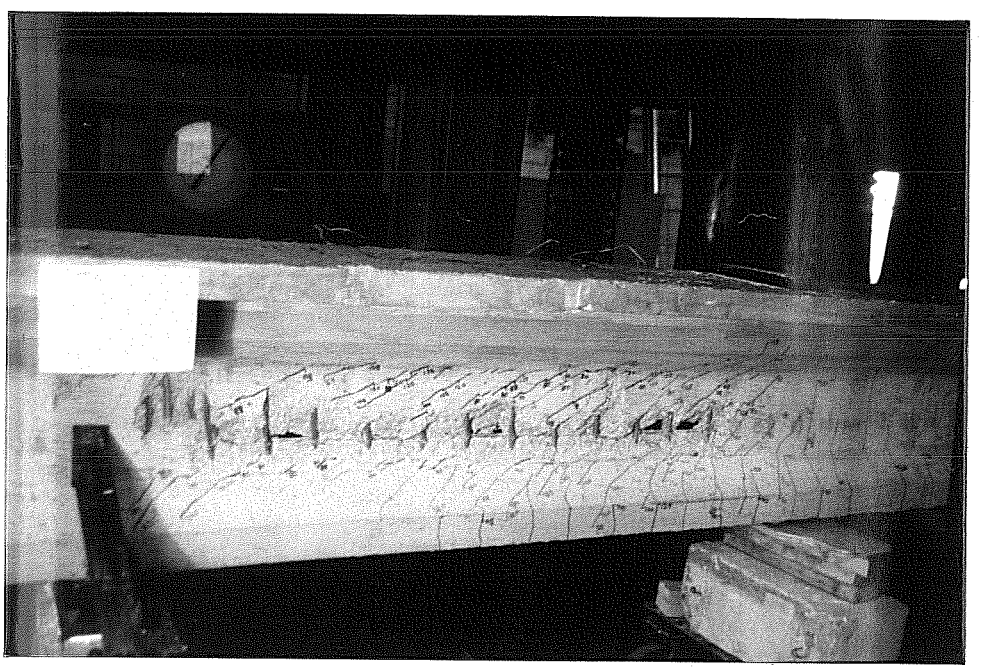

Fig. 5.24 Specimen 2-2 at failure.

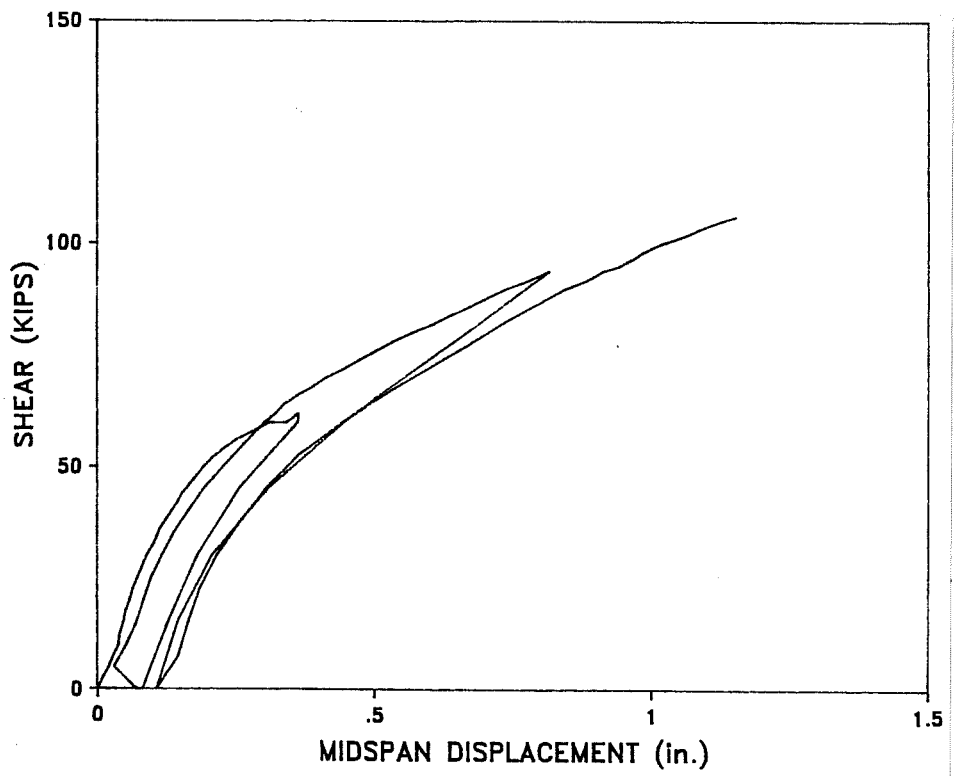

Fig. 5.25 Load-deflection curve for Specimen 2-2.

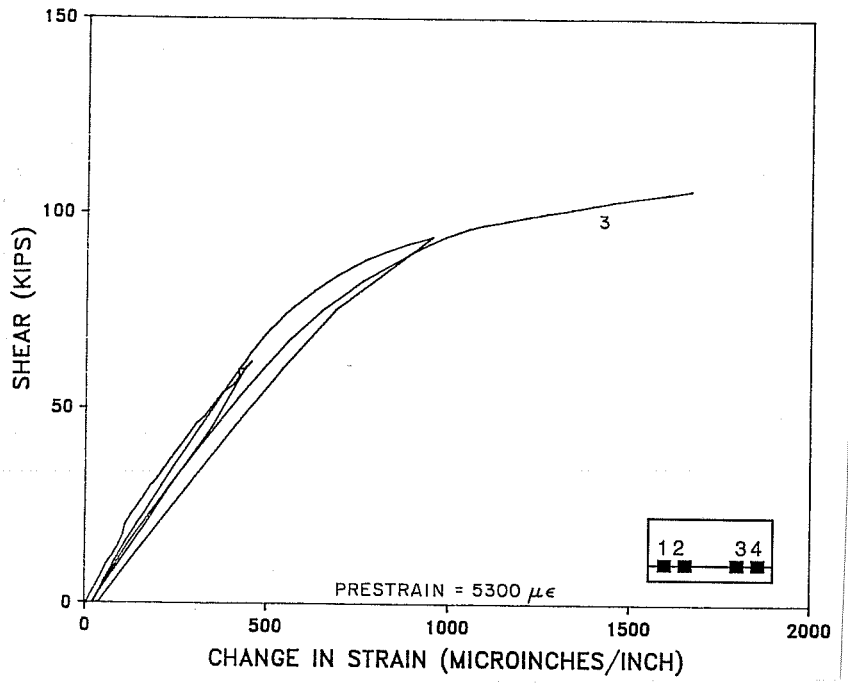

Fig. 5.26 Strand strain from Gauge 5 throughout the loading of Specimen 2-2.

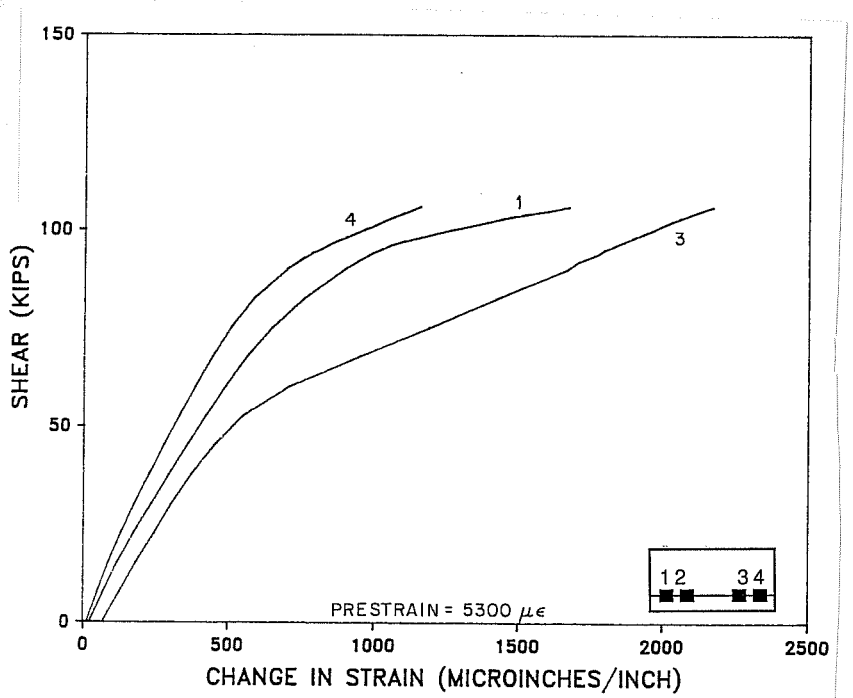

Fig. 5.27 Strand strains for final load cycle of Specimen 2-2.

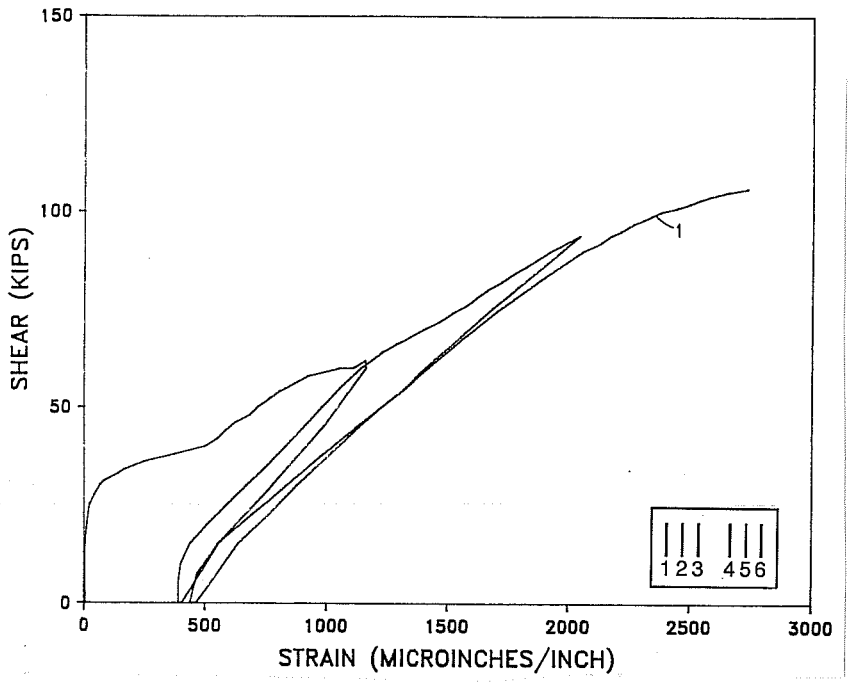

Fig. 5.28 Stirrup strains through complete loading cycle for Specimen 2-2 measured by Gauge 2.

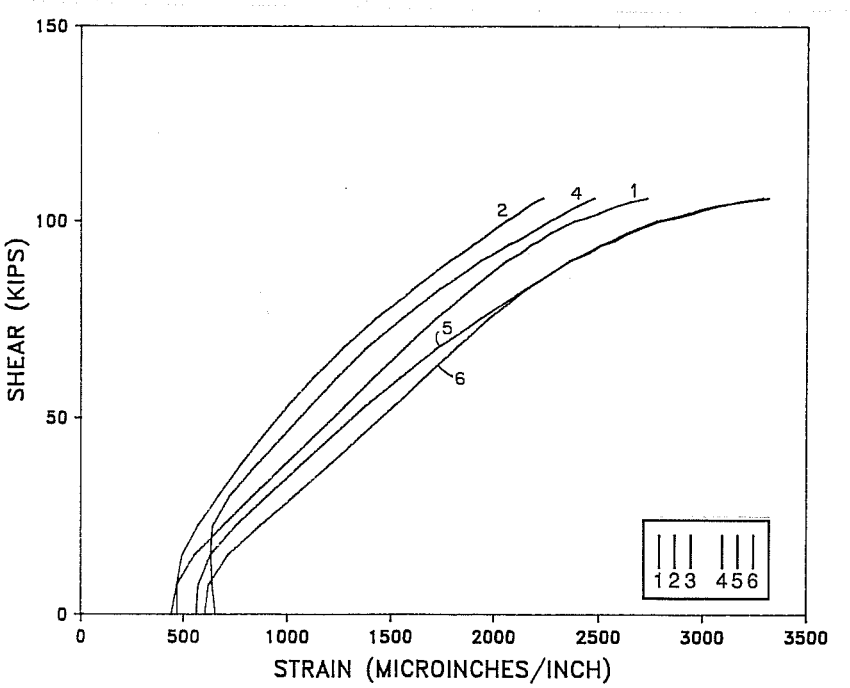

Fig. 5.29 Stirrup strains measured on final load cycle of Specimen 2-2.

held some strain between cycles of load. Figure 5.29 shows all the stirrups during the last cycle. Some of the stirrups did reach yield.

Specimen 2-2 had a very large number of cracks. Crack widths in general were 0.004 in. or less out to failure. Crack angles were generally from 28° to 35°.

5.2.6 Specimen 2-3. Specimen 2-3 had a nominal $V_s = 15\sqrt{f'_c}b_w d$ for f'_c = 12000 psi. Specimen 2-3 stirrups were designed to provide the prestressing strands with added confinement. It was loaded in 2.5 kip increments to 30 kips. Cracking was noted at 34.0 kips. The cracking was very limited. The other shear span cracked at 38.0 kips. The load was then increased in two kip shear increments to 100 kips and one kip increments thereafter. The number and length of cracks increased with loading. Flexure cracks were noted at 60.0 kips. Flexure-shear cracks were noted at 90.0 kips. The cracks propagated as the load increased. Failure occurred at 104.0 kips. The mode of failure was web crushing (Fig. 5.30). The web crushed throughout the shear span. There were cracks in the deck at the support after failure. The crushed concrete extended about five inches up the web. Prior to failure no strand slip was measured.

The load-deflection plot for Specimen 2-3 is shown in Figure 5.31. The curve indicates that the member had substantial stiffness remaining up to final shear failure. Final deflection was slightly less than one inch.

Strand strains are shown in Figure 5.32. The gauges were placed in two symmetrical locations along the beam. The gauges farther into the shear span showed much larger strains for a given load. None of the gauges show enough strain to indicate yielding of the strands.

Figure 5.33 shows the performance of the nonprestressed reinforcement. The gauge was located at the same place as the outer strand gauges. The bar was not close to yield at ultimate.

The stirrups did not pick up load until after shear cracking. Figure 5.34 shows stirrup strains thoughout the loading. All but the first stirrups in from the support showed yielding at failure.

Specimen 2-3 had a large number of very fine cracks. Crack widths near failure were generally 0.004 in. or less. Individual crack angles varied from 25° to 45°. Crack angles were generally about 28°.

5.2.7 Specimen 3-1. Specimen 3-1 was one end of the first flexural specimen tested by Castrodale. The specimen had a nominal shear reinforcement of $8\sqrt{f'_c}b_w d$.

Fig. 5.30 Specimen 2-3 at failure.

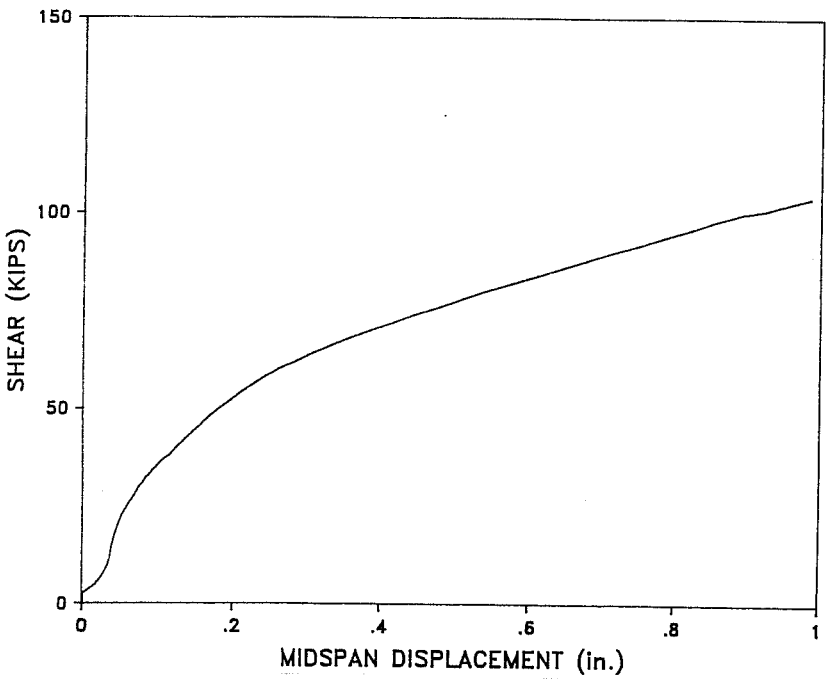

Fig. 5.31 Load-deflection curve for Specimen 2-3.

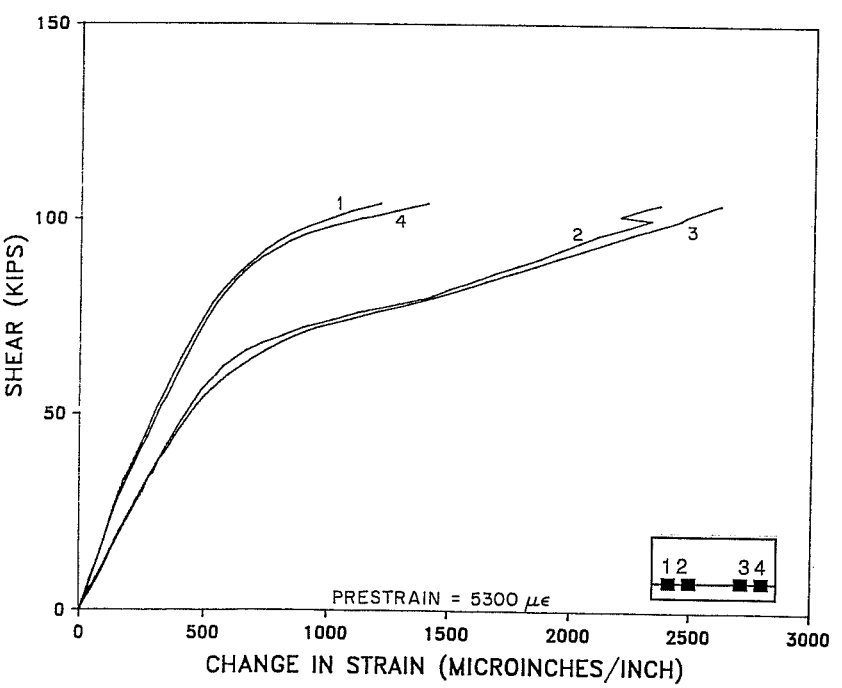

Fig. 5.32 Strand strains for Specimen 2-3.

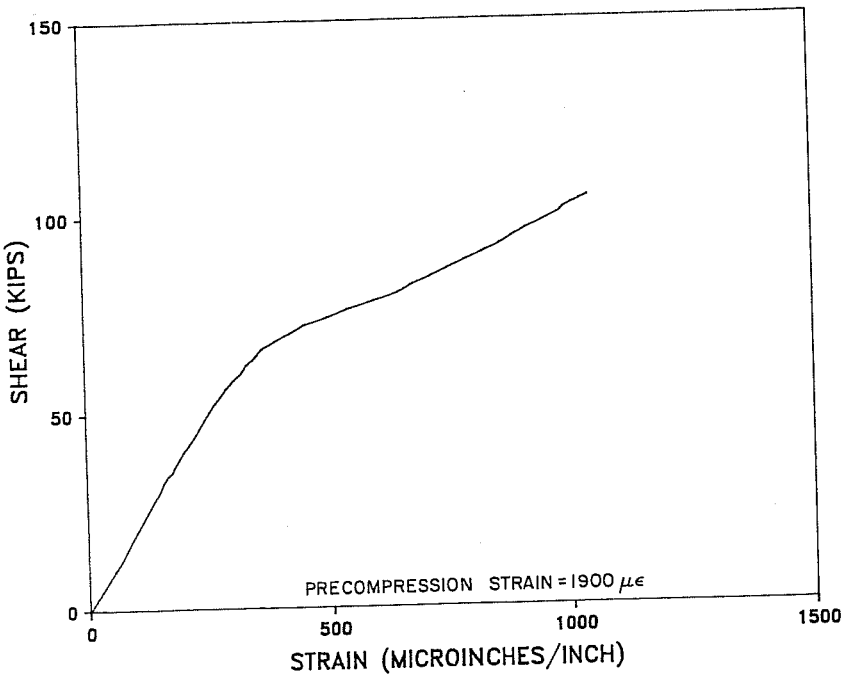

Fig. 5.33 Nonprestressed longitudinal reinforcement strains for Specimen 2-3.

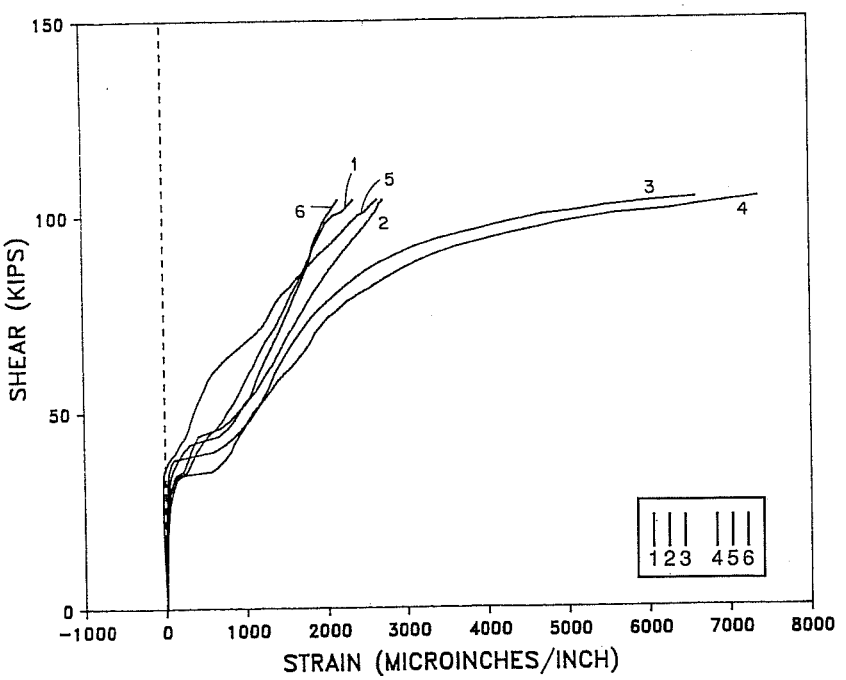

Fig. 5.34 Stirrup strains for Specimen 2-3.

Standard type stirrup details were used. The support location was modelled after that used in actual practice. Since the specimen had previously been tested in flexure it had suffered some damage. The most observable damage consisted of transverse cracks that extended through the deck and in some cases into the top flange. Additional damage due to the violent flexural failure was likely but not observed due to the prestress. Initially several load cycles were applied and discontinued due to load system difficulties. The loads exceeded those which were finally observed to cause cracking. In these preliminary cycles no crack observations were made. For these reasons the cracking load observed is of little value.

For the actual test, two load cycles were run. The first cycle was intended to determine the cracking load and the second to observe cracked behavior at low loads and then to determine the ultimate load. The first cycle went up to a shear load of 34.8 kips. Cracking was noted at a shear of 19.5 kips. The cracks were all very fine. Given the preceeding events described above it is likely that this was the reopening of existing cracks. The cracks noted extended somewhat and a few new cracks were noted during this cycle. The beam was then unloaded.

On the second cycle the specimen was loaded in five kip nominal shear increments. At 38.6 kips the test had to be suspended, the girder unloaded, and a new pressure gauge installed. The girder was then reloaded without any reading being taken until 40 kips. The first flexural cracks were observed at 44.5 kips. At 49.4 kips additional flexural cracks were observed. Shear cracks also entered into the bottom flange at this load. Failure occurred at a shear of 63.2 kips (Fig. 5.35). The failure was induced by slip of the prestressing strands (Fig. 5.36). The failure was not catastrophic since the applied load dropped rapidly with added displacement. The member still held load even after slip. Very large cracks formed right at the end of the detail steel when debonding occurred.

The load-deflection behavior of Specimen 3-1 through the last two load cycles is shown in Figure 5.37. The behavior is very consistent between the two cycles. This is partly due to the lack of flexural cracking.

Strand behavior can be seen in Figure 5.38. It will be noted that strand behavior is basically identical in both cycles. The beam was quite elastic. The gauges which were separated by 21 3/8 inches show a marked difference in behavior. Gauge 2 exhibits much more strain than gauge 1 at all load stages. Neither gauge was close to yielding of the strand.

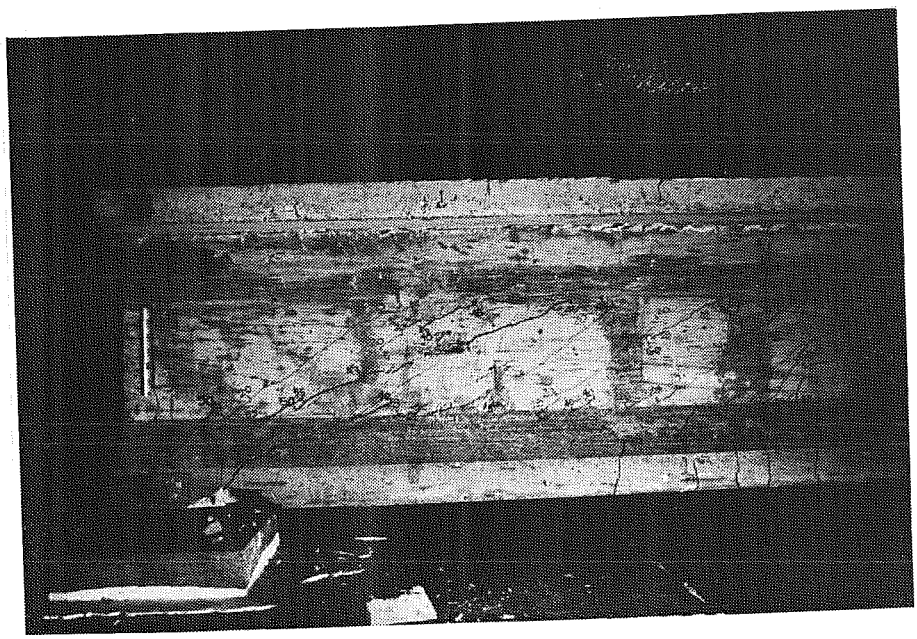

Fig. 5.35 Specimen 3-1 at failure.

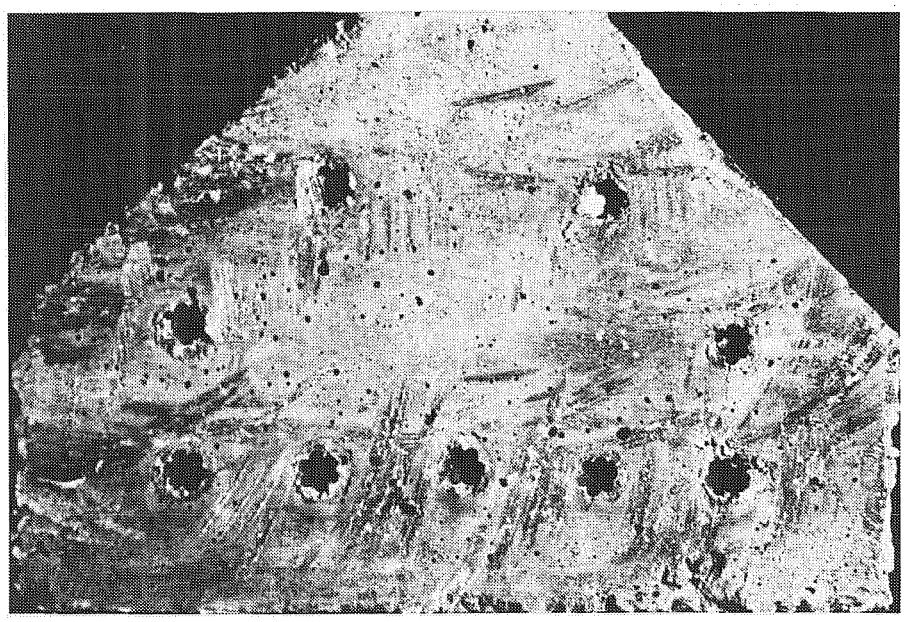

Fig. 5.36 Debonding of prestressing strands.

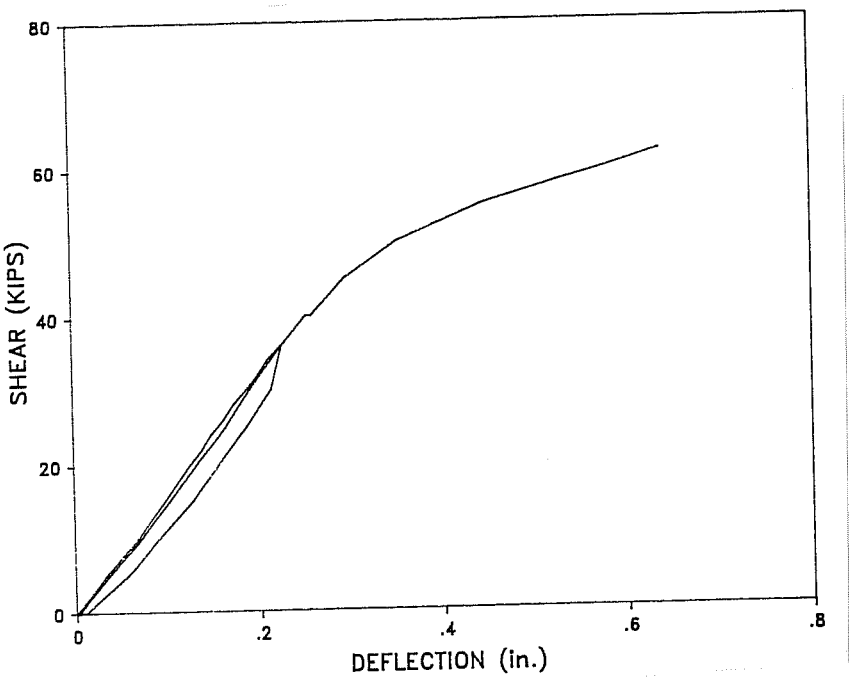

Fig. 5.37 Load-deflection behavior for Specimen 3-1.

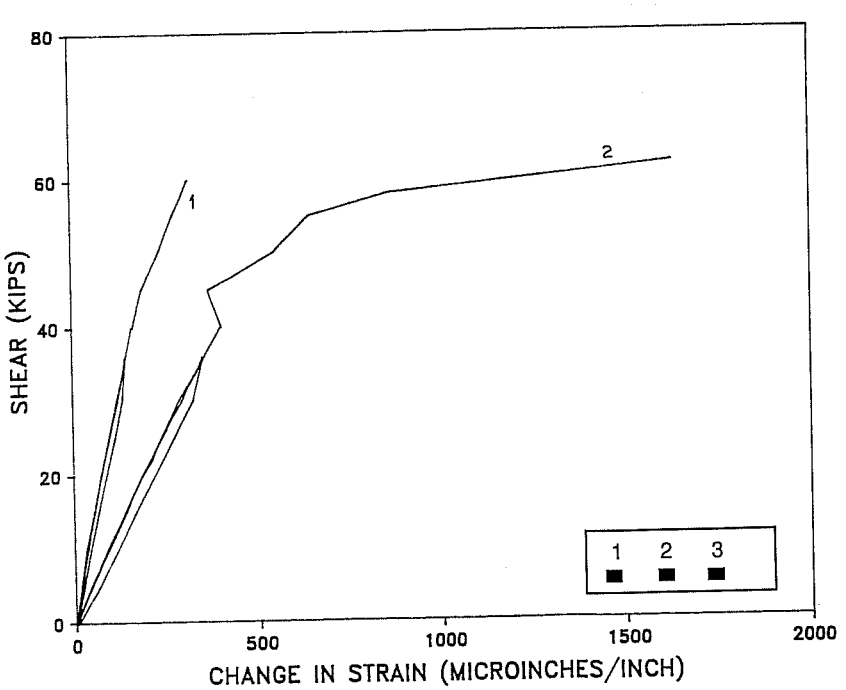

Fig. 5.38 Strand behavior for Specimen 3-1 through the last two load cycles.

The stirrups used for this specimen were #2 deformed bars. The bars after heat treatment had a yield stress of 44 ksi. The yield strain was approximately $1520\mu\epsilon$. Figure 5.39 shows strains for one of the gauges through both load cycles. It will be noted that some strain was held in the bar. It will also be noted that without the offset, behavior would be almost identical. This implies that the beam was probably cracked for the first cycle as it definitely was for the second. Figure 5.40 shows all the gauges through the second cycle. It appears that all the gauges but gauge 6, which was the closest to the load point, yielded. Gauges 4 and 5 were both just over yield.

The failure mechanism was from strand slip and thereby a loss of the tension chord. Figure 5.41 shows the load-slip behavior of the bottom row and second row of strands for the final load cycle. It shows that there was some slip before the final major slip. The draped strands showed varying degrees of slip. The top strand did not slip while the lower draped strands did slip slightly. The deck which was cast compositely did not show any significant slip throughout the loading.

Several observations were made of concrete cracking patterns. The shear cracks observed were generally inclined 25° to 35°. Shear cracks entered the bottom flange close to the support. Crack widths were not measured, but they did not appear very wide up to failure.

5.2.8 Specimen 3-2. Specimen 3-2 was the second end of the first flexural specimen tested by Castrodale. This girder had $V_s = 8\sqrt{f'_c}b_w d$. An improved stirrup detail was used for this specimen. A support location modelling actual field conditions was again used. The specimen's condition was similar to that of Specimen 3-1 except that it had not been subjected to the early shear loading cycles. Damage was assumed to be similar.

The beam was first loaded in a cracking cycle. The specimen was loaded to 33.9 kips of shear and then unloaded. Observation of the specimen had been made at 9.8 kips and no cracks were apparent. Cracking was observed at 14.7 kips. Upon unloading the cracks were apparent though somewhat closed.

The beam was reloaded in nominal five kip shear increments. The cracks were noted to have not changed substantially at 15 kips. Flexural cracking was noted beyond the load point at 38.6 kips and in the shear span at 49.4 kips. Flexure-shear cracks were observed at 54.4 kips and they reached the top of the web at 57.3 kips. The ulitmate load reached was 65.2 kips (Fig. 5.42). The failure mode was strand slip. The beam was

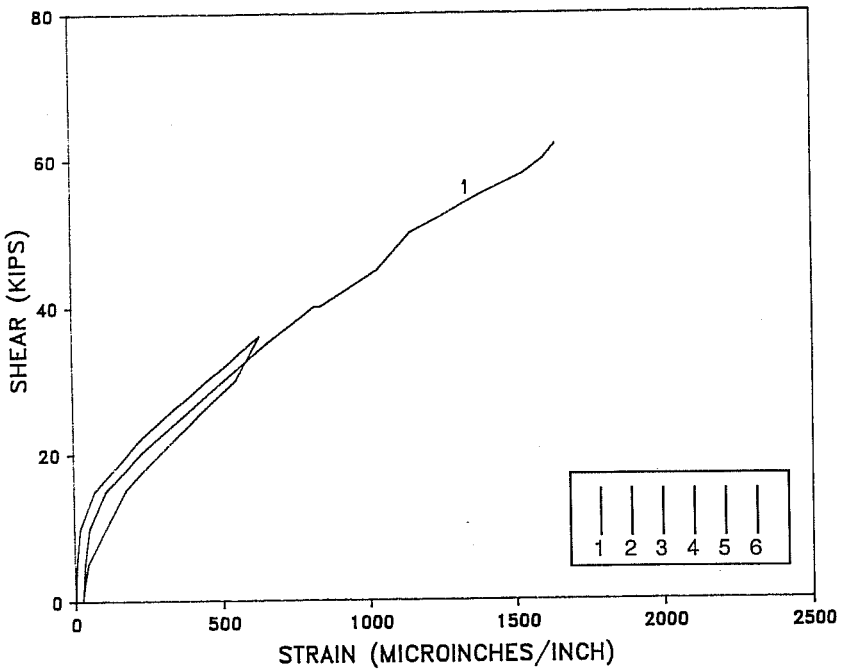

Fig. 5.39 Stirrup strains through last two load cycles of Specimen 3-1 measured by Gauge 1.

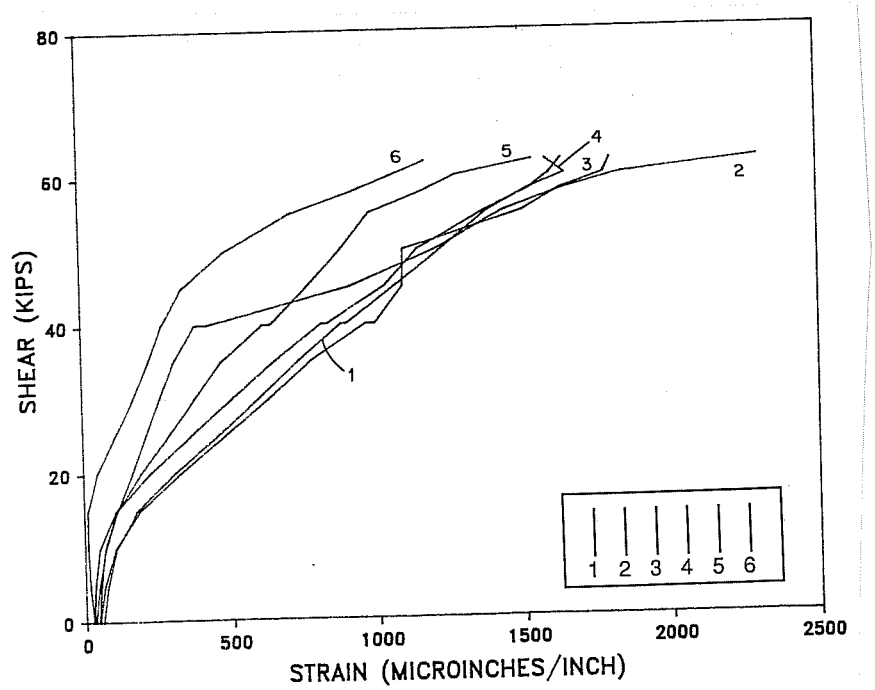

Fig. 5.40 Stirrup strains for last load cycle of Specimen 3-1.

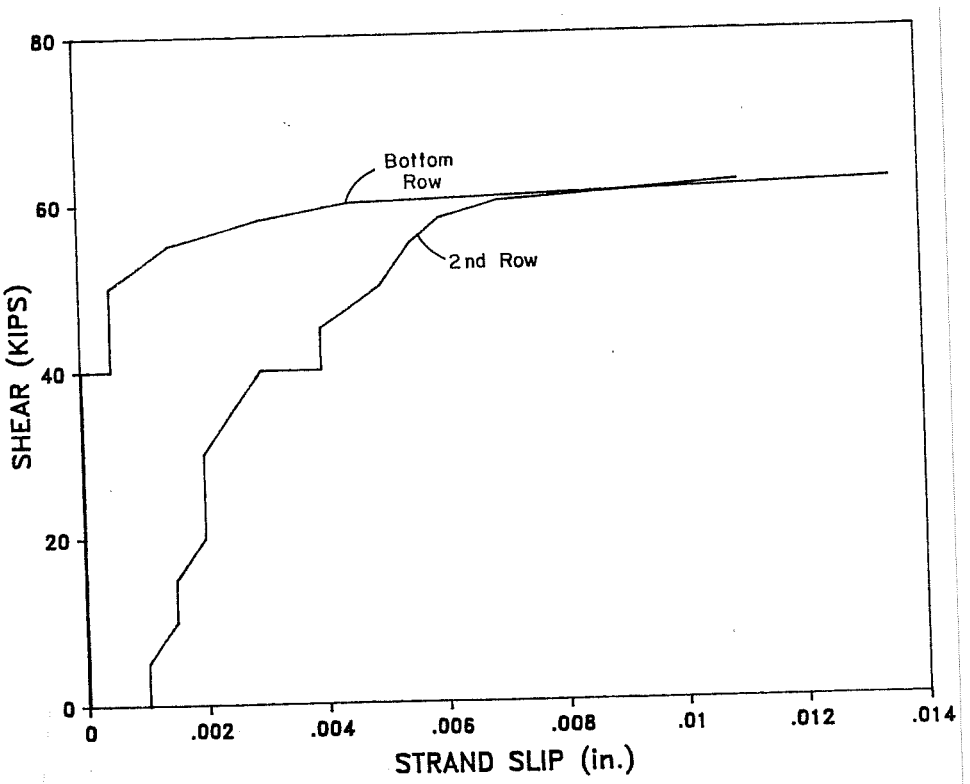

Fig. 5.41 Load-slip curve for Specimen 3-1.

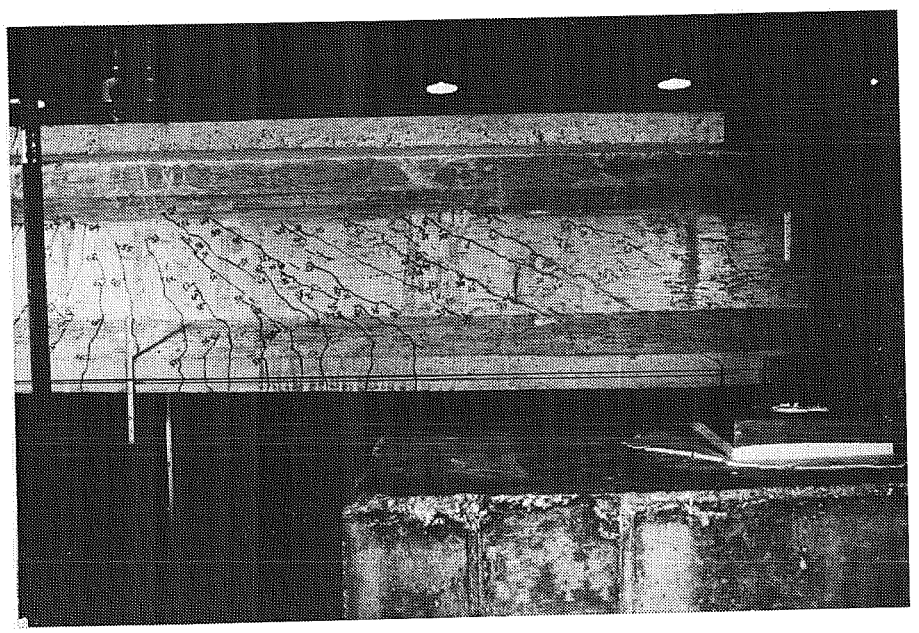

Fig. 5.42 Specimen 3-2 at failure.

able to take substantial load after slip, but did not again get to 65 kips. The strands continued to slip under added loading.

The load-deflection behavior of Specimen 3-2 is shown in Figure 5.43. Behavior between the two cycles can be seen to be similar.

Strand behavior can be seen in Figure 5.44. The strain gauges were well separated in the shear span. Both gauges show some strain set after the first cycle. If the set was taken out, the curve for the second cycle would be identical to that of the first. It will be noted that the two gauges show dramatically different amounts of change in strain. Neither gauge reached the yield strain.

Figure 5.45 shows one of the stirrups through both load cycles. Some set in the strain readings remained after the first cycle. If the second cycle is shifted to zero, the curves become identical. For the second cycle, the specimen was definitely cracked. It appears that the girder was cracked prior to testing since the first cycle shows identical behavior. The stirrup began straining immediately upon loading rather than having a period of small strains before cracking, as would be expected of a virgin specimen. Figure 5.46 shows all the stirrups for the second loading. The plot shows that all stirrups but gauge 6 had reached yield. Stirrup gauge 6 was the closest of the instrumented stirrups to the load point.

The load-slip curve for the lower levels of strands is shown in Figure 5.47. The second strand level showed some slip prior to general slip. The bottom strand slipped suddenly. The draped strands all slipped a measurable amount. Each draped strand slipped slightly more than the one above it. The deck slipped a very slight amount at failure.

The web cracking on Specimen 3-2 was typically angled at 25° to 30°. Inclined flexure-shear cracks were typically around 40° as were cracks at the support. Upon failure the major crack went through the bottom of the girder 8.5 in. from the end. Other cracking also resulted from the loss of the tension chord.

5.2.9 Specimen 3-3. Specimen 3-3 was one end of the second flexural specimen tested by Castrodale. The girder was designed for $V_s = 4\sqrt{f'_c}b_w d$. Standard stirrup details were used. Actual support locations were modelled for this girder. Specimen 3-3 had first been tested in flexure and had failed violently. There were transverse cracks across the top of the deck. The specimen also had a large number of shrinkage cracks

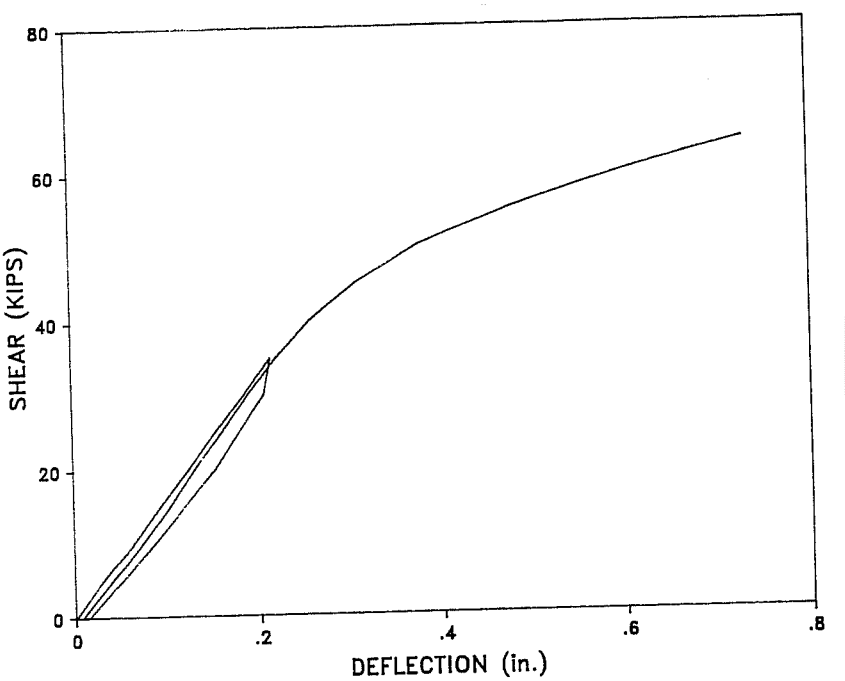

Fig. 5.43 Load-deflection behavior for Specimen 3-2.

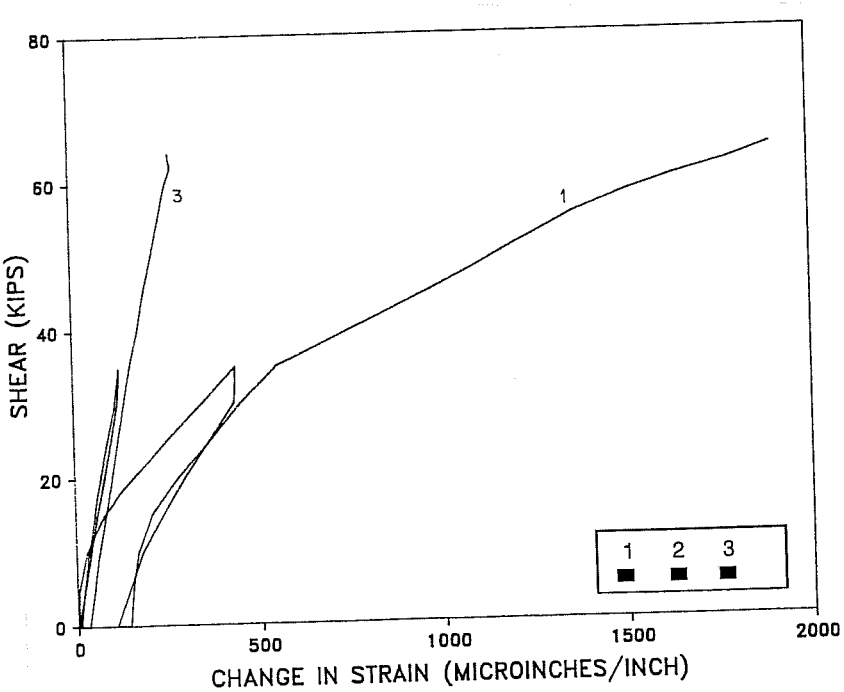

Fig. 5.44 Strand strains for final two load cycles of Specimen 3-2.

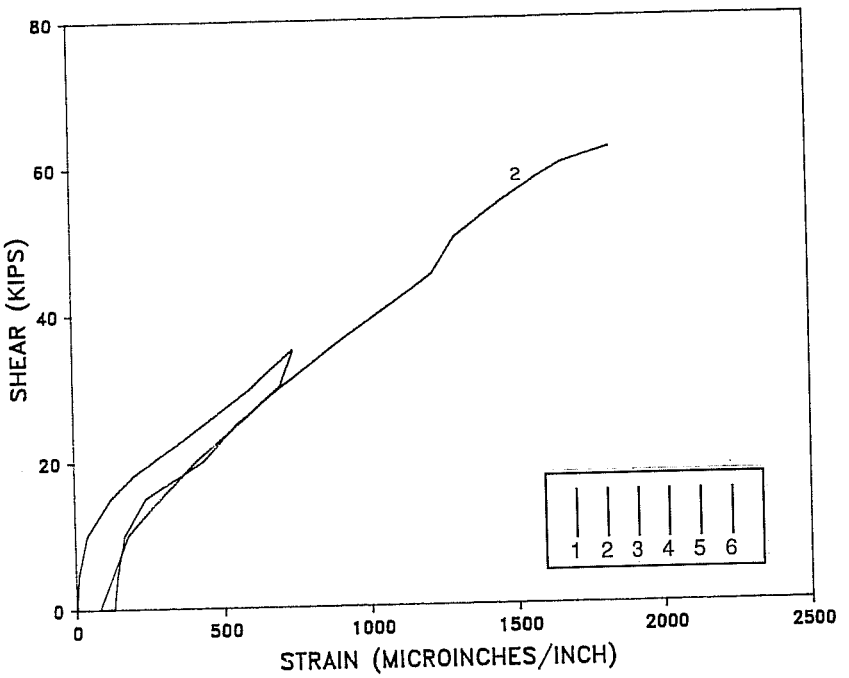

Fig. 5.45 Stirrup strain of Gauge 1 for last two load cycles of Specimen 3-2.

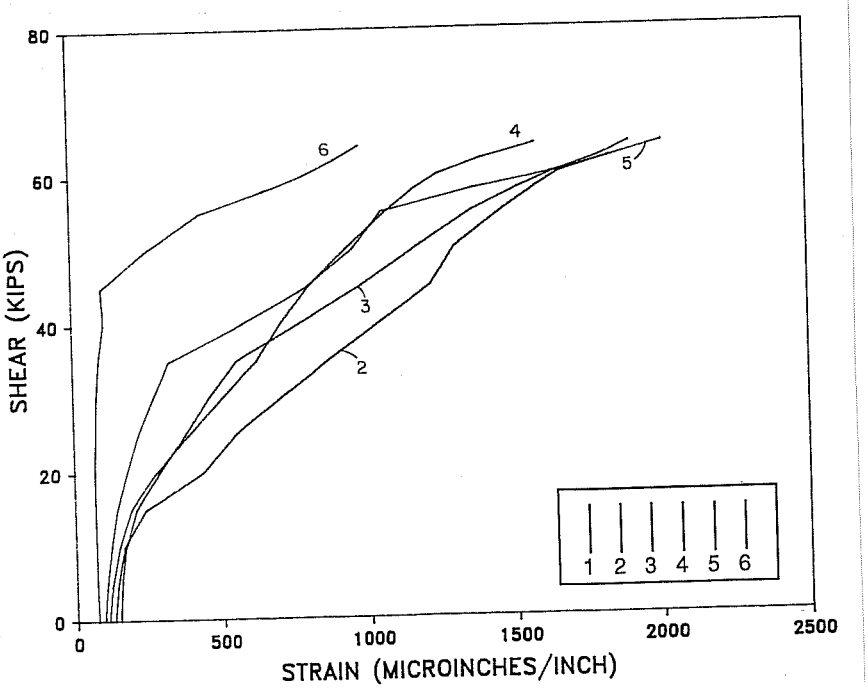

Fig. 5.46 Stirrup strains for last load cycle of Specimen 3-2.

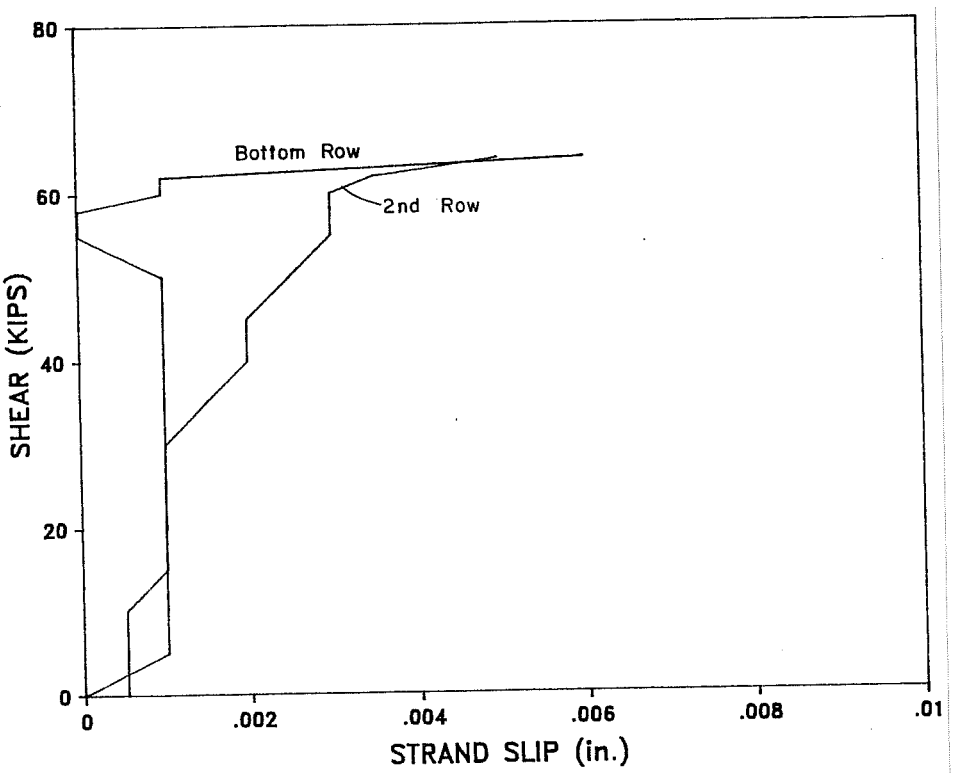

Fig. 5.47 Load-slip curve for Specimen 3-2.

throughout the section. The prestress effectively closed cracks in the web and it is believed prevented detection of existing cracks prior to the test.

The specimen was loaded in one cycle to failure. The specimen was loaded in four kip shear increments to 20 kips then two kip increments to 34 kips and one kip after that to failure. Cracks were observed near the end of the beam at eight kips. As the load increased the cracks were noted to increase in number and width. Flexure cracks were noted at 38.0 kips. Failure occurred at 41.0 kips (Fig. 5.48). The failure mode was strand slip. Prior to failure shear cracks had extended deep into the bottom flange. Shrinkage cracks close to the support were noted to not be open.

Figure 5.49 shows the load-deflection behavior of the specimens. It can be seen that the specimen had lost little stiffness up to failure. This was mainly due to the small amount of flexural cracking that occurred.

Strand behavior was measured at a number of locations along the shear span. Figure 5.50 shows gauge readings versus load through the cycle. The gauges were placed so that two gauges were relatively close to each other. The two "pair" gauges gave very similar results. The three distinctly different locations gave quite different load versus strain curves. The further away from the support that the gauge was, the greater the strain. Gauge 7 was located on the draped strand at roughly the same location as gauge 4. The gauge saw some compression early and did not go into appreciable tension until the load was about 3/4 of ultimate. Figure 5.51 shows the strains through the shear span at various load stages. None of the gauges indicated that the strand yielded prior to failure.

Stirrup gauge readings are illustrated in Figure 5.52. The gauges began to strain as soon as load was applied. This indicates that the beam was likely precracked before the shear test began. Only two of the gauges reached yield prior to the strand slip. Figure 5.53 shows the strand strains along the shear span at various loads. It shows that the stirrups near the center of the shear span yielded while the stirrups near the load point and support did not.

The failure mode was strand slip. The load-slip curve for the bottom and second rows are shown in Figure 5.54. It can be seen that the second row strand began to slip early in the loading and continued to do so by small increments until a final large slip. The bottom row stayed steady until 38.0 kips. It then slipped slightly for several load stages followed by a large and then catastrophic slip. The draped strand did not slip throughout the test. The deck did slip 0.006 in. during the test.

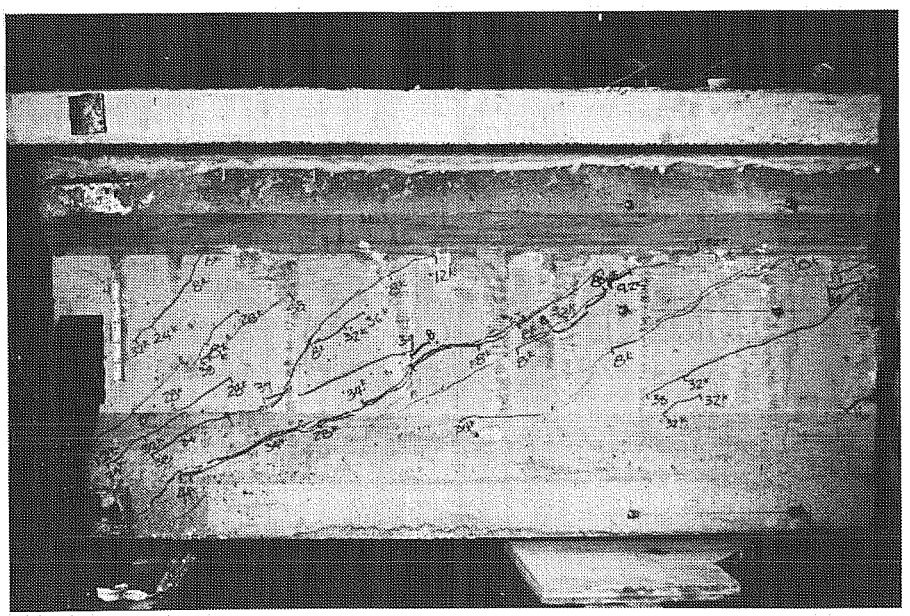

Fig. 5.48 Specimen 3-3 at failure.

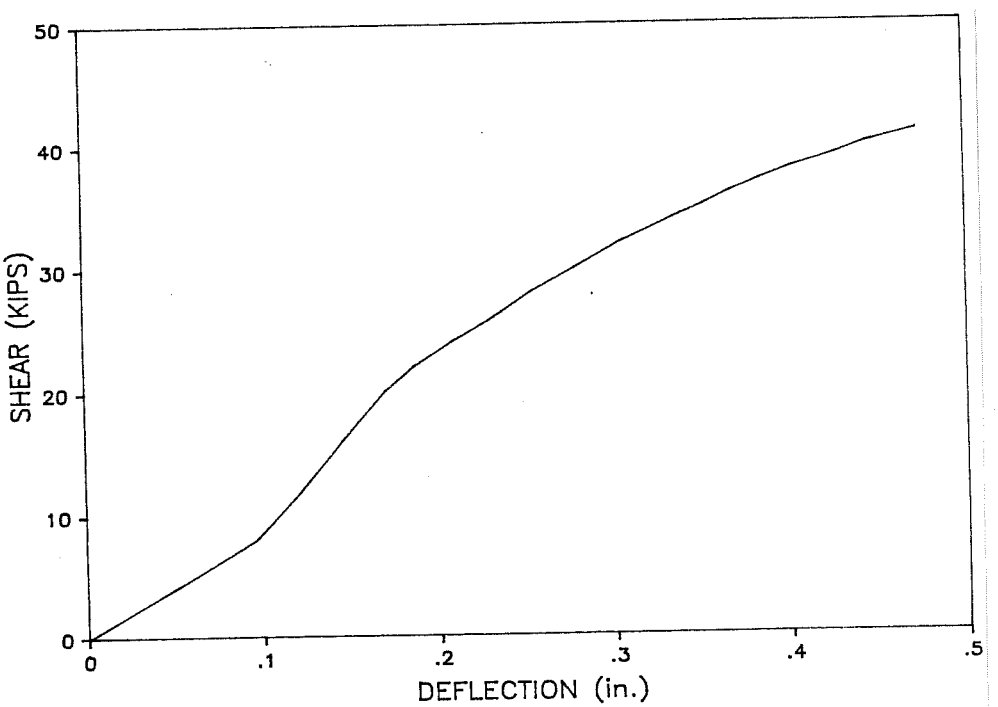

Fig. 5.49 Load-deflection curve for Specimen 3-3.

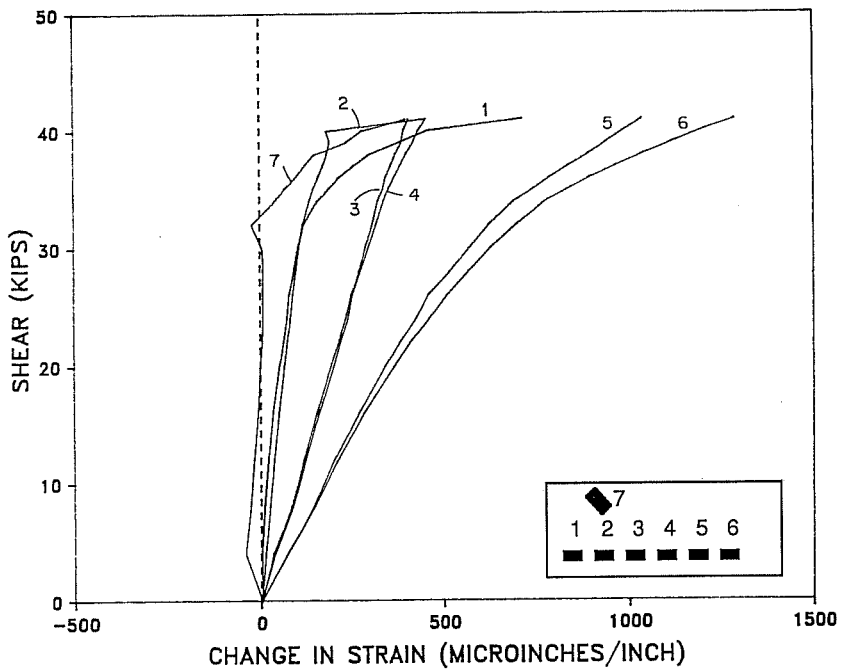

Fig. 5.50 Strand strains for Specimen 3-3.

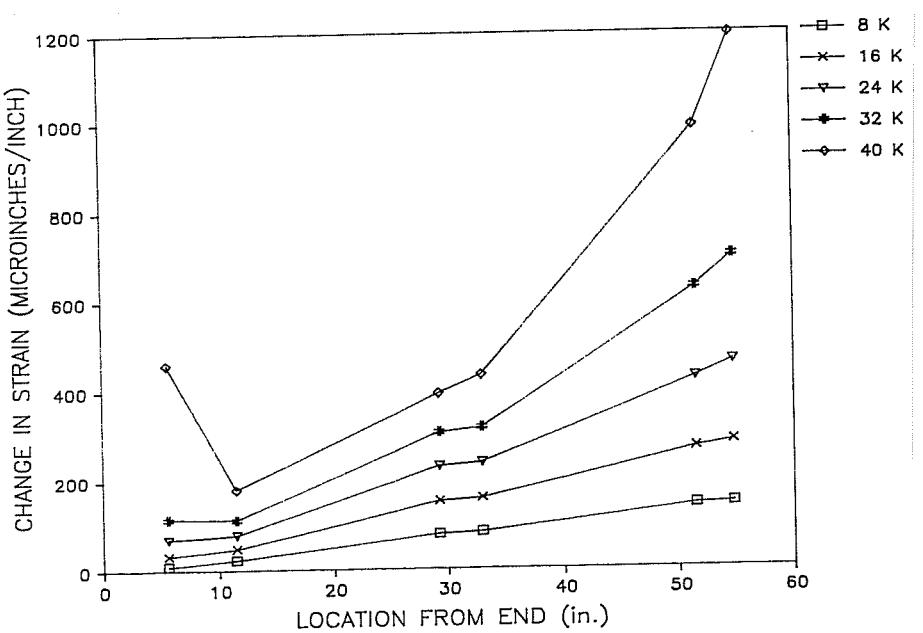

Fig. 5.51 Strand strains along length of shear span for Specimen 3-3.

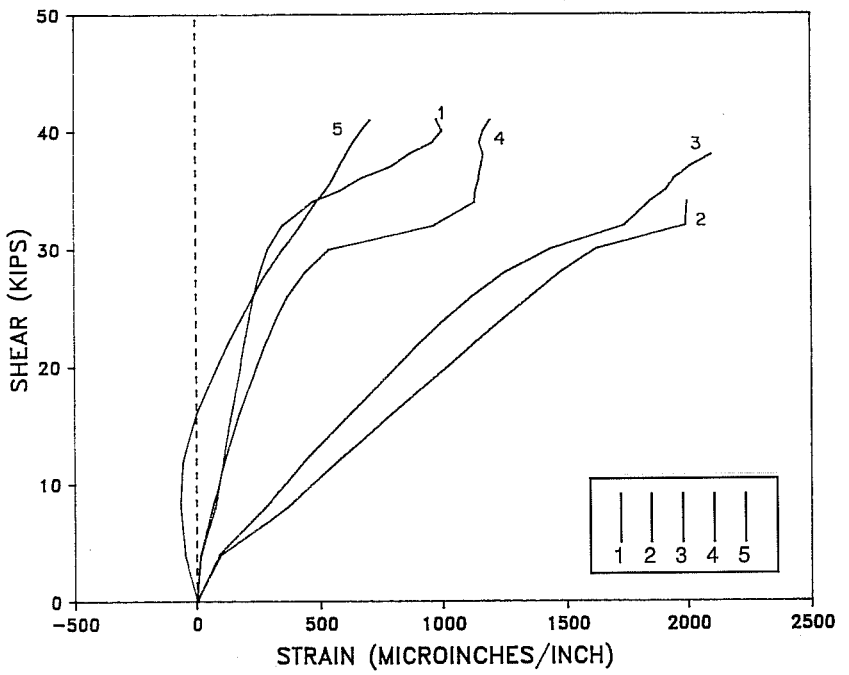

Fig. 5.52 Stirrup strains for Specimen 3-3.

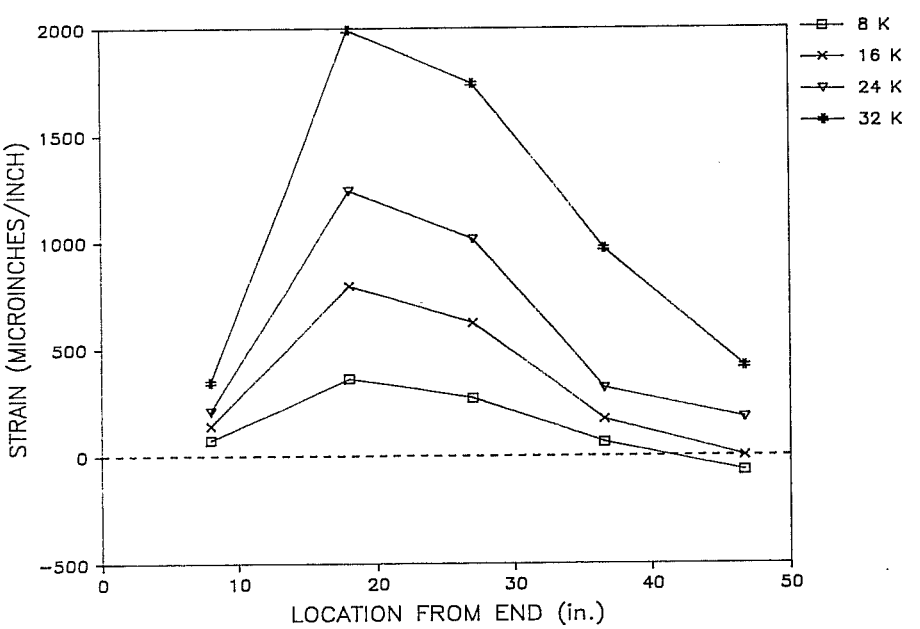

Fig. 5.53 Stirrup strains along the length of the shear span for Specimen 3-3.

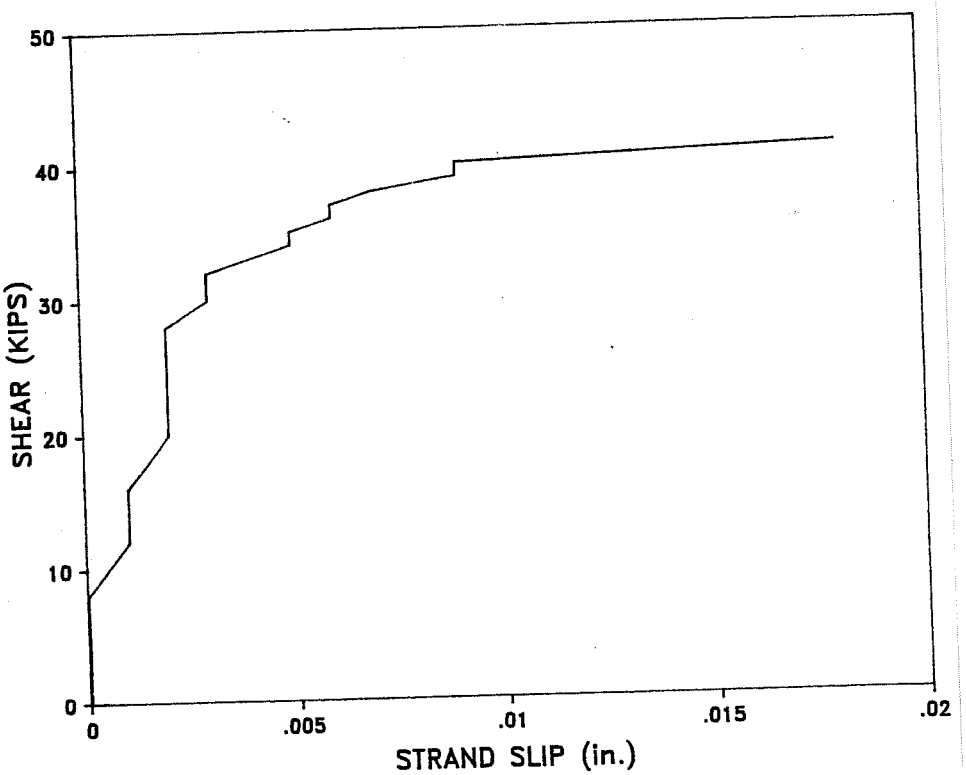

Fig. 5.54 Load-slip curve for Specimen 3-3.

Readings were taken of both crack angle and crack width. Crack angles in the middle of the shear span ranged from about 20° to 35°. Crack angles near the support and load point ranged from 40° to 55°. Crack readings were taken in the final five load stages. Crack widths on measured cracks ranged from 0.010 to 0.050 inches. These cracks were read since they were the widest ones. Other cracks had lesser widths.

5.2.10 Specimen 3-4. Specimen 3-4 was an end of the second flexural test perfomed by Castrodale. The girder was designed for a nominal $V_s = 4\sqrt{f'_c}b_w d$. Standard stirrup details were used. For this specimen an overhang to allow for more development was included. The support centerline was 8.5 in. from the specimen end. Specimen 3-4 is the second end of the girder from which Specimen 3-3 was taken. The observations about damage to 3-3 are also true for this specimen.

Specimen 3-4 was loaded in four kip shear increments to 20 kips, two kip increments to 36 kips, and one kip increments there- after. Cracks were observed at 8.0 kips. As the load was increased, cracks were marked and measured at load stages. At 34.0 kips some of the shrinkage cracks began to open as flexural cracks. Flexural cracks were observed at 40.0 kips. At 47.9 kips web crushing was observed in a localized area at the top of the web. The crushing was a slow spalling rather than the explosive failure expected with high strength concrete. The crushing originally occurred between two cracks. It appeared that the top of a diagonal compression strut was crushing. The crushing also brought about a decrease in load. Upon further loading, the load increased to 48.9 kips. At this level a second area of crushing formed. Further loading caused a third and fourth area to crush giving fairly general crushing of the web and greatly reduced capacity (Fig. 5.55). Strand slips on the order of 0.004 and 0.002 in. were noted for the second and bottom rows respectively. The slip was not of sufficient magnitude to affect the failure mode. The draped strand and deck showed no measurable slip.

The load-deflection behavior for Specimen 3-4 is shown in Figure 5.56. It will be noted that as the specimen neared the crushing load, the slope of the load-deflection curve decreased dramatically. The curve became fairly flat for about 0.15 in. and then entered a descending branch. The flat portion of the curve corresponds to the period of crushing.

Strand behavior versus load is shown in Figure 5.57. The gauges were placed throughout the shear span. The location had a significant effect on the strain measured. Those located closer to the load point had greater strain in general. A gauge was placed

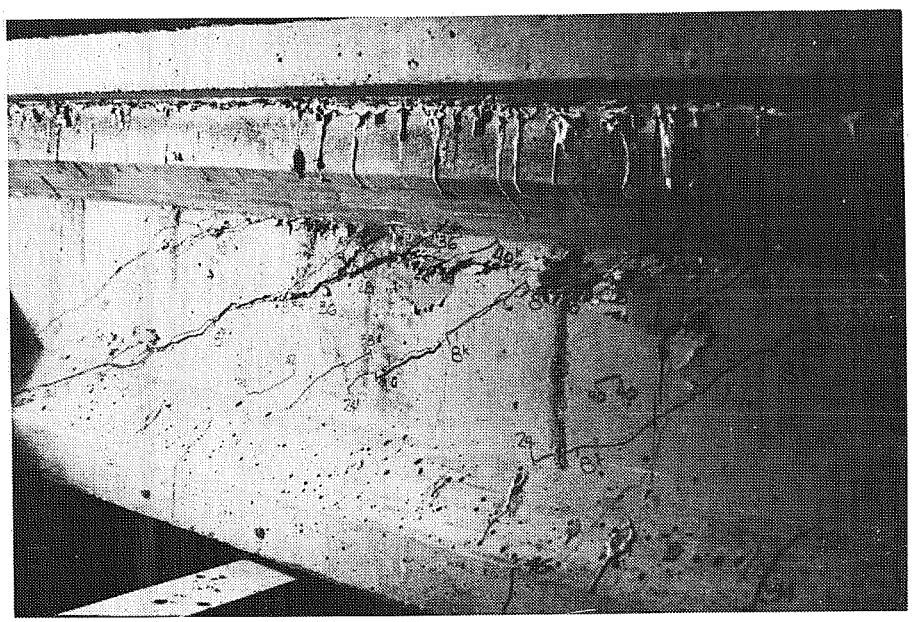

Fig. 5.55 Specimen 3-4 at failure.

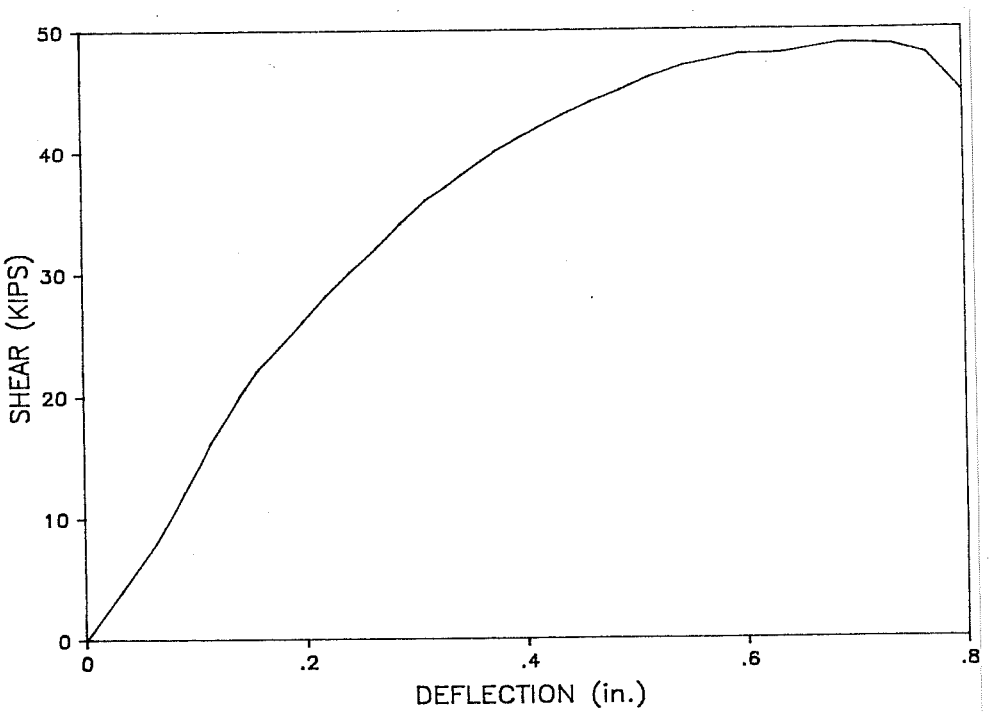

Fig. 5.56 Load-deflection curve for Specimen 3-4.

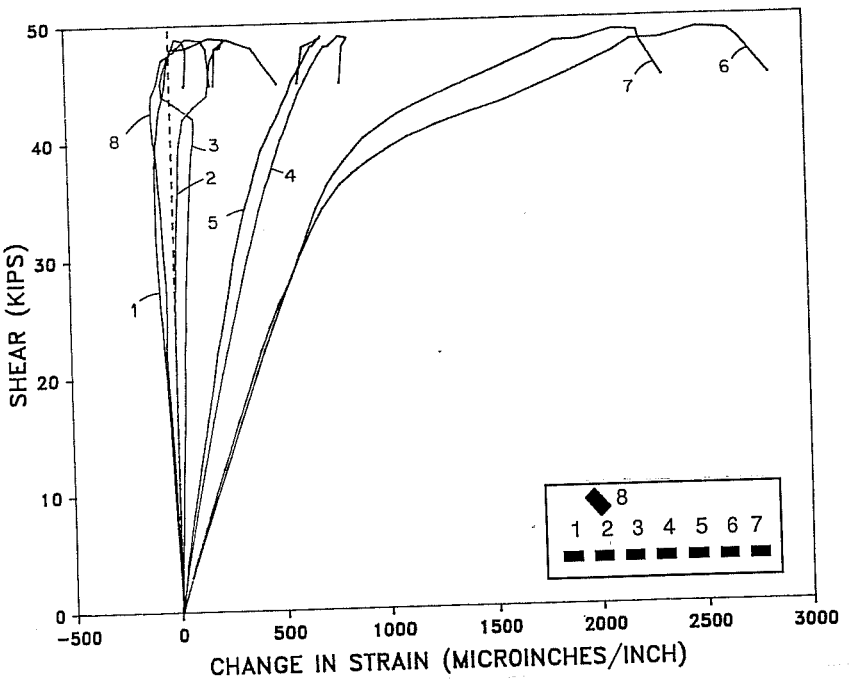

Fig. 5.57 Strand strains for Specimen 3-4.

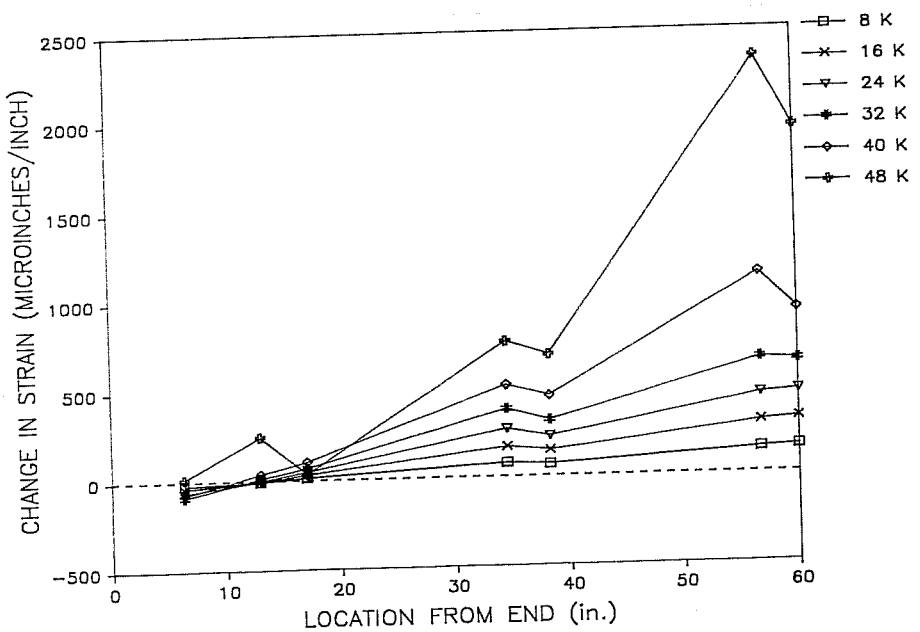

Fig. 5.58 Strand strains versus location in shear span for Specimen 3-4 (support centerline x=8.5 in.).

on the draped strand. This gauge read compression through all but the last several load cycles. A gauge was also placed 1.75 in. outside the support centerline. The gauge read compression until just prior to failure. Figure 5.58 shows strains along the shear span at various load stages. It can be seen that strains at the end of the girder changed little during loading while gauges near the load point changed considerably.

Stirrup strains versus load are shown in Figure 5.59. The readings are somewhat erratic at high loads but they do give useful information. The gauges began to strain as soon as load was applied. This indicates the beam was likely precracked. The figure also shows that three of the stirrups had reached yield. Figure 5.60 shows stirrup strain readings along the shear span. It will be noted that the three interior gauges yielded while the gauge nearest the support and nearest the load point did not yield.

5.3 Discussion of Test Results

5.3.1 General. This section will compare the individual tests to determine general properties of shear behavior in high strength prestressed concrete. As a starting point the internal behavior of the specimens will be discussed. A conceptual truss model can be used to provide a general framework for this discussion. There are five major failure mechanisms possible in a truss model including: tension chord failure, compression chord failure, stirrup tensile failure, diagonal compression strut failure, and detailing failures consisting of either debonding or slip of longitudinal reinforcement or nodal failures. Of these five mechanisms stirrup failures, diagonal compression strut failure, and slip of reinforcement were all observed and will be discussed. Additionally some general comments about strand behavior, surface strain readings, and cracking will be made.

After this general discussion the results are compared with the shear capacity model assumptions. The final and most important comparison will be between predicted and actual capacities.

5.3.2 Observations

5.3.2.1 Stirrup tensile failures. Tension failure of the stirrups is one possible mechanism for general beam failure. All but one of the specimens tested had some level of shear reinforcement. These beams can be divided into those in which general failure was initiated by stirrup failure and those which were not. Specimens 1-2 and 1-3 were controlled by failure of stirrups. Both specimens had light shear reinforcement:

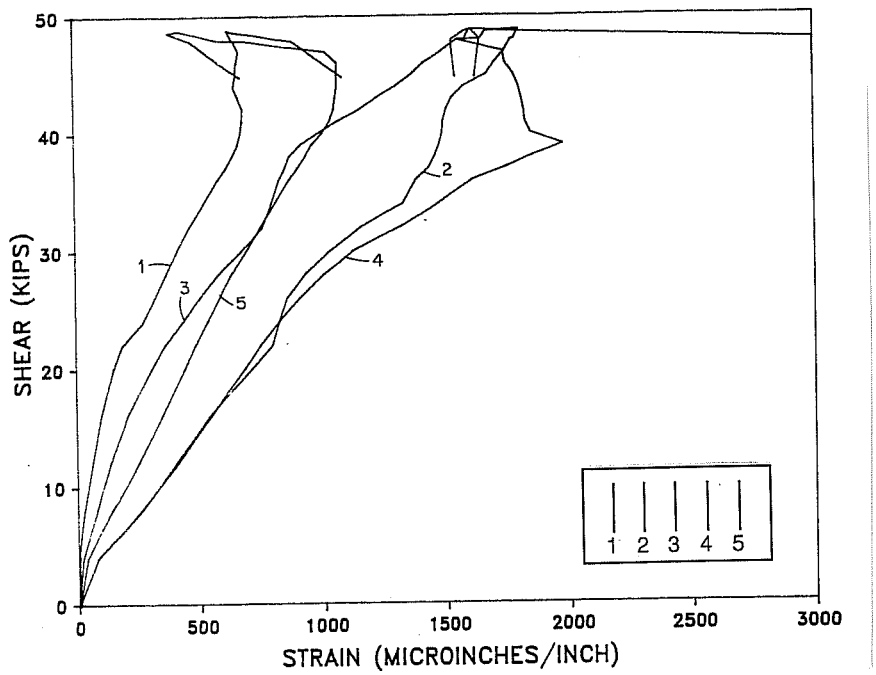

Fig. 5.59 Stirrup strains for Specimen 3-4.

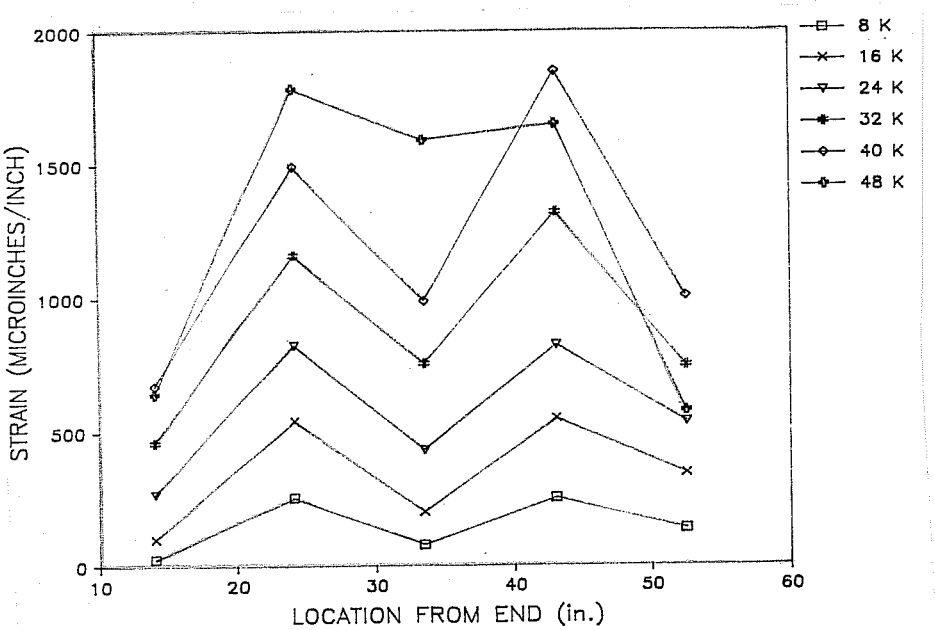

Fig. 5.60 Stirrups strains versus location in shear span for Specimen 3-4.

$\rho_v f_y = 61$ and 109 psi respectively. The prestress force, longitudinal reinforcement, and concrete were all identical.

An indication of the behavioral changes due to stirrups can be obtained by also comparing results for Specimen 1-1 which had the same prestress, concrete, etc., but no stirrups. All three girders had relatively similar cracking loads. The increasing of stirrups had several behavioral effects. Specimen 1-1, which had no stirrups, had major cracks form at initial cracking which ran from the bottom flange to the top flange. The cracks extended as the load increased but not dramatically. No additional shear cracks formed. The existing cracks grew very wide. The load which caused shear cracking was lower than that required for flexural cracking. As a result, the shear cracks became extremely wide without the bottom flange cracking from flexure. Flexure-like cracks were noted in the shear span before any formed in the constant moment region. It would appear that these cracks had to form to maintain compatibility of deformations. The concrete in the bottom flange could not deform enough to maintain compatibility with the highly deformed web. From a review of the failed specimen it is quite probable that the specimen failed from a web instability rather than crushing or strand related phenomenon.

Specimen 1-2 was designed for $\rho_v f_y$ of 50 psi. Due to material differences it actually had $\rho_v f_y = 61$ psi. The presence of that level of stirrups had little effect on the number or length of cracks which first formed. Again there was some extension of cracks with increasing load. A few new shear cracks formed. Crack widths seemed to be less than for Specimen 1-1. At high loads flexure-like cracks again formed in the shear span before they formed in the constant moment region. The number, depth, and location were all more restricted than in Specimen 1-1. The light stirrups while still allowing considerable shear crack width, held the beam together reducing compatibility problems from an extremely deformed web. The final crack width was controlled by the deformation between cracks needed to fracture the stirrups. It is most likely that one stirrup reached its fracture load and that the remaining stirrups had insufficient reserve capacity causing the beam to "unzip" and progressively fracture the remaining stirrups.

Specimen 1-3 was designed for $\rho_v f_y$=109 psi. The amount of stirrups had no apparent effect on the cracking load and no obvious effect on the initial cracking pattern. As the load increased, more new cracks formed than had been seen in either Specimen 1-1 or 1-2, although the number of cracks was still very limited number. The added stirrups helped to distribute the shear cracking. Rather than a very few wide

cracks, there were a greater number of relatively smaller cracks. For Specimen 1-3, flexure cracks first appeared in the constant moment region and then later in the shear span. The increase in stirrups decreased the web deformation at a given load. Crack widths did grow very wide as failure approached. At ultimate the collapse sequence was undoubtedly the same as for Specimen 1-2 with progressive fracturing of the stirrups.

The ultimate shear span loads were 34.5, 33.5, and 35.85 kips for Specimens 1-1, 1-2, and 1-3 respectively. For all practical purposes the failure loads were independent of shear reinforcement. Note that Specimen 1-2 did slightly poorer and Specimen 1-3 did only slightly better than Specimen 1-1 which had no stirrups. This certainly is counter to expected behavior, and it is Specimen 1-1 that behaved quite differently than expected. Between web cracking and ultimate, the beam took 8.5 kips additional shear load. The ultimate load was 1.33 times its initial inclined cracking load. The general assumption in shear design is that cracking and ultimate are the same value for members without shear reinforcement. In this beam at inclined cracking, however, both the top and bottom flanges were uncracked. The beam was able to find stable internal load paths to carry the loading. This remained true until failure. In Specimens 1-2 and 1-3 the stirrups provided the necessary hangers for the conceptual truss model. The stirrups helped to carry the load from cracking to ultimate. At stirrup fracture the stable internal mechanism lost a component. The specimen was unable to find an alternate mechanism and failed.

The stirrup strain gauges in Specimen 1-2 and 1-3 did not in general show strains of the magnitude that were obviously occurring. The gauges were slightly away from the major cracks. This also indicates that the small bars used had good bonding ability. The stirrup action crossing an extremely wide crack had essentially a localized effect on stirrup behavior.

The deformations observed and the final fracture of shear reinforcement were dependent upon no other failure mechanism occurring prematurely. Proper anchorage of the longitudinal reinforcement was essential to allow loads and deformation of the magnitude observed.

Stirrup behavior was quite different for the seven other tests. The shear reinforcement capacity V_s varied from 4 to $15\sqrt{f'_c}b_w d$. Several general trends were observed as the level of shear reinforcement increased: a) The number of initial cracks varied but their length and width decreased; b) The number of new cracks increased while the crack width declined. In these seven tests no compatibility cracks formed in the tension

flange like those in Specimens 1-1 and 1-2. The use of heavier stirrups reduced the shear deformations.

In general the instrumented stirrups yielded even for the beams with $V_s = 15\sqrt{f'_c}b_w d$. Generally the stirrups that did not yield were either close to the support or the load point. It is possible that a portion of the stirrup above or below the gauge was yielding and that the gauge location was outside the primary load resisting region. From the observations made earlier it is quite possible one portion of the bar yielded while another portion a small distance away had not reached yield.

5.3.2.2 Concrete compression diagonals. Crushing of the concrete compression diagonals was the failure mode in four of the shear tests. Of those four tests three had extremely heavy shear reinforcement. The three tests of Series 2 had $15.5\sqrt{f'_c}b_w d$ and $19.3\sqrt{f'_c}b_w d$ actual shear reinforcement. The beams were provided with a support overhang to insure proper development of the flexural reinforcement. Each specimen had a large number of very fine cracks in the web prior to failure. At failure the web blew out explosively. The concrete spalled for nearly the full shear span in each case. The crushed zone was highly irregular but tended to be in the lower portion of the web. The concrete was generally blown out down as deep as the level of the stirrups. In places it was destroyed all the way through the web. The failure gave a clear indication that for such heavy shear reinforcement values the beam set up a diagonal compression field. The cracking and crushing was distributed uniformly over the shear span. The action was that of a field rather than discrete struts.

Specimen 3-4 displayed a different mode of web crushing. This specimen had $V_s = 4\sqrt{f'_c}b_w d$ of shear reinforcement. A small overhang was provided to improve anchorage. In this specimen four major cracks defined three principle struts. There was some secondary cracking but it was limited. The major cracks had substantial width. The web crushing sequence is shown in Figure 5.61. Region 1 was the first to crush and spall. There was a significant drop in load. Upon further loading, a higher load was attained until Regions 2 and then 3 both crushed and spalled. Finally, Region 4 crushed. By the time Region 4 crushed the specimen had obviously lost the majority of its load carrying capacity. The specimen appeared to have three distinct diagonal compression struts. When strut B failed, the extra load was transferred to struts A and C. Further loading crushed each of these struts, finally destroying the member's capacity. This type of crushing may be a partial result of using high strength concrete. High strength concrete has limited capacity beyond the strain value at peak stress. It is possible that

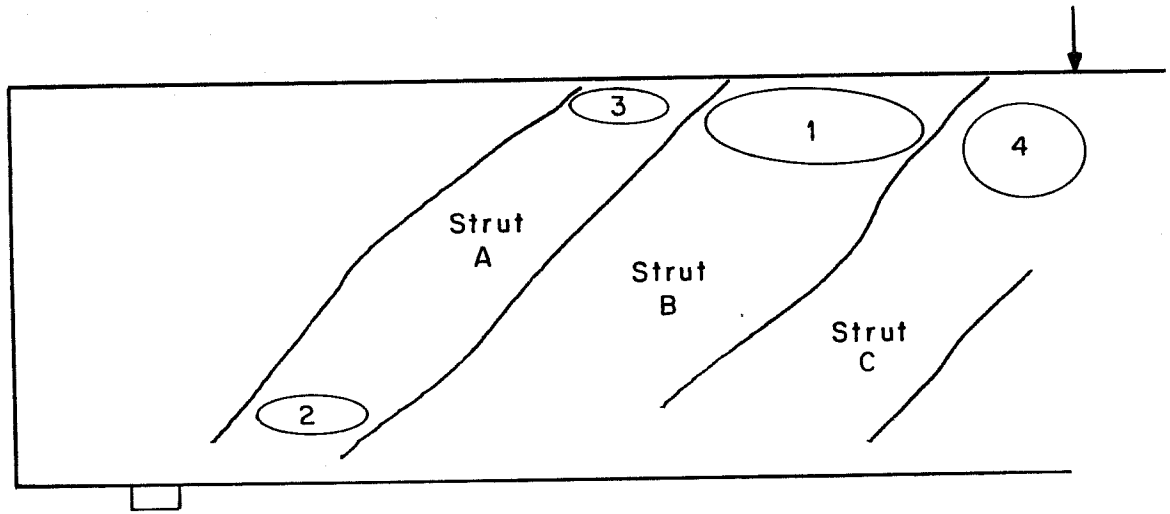

Fig. 5.61 Order of strut crushing for Specimen 3-4.

chord. A number of strain gauges were placed on the prestressing strands of each specimen as well as on nonprestressed longitudinal reinforcement when it was used. For the prestressed reinforcement a best estimate was made of the state of stress and strain in the strand at the time of test. During the test the change in strain was measured. The cumulative strain is primarily important in this discussion since it governs if the strand reached yield. So far, as internal behavior is concerned, the change in strain under load is more important.

A review of the strain readings for the prestressing strands reveals several facts. The first is that at the locations gauged the strand did not reach yield. A second observation is that change in strain readings varied along the length of the shear span.

5.3.2.5 Cracking. The cracking pattern indicated the internal response of the concrete. Some comments were made earlier with reference to the level of the shear reinforcement. This will be expanded upon in addition to the comments made on crack angles and crack widths.

The number and extent of cracks at first cracking is largely governed by the amount of shear reinforcement present. The specimens of Series 1 had a very low level of shear reinforcement. The initial inclined cracks extended from the bottom flange all the way to the top flange. For Series 2 with very heavy shear reinforcement the initial inclined cracks were very short and extremely narrow. Series 3 was very likely precracked before the shear loading so the resulting initial cracking is of little value.

The level of shear reinforcement greatly affected cracking as the load increased. In Series 1 very few additional cracks formed after initial cracking. The crack width, however, grew to extreme widths in excess of 1/8 in. Series 2 beams had a very large number of new cracks and crack extensions as the load increased. Throughout the loading most cracks were less than 0.005 in. wide. Series 3 behavior was within the bounds set by Series 1 and 2. Specimens 3-1 and 3-2, with $V_s = 8\sqrt{f'_c}b_w d$, had a considerable increase in cracking as the load increased. No crack width measurements were taken. Specimens 3-3 and 3-4, $V_s = 4\sqrt{f'_c}b_w d$, had substantially less cracking. There were a few primary cracks as well as some secondary cracking. Crack widths reached 0.050 inches. The quantity of shear reinforcement provided affects the spacing, number, and width of the shear cracks.

The angle of inclination of cracks varied somewhat throughout the program. The angle of inclination varied along the length of each beam. The angles at the end and near the load points tended to be higher. Angles as high as 55° were noted in these

regions. Away from load points and supports the cracks flattened out somewhat. There was some variation from specimen to specimen but the average crack inclination varied from 25° to 30°. The quantity of shear reinforcement and prestress did not correlate consistently with the crack angle.

5.3.2.6 Rosette strain gauges. Rosette strain gauges were used on the beams of Series 1 and 2. The rosette gauges were used in an attempt to obtain the direction and magnitude of principal stresses in the web of the girders. The gauges gave only limited success and will therefore be discussed as a group rather than for each individual girders.

The results for Series 1 were fairly consistent. Prior to cracking the principal compressive stress was inclined from about 39° to 45° towards the load point. Prior to cracking the tensile stresses indicated ranged from 300 psi to 900 psi with most values about 675 psi. This is $6.35\sqrt{f'_c}$. After cracking, the principal compression axis was in the range of 25° pointed away from the load point (Fig. 5.62). No good explaination for the principal axis inclination after cracking has been obtained. Given the strange principal direction indicated after cracking the compression strut stresses must be viewed with caution. There was considerable scatter but the average principal compression stress was 2900 psi.

The results from Series 2 are much poorer. Only Specimen 2-1 gave any results. The same trend of a large switch in principal angle direction as noted for Series 1 was again indicated. The gauges indicate that the principal tensile stress at cracking was around 1000 psi or $9.6\sqrt{f'_c}$. The higher coefficient would be expected since the beam had higher prestress than Series 1. The angle of the principal compression stress at failure was indicated to be about 33° directed away from the load point. The principal stress was about 5100 psi or just under $0.5f'_c$. Due to the low level of confidence in these measurements they will not be discussed further.

5.3.3 Comparison with Model Assumptions. Comparison of actual behavior with the assumptions used for the various shear capacity models gives an indication of the appropriateness of each model. The current test series gives only limited information so far as the AASHTO/ACI V_c term is concerned. Only the web shear equation, V_{cw}, is involved. Furthermore, only two concrete strengths and prestress forces were tested. Both results will be shown in Section 5.3.4.1. The AASHTO/ACI steel contribution assumes a 45° truss and that the shear reinforcement yields. From the cracking patterns the first assumption is not correct, but it is conservative. The assumption that

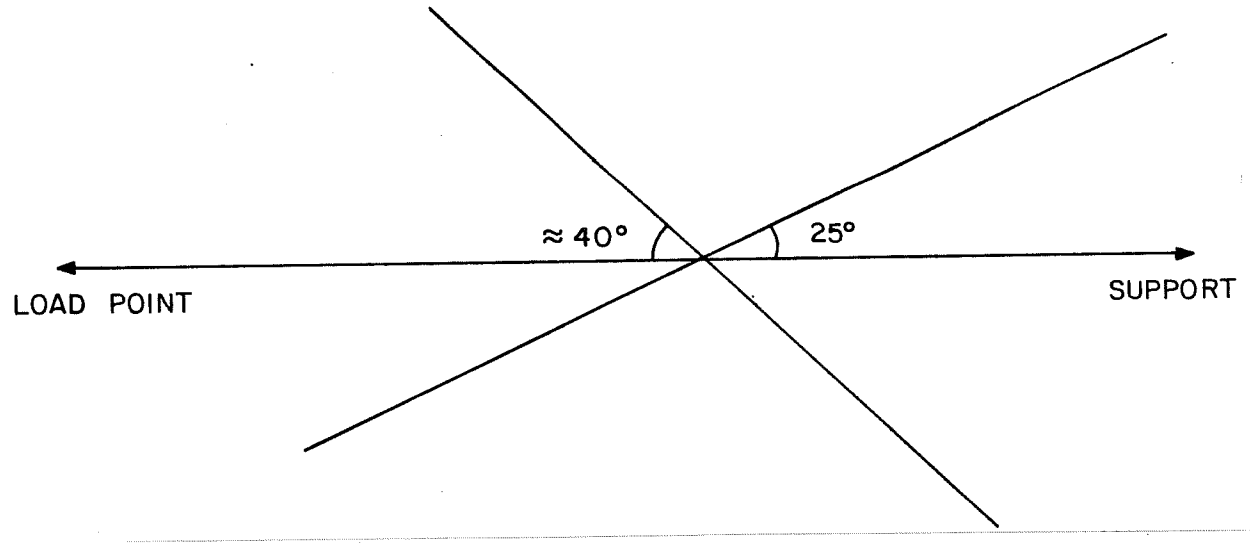

Fig. 5.62 Direction of principal compression stress before and after web shear cracking.

the stirrups yield is generally a good one even for beams reinforced well beyond current allowable limits.

The primary assumptions for the Danish plasticity model were stirrup yielding and concrete web crushing along with no yielding of the longitudinal reinforcement. As previously noted, stirrup yielding is a good assumption. Web crushing occurred principally in beams with very heavy shear reinforcement. Specimen 3-4 showed web crushing would occur for lower shear reinforcement values, but only if proper anchorage of the longitudinal reinforcement was provided. The assumption of no tension chord yielding was a good one for this program.

The Swiss plasticity model and the truss model of Ramirez are very similar and will be discussed together. The primary assumptions are that both the web and longitudinal reinforcement yield and that the concrete does not crush. Yielding of the longitudinal reinforcement was not observed in the shear span. This comes from the fact that the members are over-reinforced to insure the occurrence of a shear failure. In an actual member the shear and flexural reinforcements are designed for the same load so the assumption is not a problem. Typical failure mechanisms were stirrup fracture and concrete crushing. Both cases can be modelled with the truss model but are restricted by supplementary provisions. The case of anchorage failure is also recognized as a potential problem. The models indicate that a definite tensile requirement exists at the support.

5.3.4 Comparison of shear design models to test results

5.3.4.1 Introduction. The tests results of this project will be compared to the numerical predictions of AASHTO/ACI, the truss model, and the 1984 Canadian Code General Method. Table 5.1 contains pertinent member properties for the ten specimens of this program.

5.3.4.2 AASHTO/ACI. The AASHTO/ACI provisions are the most empirical of the three methods. Table 5.2 contains the test results and AASHTO/ACI predictions. The concrete contribution could be compared only for Series 1 and 2. All the initial cracking was web shear cracking. The AASHTO/ACI equation for V_{cw} was very close in three tests and conservative in the other three tests. The average test/predicted value was 1.06. The two primary variables in the V_{cw} equation are concrete strength and level of concrete prestress at the centroid. Figure 5.63 shows that for the data of this program no conclusions can drawn for the effect of changes in concrete strength. Figure 5.64 shows the results plotted against f_{pc}. Again, no trends are apparent.

Table 5.1 Member properties for current test series

	1-1	1-2	1-3	2-1	2-2	2-3	3-1	3-2	3-3	3-4
f'c @ TEST (girder)	11300	11300	11300	10800	10800	10800	13000	13160	11500	11500
f'c @ test (slab)	---	---	---	---	---	---	3300	3300	5350	5350
span (in.)	156	156	156	156	156	156	208	208	208	208
a (in.)	60.75	60.75	60.75	55.83	55.83	55.83	52	52	52	52
a/d	3	3	3	3	3	3	3.2	3.2	3.2	3.2
s (in.)	---	11.8	9.8	5	4	4	2.375	2.375	4.75	4.75
Avfy (psi)	0	1450	2150	16060	16060	16060	4290	4290	4290	4290
pvfy (psi)	0	61	109	1610	2010	2010	900	900	450	450
x √f'c (actual)	0	.57	1.02	15.5	19.3	19.3	7.9	7.8	4.2	4.2
d rebar	---	---	---	19	19	19	---	---	---	---
fse (ksi)	170	170	170	154	154	154	140.5	143.1	156.8	156.8
dp (in.) (all)	17.75	17.75	17.75	16.94	16.94	16.94	14.74	14.78	17.49	17.49
dp (in.) (tension)	20.25	20.25	20.25	18.57	18.57	18.57	18.4	18.31	18.78	18.7
d (in.)	20.25	20.25	20.25	18.61	18.61	18.61	16.2	16.2	16.2	16.2
z (in.)	19.94	19.94	19.94	17.58	17.58	17.58	14.74	14.74	16.76	16.76
Cracking (K)	26.9	22.9	26.7	32.9	32.9	35.9	---	---	---	---
Ultimate (K)	35.4	34.4	36.7	97.9	106.9	104.9	64.2	66.2	42	49.8

Table 5.2 Test results and AASHTO/ACI predictions for current test program

SPECIMEN	LOAD STAGE	TEST (K) (1)	ACI 1 (K) (2)	(1)/(2)	ACI 2 (K) (3)	(3)/(1)
1-1	Vc	26.9	23.4	1.15		
	Vu	35.4	23.4	1.51		
1-2	Vc	22.9	23.4	.98		
	Vu	34.4	25.9	1.33		
1-3	Vc	26.7	23.4	1.14		
	Vu	36.7	27.8	1.32		
2-1	Vc	32.9	33.1	.99		
	Vu	97.9	93	1.05		
2-2	Vc	32.9	33.1	.99		
	Vu	106.9	107.9	.99		
2-3	Vc	35.9	33.1	1.08		
	Vu	104.9	107.9	.97		
3-1	Vu	64.2	61.2	1.05	64.9	.99
3-2	Vu	66.2	61.6	1.07	65	1.02
3-3	Vu	42	36.6	1.15	39.5	1.06
3-4	Vu	49.8	36.7	1.36	39.4	1.26
			Vc ave	1.06	Vu ave	1.08
			Vc std	.09	Vu std	.11
			Vu ave	1.18		
			Vu std	.18		

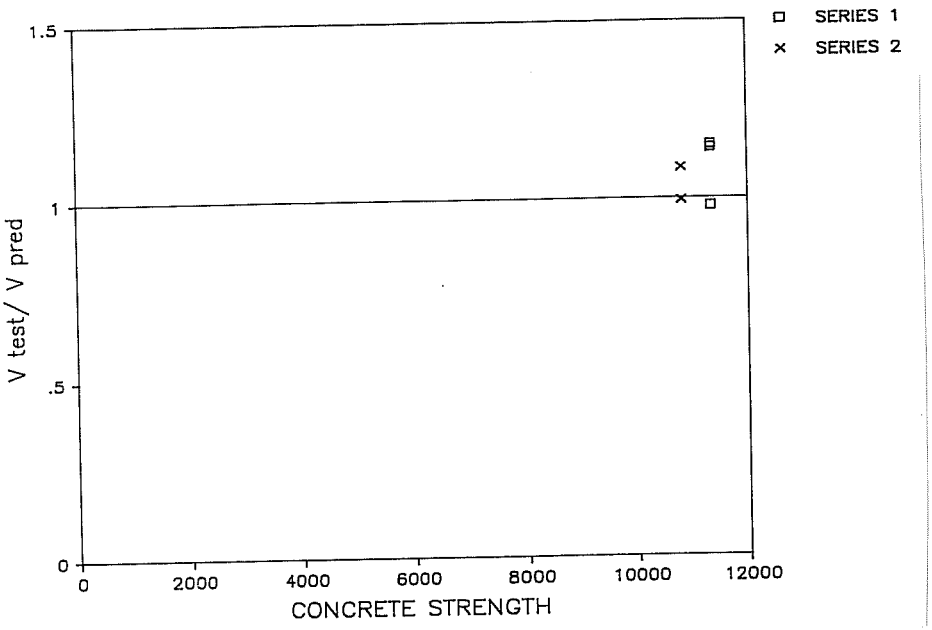

Fig. 5.63 Relative conservatism of cracking loads versus AASHTO/ACI equations for concrete contribution plotted against concrete strength.

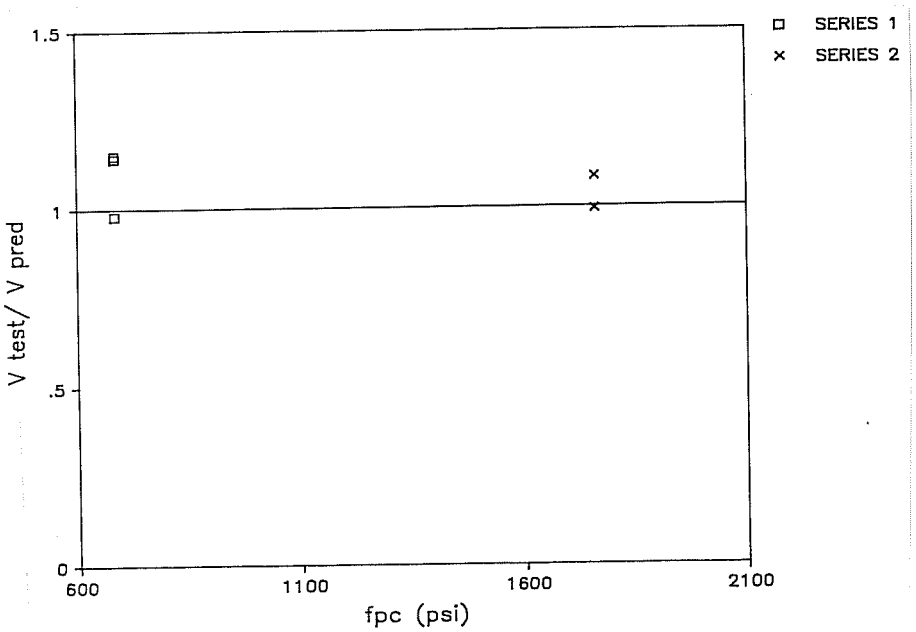

Fig. 5.64 Relative conservatism of cracking loads divided by AASHTO/ACI predictions versus stress at centroid due to prestress force.

The AASHTO/ACI provisions were generally conservative in ultimate strength predictions. The lowest value was only below unity. Plotting the results versus concrete strength gives no information (Fig. 5.65). Plotting the results against $\rho_v f_y$ does show interesting behavior (Fig. 5.66). Specimen 1-1 had no shear reinforcement. The AASHTO/ACI equation becomes less conservative and in fact very slightly unconservative as $\rho_v f_y$ increases. In fairness, the AASHTO/ACI maximum V_s limit of $8\sqrt{f'_c} b_w d$ would prohibit values of $\rho_v f_y$ above about 800 psi. In Table 5.2 two values are given for Series 3 predictions. Series 3 is not as simple as Series 1 and 2 since it has both draped strands and a low-strength composite deck. The question arises as to what is the correct value of d. The first column is based on d=.8h as allowed by the Code. The results are quite good indicating that the assumption is acceptable. The second column comes from a more refined set of assumptions. First all strands are used for computation of f_{pc}. The depth used for the first term of the V_c calculations is the distance from the centroid of the nondraped strands to the top of the pretensioned girder section. A second term of $V_c = 2\sqrt{f'_c} b_w t$, where t is the deck thickness and f'_{cd} is the deck concrete strength is calculated and added to the previous V_c term. Finally for V_s, d is taken as the distance from the centroid of the nondraped strands to the top of the section. This second method gives slightly more accurate results with less scatter. The improvement in the prediction is not, however, proportional to the added work.

5.3.4.2 Canadian Code. The evaluation procedure used in this section is identical to that described in Section 3.6.3.2. The results are tabulated in Table 5.3. Only Specimen 1-1 will be evaluated for cracking strength against Equation 3.72. Specimen 1-1 will be discarded in statistical evaluations.

Specimen 1-1 evaluated by the Canadian Code cracking equation is quite conservatively predicted. The test/predicted ratio was 1.89 which is very close to the average of 1.85 for tests reported in the literature.

The remainder of the specimens had some level of shear reinforcement. Tests plotted against concrete strength show large scatter and no trends (Fig. 5.67). All the results of the test program are conservative. Plotting the results versus $\rho_v f_y$ gives much greater insight into behavior (Fig. 5.68). The two specimens of Series 1 with light shear reinforcement were predicted very conservatively. Specimen 1-2 with the lightest shear reinforcement had the largest factor of safety. The specimens of Series 2 with their extremely heavy shear reinforcement were predicted with a reasonable amount of conservatism. All specimens of Series 3 were conservatively predicted. Even the

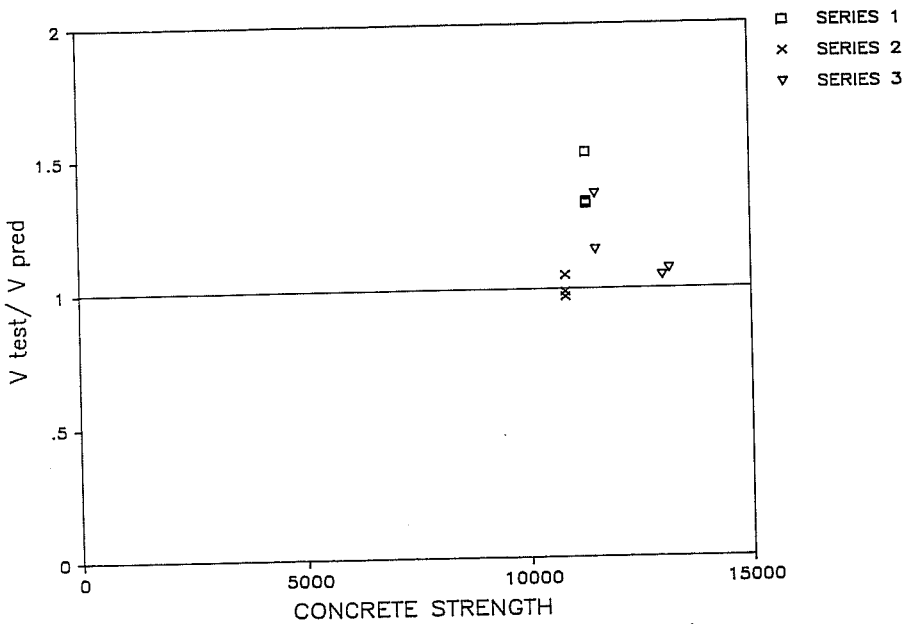

Fig. 5.65 Test results/(AASHTO/ACI) predictions at ultimate plotted versus concrete strength.

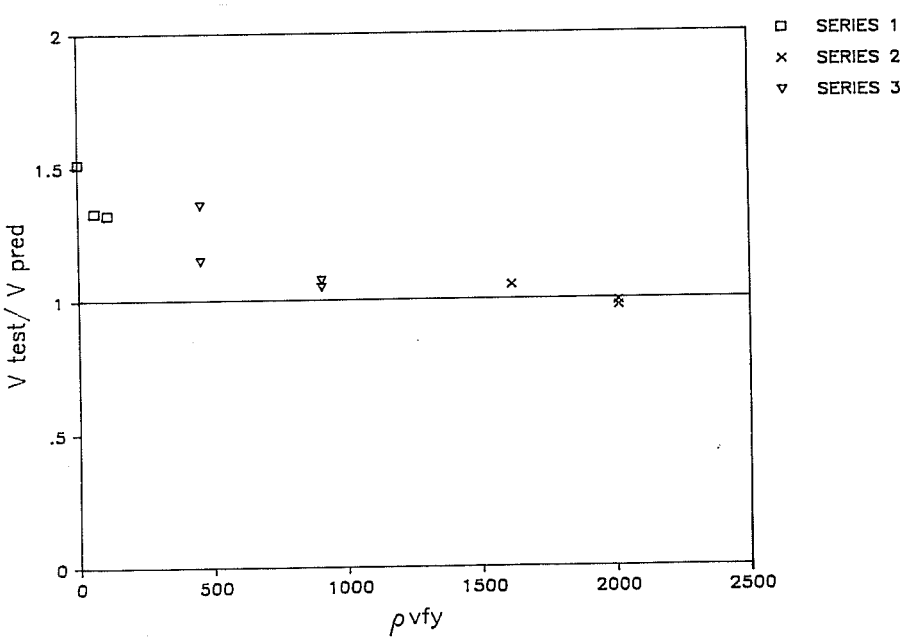

Fig. 5.66 Test results/(AASTHO/ACI) predictions at ultimate plotted against $\rho_v f_y$.

Table 5.3 Test results and Canadian Code general method prediction for current test series

SPECIMEN	TEST (K)	CANADIAN (K)	TEST / CAND.
1-1	26.9	14.2	1.89
1-2	34.4	9.1	3.78
1-3	36.7	14.4	2.55
2-1	97.9	76.4	1.28
2-2	106.9	86.3	1.24
2-3	104.9	86.3	1.22
3-1	64.2	48.1	1.33
3-2	66.2	48.3	1.37
3-3	42	33	1.27
3-4	49.8	33	1.51
		AVE	1.74
		STD DEV	.78

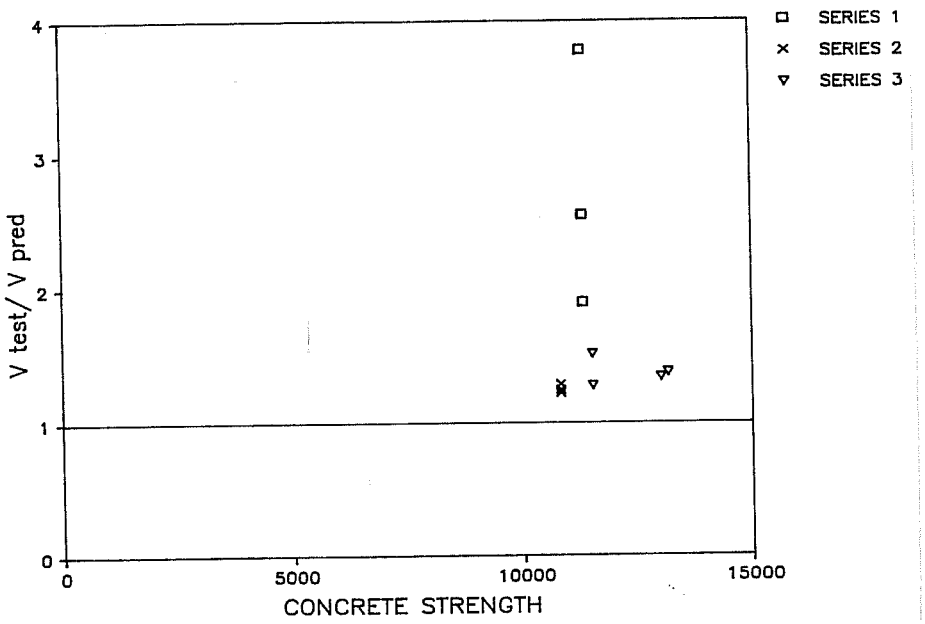

Fig. 5.67 Test results/Canadian Code at ultimate versus concrete strength.

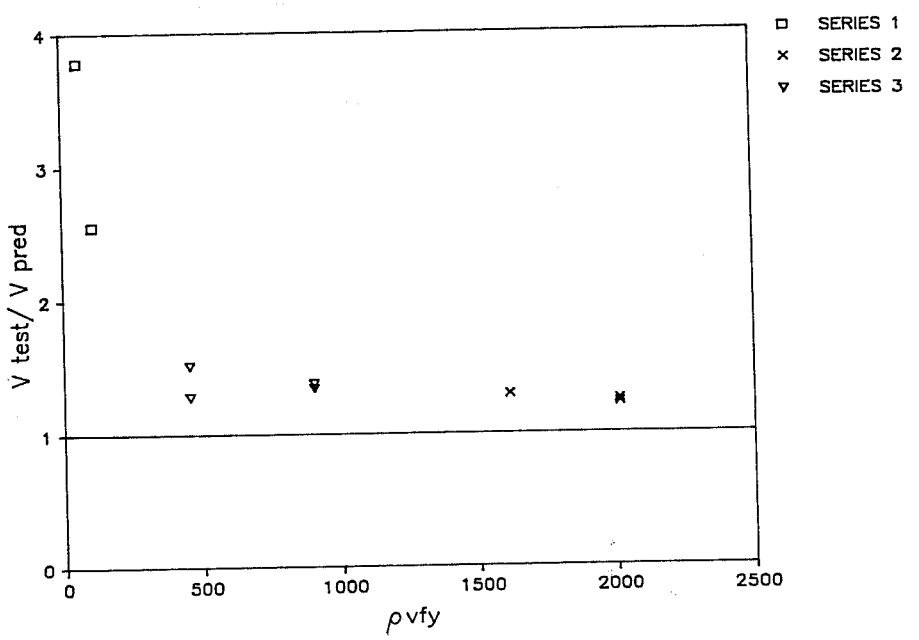

Fig. 5.68 Test results/Canadina Code at ultimate versus $\rho_v f_y$.

specimens which had shear- anchorage failures were acceptable. Specimen 3-4 with its web crushing was the most conservative of this series. The data shows the same trend for increasing $\rho_v f_y$ as noted for tests reported in the literature. The predictions show comparable conservatism between groups as well. The theory that the high conservatism for specimens with low shear is due to improper accounting of a concrete contribution seems to have even more support. More importantly, the method is conservative for values of shear reinforcement far in excess of reinforcement values that will be allowed in actual practice.

5.3.4.4 Truss model. The procedures used to evaluate the specimens with the Ramirez truss model are the same as described in Section 3.6.4.3. Table 5.4 contains the cracking loads and the maximum concrete contribution allowed. This comparison is merely a check to see that the limit placed on V_c is conservative. The limit is conservative in all cases and very much so for Series 2. Figure 5.69 shows the results versus concrete strength. Figure 5.70 shows the results against f_{pc}. This figure indicates that the method does not properly account for the effect of prestress. Conservatism increases rapidly as f_{pc} increases.

The main analysis with the truss model is for the ultimate capacity of girders with stirrups. Table 5.5 contains the results for beams with stirrups. All of the predicted values are conservative. The test/predicted values plotted against concrete strength give little information (Fig. 5.71). Plotting the results versus $\rho_v f_y$ indicates some very interesting behavior (Fig. 5.72). Specimens with light shear reinforcement were quite conservative although not to the extent noted in the literature. Specimens 3-3 and 3-4 with moderate shear reinforcement were conservative but much less so than the Series 1 beams. All the other specimens became more conservative as $\rho_v f_y$ increased. When computing capacities the reason for this quickly becomes apparent. For girders with heavy shear reinforcement the Ramirez truss model limit on the stress in the compression diagonals places constraints on α. The higher $\rho_v f_y$ is, the higher α must be to keep f_d below $30\sqrt{f'_c}$. Table 5.5 indicates that something is clearly wrong. Specimen 2-1 with $\rho_v f_y = 1610$ psi has a computed capacity of 54.8 kips while Specimens 2-2 and 2-3 with $\rho_v f_y = 2010$ psi have a computed capacity of 52.5 kips. Given two otherwise identical beams it is unreasonable to expect less capacity out of the one with more shear reinforcement. At the very least the beams should give the same capacity. Again the arbitrary $30\sqrt{f'_c}$ limit on the compressive strut stress imposes a severe limit.

Table 5.4 Truss model cracking load predictions

SPECIMEN	TEST (K) (1)	TRUSS (K) (2)	TEST TRUSS
1-1	26.9	15.1	1.78
1-2	22.9	15.1	1.52
1-3	26.7	15.1	1.77
2-1	32.9	14.6	2.25
2-2	32.9	14.6	2.25
2-3	35.9	14.6	2.46
		AVE	2.01
		STD DEV	.34

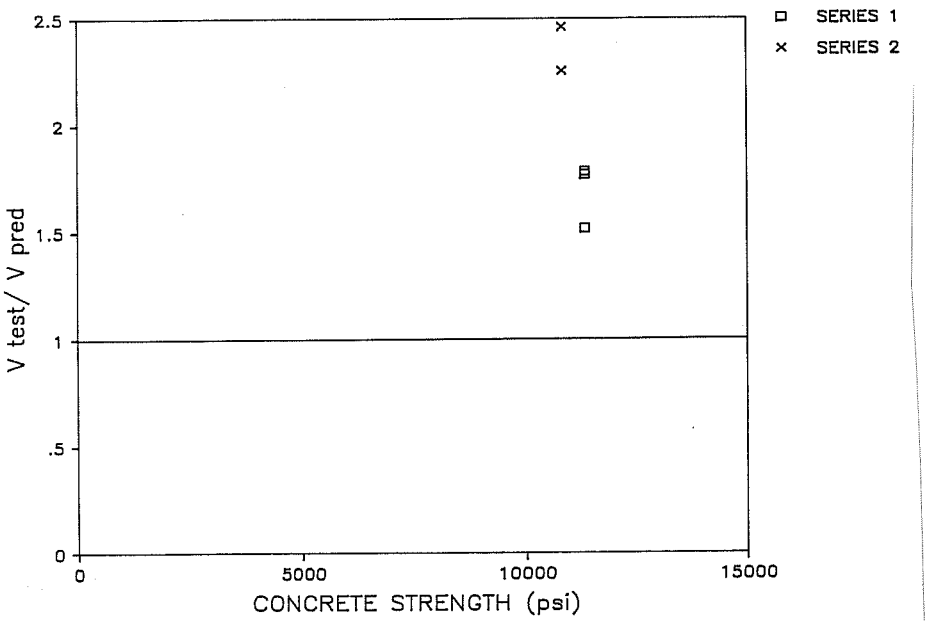

Fig. 5.69 Cracking load/truss model concrete contribution versus concrete strength.

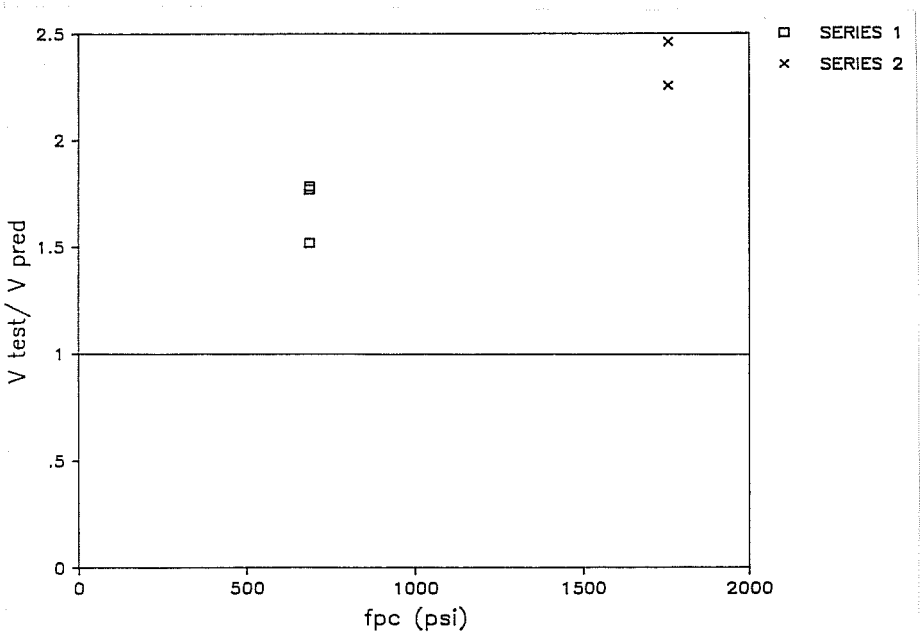

Fig. 5.70 Cracking load/truss model concrete contribution versus stress at centroid due to prestress.

Table 5.5 Test results and truss model ultimate capacity predictions

SPECIMEN	TEST (K) (1)	TRUSS (K) (2)	TEST TRUSS
1-2	34.4	17.4	1.98
1-3	36.7	19.2	1.91
2-1	97.9	54.8	1.79
2-2	106.9	52.5	2.04
2-3	104.9	52.5	2.00
3-1	64.2	44.4	1.45
3-2	66.2	44.6	1.48
3-3	42	32.3	1.30
3-4	49.8	32.3	1.54
		AVE	1.72
		STD DEV	.26

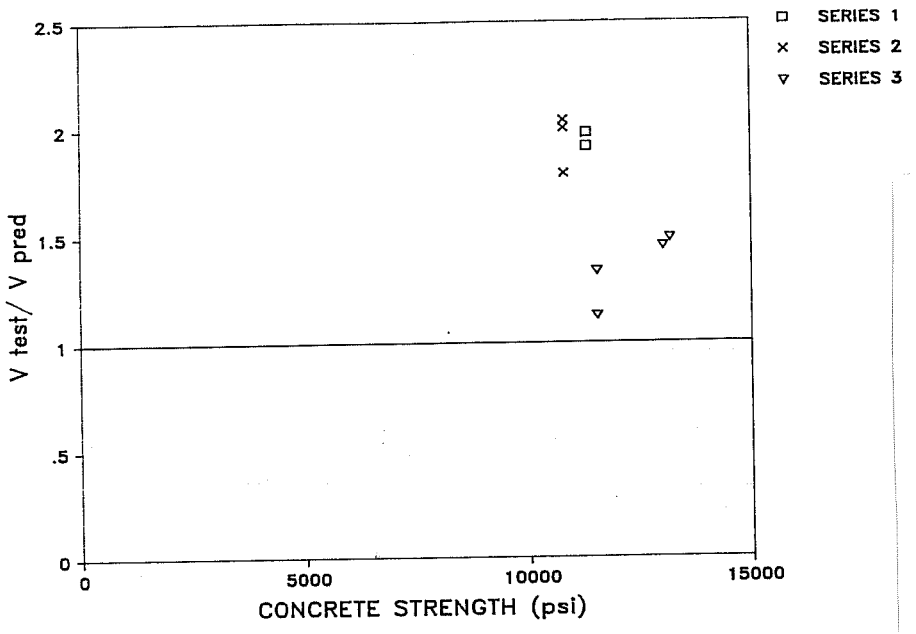

Fig. 5.71 Test results/truss model at ultimate versus concrete strength.

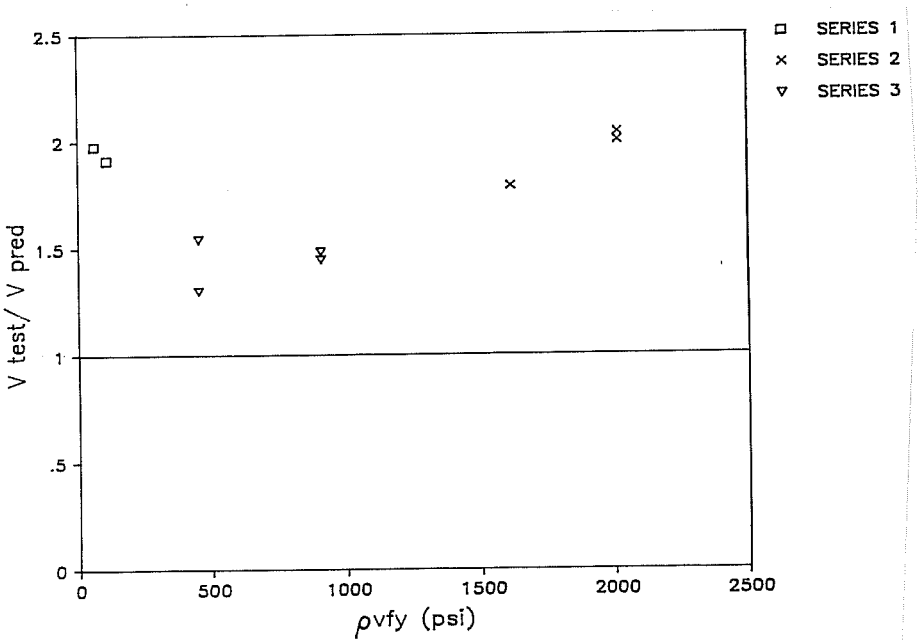

Fig. 5.72 Test results/truss model at ultimate versus $\rho_v f_y$.

Figure 5.73 shows how $30\sqrt{f'_c}$ decreases as a percentage of f_c as f'_c increases. The square root function increases much more slowly than f'_c. As a result allowable strut stresses decrease considerably as a percentage of f'_c as the strength increases. Setting the limit on f_d as a fixed percentage of f'_c may be a more proper course. This idea was used by Schlaich in Reference [42]. Table 5.6 contains recomputed truss model predicted values if $f_d \leq 0.5f'_c$. Even with f_d as high as 0.5 f'_c the results are all conservative. A look at Figure 5.74 shows the results plotted against $\rho_v f_y$. Using $f_d \leq .5f'_c$ gives almost constant conservatism for $900 \leq \rho_v f_y \leq 2010$ psi. None of the other tests of this series nor of the tests from the literature would be affected since the strut stress was below the allowable stress. They did, however, have relatively low shear reinforcement values. Using the current $f_d \leq 30\sqrt{f'_c}$, $\rho_v f_y$ must be greater than $5.36\sqrt{f'_c}$ for any constraints to be placed on the angle α.

5.3.4.5 Comparison of model predictions. A comparison of model predictions allows judgement as to the relative accuracy of the various methods for predicting the capacity of the members tested. Cracking and ultimate are two load stages at which model comparisons are of interest. The statistical analysis of this section is identical to that in Section 3.6.5. Also as in Section 3.6.5 cracking load predictions based on the Canadian Code will be omitted since they are not part of actual capacity predicting procedures.

Table 5.7 contains the results of the statistical analysis. The upper and lower limits are quite wide for all of the methods (Fig.5.75). This is largely a function of the fact that only a few data points were used. The AASHTO/ACI equations seem quite acceptable for this data. The lower confidence limits are below one but the range is fairly small both at cracking and at ultimate. The Canadian Code General Method did quite poorly. More important than the actual confidence limits themselves is the extreme relative width. At cracking the truss model did rather poorly. The lower limit is unconservative while the upper limit is quite high. At ultimate the truss model did relatively well. The lower confidence limit was greater than one and the range was not too bad. In general, the AASHTO/ACI method was the best for this experimental series. The average value was close to one and the method had the smallest scatter.

One other comparison of interest in the truss model is the effect on the predictions due to a change in the f_d limit from $f_d \leq 30\sqrt{f'_c}$ to $f_d \leq 0.5f'_c$. Use of $f_d \leq 0.5f'_c$ gives an average prediction ratio that is substantially improved. The scatter increases slightly.

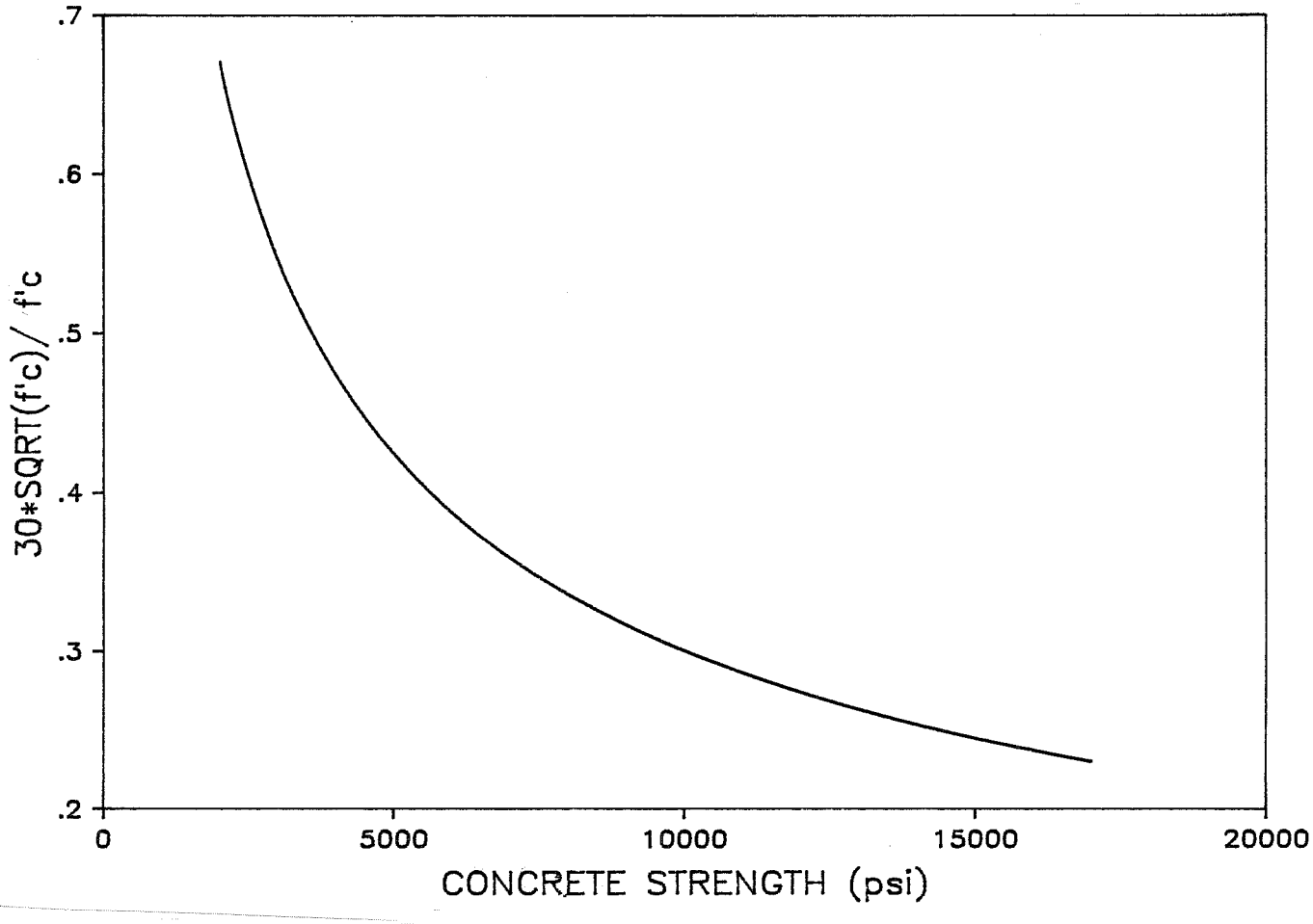

Fig. 5.73 Allowable diagonal compression strut stress as a percentage of $\sqrt{f'_c}$ versus f'_c.

Table 5.6 Truss model prediction with $f_d \leq 0.5f'_c$

SPECIMEN	TEST (K) (1)	TRUSS (K) (2)	TEST TRUSS
1-2	34.4	17.4	1.98
1-3	36.7	19.2	1.91
2-1	97.9	86.8	1.13
2-2	106.9	91.8	1.16
2-3	104.9	91.8	1.14
3-1	64.2	56.9	1.13
3-2	66.2	56.9	1.16
3-3	42	32.3	1.30
3-4	49.8	32.3	1.54
		AVE	1.38
		STD DEV	.32

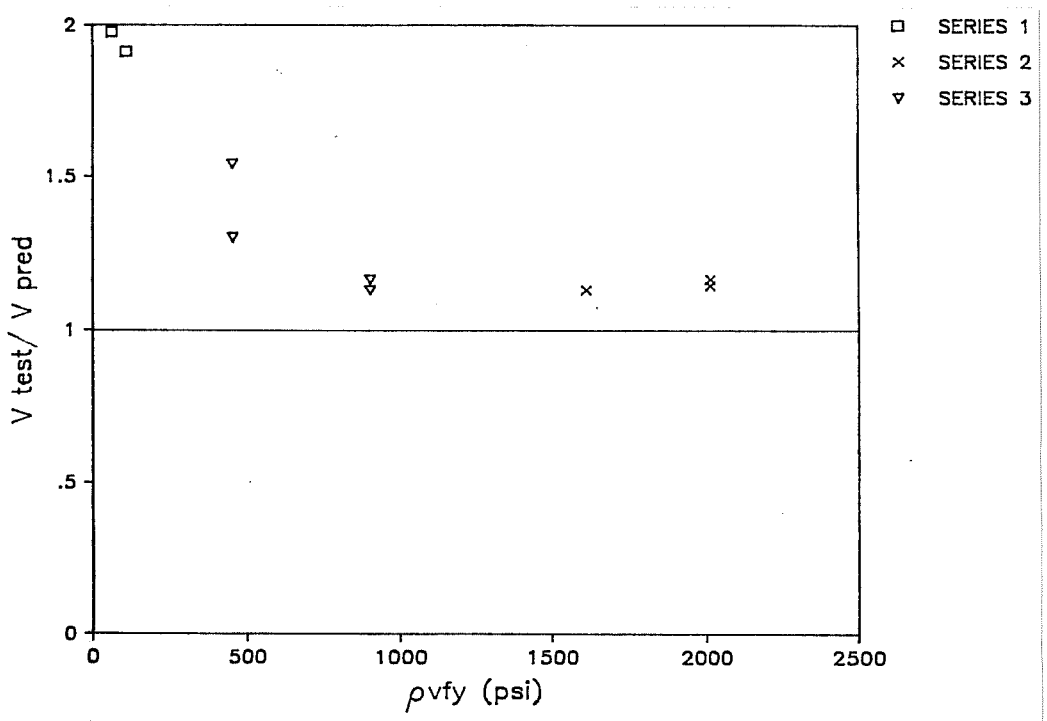

Fig. 5.74 Test results/truss model at ultimate with $f_d \leq 0.5\ f'_c$ versus $\rho_v f_y$.

Table 5.7 Statistical comparison for the current test series

METHOD		CRACKING	ULTIMATE
ACI	MEAN	1.06	1.18
	STD DEV	.09	.18
	UP. LIMIT	.79	1.6
	LOW LIMIT	1.33	.76
CANADIAN	MEAN	---	1.74
	STD DEV	---	.78
	UP. LIMIT	---	3.55
	LOW LIMIT	---	-.07
TRUSS	MEAN	2.1	1.72
	STD DEV	.47	.26
	UP. LIMIT	.71	2.32
	LOW LIMIT	3.49	1.12
MODIFIED TRUSS	MEAN	2.1	1.38
	STD DEV	.47	.32
	UP. LIMIT	.71	2.12
	LOW LIMIT	3.49	.64

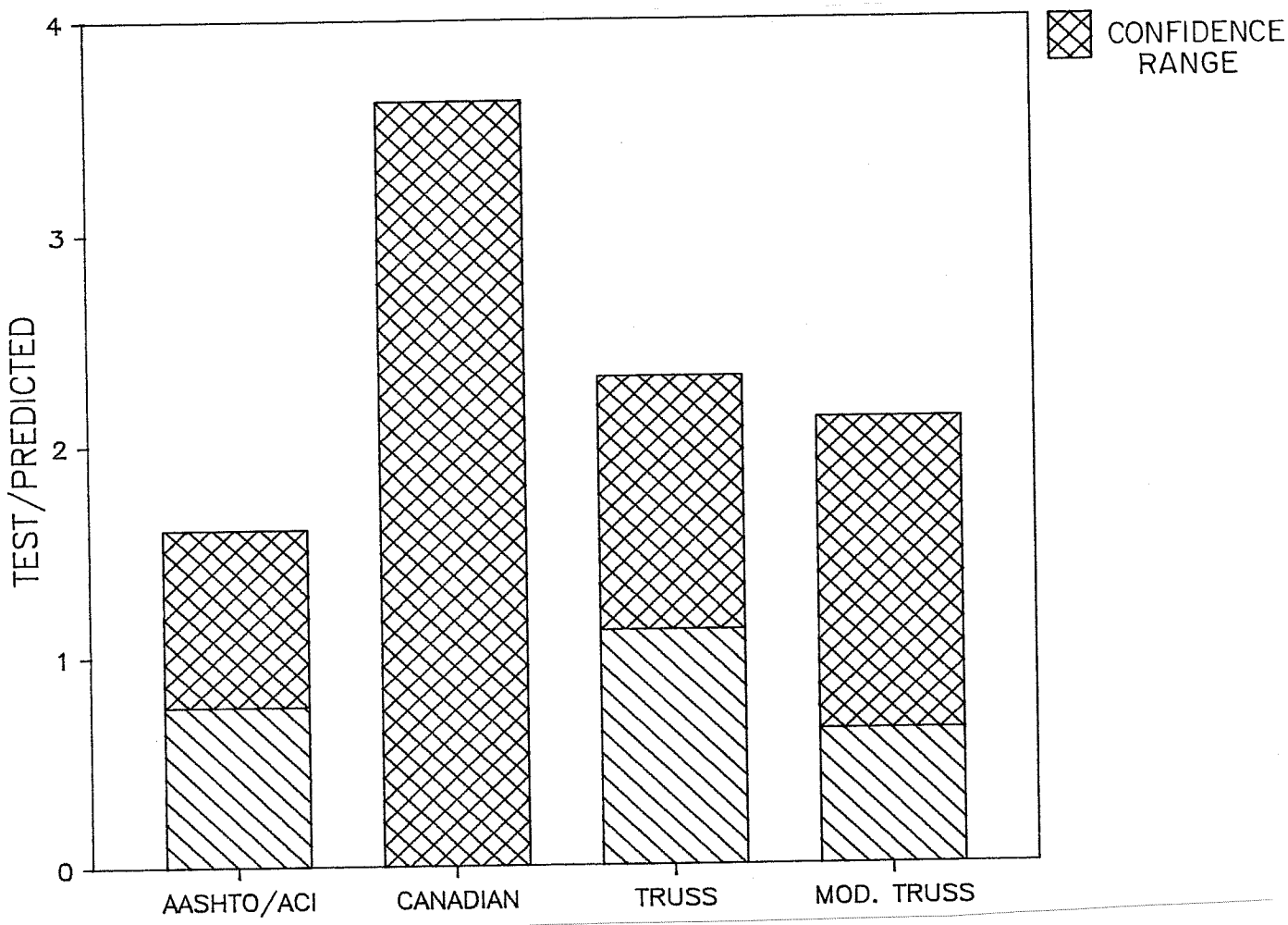

Fig. 5.75 Confidence ranges for the current test series at ultimate.

The question arises over how a set of empirical equations can give more accurate results than supposedly rational and physically based models. The AASHTO/ACI equations were originally derived and calibrated to existing test data. Given a reasonably complete set of primary variables including concrete strength, longitudinal reinforcement, shear reinforcement, prestress force, and shear span- to-depth ratio, fairly accurate results could be expected. In high strength concrete, concrete strength is the only variable which has changed. More importantly the relationship between compressive strength and tensile strength stays about the same for high strength concrete. Given this it is not extraordinary that the current AASHTO/ACI equations give good results.

The question then is why do the Canadian Code General Method and truss model do poorly? For this discussion $f_d \leq 0.5f'_c$ will be used. Figures 3.38, 3.43, 3.46, 5.66, 5.68, and 5.72 show an interesting trend. There is extreme conservatism for low $\rho_v f_y$ decreasing to near unity for higher $\rho_v f_y$. If Specimens 1-2 and 1-3 from the current test series are omitted, the average test/predicted ratio for the Canadian model would be 1.32 with a standard deviation of 0.10. If the same were done with the truss model, the average would be 1.22 with a standard deviation of 0.15. Improvements in average performance would be noted in tests reported in the literature as well if tests with very low $\rho_v f_y$ were excluded. As a practical matter, however, most beams are at the low end of the $\rho_v f_y$ scale. This means that both the Canadian Code and the truss model have a serious practical weakness. They do not properly account for concrete's contribution to shear capacity for low values of $\rho_v f_y$. At higher values of $\rho_v f_y$ the variable angle truss models can give an accurate prediction of shear capacity. Very interestingly, concrete strength is not the principal variable as witnessed by the lack of trends evident when strength ratios were plotted versus concrete strength.

The Canadian Code General Method does not currently have any avenue through which to improve its performance at low values of $\rho_v f_y$. This is a very serious practical weakness to the whole method. The truss model on the other hand has the framework in place to handle this difficulty. Increasing the allowable V_c to more realistic values and possibly extending the transition zone would allow this model to give very good results. From Tables 3.9 and 3.10 it can be seen that the current maximum contribution allowed by the truss model gave average values of 1.67 and 2.38 for reinforced and prestressed beams respectively. Improving these predictions would likely improve predictions at low $\rho_v f_y$ enough to make the truss model a viable, practical model.

CHAPTER 6
SUMMARY AND CONCLUSIONS

6.1 Summary of Results

6.1.1 Experimental program. The experimental portion of this project consisted of ten pretensioned high strength concrete girders. The girders were built with widely varying levels of shear reinforcement. This allowed behavioral observations to be made on members with very low, medium, and very high shear reinforcement levels. By varying shear reinforcement and support locations three separate failure modes were observed.

A number of observations and measurements were made during testing. Determination of the cracking load was of particular importance since current American practice assumes this is the concrete's contribution to shear capacity. Load-deflection behavior for the beams was observed as well. A number of internal strain measurements were taken. The strain readings gave an indication of internal behavior and thereby were of use comparing shear model assumptions and actual behavior. Additionally, observations were made on crack angles and crack widths. This gave information on how the concrete was working under load. Comparing various tests indicated behavioral changes that occurred as the shear reinforcement and support locations changed.

6.1.2 Model comparisons. A number of shear capacity models were evaluated. The evaluations consisted of a description of underlying assumptions and a comparison of these assumptions to observations made during the experimental portion of this program. The models evaluated ranged from highly empirical, such as current AASHTO/ACI methods, to highly theoretical, like the plasticity models.

A comparison was also made between the model capacity predictions and actual capacity obtained from tests. The shear tests on high strength concrete reported in American literature and the results of the current test program were used for this comparison. Both reinforced and prestressed results were analyzed to determine if major differences in conservatism of model predictions were occurring for high strength concrete. The last step was to compare the relative accuracy of the various models.

6.2 Conclusions

Evaluation of the experimental portion of this program gives rise to the following conclusions:

1. Stirrups generally reach yield even when the beam has shear reinforcement values on the order of $19.3\sqrt{f'_c}$.
2. Stirrups see very small strains until after shear cracking.
3. Crack widths are highly dependent upon the quantity of shear reinforcement.
4. Number and extent of cracks are dependent upon level of shear reinforcement.
5. Bottom rows of strands show little or no slip until shortly before shear-anchorage failures. Middle rows of strands show slow gradual slip throughout loading.
6. Two types of crushing failures can occur. They are crushing of individual struts for moderate levels of shear reinforcement or a compression field crushing for very heavy shear reinforcement.
7. Shear-anchorage failures were the primary mode of failure of prestressed beams without support overhangs. This was accentuated by poor modelling of strand development but needs to be carefully checked in prototype applications.
8. Prestressing strands did not reach yield within the shear span for any of the tests.

From model comparisons the following additional conclusions can be drawn:

1. AASHTO/ACI, the 1984 Canadian Code General Method, and the truss model all give generally conservative predictions of high strength concrete's shear capacity. This includes high strength concrete tests reported in the literature and those conducted by this project. This indicates that the methods are acceptable for concrete strengths to at least 12000 psi.
2. AASHTO/ACI gives the most accurate results with the least scatter of the three methods.
3. AASHTO/ACI becomes slightly unconservative in the range of $V_s = 19.3\sqrt{f'_c}$.
4. There are no strong trends apparent in the conservatism of the three methods related to increases in concrete strength.
5. Both the 1984 Canadian Code General Method and the truss model show decreasing conservatism as $\rho_v f_y$ increases.

6. The Canadian Code General Method is very conservative at low $\rho_v f_y$ values. For reinforced beams this is $\rho_v f_y \leq 100$ psi and for prestressed beams $\rho_v f_y \leq 350$ psi.

7. The truss model is very conservative for prestressed beams with $\rho_v f_y$ less than 350 psi.

8. The Canadian Code General Method and the truss model are conservative for tests with high $\rho_v f_y$ values.

9. The truss model, with the current limit on f_d, is unable to properly predict capacities for high strength concrete beams with very heavy shear reinforcement.

10. Based on this study the truss model allowable stress in the compression diagonals could conservatively be raised to 0.5 f'_c.

APPENDIX A

This Appendix contains information about the high strength concrete used throughout this project. Table A.1 gives material properties for the various concrete constituents. Table A.2 contains the batch weights and some physical properties for the concrete. It should be noted that the quantities of water reducing and retarding agents and high range water reducers used were dependent upon the temperature on the day of cast.

TABLE A.1

MIX CONSTITUENTS	PROPERTIES
Cement	ASTM C150 Type I
Fly ash	ASTM C618 Class C TSDH&PT Type B BSG = 2.64
Coarse aggregate	Crushed limestone ASTM C33 No. 8, 3/8-in. to #8 DRUW = 100 pcf BSG_{ssd} = 2.79 AC_{ssd} = 0.5%
Fine aggregate	Natural river sand BSG_{ssd} = 2.62 AC_{ssd} = 1.0%
Water reducing and retarding admixture (Gifford-Hill - R-Plus)	ASTM C494 Type D Polymer-based S. G. = 1.24 % solids = 42% Dosage rates: 2-4 oz./cwt
High range water reducing admixture (Gifford-Hill - PSI-Super)	ASTM C494 Type F Naphthalene-based S. G. = 1.21 Dosage rates: 6-16 oz./cwt

TABLE A.2

Design strength @ 28 days	12000 psi
MIX DESIGN	lbs/cubic yard
Cement	698
Fly ash	298
Coarse aggregate	1821
Fine aggregate	1039
Water	249
Water reducing and retarding admixture	20-40 oz
High-range water reducing admixture	60-160 oz
MIX PROPERTIES	
Slump	1 in. at batch plant prior to addition of HRWR 10 in. at laboratory after second HRWR dose
Unit weight	150 pcf
Water/cementitious material ratio	0.25
Cemetitious materials (sacks/ cu. yard)	10.5
Air content	1.3%
Percent fly ash replacement	30%
Percent DRUW	67%

APPENDIX B

Development refers to the general topic of the transfer of force between the steel and the concrete in reinforced and prestressed concrete. The term development length refers to the distance required for the force transfer. Knowledge of the development characteristics of the reinforcement used is important since it indicates the location that the full capacity of the reinforcement can be counted on. If the full capacity is not available, knowledge of the percentage that can be obtained is important. The development length of prestressing strands is the area of current interest. Only pretensioned members will be discussed herein. The development of prestressing strands consists of two distinct mechanisms. The first is termed transfer and the second is flexural bond.

The discussion will begin with a coverage of the two development mechanisms followed by factors that affect them. The current equations for development will be covered. Then a comparison of model and prototype development lengths will be made.

The first development phase is transfer. Transfer occurs when the prestressing strands are released from the supports which held them during casting. Since the prestressing strands are tensioned they try to contract to their original length. The concrete resists this contraction and forces are transferred between the strands and the concrete until equilibrium is achieved. The equilibrium condition in the strand is one of zero stress at the exterior of the concrete increasing to the effective prestress force at the end of the transfer length. Friction between the concrete and the steel is generally attributed the greatest importance in transfer [B3,B8,B9,B12]. When a prestressing strand is originally tensioned the cross-sectional area decreases slightly. Upon release the strand tries to shorten. As it does so, the diameter of the strand increases. This is called the Hoyer effect. [B12]. The increase in cross-section causes a radial pressure to develop against the hardened concrete. A high friction force is present as the strand tries to move into the concrete due to this radial pressure. This friction is enough to prevent further slip of the strand into the concrete and thereby provide transfer.

The second development phase is flexural bond. Flexural bond mechanisms are activated after cracking when steel stresses in excess of the effective prestress stress are required for equilibrium. This added stress must be transferred to the concrete. The mechanisms of flexural bond must be different than those of transfer since the strand constricts as it elongates [B8,B9]. Two mechanisms are thought to be at work in flexural bond. The first is adhesion between the concrete and the steel. This comes from concrete

filling the irregularities in the steel surface. This is generally felt to be of fairly minor importance. The second mechanism of flexural bond is mechanical resistance. The helical shape provides a nonuniform cross- section that allows for mechanical resistance. This mechanical resistance is, however, fairly low since the strand is able to twist in the groove formed by the strand in the concrete. The mechanisms of flexural bond are not nearly as effective as those of transfer.

A number of factors have been found to affect the mechanisms described above and thereby the development length. The most important parameter is the force to be transferred. The larger the force in the strand, the larger the force to be transferred. The size of the strand also effects the development length. The larger the strand, the greater surface area there is for transfer. The surface condition of the strand can have an effect on development. Research has shown behavior goes from good to bad for rusted, clear, and oiled strands. [B7,B8,B9]. The literature has attributed only a small influence to concrete strength. However, recent tests by Castrodale seem to contradict this [B6,B10]. The method of release whether sudden or gradual can have a influence on transfer length. The sudden release such as by flame cutting can considerably increase development length. [B5,B10,B11]. Proper consolidation has been found to be an important practical method of obtaining good development characteristics [B4,B5]. Finally the amount of cover has been found to effect performance.

The ACI Code has several provisions dealing with the development length of prestressing strands. It calls for a development length of: $I_d = (f_{ps} - (2/3)f_{se})d_b$ beyond the critical section where f_{ps} and f_{se} are in kips per square inch and l_d and d_b are inches. The added provision is given that if strands are debonded and there is tension in the concrete the length computed needs to be doubled. In the section on shear ACI calls for a development length of 50 d_b. For computations of the concrete's contribution to shear, the prestress can be assumed to vary linearly from zero at the end of the member to full prestress at the end of the transfer length.

The equation given for development length is a condensed form of the following:

$$I_d = [f_{se}/3 + (f_{ps} - f_{se}) * d_b)]$$

This shows more clearly the two phases of development discussed previously (Fig. B-1). The first term represents the transfer length. The second represents the length required for flexural bond. Each phase of development is shown to be a function

of a change in stress times the strand diameter. These factors indicate the force to be transferred and the surface area over which this transfer takes place are the most important factors. It can be seen that transfer is three times as effective as flexural bond. In this form it is also possible to see the origin of 50 diameters as used in the shear provisions. When the original tests were conducted 250-ksi strands were common as opposed to the current use of 270-ksi strands. In both cases, given an initial prestress of .7 f_{pu} and 20% losses, transfer becomes 47 and 51 strand diameters respectively [A13].

One major question is how 3/8" diameter strands in a 1/3 scale model test compare to 1/2" diameter strands in a prototype specimen. Table B-1 shows a comparison. It can be seen that the development of 1/2" strand in a prototype is poorly modelled by the use of 3/8" strands in these 1/3 scale models. If the actual development requirement of 3/8" strands is multiplied by the scale factor of 3, very long development lengths are required when compared to the development of 1/2" strand in a prototype. In retrospect, these model girders were poorly scaled for strand anchorage. It can be easily computed that the 3/8" strands would give a prototype development length 2.25 times as long as the 1/2" strands.

While development in the prototype can be seen to be comparatively better the possible failure mechanisms remain the same. Thus there still is a possibility that debonding of strand might occur in the prototype as well as the model. This should always be checked.

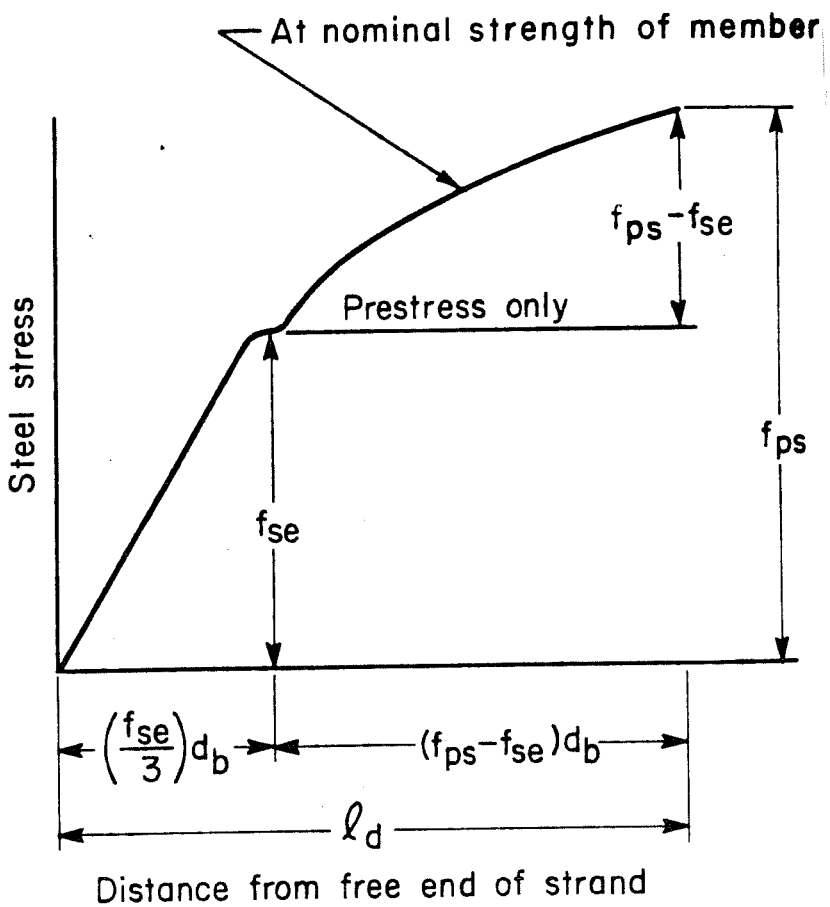

Fig. B-1 Variation of steel stress with distance from free end of strand [Ref. B2]

TABLE B.1

STRESS (x fpu)	1/2" STRAND (in.)	3/8" STRAND (in.)	3/8" PROTOTYPE (in.)
.5	67.5	50.6	151.9
.6	87.0	60.7	182.2
.7	94.5	70.9	212.6
.8	108.0	81.0	243.0
.9	121.5	91.1	273.4
1.0	135.0	101.2	303.8

REFERENCES

B1. American Concrete Institute, *Building Code Requirements for Reinforced Concrete (ACI 318-83)*, Detroit, 1983, 111pp.

B2. American Concrete Institute, *Commentary on Building Code Requirements for Reinforced Concrete (ACI 318-83)*, Detroit,.

B3. Badaliance, R. and Van Horn, D.A., "Ultimate Flexural Bond inBeams Pretensioned withHigh Strength Strands," Fritz Engineering Laboratory Report No. 309.3, Lehigh University, Jan., 1967.

B4. Base, G.D., "An Investigation of the Use of Strand in Pretensioned Concrete," *Research Report No. 11*, Cement and Concrete Association, London, 1963.

B5. Base, G.D., "An Investigation of Transmission Length in Pretensioned Concrete," *Research Report No. 5*, Cement and Concrete Association, London, August, 1958.

B6. Castrodale, R.W., " ", unpublished Ph.D. dissertation, The University of Texas at Austin, ,.

B7. Hanson, N.W., "Influence of Surface Roughness of Prestressing Strand in Bond Performance," *Journal*, Prestressed Concrete Institute, V.14, No.1, Jan.-Feb. 1969, pp. 32-45.

B8. Hanson, N.W. and Kaar, P.H., "Flexural Bondof Pretensioned Prestressed Beams," *ACI Journal*, Proceedings, V. 55, No. 7, January, 1959, pp. 783-803.

B9. Janney, J.R., "Nature of Bond in Pretensioned Prestressed Concrete," *ACI Journal*, Proceedings, V. 50, No. 9, May, 1954, pp. 717-736.

B10. Kaar,P.H., Lafraugh, R.W., and Mass, M.A., "Influence of Concrete Strength on Stranad Transfer Length," *PCI Journal*, V. 8, No. 5, October, 1963, pp. 47-67.

B11. Swamy, R.N. and Anand, K.L., "Transmission Length and Prestress Lossed in High Strength Concrete," Paper presented at the Seventh International Congress of the Federation Internationale de la Precontrainte, New York, N.Y., May-June, 1974.

B12. Tulin, L.G. and Al-Chalabi,M.M., "Bond Strength as a Function of Strand Tension and Cement Paste Content for Lightweight Aggregate Concrete," *ACI Journal*, Proceedings, V. 66, No. 10, October, 1969, pp. 840-846.

B13. Zia, P. and Mostafa, T.,"Development Length of Prestressing Strands," *PCI Journal*, V. 22, No. 5, September-October 1977, pp. 54-65.

REFERENCES

1. Ahmad, S.H., Khaloo, A.R., and Poveda, A., "Shear Capacity of Reinforced High-Strength Concrete Beams," *ACI Journal, Proceedings* Vol. 83, No. 2, Mar.-Apr. 1986, pp.297-305.

2. American Association of State Highway and Transportation Officials, *Standard Specification for Highway Bridges*, Thirteenth Edition, Washington, D.C., 1983.

3. American Concrete Institute, *Building Code Requirements for Reinforced Concrete (ACI 318-63)*, Detroit, 1963, 144 pp.

4. American Concrete Institute, *Building Code Requirements for Reinforced Concrete (ACI 318-83)*, Detroit, 1983, 111 pp.

5. American Concrete Institute, *Building Code Requirements for Reinforced Concrete (ACI 318-71)*, Detroit, 1971, 78 pp.

6. American Concrete Institute, *Commentary on Building Code Requirements for Reinforced Concrete (ACI 318-63)*, SP10 Detroit, 1965, 91 pp.

7. American Concrete Institute-American Society of Civil Engineers Committee 326, "Shear and Diagonal Tension," *Proceedings*, American Concrete Institute, V.59, Jan., Feb., and Mar., 1962, pp. 1-30, 277-334, and 353-396.

8. American Concrete Institute-American Society of Civil Engineers Committee 426, "The Shear Strength of Reinforced Concrete Members," Journal of the Structural Division, *Proceedings*, ASCE, V.99, No. ST6, June 1973, pp. 1091-1187.

9. American Concrete Institute Committee 211.D, "Guide for Selecting Proportions for High Strength Concrete," Committee proposal, July 1986.

10. American Concrete Institute Committee 363, "State-of-the-Art Report on High-Strength Concrete," *ACI Journal, Proceedings*, Vol. 81, No. 4, July-Aug. 1984, pp. 363-411.

11. Carrasquillo, P.M. and Carrasquillo, R.L., "Guidelines for Use of High Strength Concrete in Texas Highways," *Research Report 367-1F*, Center for Transportation Research, The University of Texas at Austin, Aug. 1986, 227 pp.

12. Carrasquillo, R.L., Nilson, A.H., and Slate, F.O., "Properties of High Strength Concrete Subject to Short-Term Loads," *ACI Journal, Proceedings* Vol. 78, No. 3, May-June 1981, pp. 171-178.

13. Castrodale, R.W., "A Study of Pretensioned High Strength Concrete Girders in Composite Highway Bridges" unpublished Ph.D. dissertation, The University of Texas at Austin, 1988, pp. 662.

14. Colaco J.P., "75-Story Texas Commerce Plaza, Houston - The Use of High-Strength Concrete," *High Strength Concrete*, SP-87, American Concrete Institute, Detroit, 1985, pp. 1-8.

15. Collins, M.P. and Mitchell D., "A Rational Approach to Shear Design - The 1984 Canadian Code Provisions," *ACI Journal, Proceedings*, V. 83, No. 6, Nov.-Dec. 1986, pp. 925-933.

16. Collins, M.P. and Mitchell D., "Shear and Torsion Design of Prestressed and Non-Prestressed Concrete Beams," *PCI Journal*, Vol. 25, No. 5, Sept.-Oct. 1980, pp. 32-100.

17. Collins, M.P., "Towards a Rational Theory for RC Members in Shear," Journal of the Structural Division, *Proceedings*, ASCE, V. 104, No. ST4, April 1978, pp. 649-666.

18. Comite Euro-International du Beton, *CEB-FIP Model Code for Concrete Structures*, CEB-FIP International Recommendation, Third Edition, Paris, April 1978, 348 pp.

19. Danielsen, S.W., "Optimizing Aggregate Properties for High Strength Concrete," *Utilization of High Strength Concrete*, Proceedings Symposium in Stauanger, Norway, June 15-18,1987, No. 1.6, pp 73-84.

20. de Larrad, F., Acker, P., Malier Y., "Very High-Strength Concrete: From the Laboratory to the Construction Site," *Utilization of High Strength Concrete*, Proceeding Symposium in Stauanger, Norway, June 15-18, 1987, No. 4.12, pp. 509-516.

21. *Design of Concrete Structures for Buildings (CAN3-A23.3- M84)*, Canadian Standards Association, Rexdale, 1984, 281 pp.

22. Drake, K.D., "High-Strength Concrete in Seattle," *High Strength Concrete*, SP-87, American Concrete Institute, Detroit, 1985, pp. 21-34.

23. Elzanaty, A.H., Nilson, A.H., and Slate, F.O., "Shear- Critical High Strength Concrete Beams," *Research Report No. 85- 1*, Depatment of Structural Engineering, Cornell University, Feb. 1985, 216 pp.

24. Fergestad, S., Jordet, E.A., Nielsen, K.H., and Walstad, T., "An Evaluation of the Economical and Technical Potential of High Strength Concrete in Long Span Concrete Bridge Construction," *Utilization of High Strength Concrete*, Proceeding Symposium in Stauanger, Norway, June 15-18, 1987, No. 5.4, pp. 597-607.

25. Glaever, N.A., Hoysaeter, E., and Odervd H.T., "High Strength Concrete-Applications in Bridge Construction," *Utilization of High Strength Concrete*, Proceedings Symposium in Stauanger, Norway, June 15-18, 1987, No. 5.2, pp. 573-584.

26. Grob, F. and Thurlimann, B., "Ultimate Strength and Design of Reinforced Concrete Beams Under Bending and Shear," Publications, No. 36-II, IABSE, Zurich, 1976, pp. 105-120.

27. MacGregor, J.G. and Hanson, J.M., "Proposed Changes in Shear Provisions for Reinforced and Prestressed Concrete Beams," *Proceedings*, American Concrete Institute, V. 66, No. 4, April 1969, pp. 276-288.

28. Martin, J.B., *Plasticity: Fundamentals and General Results*, The MIT Press, Cambridge, Mass., 1975, 931 pp.

29. Martinez, S., Nilson, A.H., Slate, F.O., "Short-term Mechanical Properties of High-Strength Light-Weight Concrete," *Research Report No. 82-9* Vol. 81, No.5, Sept.-Oct. 1984, pp. 431-442.

30. Mphonde, A.G., and Frantz, G.C., "Shear Strength of High Strength Reinforced Concrete Beams", *Research Report C#84-157*, Department of Civil Engineering, University of Connecticut, June 1984, 260 pp.

31. Natrella, M.G., *Experimental Statistics*, National Bureau of Standards, 1966

32. Nielsen, M.P., Braestrup, M.W., Jensen, B.C., and Bach, F., "Concrete Plasticity: Beam Shear–Shear in Joints–Punching Shear," Danish Society for Structural Science and Engineering, Structural Research Laboratory, Technical University of Denmark, Lyngby, Special Publication, Oct. 1978, pp. 1-89.

33. Nielsen, M.P., *Limit Analysis and Concrete Plasticity*, Prentice-Hall Inc. 1984, 420 pp.

34. Nielsen, M.P., and Braestrup, N.W., "Plastic-Shear Strength of Reinforced Concrete Beams," *Bygningsstatiske Meddeleser*, V. 46, No. 3, 1975, pp. 61-99.

35. Nilson, A.H., "High Strength Concrete - An Overview of Cornell Research," *Utilization of High Strength Concrete*, Proceedings Symposium in Stauanger, Norway, June 15-18, 1987, No. 1.2, pp. 27-38.

36. Peterman, M.B., and Carrasquillo, R.L., "Production of High Strength Concrete," *Research Report 315-1F*, Center for Transportation Research, The University ofTexas at Austin, Oct. 1983, 286 pp.

37. Radjy, F.F., Bogen, T., Sellevoid, E.J., and Loeland, K.E., "A Review of Experiences with Condensed Silica-Fume Concretes and Products," *Fly Ash, Silica Fume, Slag, and Natural Pozzolans in Concrete*, SP-91, Proceedings Second International Conference, Madrid, Spain, Vol. II, American Concrete Institute, Detroit, 1986, pp. 1135-1152.

38. Ramirez, J.A. and Breen, J.E., "Experimental Verification of Design Procedures for Shear and Torsion in Reinforced and Prestressed Concrete," *Research Report 248-3*, Center for Transportation Research, The University of Texas of Austin, Nov. 1983, 300 pp.

39. Ramirez, J.A. and Breen, J.E., "Proposed Design Procedures for Shear and Torsion in Reinforced and Prestressed Concrete," *Research Report 248-4F*, Center for Transportation Research, The University of Texas at Austin, Nov. 1983, 254 pp.

40. Ramirez, J.A. and Breen, J.E. "Review of Design Procedures for Shear and Torsion in Reinforced and Prestressed Concrete," *Research Report 248-2*, Center for Transportation Research, The University of Texas at Austin, Nov. 1983, 186 pp.

41. Russel, H.G., "High-Strength Concrete in North America," *Utilization of High Strength Concrete*, Proceedings Symposium in Stauanger, Norway, June 15-18, 1987, No. 5.1, pp. 561-572.

42. Schlaich, J., Schafer, K., and Jennewein, M., "Towards a Consistent Design of Structural Concrete," *PCI Journal*, Vol. 32, No. 3, May-June 1987, pp. 74-150.

43. Shah, S.P. and Ahmad, S.H., "Structural Properties of High Strength Concrete and Its Implications for Precast Prestressed Concrete," *PCI Journal*, Vol. 30, No. 6, Nov.-Dec. 1985, pp. 91- 117.

44. Smadi, M.M., Slate, F.O., and Nilson, A.H., "High-, Medium-, and Low-Strength Concretes Subject to Sustained Overloads-Strains, Strengths, and Failure Mechanisms," *ACI Journal, Proceedings*, V. 82, No. 5, Sept.-Oct. 1985, pp. 657-664.

45. Sozen, M.A. and Hawkins, N.M., Discussion of "Shear and Diagonal Tension," by ACI-ASCE Committe 326, *ACI Journal, Proceedings*, V. 59, Sept. 1962, pp. 1341-1347.

46. Thurlimann, B., "Plastic Analysis of Reinforced Concrete Beams," Berich 86, Institut fur Baustatik und Konstruktion ETH, November, 1978, Zurich 20 pp.

47. Thurlimann, B., "Shear Strength of Reinforced and Prestressed Concrete Beams – CEB Approach," SP-59, American Concrete Institute, Detroit, 1979, pp. 93-115.

48. Thurlimann, B., unpublished class notes for "CE397: Strength of Reinforced and Concrete and Prestressed Concrete Beams under Shear, Torsion, and Combined Actions," The University of Texas at Austin, Oct. 1978.

49. Vecchio, F.J. and Collins, M.P., "The Modified Compression- Field Theory for Reinforced Concrete Elements Subjected to Shear," *ACI Journal, Proceedings*, V. 83, No. 2, March-April, 1986, pp. 219-231.